The Dissertation Committee for Julia Nicole Roberts Certifies that this is the approved version of the following dissertation:

Field Evaluation of Large-Scale, Shallow Ground Improvements to Mitigate Liquefaction Triggering

Committee:

Kenneth H. Stokoe, II, Supervisor

Ronald D. Andrus

Brady R. Cox

Ellen M. Rathje

Clark R. Wilson

Field Evaluation of Large-Scale, Shallow Ground Improvements to Mitigate Liquefaction Triggering

by

Julia Nicole Roberts

Dissertation

Presented to the Faculty of the Graduate School of

The University of Texas at Austin

in Partial Fulfillment

of the Requirements

for the Degree of

Doctor of Philosophy

The University of Texas at Austin

December 2017

Dedication

To the reader.

Acknowledgements

The work completed in this dissertation could not have been done without the help of many individuals over the past six years. First and foremost, I wish to thank Dr. Kenneth H. Stokoe II, for his guidance as my research advisor and for answering my endless stream of questions regarding soil dynamics. I am also deeply grateful for the invaluable guidance from Dr. Brady R. Cox regarding the work done on this dissertation as well as other research projects.

I also extend my deepest gratitude to the staff Alicia Zapata, Cecil Hoffpauir, Dr. Farnyuh Menq, Robert Kent, and Andrew Valentine, without whom none of this research would be possible, nor would it be nearly as much fun. I extend an additional thanks to my classmate and partner in crime out in the field, Sungmoon Hwang, for great times on past projects. To fellow classmate Benchen Zhang, who has been trained as my replacement, I wish nothing but good luck and good weather for all future projects.

Thank you to Dr. Gilbert, Dr. Rathje, Dr. Zornberg, and Dr. El Mohtar from whom I have taken courses or interacted with over the past few years, for creating an excellent community of learning and research in our geotechnical engineering program here at The University of Texas at Austin. A special thank you goes to Dr. Andrus and Dr. Wilson for also being a part of my dissertation committee and providing invaluable feedback on my research.

To those who first inspired me to go into geotechnical engineering, I extend a special acknowledgement to Dr. Lucy Jen and Dr. John Germaine, formerly of the Massachusetts Institute of Technology. Thank you for teaching me that “it is what it is” when it comes to soil, for introducing me to the excitement of research, and for overconsolidating me for the rest of my life.

To my friends here in Austin and scattered around the world, I am most appreciative of all the good times, the support, and the invaluable life advice I can always count on.

To my family, I am grateful for your continued support over the course of my life and my studies. The greatest gift of all has been access to an education that has repeatedly taught me the love of learning along with the freedom to make my own mistakes. You each, in your own way, inspire me every day to work harder and be smarter in hopes of making tomorrow better.

Field Evaluation of Large-Scale, Shallow Ground Improvements to Mitigate Liquefaction Triggering

Julia Nicole Roberts, Ph.D.

The University of Texas at Austin, 2017

Supervisor: Kenneth H. Stokoe, II

Much of the devastation wrought by the 2010-2011 Canterbury Earthquake Sequence (CES) in Christchurch, New Zealand, was caused by extreme levels of liquefaction-induced damage to structures with shallow foundations. In response to this disaster, the New Zealand Earthquake Commission (EQC) funded a large study known as the Ground Improvement Trials to evaluate and identify shallow ground improvement methods that are not only effective at increasing the soil's resistance to soil liquefaction, but are also cost effective and practical to build for lightweight structures. Of the nine ground improvement methods included in the trials, three were selected for extensive analysis in this dissertation. These three ground improvement methods are the Rapid Impact Compaction (RIC), the Rammed Aggregate Piers^{TM} (RAP), and the Low-Mobility Grout (LMG).

At three test sites along the Avon River in Christchurch neighborhoods that were among the worst hit by liquefaction-related damage, full-scale test panels of natural soil and ground-improved soil were constructed and evaluated using a variety of in situ test methods. The analysis in this dissertation primarily relies on data from excavation trenching, cone penetrometer testing (CPT), direct-push crosshole testing (DPCH), and shake testing with T-Rex. These tests capture changes in density and stiffness, and

therefore liquefaction resistance, due to the ground improvement methods in comparison to the natural soil. Shake testing with T-Rex is further able to define the relationship between cyclic shear strain and the generation of excess pore pressure that ultimately determines whether or not a soil will liquefy under cyclic loading. Under this framework, the effectiveness of each of the three ground improvement methods is evaluated and discussed.

Table of Contents

List of Tables

List of Figures

Chapter 1: Introduction

1.1 INTRODUCTION

This dissertation covers the evaluation of three ground improvement methods and their effectiveness to reduce the susceptibility of soil liquefaction triggering during an earthquake. This work was part of a large study, known as the Ground Improvement Trials, that was funded by New Zealand Earthquake Commission (EQC) to identify and assess shallow ground improvement methods that would reduce liquefaction-related damage to lightweight residential structures during future earthquakes and it represents only a small part of a highly collaborative study that was led and managed by the engineering firm Tonkin & Taylor Ltd.

The scale of the Ground Improvement Trials was remarkable because it featured the construction of dozens of full-scale ground improvement test panels at three separate sites in the Christchurch area. These sites and test panels were subjected to a battery of investigations that included borings, cone penetrometer tests (CPT), direct-push crosshole tests (DPCH), dilatometer tests (DMT), shake testing with T-Rex, blasting, excavation trenches, resonant column tests (RC), laboratory classifications of soils, and cyclic triaxial tests, resulting in the systematic collection of massive quantities of data by scores of researchers and engineers.

The impetus for the Ground Improvement Trials was the extensive liquefaction-related damage to residential areas in Christchurch, New Zealand, from the 2010-2011 Canterbury Earthquake Sequence (CES) and the desire to prevent a similar catastrophic scenario in the future. The cumulative toll of the 2010-2011 CES includes the deaths of 185 individuals and costs greater than 40 billion NZD to repair and rebuild the city, a process that is ongoing and estimated to continue at least through the year 2020.

Of the six main events that made up the CES, there were two earthquakes in particular that were responsible for much of the widespread liquefaction-related damage: (1) the 4 September 2010 Darfield Earthquake with a moment magnitude M_W of 7.1 and (2) the 22 February 2011 Christchurch Earthquake with a moment magnitude M_W of 6.2. The repeated liquefaction throughout the suburbs of Christchurch caused by these earthquakes highlighted the vulnerability of the city's built environment and foreshadowed the decision to eventually abandon some neighborhoods entirely because the process of improving the worst-performing soils in those areas was deemed too costly.

1.2 PROJECT SCOPE

The scope of the work covered in this dissertation will cover only part of the contribution that a team of researchers from The University of Texas at Austin made to the Ground Improvement Trials. This team consisted primarily of professors Dr. Kenneth H. Stokoe and Dr. Brady R. Cox, graduate students Julia N. Roberts and Sungmoon Hwang, research associate Dr. Farnyuh M. Menq, and support staff Cecil Hoffpauir, Andrew Valentine, and Robert Kent.

The work presented in this dissertation was performed in Christchurch, New Zealand, during two separate trips in 2013. The first trip took place over the course of four weeks in June and July of 2013 and the second trip took place over the course of six weeks in September and October of 2013.

While the work by the research team from The University of Texas at Austin in the Ground Improvement Trials encompassed significantly more than what is presented herein, this dissertation will focus only on testing related to the evaluation of three ground improvement methods that at the time were considered the most promising methods available. Some of the work from this dissertation, as well as from other aspects of the Ground Improvement Trials, have previously been published in Stokoe et al. 2014, van Ballegooy et al. 2015, Roberts et al. 2016, Stokoe et al. 2016, Wang et al. 2017, and Hwang et al. 2017. Additional publications related to the work of The University of Texas at Austin researchers for the Ground Improvement Trials are forthcoming.

1.3 ORGANIZATION OF DISSERTATION

The main objective of this dissertation is to evaluate the effectiveness of three ground improvement methods using three in-situ testing techniques as part of the Ground Improvement Trials.

Chapter 1 introduces the motivation for the Ground Improvement Trials and the need to evaluate the effectiveness of various ground improvement methods. It also outlines the scope of this dissertation and explains how the work of this dissertation fits into the bigger picture of the Ground Improvement Trials, providing pertinent context.

Chapter 2 reviews literature related to the triggering of soil liquefaction. This includes a review of in-situ tests and analysis methods that represent the best way of evaluating the liquefaction susceptibility of natural deposits in the field as well as a review of primarily laboratory research that investigate the effects of degree of saturation and non-plastic fines content on the cyclic resistance of soils.

Chapter 3 provides background and context for understanding the portion of the Ground Improvement Trials that is included in this dissertation. It includes an overview of the three test sites and the 15 test panels (five test panels at each test site) as well as full descriptions of the construction processes for the three ground improvement methods.

Chapter 4 focuses on the characterization of the natural soils. Because there are differences between the soil layering at each of the three test sites, the natural soils at each of the test sites were characterized separately. The characterization of the natural soils includes CPT tests to identify subsurface layering, DPCH tests to develop compression and shear wave velocity profiles, and excavation trenches to visually confirm subsurface layering and obtain disturbed samples for laboratory soil classification.

Chapter 5 evaluates the effectiveness of the ground improvement methods using CPT and DPCH testing. The results of these tests at the ground-improved soil are assessed

in comparison to those from the natural soil to identify relative values of change. Excavation trenches of the ground-improved test panels are used to visually assess the construction quality of the ground improvements as well.

Chapter 6 provides an overview of shake testing with T-Rex as it was performed for the Ground Improvement Trials. This includes a brief overview of the sensors, the installation process, the various instrumentation arrays used at different test panels, and the typical staging of a shake test with T-Rex. This chapter also discusses how the excess pore pressure ratio, shear strain, and the shear-wave velocity based cyclic resistance ratio are calculated, as well as two modifications to the method of calculating shear strain and its impact on the accuracy of results.

Chapter 7 evaluates the effectiveness of the ground improvement methods using stiffness profiles from shake testing with T-Rex. The stiffness profiles are used to indicate the stiffness of the soil in the top 4.0 m over a large range of shear strains. The performance of the ground-improved soils are considered in comparison to the performance of the natural soils.

Chapter 8 introduces four categories of behavior based on the relationship between the generation of residual excess pore pressure and cyclic shear strain, and investigates how soil type, relative density, and degree of saturation influences this relationship. These four categories range in behavior from highly susceptible to soil liquefaction in Category 1 to not liquefiable in Category 4 under cyclic loading conditions. The effectiveness of the ground improvement methods are further evaluated by investigating how the ground improvement method may influence the soil's relationship between the generation of residual excess pore pressure and shear strain, and therefore its susceptibility to liquefaction triggering under cyclic loading conditions.

Chapter 9 summarizes the work presented in this dissertation and offers salient conclusions based on its work.

Appendix A includes graphs of data related to the evaluation of the stiffness profiles that were presented in Chapter 7.

Chapter 2: Literature Review

2.1 INTRODUCTION

The current state of knowledge regarding soil liquefaction comes from decades of research in the field and laboratory. Case studies following devastating earthquakes often provide the greatest insight into the complex behavior of soil post-liquefaction as well as the characteristics of soils that are most likely to liquefy and of soils that are considered non-liquefiable. The laboratory provides highly-controlled conditions in which to study the varying effects of properties such as degree of saturation, fines content, confining pressure, and density on the liquefaction susceptibility and cyclic resistance of soils. Among the topics that continue to be the focus of researchers today are the accurate evaluation of the cyclic resistance of in situ soils using field testing methods and the influence that the degree of saturation and fines content have on the cyclic resistance of soils. A greater understanding of these areas will lead to fewer over- and under-predictions of soil liquefaction in future earthquakes, as well as a better understanding of how these factors will influence the effectiveness of various ground improvement methods intended to prevent the triggering of soil liquefaction.

In Section 2.2, the work of Youd et al. 2001 will be reviewed to show the state of practice regarding in situ methods of estimating the cyclic resistance of the soil. In Section 2.3, the effect of degree of saturation on the cyclic resistance of soils as well as methods for estimating the degree of saturation in the laboratory and the field are discussed and summarized. In Section 2.4, there is a brief overview of the updated criteria for considering the liquefaction-susceptibility of a soil based on its soil type as well as a review of literature regarding the effects of varying fines content on the cyclic resistance of soils.

2.2 YOUD ET AL. (2001) – LIQUEFACTION RESISTANCE OF SOILS

In 2001, a summary report authored by twenty-one contributors laid out the known testing and analysis methods for predicting the earthquake-induced liquefaction susceptibility of in-situ soils (Youd et al. 2001). The authors are acknowledged leaders in the field of geotechnical earthquake engineering research and their collaboration on this publication stems from two workshops on the subject of evaluating the liquefaction resistance of soils. The objectives of the workshop and the report were to standardize some liquefaction testing and data analysis procedures as well as to reach a consensus on soil behavior models given the prior experience of each of the contributors.

This report first outlines the simplified procedure for evaluation the cyclic stress ratio (CSR) imposed on the soil during a given earthquake event. The CSR is defined simply as the ratio of shear stress to the initial vertical effective stress ($CSR = \tau/\sigma'_{vo}$). While the in-situ vertical effective stress is typically straight forward to calculate, it is very difficult to accurately ascertain the dynamic shear stress imposed by an earthquake throughout the soil deposit. The simplified procedure first suggested by Seed and Idriss 1971 estimates the CSR using the following equation:

$$CSR = 0.65(\frac{a_{max}}{g})(\frac{\sigma_{vo}}{\sigma'_{vo}})r_d \quad (1)$$

where a_{max} is the maximum horizontal acceleration at the ground surface during an earthquake, g is the acceleration of gravity, σ_{vo} is the total vertical stress, σ'_{vo} is the effective vertical stress, and r_d is the stress reduction coefficient. In the intervening decades, some updates have been made to the estimation of the stress reduction coefficient r_d but the overall simplified procedure to calculate CSR has remained the same.

In much the same way that the CSR is a measure of the stresses imposed on the soil during the earthquake, the cyclic resistance ratio (CRR) is a measure of the soil's innate

ability to resist the triggering of liquefaction in relation to the CSR. It is simple to evaluate the CRR of a soil specimen in the laboratory, but it difficult to do the same for in situ soil deposits. As a result, the experts began developing empirical relationships correlating the results from in situ test methods to the CRR of natural deposits. This process has involved using hundreds of case studies from previous earthquake events and correlating the results of in situ testing with instances in which sites either experience or did not experience soil liquefaction.

At the time of the publication in 2001, there existed four well-known field methods for evaluating the potential for earthquake-induced liquefaction in granular soils, all of which are indirect. The testing methods include the standard penetration test (SPT), the cone penetration test (CPT), the Becker penetration test (BPT), and shear wave velocity (V_S) measurements. The results from each method generally indicate the stiffness or density of the soil, properties that play a role in determining the liquefaction-susceptibility of a soil but are not the only controlling factor. The models derived from the test-obtained data are verified by comparison against visually confirmed surface manifestations of soil liquefaction at specific sites for approximately magnitude 7.5 earthquakes, though scaling factors can be applied to adjust the models for earthquake magnitudes ranging from 5.5 to 8.5. Proposed relationships for estimating the magnitude scaling factor for given earthquake magnitude are presented in Figure 1. The baseline of these soil liquefaction susceptibility models is also applicable only for clean sands (no fines content), but there exist corrections that can be applied for varying percentages of fines content.

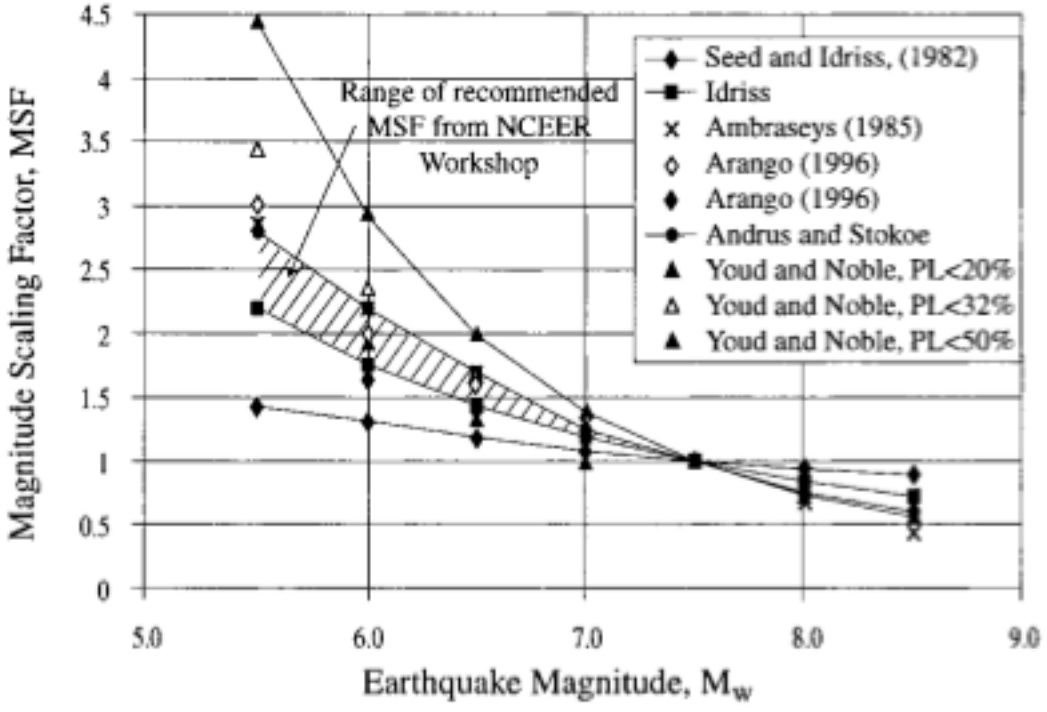

Figure 1: Magnitude Scaling Factors suggested by different researchers to adjust the soil liquefaction susceptibility models for earthquake magnitudes other than 7.5 (from Youd and Noble, 1997).

The first and most common method outlined in the report is the standard penetration test (SPT), which is preferred by many engineers because it is relatively quick, inexpensive, and the equipment is readily available. As a result, there is a large repository of SPT-collected data to reference. SPTs are good because not only are they indicative of strength of the soil through a blow count, but they also allow disturbed soil samples to be taken from depth for further analyses. Among the limitations of the test are: (1) the inability to test large grained materials such as gravels, (2) very localized large-strain deformations with loading conditions dissimilar to earthquake conditions, (3) the lack of pore water pressure measurements, and (4) lack of consistency with the hammer energy. Figure 2 shows SPT Sand Base Curves with supporting data for magnitude 7.5 earthquakes. The

fines content in the sands for the SPT Sand Based Curves range from 0 % to 35 %. The corrected blow count, $(N_1)_{60}$, is normalized to a 1 ton/ft^2 (100 kPa) overburden pressure and a 60 % hammer energy efficiency.

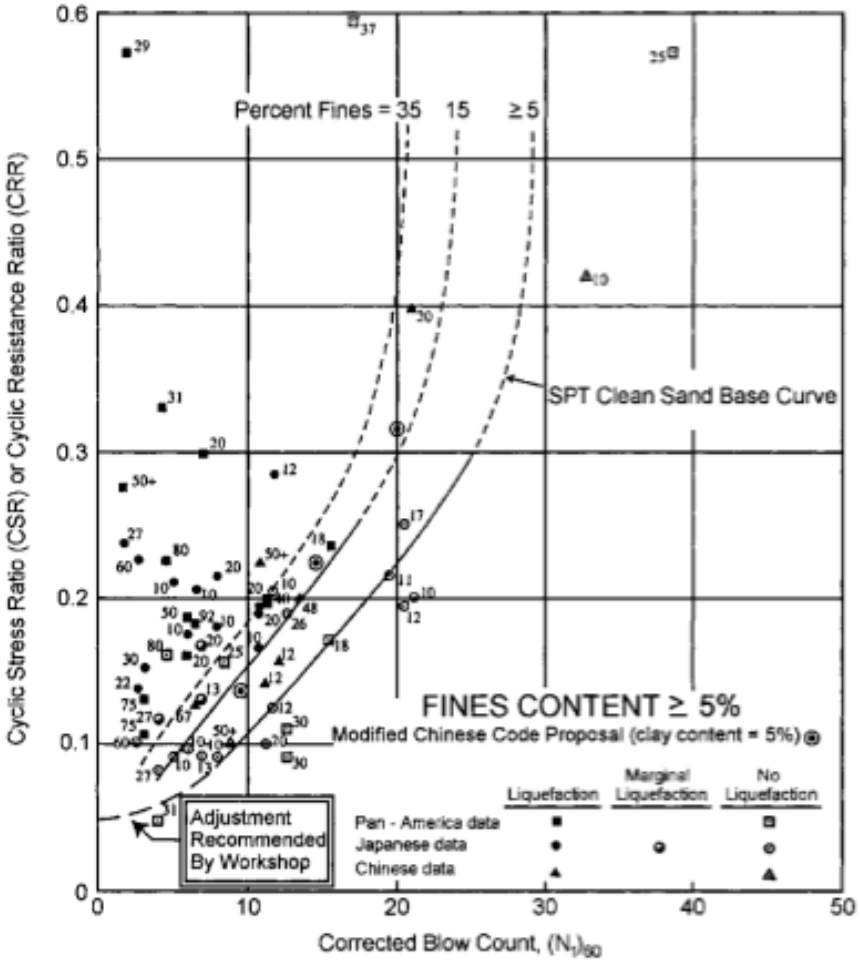

Figure 2: SPT Sand Base Curves for sands with fines contents ranging from 0% to 35%. These curves are applicable for 7.5 Magnitude earthquakes (from Seed et al, 1985).

The CPT is a more intricate testing technique than the SPT and can offer higher quality data. Unlike the SPT, the CPT is not operator dependent, meaning the results of the test should be the same regardless of the equipment and personnel used to obtain them as

long as the sensors are correctly calibrated and proper procedure are followed. Additional advantages the CPT has over the SPT are: (1) the measurement of pore water pressure, (2) nearly-continuous measurements over the entire test depth range, and (3) an estimation of the soil behavior type. Unlike the SPT, however, it cannot retrieve a soil sample from depth without special tooling. As with the limitations of the SPT, the CPT typically is not reliable in gravels and its testing procedure relies on very localized large strain deformation with loading conditions dissimilar to earthquake conditions. Figure 3 presents the CPT Clean Sand Based Curve with supporting data for magnitude 7.5 earthquakes. The fines content for the sands in this model is less than 5 %.

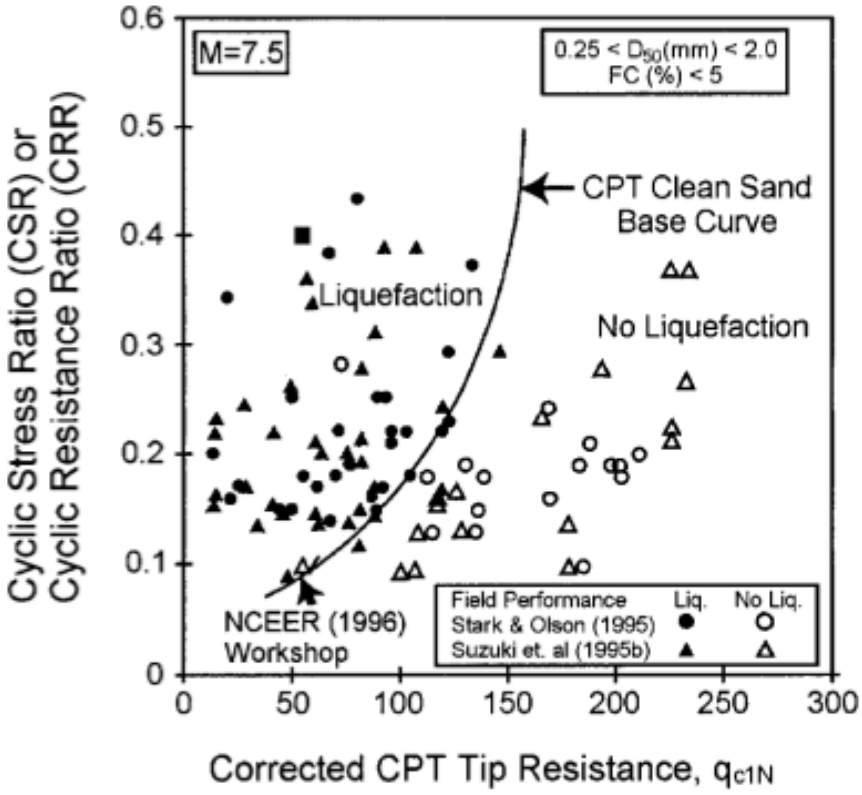

Figure 3: CPT Clean Sand Base Curve applicable for 7.5 magnitude earthquakes (from Robertson and Wride, 1998).

For gravel and cobbles that are not testable by the SPT and CPT, the BPT has been developed specifically for these hard-to-test soils. The application of the BPT for soil liquefaction susceptibility studies has been much more limited than that of SPT or CPT and as a result there is not much available data. At the time of the report's publication in 2001, results from BPTs were evaluated by converting the blow counts into equivalent SPT values and then commencing the evaluation of liquefaction susceptibility, which is not an ideal procedure because of the uncertainty inherent in adding a calculation based on equivalency. Other than its ability to test soils with gravels and cobbles, this testing technique has not been able to contribute significantly to soil liquefaction research in general because it has not been utilized extensively and it also produces very localized large-strain deformations with loading conditions dissimilar to earthquake conditions.

The fourth testing method discussed in the report is the use of shear wave velocities. Shear wave velocities are a direct measure of the small-strain shear stiffness of soil and can be correlated to soil liquefaction susceptibility in the same way as the STP and CPT methods. In general, the database of measured in-situ soil shear wave velocities is not nearly as extensive as those of SPTs and CPTs, so the verification of liquefaction susceptibility models is less robust. The advantages of using shear wave velocity testing techniques is that it can be employed in any soil type and that its measurement represents a soil property over a less localized region than SPTs and CPTs. Figure 4 presents the Vs Sand Based Curves with supporting data from assembled case histories. These curves are applicable for 7.5 magnitude earthquakes, but the note in the top left corner indicates scaling factors for other magnitudes. The fines contents in the sands for this model range from 0 % to greater than 35 %.

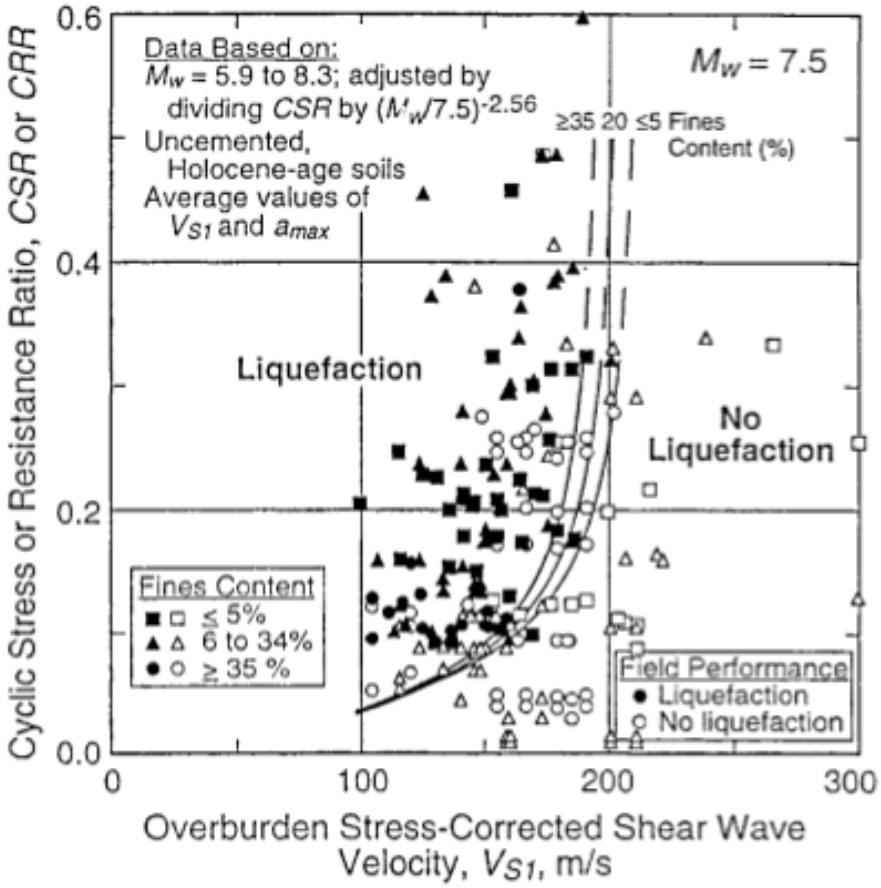

Figure 4: V_S Sand Based Curves for magnitude 7.5 earthquakes and fines contents ranging from 0% to greater than 35% (from Andrus and Stokoe, 2000).

At the time of the publication by Youd et al, 2001, these four testing methods represented the best techniques available to researchers to develop soil liquefaction susceptibility models based on data derived from in-situ field tests.

2.3 EFFECTS OF PARTIAL SATURATION ON THE CYCLIC RESISTANCE OF SOILS AND USING THE COMPRESSION WAVE VELOCITY TO ESTIMATE IN-SITU DEGREE OF SATURATION

The effect of partial saturation on the cyclic resistance of soils is fairly well documented in laboratory tests but not well understood for similar conditions in the field. Traditional crosshole, downhole, and p-s suspension logging tests in the field have consistently shown that regions of partial saturation are common to depths several meters below the water table (Kokusho 2000, Ishihara et al. 2001, Fourie et al. 2001, Tsukamoto et al. 2002, Ishihara & Tsukamoto 2004). Based on laboratory testing, it is believed that the cyclic resistance of these partially-saturated zones is significantly higher than that of fully-saturated soils; current liquefaction susceptibility evaluation methods, however, have difficulty effectively transferring this knowledge from the laboratory to field conditions where it is difficult to estimate the in situ degree of saturation. The compression wave velocity has emerged as the most reliable link for estimating the degree of saturation in both the laboratory and the field. The relationship between the compression wave velocity and degree of saturation, however, is not unique and must be defined for specific soil types and conditions.

The effect of partial saturation on the cyclic resistance of sands has been documented as early as the 1970s by Sherif et al. 1977 and Martin et al. 1978. Since then, results from cyclic triaxial tests have consistently shown that relatively small decreases in the degree of saturation result in large increases in the cyclic resistance. From the work presented in Yoshimi et al. 1989, the data in Figure 5 show the cyclic resistance versus the number of cycles to achieve a double amplitude shear strain of 5 % (defined as the onset of liquefaction for these cyclic triaxial tests) for soils with degrees of saturation ranging from 70 to 100 %; the sand used for these tests was Toyoura sand, pluviated dry to a relative

density of 60 %. These results show a doubling and tripling of the cyclic resistance at 90 % and 70 % degrees of saturation, respectively, in comparison to fully-saturated specimens (Yoshimi et al. 1989).

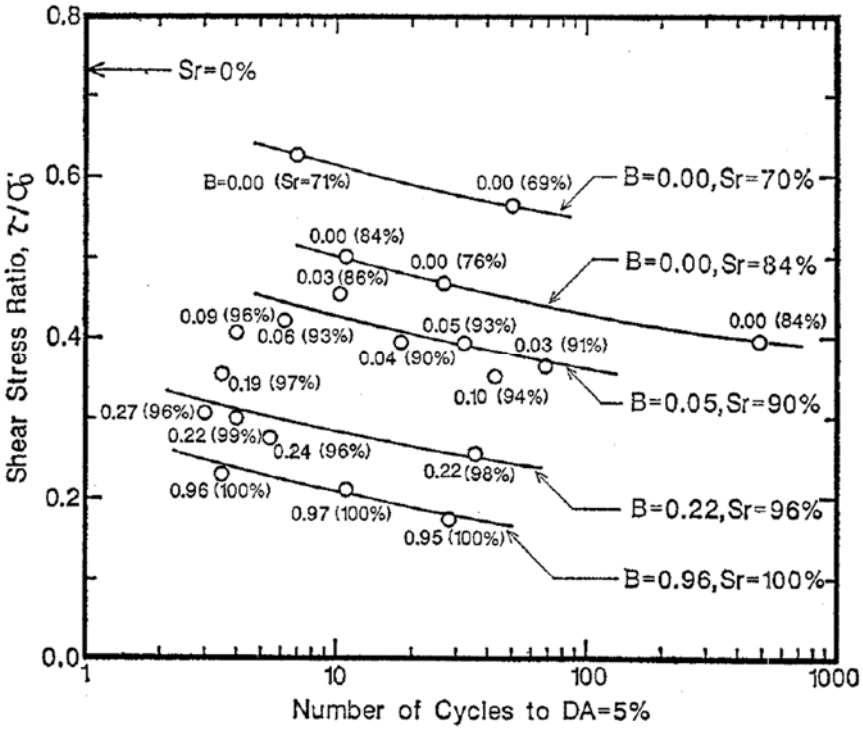

Figure 5: Effects of degree of saturation on liquefaction characteristics of sand (from Yoshimi et al. 1989).

In the past two decades, it has become more common for laboratory tests such as cyclic triaxial or resonant column tests to incorporate bender elements in the test apparatus to measure compression and shear wave velocities of the specimens as a way of estimating the degree of saturation. Test results presented in Ishihara et al. 2001 come from a cyclic triaxial setup with bender elements to measure the compression wave velocity and use it as a measure of the soil's saturation along with the B-value. The soils used in these experiments are clean sands from a soil deposit near Niigata, Japan, compacted to a relative density of 62 %. The relationship of the compression and shear wave velocities measured

using bender elements versus the B-value in Figure 6 shows the sensitivity of the compression wave to variations in saturation when the B-value is greater than 0 (S_r ~ 85-90 %). The shear wave velocity is unaffected by the variation in the degree of saturation (Ishihara et al. 2001).

In a separate set of experiments by Valle-Molina 2006, bender elements in a resonant column test setup are used to focus more closely on the sensitivity of the compression wave velocity and the B-value to the degree of saturation at high levels of saturated (S_r > 97 %). The results in Figure 7 show the compression wave velocity versus the degree of saturation and in Figure 8 show the B-value versus the degree of saturation for samples of Ottawa Sand and washed mortar sand. These relationships show that both the compression wave velocity and B-value can be used to estimate the degree of saturation in soils that are nearly to fully saturated with a level of high precision (Valle-Molina 2006).

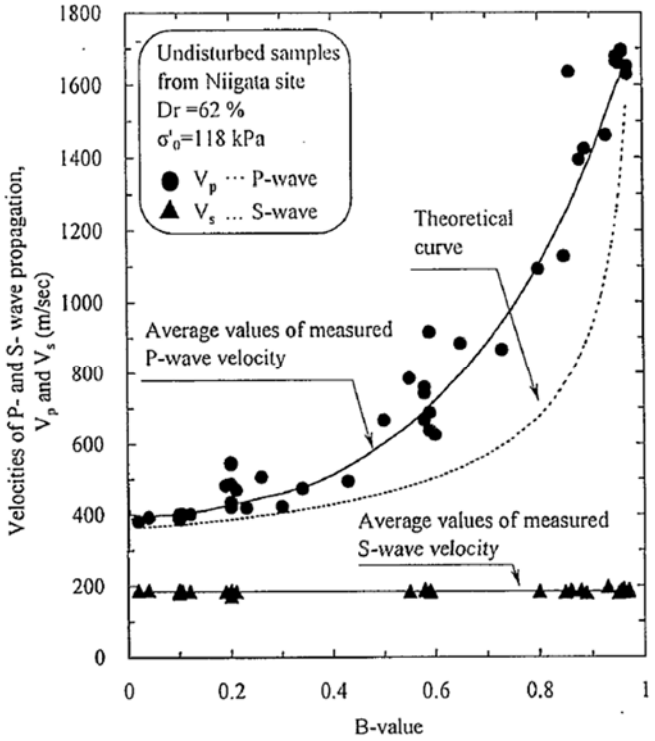

Figure 6: Velocities of P-wave and S-wave propagation versus the B-value (from Ishihara et al. 2001).

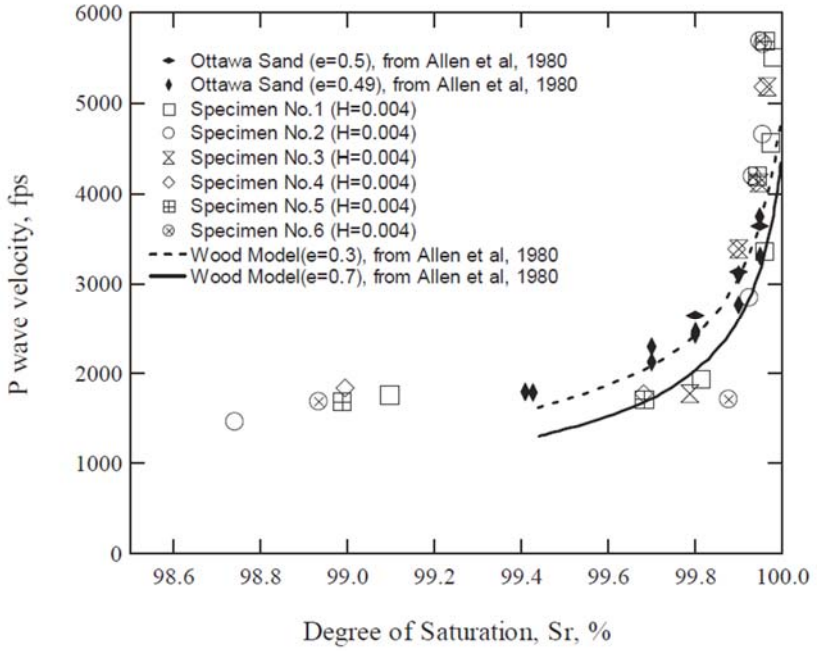

Figure 7: Comparison of the Relationship between Degree of Saturation (S_r) and Compression Wave Velocity (from Valle-Molina 2006).

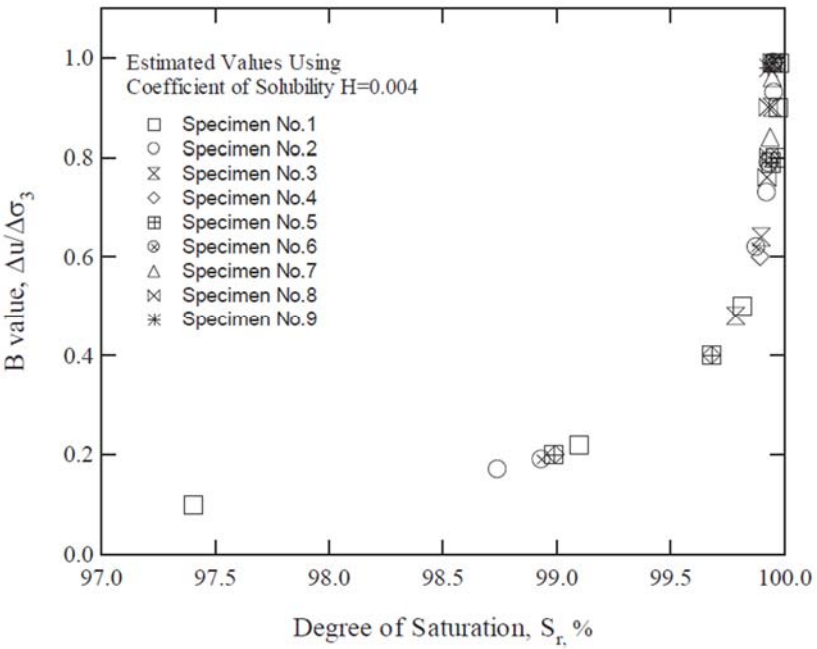

Figure 8: Comparison of the Estimated Degree of Saturation (S_r) and the B Values (from Valle-Molina 2006).

Ishihara et al. 2001 uses the data from cyclic triaxial testing to present the cyclic resistance versus compression wave velocity in Figure 9, versus the degree of saturation in Figure 10, and versus the B-value in Figure 11. Both the compression wave velocity and the B-value are similarly sensitive to changes in saturation at values greater than 99 %, providing a high amount of precision for the behavior of the soil in that range of nearly saturation. The ratio between the cyclic resistance of a partially saturated soil and that of a fully saturated soil is plotted against the compression wave velocity in Figure 12, showing a clear and strong relationship between the two parameters for a variety of sand types and relative densities. Collectively, this work provides the basis for using compression wave velocities to connect research on the cyclic resistance of partially saturated sands in the laboratory to evaluations in the field.

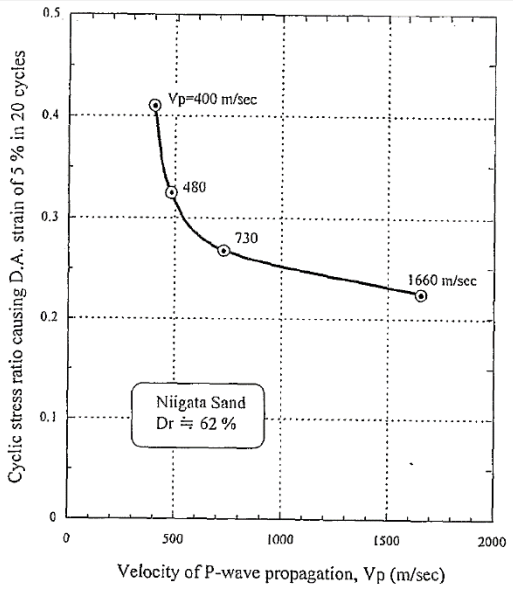

Figure 9: Cyclic strength of sand versus the velocity of P-wave propagation (from Ishihara et al. 2001).

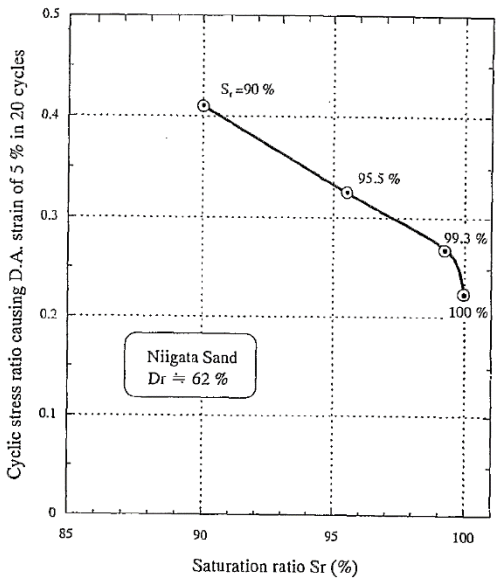

Figure 10: Cyclic strength versus the saturation ratio (from Ishihara et al. 2001).

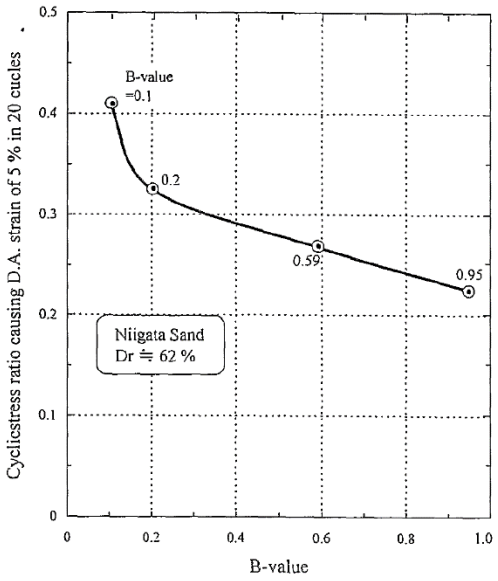

Figure 11: Cyclic strength versus B-value (from Ishihara et al. 2001).

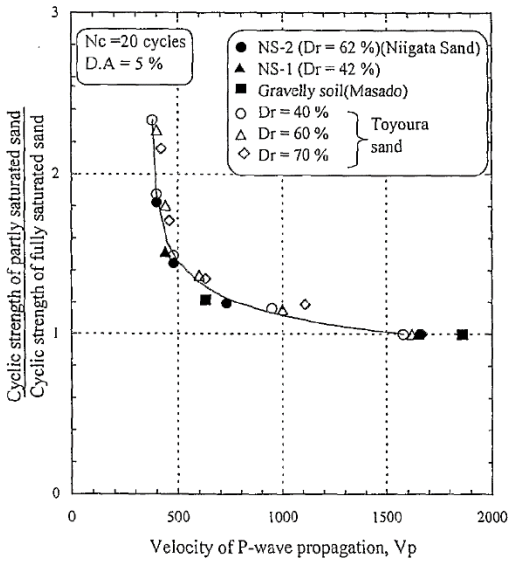

Figure 12: Ratio of cyclic strength between partially fully saturated sand (from Ishihara et al. 2001).

Partial saturation is a key area of research within the topic of soil liquefaction because it results in an increase in cyclic resistance when compared to fully saturated conditions. Cyclic triaxial tests consistently show that the cyclic resistance of clean sands roughly doubles when the degree of saturation decreases from 100 to 90 % and triples when the degree of saturation decreases from 100 to 70 % (Yoshimi et al. 1989, Tsukamoto et al. 2002, Ishihara & Tsukamoto 2004). Further, relationships between the B-value and the compression wave velocity developed from laboratory testing make it possible to estimate the degree of saturation in situ because of high confidence in the accuracy of compression waves measured both in the laboratory and the field (Kokusho 2000, Fourie et al. 2001, Ishihara et al. 2001). Recent attempts to incorporate this knowledge into liquefaction evaluation methods for the field include a suction-based method by Unno et al. (2008) and an update to the K_S correction factor for unsaturated conditions in calculating the cyclic resistance ratio, CRR, by Hossain et al. (2013). Without large-scale testing in the field, however, it remains to be seen whether the increases in cyclic resistance seen in the laboratory for unsaturated specimens will apply to unsaturated soils seen in the field.

2.4 EFFECT OF NONPLASTIC FINES ON THE CYCLIC RESISTANCE OF SOILS

Case studies from recent earthquake events show that soils with very high fines contents (and some plasticity) are able to liquefy under dynamic loading. Examples of silty soil sites with evidence of soil liquefaction include Moss Landing during the 1989 Loma Prieta earthquake (Boulanger et al. 1997 and Boulanger et al. 1998), the city of Adapazari during the 1999 Kocaeli earthquake (Bray et al. 2004 and Sancio et al. 2002), and the cities of Nantou, Wufeng, and Yuanlin in Taiwan during the 1999 Chi-Chi earthquake (Chu et al. 2004). These case studies have helped inform researchers reassess the criteria with which soils are classified as liquefiable or non-liquefiable (Bray & Sancio 2006 and Boulanger & Idriss 2006).

The work by Bray & Sancio (2006) focused on results from cyclic triaxial testing as well as field data to update the Chinese criteria (Wang 1979). They suggest that a soil should be considered liquefiable if it has a water content to liquid limit ratio greater than 0.85 ($w_c/LL > 0.85$) and a plasticity index less than 12 ($PI < 12$). A soil should be considered moderately liquefiable if has a water content to liquid limit ratio greater than 0.80 ($w_c/LL > 0.80$) and a plasticity index between 12 and 18 ($12 < PI < 18$). The results in Figure 13 from Bray & Sancio 2006 show how well five sets of data match the predictions from the new liquefaction criteria for (a) results from cyclic triaxial testing, (b) field testing in Adapazari, Turkey following the 1999 Koeceli earthquake, (c) field testing in Potrero Canyon, (d) field testing from China following the 1975 Haicheng and 1976 Tangshan earthquakes, and (e) field testing from Tawain following the 1999 Chi-Chi earthquake.

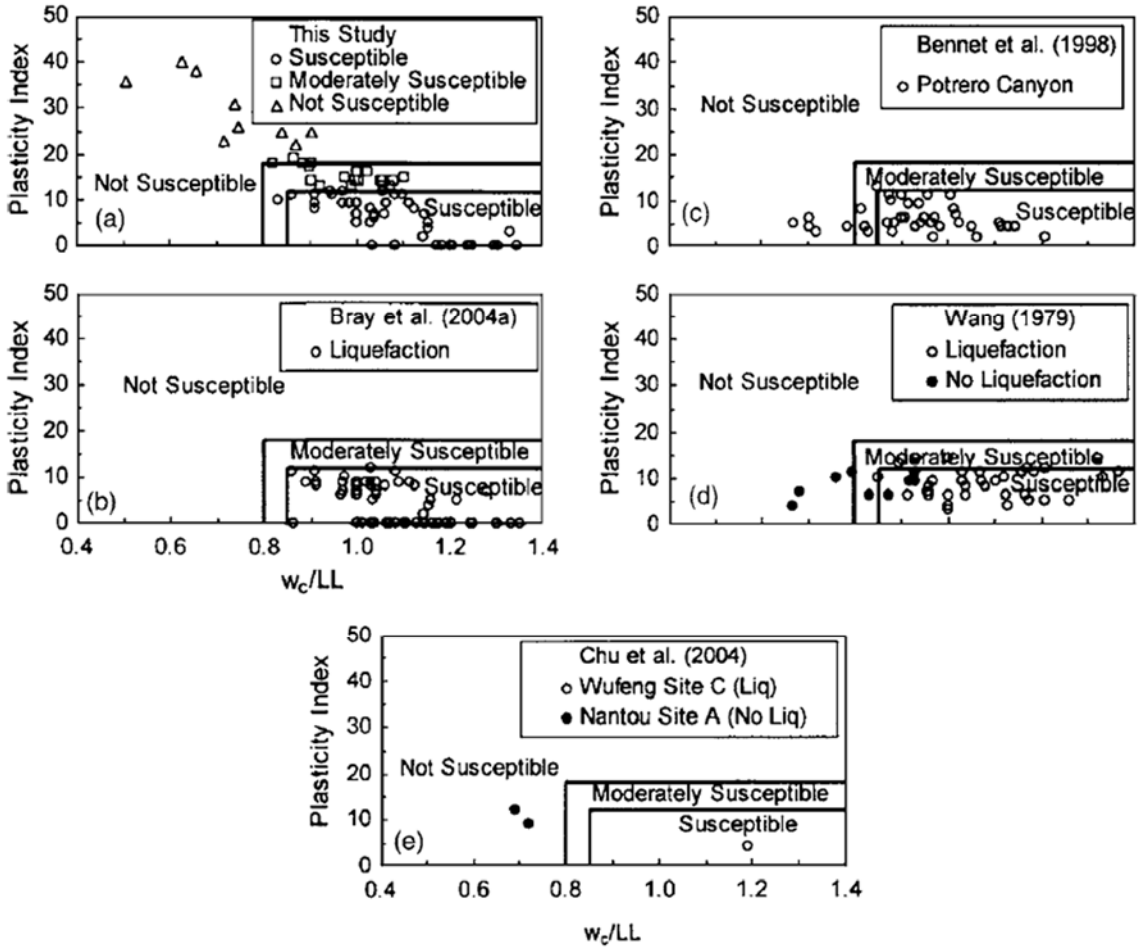

Figure 13: Graphical representation of the proposed liquefaction susceptibility criteria: (a) isotropically consolidated CTX testing data from this study; (b) field data from Bray et al. (2004); (c) Potrero Canyon field data from Bennett et al. (1998); (d) field data from Wang (1979); and (e) field data from Chu et al. (2004). (from Bray & Sancio 2006)

Boulanger & Idriss 2006 tackle the question of liquefaction susceptibility by dividing soils into those than have sand-like or clay-like behavior during monotonic and cyclic undrained loading tests and suggest improvements to processes for estimating strains and strength loss that results from seismic loading. Importantly, their test results identify a transition zone between the sand-like and clay-like behavior that is dependent on the plasticity index of the material. The graph in Figure 14 shows that in the absence of

laboratory testing, soils with a plasticity index less than 7 should be considered to have sand-like behavior while soils with a plasticity index greater than 7 should be considered to have clay-like behavior. If results from laboratory testing are available, the boundary between sand-like and clay-like behavior can be ascertain with greater accuracy, allowing for less conservative definitions of sand-like or clay-like behavior if appropriate.

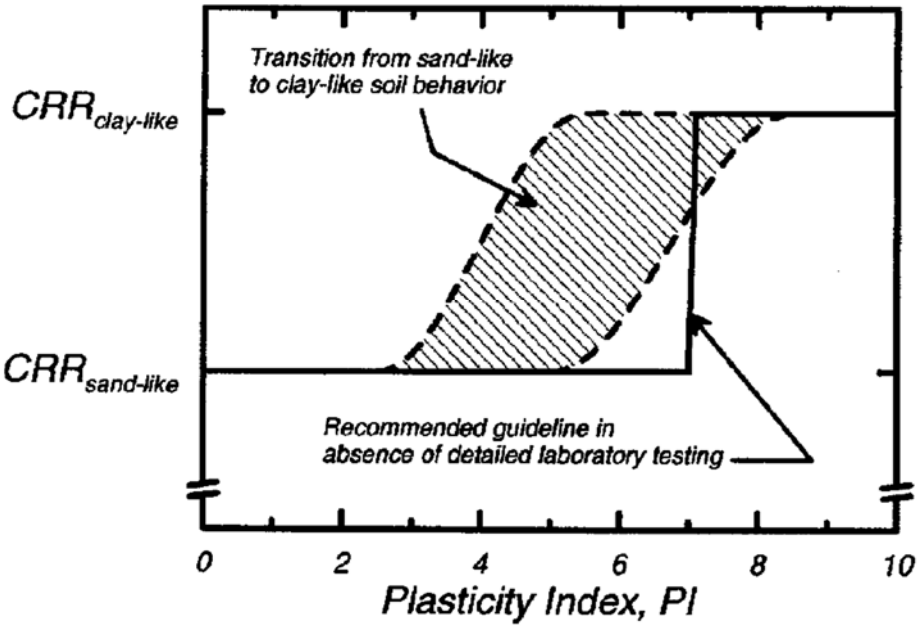

Figure 14: Schematic illustration of the transition from sand-like to clay-like behavior for fine-grained soils with increasing PI, and the recommended guideline for practice. (from Boulanger & Idriss 2006)

Knowing that soils with high fines contents are liquefiable, the effect of varying levels of nonplastic fines on the cyclic resistance of soils has also been studied extensively in the laboratory since the 1970s, unfortunately without achieving clear guidelines regarding this effect. Different researchers have shown relationships from laboratory testing that support these four different conclusions: 1) the cyclic resistance increases with increasing fines content (Seed et al 1983, Tokimatsu & Yoshimi 1983, Robertson & Campanella 1985, Pitman et al. 1994, Amini & Qi 2000), 2) the cyclic resistance decreases

with increasing fines content (Sladen et al. 1985, Lade & Yamamuro 1997, Yamamuro & Lade 1997, Zlatovic & Ishihara 1997, Huang et al. 2004, Liu & Mitchell 2006), 3) the cyclic resistance first increases then decreases with increasing fines content (Singh 1996, Askari et al 2010), 4) the cyclic resistance first decreases then increases with increasing fines content (Xenaki & Athanasopoulos 2003, Polito & Martin 2001).

In many cases, however, the contraction in these four conclusions may be due to different specimen preparation methods, varying silt contents and densities, different confining stresses and loading conditions, and different criteria for defining liquefaction and/or the CSR (Liu & Mitchell 2006). Analyses performed using the indices relative density or the global void ratio of the soil seem to provide a more consistent approach to comparing soils with varying fines contents than any other method reviewed (Amini & Qi 2000, Xenaki & Athanasopoulos 2003, Huang et al. 2004, Liu & Mitchell 2006, Polito & Martin 2001).

In terms of classifying the behavior of the soil as either dominated by granular or fine-grained characteristics, several researchers have proposed that until the volume of fines content exceeds the void spaces between sand grains, the sand skeleton will remain intact and control the overall behavior while the silt has a secondary influence. At fines contents greater than this threshold fines content, the sand grains will float within the silt matrix and the silt will control the overall behavior (Polito & Martin 2001, Thevanayagam et al. 2002). Polito & Martin 2001 found that in a review of various sands and silts, the threshold silt content primarily ranges from 25 to 45 %, which helps explain why a number of studies found that the cyclic resistance of soils decreased or stayed constant as the fines content was increased until about 30 to 40 % before causing an increase in the cyclic resistance for increasing fines contents above that threshold (Polito & Martin 2001, Liu & Mitchell 2006). The results from Polito & Martin 2001 in Figure 15 show the effect of silt

content on Monterey sand at a constant void ratio and Figure 16 show the effect of silt content on Yatesville sand at a constant 30 % relative density, illustrating the complexity of finding a fair metric with which to compare specimens of varying silt contents, void ratios, relative densities, etc.

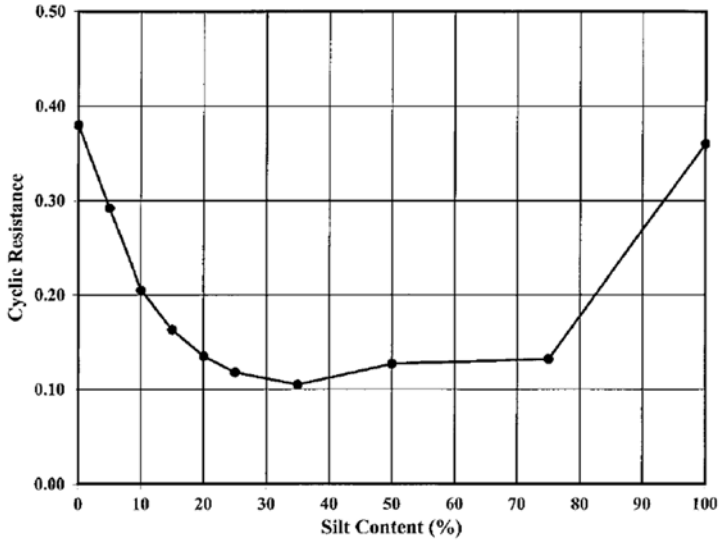

Figure 15: Cyclic resistance of Monterey Sand at constant void ratio with variation in silt content (from Polito & Martin 2001)

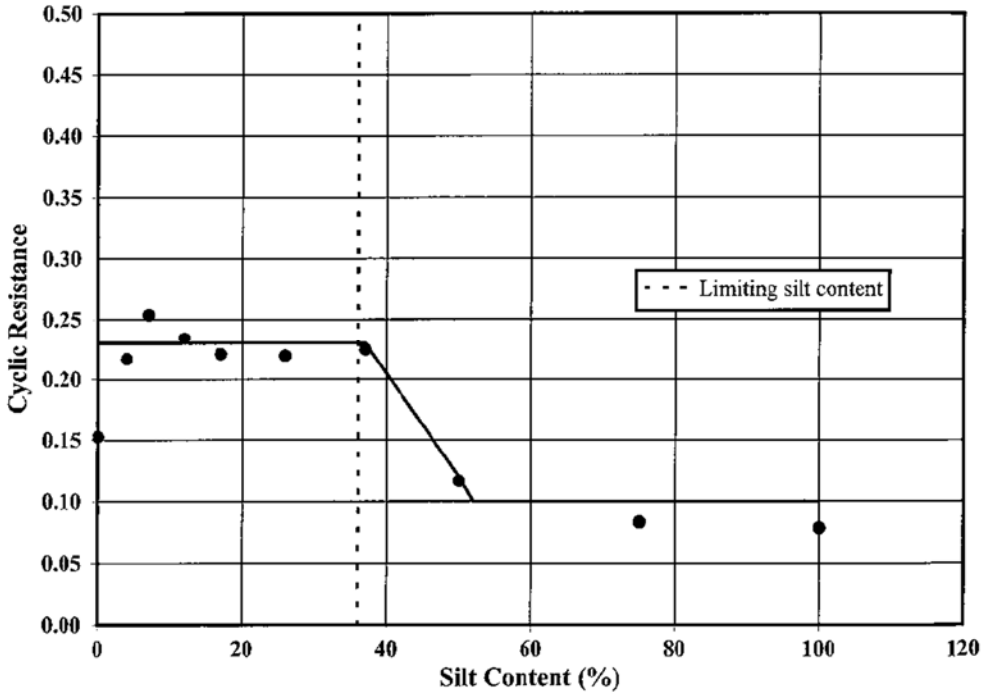

Figure 16: Variation in cyclic resistance with silt content for Yatesville sand specimens prepared by moist tamping adjusted to 30 % relative density (from Polito & Martin 2001)

These laboratory studies provide important insight into the cyclic behavior of soils with non-plastic fines contents ranging from 0 to 100 %, but the conditions in the laboratory frequently are not representative of conditions found in the field. They are not able to account for the influence of adjacent layers may have in terms of the dynamic response and redistribution of excess pore pressures across layers with varying cyclic resistances that lead up to liquefaction (Cubrinovski et al. 2017). It is important to also note that in the field, it is difficult to isolate the effect of fines content when many other properties and parameters such as degree of saturation, aging, confining pressure, and density simultaneously vary and also influence the cyclic resistance of the soil within a single soil deposit.

2.5 SUMMARY

The previous sections provide an overview of the state of knowledge regarding the triggering of soil liquefaction and the factors that affect the cyclic resistance of soils. The summary in Section 2.2 provides an overview of the SPT, CPT, BPT, and Vs-based methods for estimating the in situ cyclic resistance ratio (CRR) and describes the advantages and disadvantages of each of the methods. These four methods are the most effective tools existing today for predicting whether or not a soil deposit will experience soil liquefaction during an earthquake and they continue to be refined as more field tests and case studies become available.

The overview of literature in Section 2.3 shows there is a strong general consensus regarding the influence that the degree of saturation has on the cyclic resistance of soils. Many researchers have found in the laboratory that a reduction in the degree of saturation from 100 % to 90 % results in a doubling of the cyclic resistance ratio in a sand. There is great difficulty, however, in directly estimating the degree of saturation for soils in situ, and as a result, researchers have turned to using the compression wave velocity as a reliable, indirect measure of the degree of saturation.

The overall effect of fines content and soil type is explored in Section 2.3. Case studies from recent earthquakes and accompanying laboratory experiments have focused on redefining what it means to be classified as liquefiable or non-liquefiable based on soil type. Other studies in the laboratory have focused on understanding how the cyclic resistance of a soil varies as a function of fines content, though there is little consensus on the best way to control for the variation of other parameters such as the void ratio and density while varying the fines content.

Chapter 3: Test Sites and Ground Improvement Methods

3.1 THE TEST SITES: SITE 3, SITE 4, AND SITE 6

The three sites used for evaluating the ground improvement methods are referred to as Site 3, Site 4, and Site 6. These sites were selected after preliminary site investigations at nine locations in the Christchurch area using CPT and/or direct-push seismic crosshole testing to find optimal testing conditions. The map of liquefaction damage in Christchurch in Figure 17 shows the location of these three sites along the Avon River and in neighborhoods that experienced moderate-to-severe land damage during the 2010-2011 Canterbury Earthquake Sequence (CES). Site 3 is located at 1046 Avonside Drive in the Wainoni neighborhood. Site 4 is located approximately one kilometer north of Site 3 at 1134 Avonside Drive in the Avondale neighborhood. Site 6 is approximately three kilometers east of Sites 3 and 4 at 18 Wairoa Street in the Bexley neighborhood. The edge of each site is no further than 45 meters from the bank of the Avon River, separated only by a residential road.

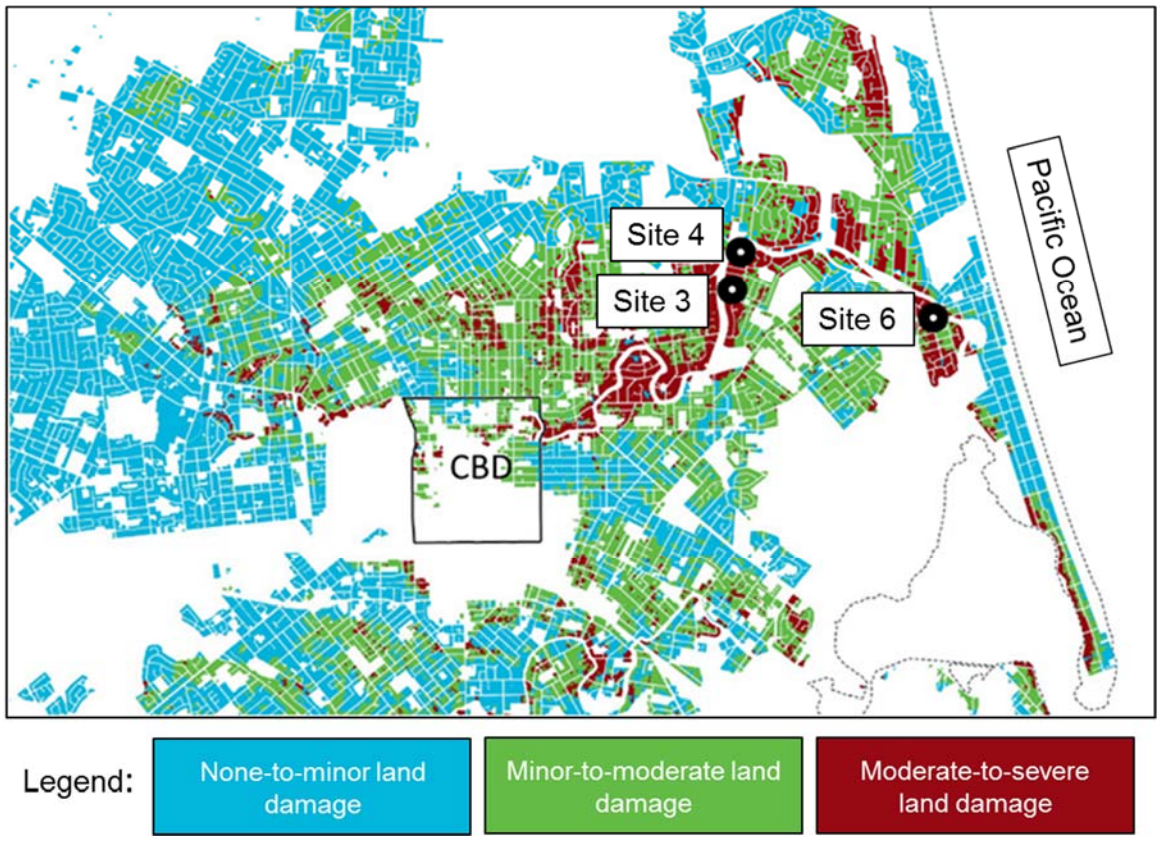

Figure 17: Map of Christchurch overlain with regions of liquefaction-damage highlighted. The location of the Central Business District (CBD) is outlined in black and the locations of the three test sites are identified (modified from van Ballegooy et al. 2017). Damage levels are (1) none-to-minor shown in blue, (2) minor-to-moderate shown in green, and (3) moderate-to-severe shown in red.

The Wainoni, Avondale, and Bexley neighborhoods are three of the neighborhoods in the Christchurch area in which the government decided not to rebuild after the CES because the cost of improving the soil conditions would be too high. The ground improvement trials were held in these areas where the soils are most susceptible to soil liquefaction under the theory that if the ground improvement methods have a remediating effect on these difficult soils, they will also work well in areas that experienced less devastating consequences from soil liquefaction.

Prior to commencement of the trials, the damaged homes at each site were razed and the land cleared to provide an open area for testing. A total of nine ground improvement methods were included in the trials, but only the three of these methods are evaluated in this dissertation. The three methods studied herein are the Rapid Impact Compaction (RIC), the Rammed Aggregate Piers™ (RAP), and the Low-Mobility Grout (LMG). While some ground improvement methods were tested only at one site (Site 4), test panels using the RIC, RAP, and LMG methods were built and tested at all three sites, providing an opportunity to assess the ground improvement methods over a range in ground conditions as well as to judge consistency in construction quality.

In addition to RIC, RAP, and LMG test panels, each site had at least two control test panels of natural soil that represent the starting, in-situ conditions to be used as a baseline for comparing the performance of the ground improvement methods. The naming convention for labeling each of these test panels has three identifying parts: (1) the site number, (2) the test panel type, and (3) sequential numbering for test panels of the same type at the same site. Table 1 provides a summary of each test panel with its test site location, ground improvement method, and sequential numbering.

Table 1: List of test panels labelled according to their site location, ground improvement method, and sequential numbering.

Test Panel	Test Site	Ground Improvement Method	Sequential Numbering
3-NS-1	3	None - Natural Soil (NS)	1
3-NS-2	3	None - Natural Soil (NS)	2
3-RIC-1	3	Rapid Impact Compaction (RIC)	1
3-RAP-1	3	Rammed Aggregate Piers^{TM} (RAP)	1
3-LMG-1	3	Low-Mobility Grout (LMG)	1
4-NS-1	4	None - Natural Soil (NS)	1
4-NS-2	4	None - Natural Soil (NS)	2
4-RIC-1	4	Rapid Impact Compaction (RIC)	1
4-RAP-1	4	Rammed Aggregate Piers^{TM} (RAP)	1
4-LMG-1	4	Low-Mobility Grout (LMG)	1
6-NS-1	6	None - Natural Soil (NS)	1
6-NS-2	6	None - Natural Soil (NS)	2
6-RIC-1	6	Rapid Impact Compaction (RIC)	1
6-RAP-1	6	Rammed Aggregate Piers^{TM} (RAP)	1
6-LMG-1	6	Low-Mobility Grout (LMG)	1

Each test panel covers a rectangular area with dimensions of approximately 7.5 m by 7.5 m; for test panels that have been subjected to ground improvement, the zone of the primary ground improvement is fully contained within this area. At Site 3, test panels 3-NS-1, 3-RIC-1, 3-RAP-1, and 3-LMG-1 were located within a 22 by 22 m^2 region as shown in Figure 18. Test panel 3-NS-2 was not included in the original test setup and had to be located approximately 50 m from the other test panels due to space constraints. At Site 4, test panels 4-NS-1, 4-RIC-1, 4-RAP-1, and 4-LMG-1 were located within a 33 by 20 m^2 region as shown in Figure 19. Test panel 4-NS-2 was positioned near the test panels of other ground improvement methods that are not included in this analysis. As a result, it is located approximately 50 m from test panel 4-NS-1. At Site 6, test panels 6-NS-1, 6-NS-2, 6-RIC-1, 6-RAP-1, and 6-LMG-1 are located within a 30 by 30 m^2 region as shown in Figure 20.

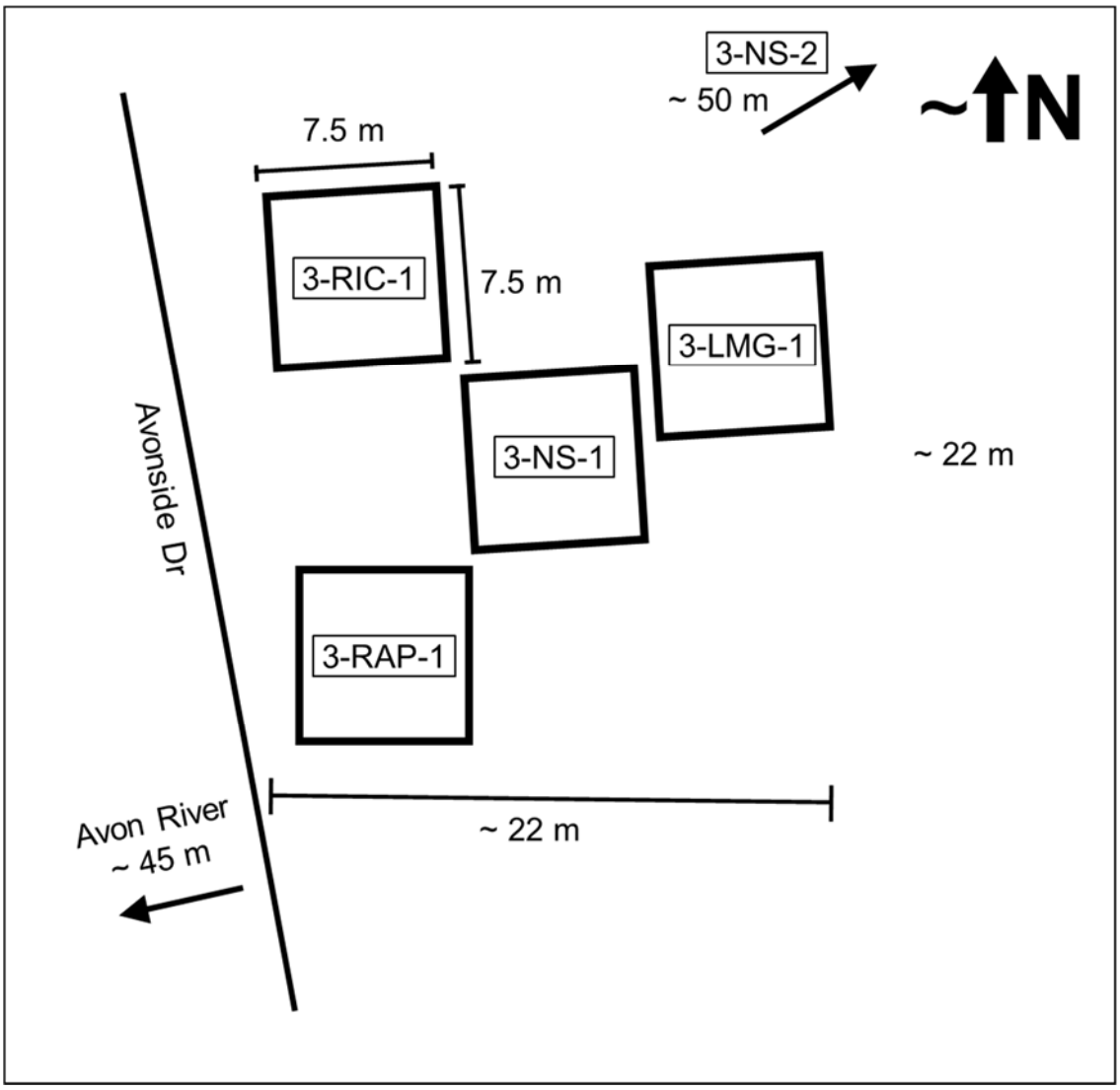

Figure 18: Map showing the relative locations of the five test panels analyzed at Site 3.

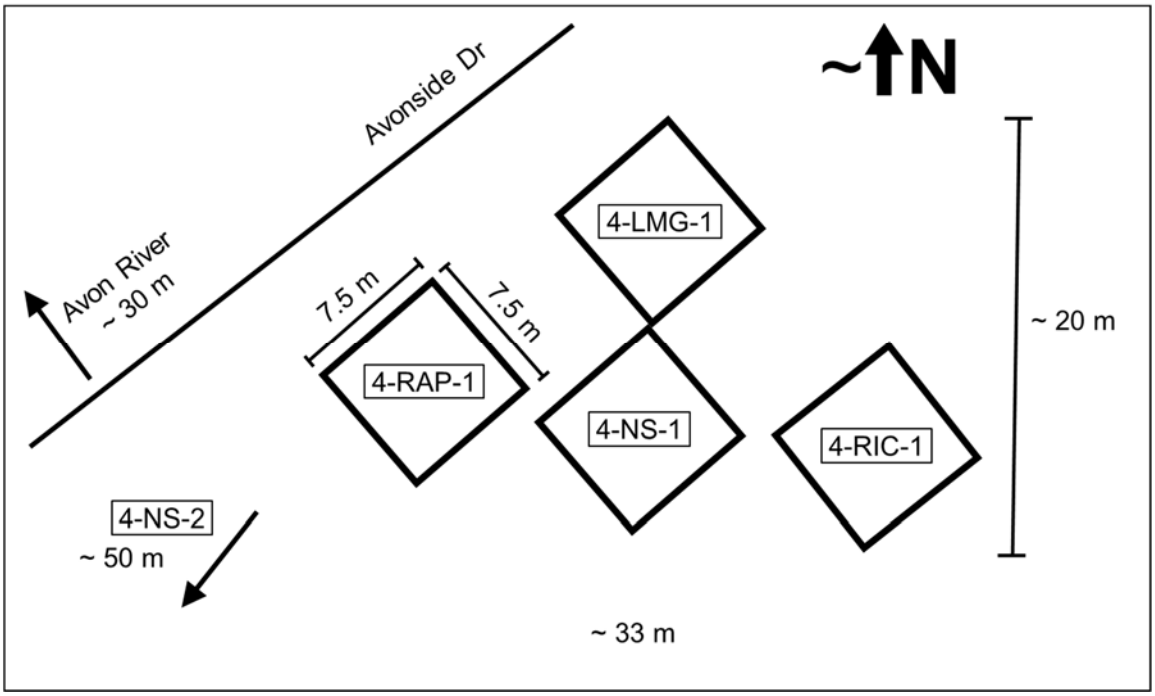

Figure 19: Map showing the relative locations of the five test panels analyzed at Site 4.

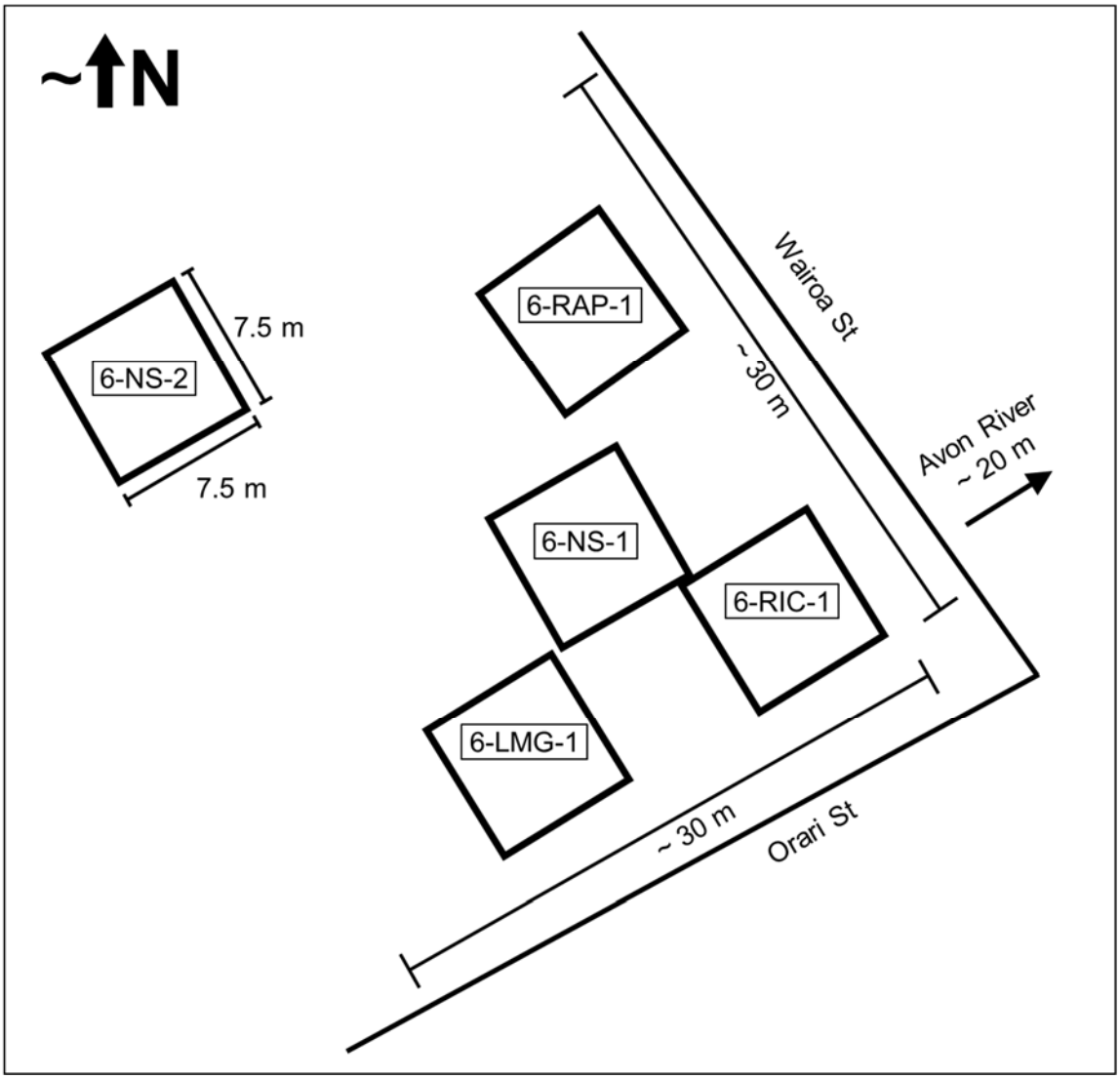

Figure 20: Map showing the relative locations of the five test panels analyzed at Site 6.

3.2 GROUND IMPROVEMENT METHODS

The ground improvement methods selected for this study are intended to increase the resistance to soil liquefaction in the top 4.0 m of the ground surface, above which light-weight structures such as a single family home could be built and survive future earthquakes without sustaining critical damage. The idea for a shallow ground improvement method is based on Dr. Kenji Ishihara's 1985 paper, "Stability of natural deposits during earthquakes" (Ishihara 1985). In the paper, Ishihara proposes the concept that if a liquefiable layer is overlain by a non-liquefiable layer, or crust, of sufficient thickness, the soil in the lower layer can liquefy with minimal impact on structures at the ground surface. The criteria for ground improvement down to a depth of 4.0 m comes from an extensive study in the Christchurch area following the CES found that single-family houses founded on an intact, relatively stiff non-liquefying crust of at least 3.0 m survived the earthquakes with less structural damage than houses in areas without the thick crust (van Ballegooy et al. 2017). It should be noted that this approach is only applicable for level-ground sites that are at least 300 m from a free face (Ishihara 1985).

In the following sections, the construction methods for the RIC, RAP, and LMG test panels are described. These descriptions have been taken directly from an unpublished draft report from Tonkin & Taylor Ltd titled "Christchurch Ground Improvement Trials Report" that is being prepared for the New Zealand Earthquake Commission (EQC). The final report is expected to be published in 2018 and will likely contain minor variations in formatting and wording from the text presented herein, but the material substance and accuracy of the descriptions should remain the same. The figures in this section include figures taken directly from the report where noted as well as original content. Object references have been updated to reflect the placement of text, figures, and tables in relation to their position within this dissertation rather than their original position in the draft report.

3.2.1 Rapid Impact Compaction (RIC) Construction Method

"RIC is a type of dynamic compaction, downscaled from the traditional methodology where a large weight is repeatedly raised and dropped onto the ground from a great height utilizing a crane. The smaller scale plant is typically more cost effective on sites where shallow improvement (i.e. depths less than about 3 to 5m) is all that is required, and can be used on sites with access constraints that would prevent the use of large cranes. Like dynamic compaction, RIC increases the density and stiffness of relatively clean sands through controlled and repeated impact loading.

RIC consists of hydraulically raising and dropping a heavy weight (i.e. 5 to 7 tonnes) with a piling hammer from a height of about 1.2 to 1.5m using a conventional tracked excavator. The weight is dropped onto a 1 to 1.5m diameter circular anvil or "foot" at a typical rate of between 40 and 60 blows per minute.

An electronic control and data acquisition system installed in the excavator's operator cab allows the drop height and rate to be controlled, and records parameters such as the number of hammer blows and ground penetration of the anvil plate per blow.

Golder Construction Limited undertook the construction of the RIC ground improvement work for the ground improvement trials.

One RIC test panel was constructed at each of Sites 3, 4 and 6 using a 35 tonne tracked excavator. Prior to constructing the test panels, a spacing trial was conducted at Sites 3, 4 and 6 to optimize the impact pattern (refer to Section 6 for a detailed discussion of the analyses and results from the spacing trials). The center-to-center spacing of RIC impact points was 1.5, 3 and 6m for the spacing trials. Based on the results of spacing trials, a RIC spacing of 1.5m in a square pattern was selected for construction of all of the test panels constructed at Sites 3, 4 and 6. The layouts of RIC impact points within the test panels at Sites 3, 4 and 6 are shown in Figure 21.

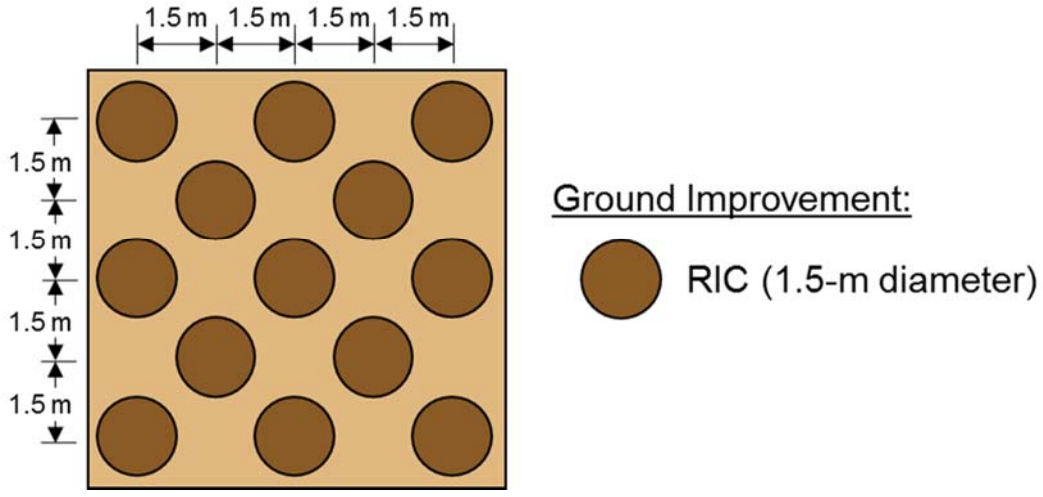

Figure 21: Plan view of the RIC impact points layout used at Sites 3, 4, and 6.

RIC was undertaken at Sites 3, 4 and 6 as follows:

a) An approximately 400mm thick working platform constructed of gravel or crushed concrete (demolition debris) was laid down to form a stable surface for the excavator. This was necessary because of the wet ground conditions which had the potential to bog down the equipment;

b) The RIC points were measured out on the ground surface and marked with paint or a wooden stake; and

c) Compaction was performed at each point using a 7 tonne weight dropped from a height of 1m, at a rate of between 40 and 60 blows per minute onto an anvil measuring 1.5m in diameter. The weight was dropped until either:

- 500mm of settlement occurred below the anvil (i.e. the limit of anvil reach);
- The individual blows resulted in settlement of 10mm or less; or
- The total number of blows reached 40.

The hammer drop height was set at 1m (approximately 75% of maximum available impact energy) in order to reduce the ground surface vibrations generated during

compaction. The operating settlement limit of the ground supporting the anvil is 500mm. The limit of 40 blows is a typical value because above this number, the increase in soil density is relatively small but the impact vibrations can increase significantly. A schematic diagram illustrating the RIC methodology shown in Figure 22.

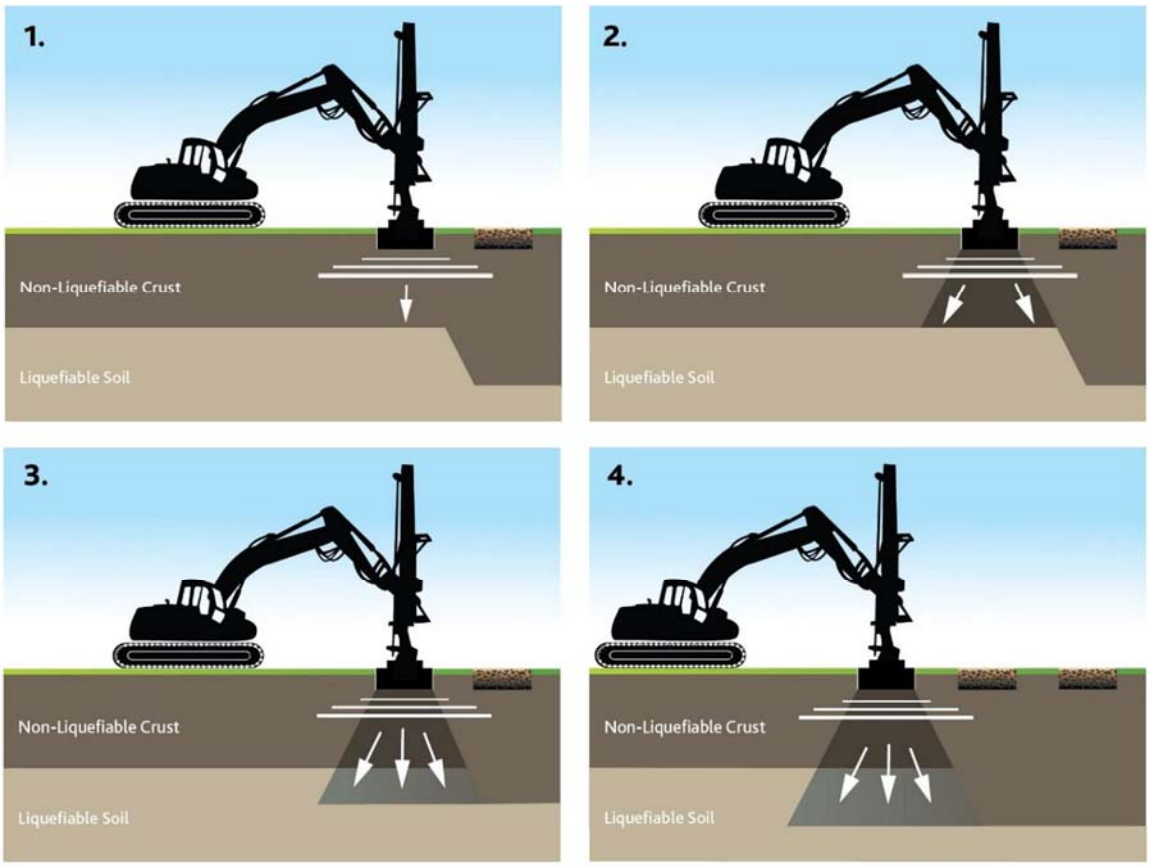

Figure 22: Rapid Impact Compaction (RIC) construction methodology (from van Ballegooy et al. 2017).

Each 7m x 7m test panel included 13 impact points. The construction sequence was to undertake the eight outside points and single center point first, then stopping work for 1 hour to allow the ground to "rest." The four remaining intermediate points were then compacted. The "rest" period allowed dissipation of excess pore pressure generated by the

impact process in order to help optimize the compaction of the soils. This 1 hour "rest" period typically occurs without stopping work when RIC is applied over larger areas. For example, an initial pass is undertaken in a (typical) 3m center-to-center square spacing pattern followed up by a second pass with the same pattern offset by 1.5m. At the completion of the RIC process, the impact point depressions were backfilled with gravel and the ground surface in the test panels was levelled for subsequent testing.

The number of hammer drops and total settlement per impact point were recorded during the RIC process, but not the settlement per hammer drop, which is higher for the first few hammer drops at each impact point, and lower towards the end of each impact point as the soils become more densified."

3.2.2 Rammed Aggregate Pier™ (RAP) Construction Method

"The Geopier Rammed Aggregate Pier™ (RAP) System is a patented/proprietary ground improvement system in which aggregate is compacted into the soil to form stiff, high density columns. RAPs are constructed by vibratory driving of a specially designed pipe mandrel, fitted with a tamper foot into the ground. A flat sacrificial steel plate is attached to the bottom of the mandrel to:

- Minimize spillage of aggregate at the ground surface;
- Prevent soil from entering the tamper foot and mandrel during driving; and
- Displace soils laterally.

Upon reaching the desired depth, the specified aggregate is top-loaded into the mandrel, and the mandrel is raised a short distance to partially fill the formed hole with aggregate, then hydraulically driven back down (all under vertical vibration) to compact the aggregate and displace and densify the surrounding soil. The process is repeated to

construct a column or "pier" comprised of a series of relatively thin lifts of dense aggregate extending to the ground surface.

Golder Construction Limited undertook the construction work of the RAP ground improvement work for the ground improvement trials.

RAP piers were installed in a single 7m x 7m test panel at Sites 3 and 6, and in four test panels at Site 4. Prior to constructing the test panels, spacing trials were conducted at Sites 3, 4 and 6 to optimize the pier pattern (refer to Section 6 for a detailed discussion of the analyses and results from the spacing trials). A triangular grid pattern was used for the spacing trial with a center-to-center spacing of RAP piers of 1.5, 1.75, 2, 2.25, 2.5, 2.75 and 3m. The spacing trial Area Replacement Ratios (ARR, defined as the ratio between the total cross-sectional area of the gravel piers and the total improved area of the test panel) ranged from approximately 4 to 14%. The RAP layout plans are shown in Figure 23. Based on the results of spacing trials, a RAP center-to-center pier spacing of 2m on a triangular grid (ARR ~ 8%) was selected for construction of all of the test panels constructed at Sites 3, 4 and 6.

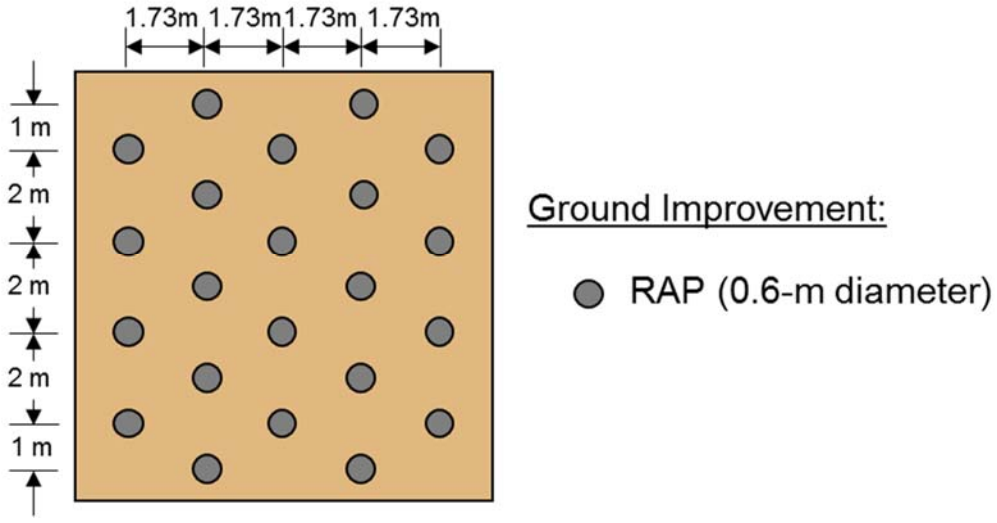

Figure 23: Plan view of the RAP impact points layout used at Sites 3, 4, and 6.

Each 7m x 7m test panel contained 22 RAP piers. The mandrel was pushed into the ground to a constant depth of 4m for all spacing trial and test panels apart from one test panel at Site 4 (4-RAP-2), where the mandrel was pushed to 3m and another test panel at Site 4 (4-RAP-3) where the mandrel was pushed to 2m.

The RAP construction process used at Sites 3, 4 and 6 is summarized below:

a) An approximately 400mm thick working platform constructed of gravel or crushed concrete (demolition debris) was laid down to form a stable surface for the excavator with the mounted RAP unit. This was necessary due to wet ground conditions which had the potential bog down the equipment;
b) The 250mm diameter mandrel and tamper foot were driven to the target depth of between 2 and 4m;
c) After driving the mandrel to the target depth, aggregate was loaded into a top-feed hopper, and the mandrel raised approximately 1.2m to allow the aggregate to fill the resulting void at the bottom of the hole. The mandrel was then driven back down approximately 900mm to form a 300mm thick lift of compacted aggregate. The process was repeated as necessary until there was a sufficient resistance when driving the mandrel back down, before repeating the process 300mm higher to construct a column of dense aggregate extending to the ground surface. The lengths of the compaction strokes were adjusted to suit the specific ground conditions at each test panel; and
d) At completion of each RAP pier, the hopper and mandrel were emptied of any remaining aggregate and the net aggregate volume consumed was measured.

The RAP process is schematically illustrated in Figure 24.

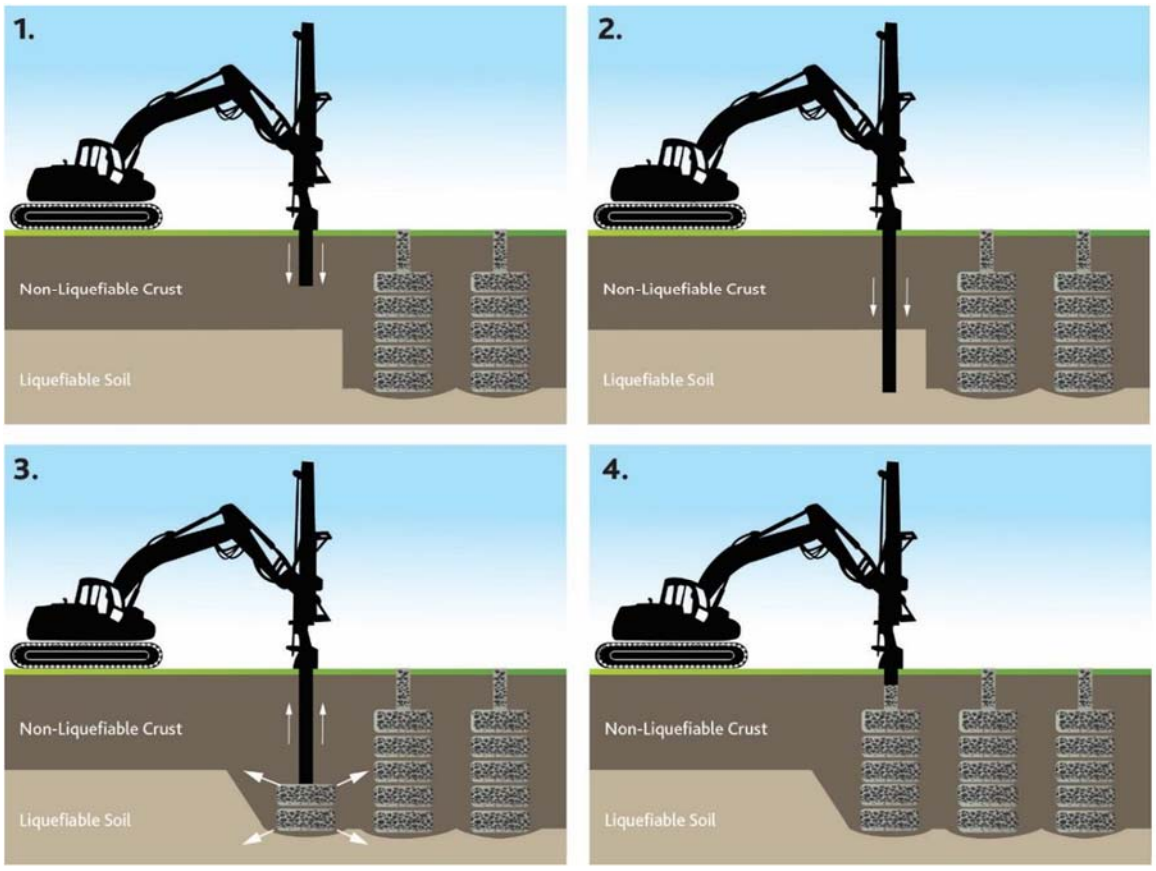

Figure 24: Rammed Aggregate Pier (RAP) construction methodology (from van Ballegooy et al. 2017).

The diameter of the completed aggregate piers was typically 600mm. The aggregate used for RAP construction comprised open-graded gravel with a maximum nominal particle size of 80mm and minimum nominal particle size of 10mm. Most of the aggregate ranged between 20 to 50mm (D10 to D90 respectively).

It is noted that the ARR have been calculated by assuming that the volume of aggregate used for each pier is evenly distributed over the mandrel depth. However, based on the CPT and crosshole VS results, the aggregate appears to have been typically pushed 1m below the target mandrel depth. Therefore, adjusted ARR values include an additional 1m of pier length below the mandrel target depth."

3.2.3 Low-Mobility Grout (LMG) Construction Method

"LMG, also known as compaction grouting, is a well-proven method for relevelling structures, and has also been used to improve liquefaction-prone soils through densification. The LMG solution involves pumping a stiff grout into the soil under relatively high pressure to laterally displace and densify the soil. Typically, a series of grout "bulbs" are injected, one upon another from the bottom up to form a grout "column." In some cases, the top or shallowest bulb is injected first and allowed to set and form a confining layer prior to injecting the deeper bulbs.

Relevel Limited undertook the LMG ground improvement work for the ground improvement trials.

LMG was undertaken in a single 7m x 7m test panel at Sites 3, 4 and 6. Prior to constructing the test panels, a spacing trial was conducted at Sites 3, 4 and 6 to optimize the injection pattern and grout bulb injection sequence. Triangular injection spacings of 1.5, 2, and 2.5 and 3m (center-to-center) were utilized in the spacing trials. Based on the results of spacing trials, a LMG center-to-center injection spacing of 2m on a triangular grid was selected for the test panels constructed at Sites 3, 4 and 6.

The layout of LMG injection points within the test panels at Sites 3, 4 and 6 are shown in Figure 25. Each 7m x 7m test panel contained 22 LMG injection locations. The injection tubes were installed to a constant target depth of 4m within each test panel.

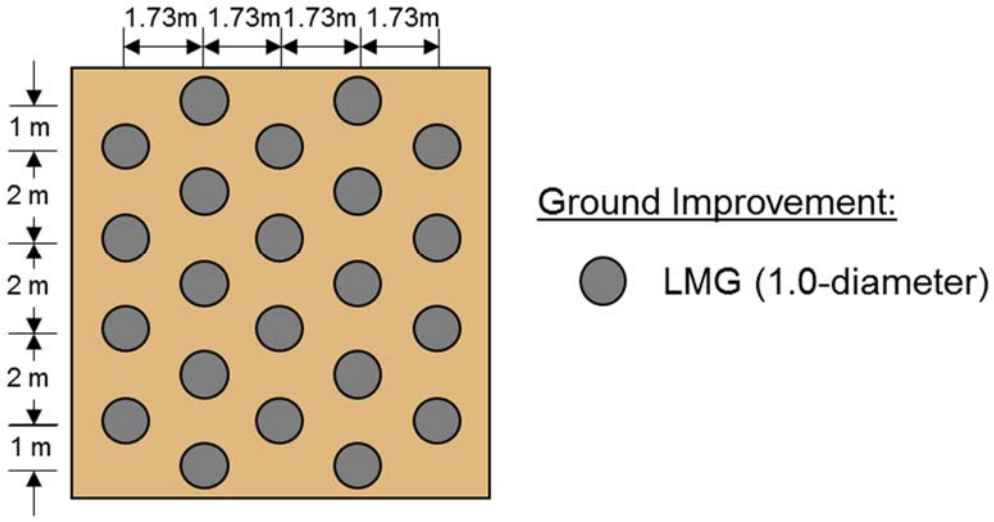

Figure 25: Plan view of the LMG impact points layout used at Sites 3, 4, and 6.

The LMG construction process used at Sites 3, 4 and 6 is summarized below:

a) Using a 3 tonne excavator equipped with either a compressed air hammer or hydraulic "rock breaker" attachment, a steel casing was driven into the ground to a depth of 1.5m at each injection point location;

b) A stiff, low viscosity grout mix was pumped from a mixer truck and through the steel casing into the ground to form the 'top bulb' of each injection point. Pumping was stopped when ground surface heave started to occur (monitored using a zip level);

c) The steel casings were removed using an electric powered hydraulic jack, the entire process (a-c) was repeated for all injection point locations within the test panel;

d) The following day, steel casings were driven into the ground at the same installation points as the previous day, down to a depth of 2.9 to 4m;

e) LMG was then pumped into the ground until ground surface heave started to occur; and

f) When pumping was completed at a particular depth, the casing was lifted approximately 500mm and the pumping process was repeated. This was continued until a 'column' of grout bulbs was completed between the starting depth of 2.9 to 4m and the top bulb, formed the previous day (at 1.5m depth). The ground surface heave during the injection of LMG at any one depth was typically limited to 50mm, and the total ground surface heave from the injection of LMG at all the depths was typically limited to 100mm.

The LMG installation process is schematically illustrated in Figure 26.

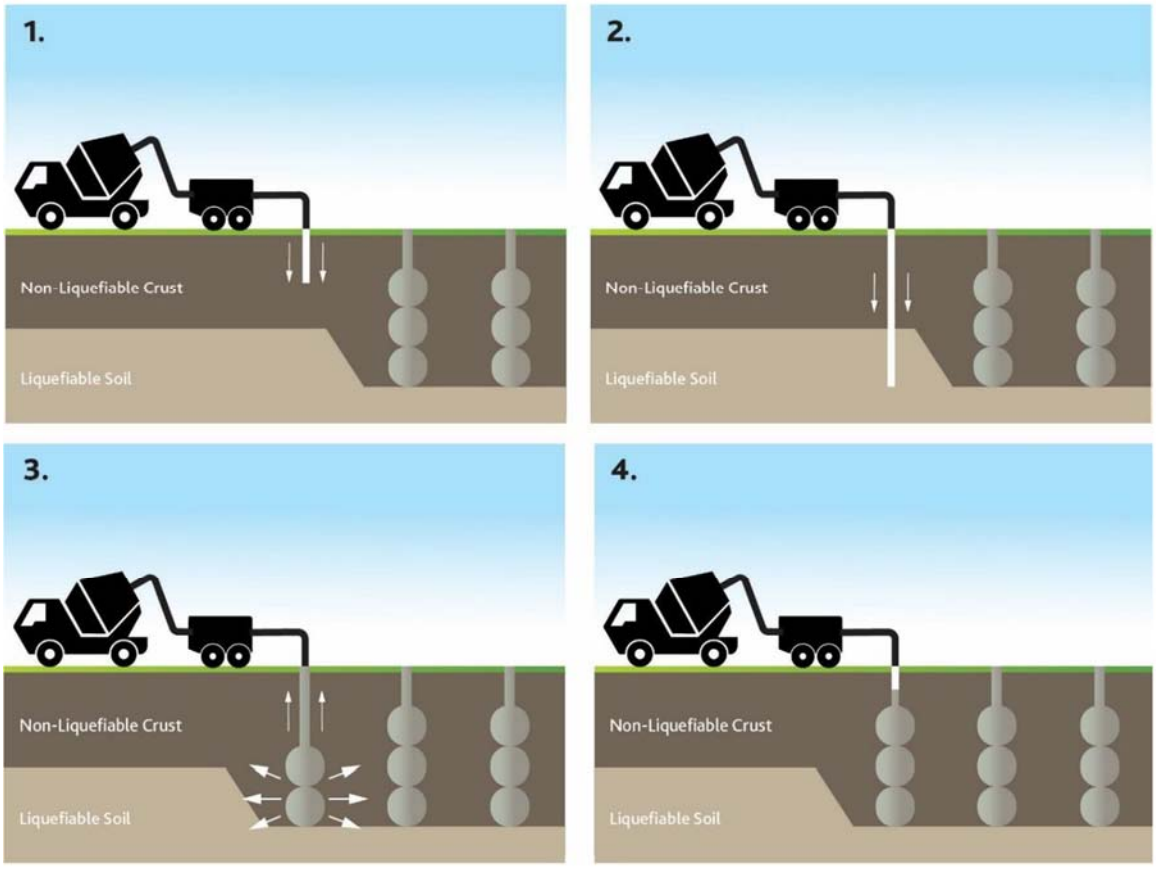

Figure 26: Low Mobility Grout (LMG) construction methodology (from van Ballegooy et al. 2017).

The LMG contractor provided limited information about the properties of LMG due to commercial sensitivity. The LMG consisted of mixture of cement, sand, aggregate (up to 10mm particle size), water and “approved additives.” The grout slump target was less than 50mm and the minimum specified strength was 10MPa after 28 days.”

3.3 SUMMARY

This chapter provides background and an overview of the three locations where the ground improvement trials took place as well as the construction methods for each of the reviewed ground improvement methods. All three of the sites (Site 3, Site 4, and Site 6) are located in residential neighborhoods along the Avon River to the east of the Central Business District where liquefaction-induced damage was severe, providing ideal conditions for testing various ground improvement methods.

Test panels using the Rapid Impact Compaction (RIC), the Rammed Aggregate Piers^{TM} (RAP), and the Low-Mobility Grout (LMG) ground improvement methods were built at all three of the test sites. Additional test panels of undisturbed, natural soil were designated at each of the test sites as well to serve as a baseline of comparison against which to compare the ground-improved soils. The construction processes of the RIC, RAP, and LMG ground improvements were summarized in this chapter as well.

Chapter 4: Site Characterization

4.1 Overview of Site Characterization Program

An extensive site characterization program was undertaken at each test panel to gather as much information as possible regarding the subsurface conditions of the natural soil and ground-improved soil. This site characterization program included three main activities: 1) trenching, 2) cone penetrometer testing (CPTs), and 3) direct-push crosshole testing (DPCH). The trenching operation was organized and reported by engineering geologists employed by the engineering firm Tonkin & Taylor Ltd. The CPTs were pushed by various contractors and the raw data were analyzed by the author. The DPCH tests were performed by The University of Texas at Austin research team and analyzed by fellow graduate student Sungmoon Hwang.

The location of the CPTs and direct-push crosshole tests included in the analysis are shown in Figure 27 through Figure 29 for Sites 3, 4, and 6, respectively.

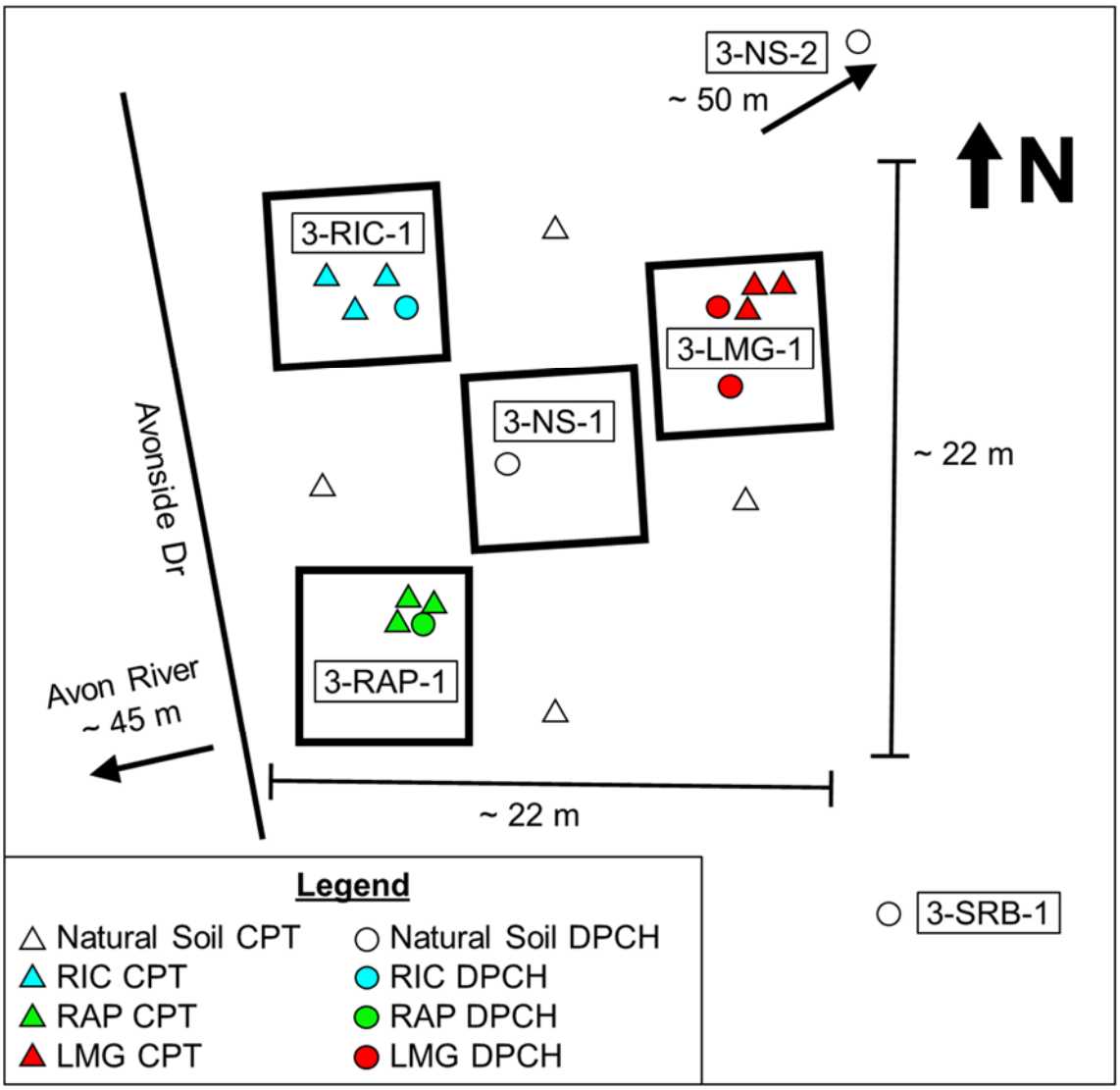

Figure 27: Location of CPT and DPCH tests performed at Site 3.

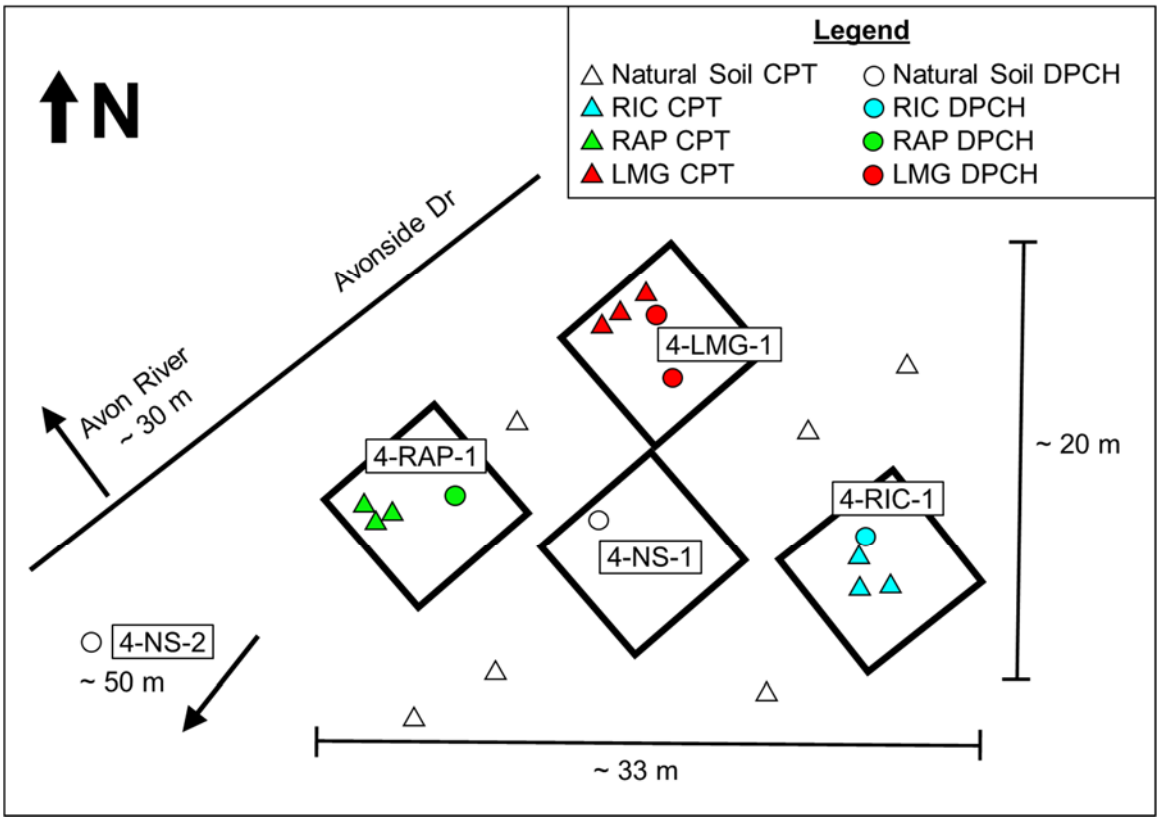

Figure 28: Location of CPT and DPCH tests performed at Site 4.

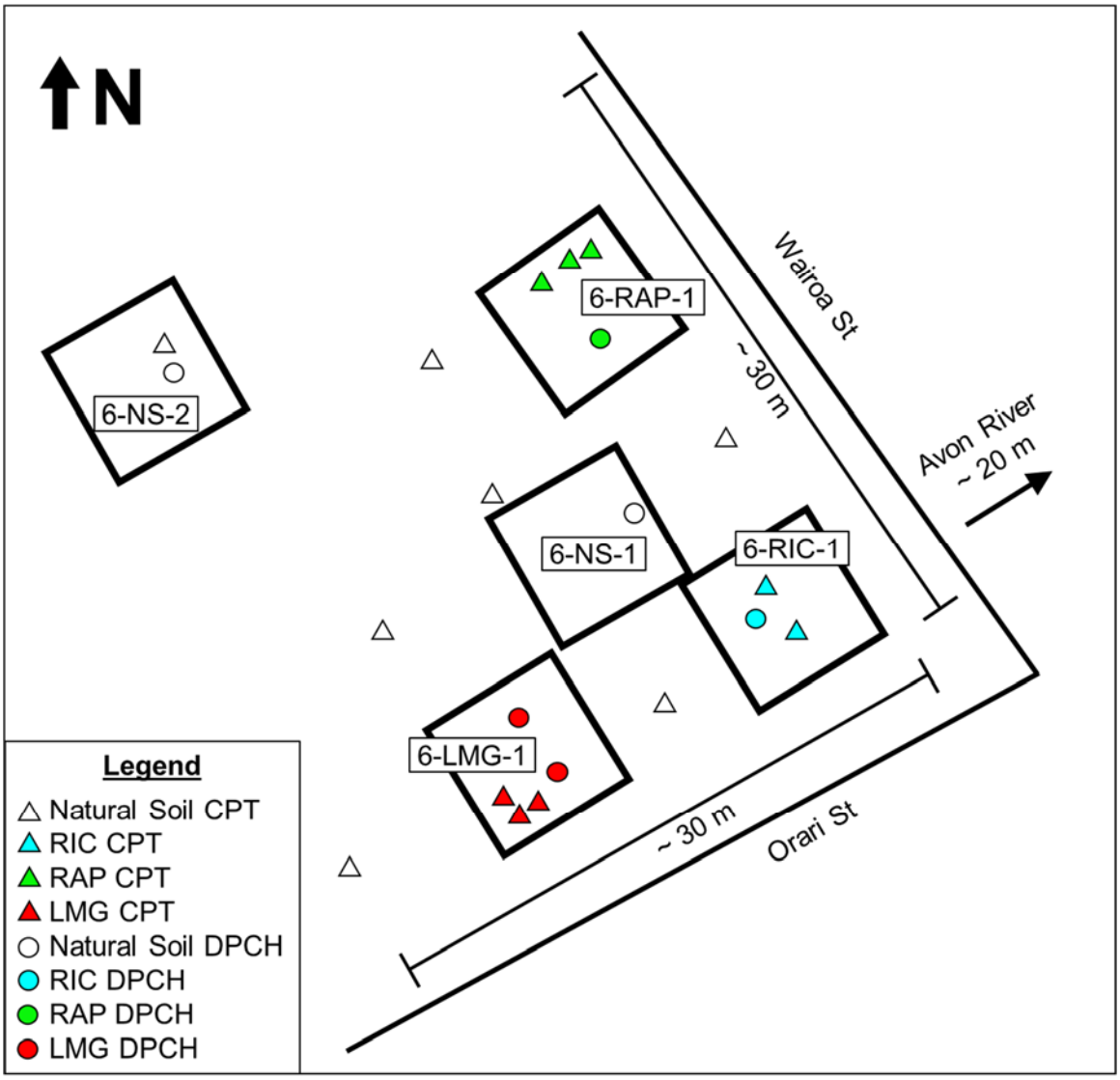

Figure 29: Location of CPT and DPCH tests performed at Site 6.

4.1.1 Objectives of Trenching and CPTs

The objective of the trenching, which was performed at the end of the project because it destroyed the test panels, was to identify and categorize the soil layers as well as obtain representative soil samples for laboratory testing. Trenching also provided an opportunity to assess the construction quality of the ground improvements. Because of the relatively shallow water table at each site, de-watering spears were used to lower the water

table within the test panel during excavation to help prevent the trench from collapsing. The maximum depths of the trenches ranged from 2.6 to 5.2 m and was limited by trench collapse.

The CPT was used to evaluate the changes in soil characteristics resulting from the ground improvement methods and to identify layering in the subsurface using a soil behavior index. CPTs were pushed at locations between the test panels to characterize the natural soil and at locations within the improved-ground test panels approximately equidistant to the impact points (RIC), gravel piers (RAP), and injection points (LMG) to provide data regarding changes in the soil due to the ground improvement. See Figure 27 through Figure 29 for CPT locations at Sites 3, 4, and 6, respectively. Changes in the cone tip resistance and the side friction values measured at the improved-ground locations versus those at the natural soil locations indirectly indicate changes in soil strength and/or soil density. At the ground-improved test panels, CPTs were typically pushed after improvement at 14-day, 28-day, and 90-day intervals to capture potential time effects associated with the ground improvement method. Because a time effect was not observed in the results, CPTs from the same test panel are presented without distinction.

4.1.2 Overview and Objectives of Direct-Push Crosshole (DPCH) Tests

DPCH was performed at each test panel using two linear arrays, producing two separate and independent wave velocity profiles side-by-side. The typical velocity profile started at a depth of 0.6 m below the ground surface and extended to a maximum depth of 5.0 or 6.0 m, advancing in 0.2 m increments. The horizontal distance between the source and receiver rods ranged from 1.0 to 1.8 m. At the natural soil test panels, both velocity profiles characterize the natural soil. At the ground-improved test panels, one set of velocity profiles characterizes the soil in between improvements (i.e. the RIC impact

points, RAP piers, or LMG columns) and the other set performed across improvements characterizes the combination of the soil and improvement method. As shown in Figure 30a for the RIC test panels, one linear array is positioned across an impact point and the other linear array is positioned between two impact points to characterize the changes in the soil due to the improvement method and identify potential variability in the densification. As shown in Figure 30b for the RAP and in Figure 30c for the LMG test panels, one linear array is positioned across the gravel pier or grout column to characterize the properties of the soil/column matrix while the other linear array is positioned between two columns to characterize the changes in the soil due to the ground improvement. Two sets of DPCH were performed at all LMG test panels to verify the data due to surprising and controversial results that were identified by Sungmoon Hwang and Dr. Stokoe during data collection. The locations of DPCH testing are shown in Figure 27 through Figure 29 for Site 3, Site 4, and Site 6, respectively.

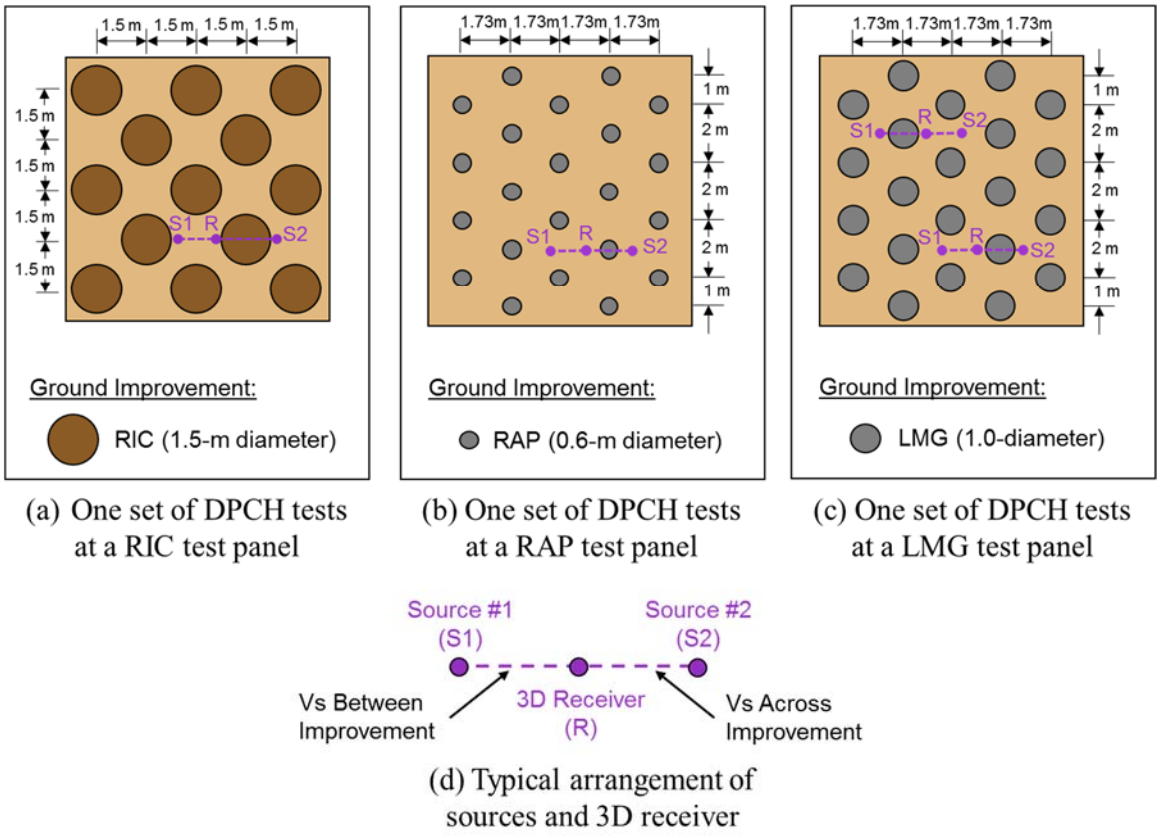

(a) One set of DPCH tests at a RIC test panel

(b) One set of DPCH tests at a RAP test panel

(c) One set of DPCH tests at a LMG test panel

(d) Typical arrangement of sources and 3D receiver

Figure 30: Plan view of DPCH test locations at the three ground improvement test panels (a) RIC, (b) RAP, and (c) LMG and (d) the typical arrangement of sources and 3D receiver for the DPCH test.

The methodology and procedure of DPCH is described in detail in Stokoe et al. (2014) and Stokoe et al. (2015); beyond this brief introduction, only the results of DPCH testing will be presented and discussed herein as part of the site characterization. The objective of DPCH testing was to obtain both constrained-compression wave and shear wave velocity profiles. The work of Valle-Molina & Stokoe (2012) and Valle-Molina (2006) offer empirical data for correlating the compression wave velocity with the degree of saturation in sands, providing an opportunity to estimate the degree of saturation in situ using the compression wave velocity profile determined from DPCH testing. A compression wave velocity greater than 1,450 m/s indicates a sandy soil is 100 % saturated.

A compression wave velocity of 750 m/s corresponds to a sandy soil that is approximately 99.6 % saturated (Valle-Molina & Stokoe (2012) and Valle-Molina (2006)).

While the effect that degree of saturation has on the triggering of soil liquefaction is not the focus of the ground improvement trials, it is believed that soils with a compression wave velocity greater than 750 m/s exhibit fully-saturated behavior under dynamic loading. Soils with compression wave velocities less than 750 m/s are expected to generate less residual excess water pressure under dynamic loading conditions due to the compressible nature of air in comparison to the water and soil particles, making this condition less susceptible to the triggering of soil liquefaction.

The field shear wave velocities obtained from DPCH testing provide as close a indirect measure of the material's small-strain stiffness as any field dynamic measurement. The small-strain stiffness is the shear modulus (G_{max}). The relationship between the shear wave velocity and G_{max} is $G_{max} = \rho \times V_S^2$ where ρ is the mass density of the soil and V_S is the shear wave velocity. A mass density of 1.89 g/cm^3 was used for soils above the water table and of 1.99 g/cm^3 for soils below the water table. At Site 3 and Site 4, the water table was located approximately 0.7 m below the ground surface. At Site 6, the water table was located approximately 0.5 m below the ground surface.

The resulting G_{max} profiles are vital not only for quantifying the changes in soil stiffness resulting from the ground improvements (from measurements between improvements) but also quantifying the stiffness of the soil/column matrix (from measurements across improvements). Shear wave velocities are also important for ensuring laboratory specimens are accurate representations of field specimens by comparing the S-wave velocity measured in situ versus the S-wave velocity measured in the laboratory specimen. Further, the G_{max} evaluated from DPCH is the starting point for understanding the nonlinear shear strain behavior of the soil during shake testing with T-Rex.

4.2 CHARACTERIZATION OF THE NATURAL SOIL USING CPT AND DPCH

The natural soil at each site was characterized using results from multiple CPT soundings and DPCH tests as well as from the excavation trenches at the natural soil test panels. The locations of the CPT soundings and DPCH tests in the natural soil are shown in Figure 27 through Figure 29 for Sites 3, 4, and 6, respectively. As shown in these figures, the natural soil CPTs were pushed at locations between the test panels while the natural soil DPCH tests were performed within the boundaries of the natural soil test panels.

The CPTs and DPCH tests used to characterized the natural soil at each site are summarized in Table 2; the CPTs are labeled according to their identification number in the New Zealand Geotechnical Database and the DPCH are labeled according to the test panel in which they were performed. The summary of DPCH testing also includes the number of profiles that resulted from the test; a typical DPCH test on this project used two source-to-receiver spacings to obtain two profiles, but occasionally only one source-to-receiver spacing was used due to limitations in the field.

Table 2: Summary of CPTs and DPCH tests performed at each site to characterize the natural soil. The number of profiles obtained from each DPCH test is included in parenthesis next to the test panel.

Test Site	CPT Database ID #	DPCH Test Panels (# of profiles)
Site 3	21509, 21510, 21515, 21516	3-NS-1 (2), 3-NS-2 (1), 3-SRB-1* (2)
Site 4	21511, 21519, 21521, 21522, 34438, 34452	4-NS-1 (2), 4-NS-2 (2)
Site 6	21506, 21507, 21524, 21525, 33401, 34415, 34416	6-NS-1 (2), 6-NS-2 (2)

*Single-Row-of-Beams ground improvement test panel

Five parameters derived from the CPT and DPCH testing were used to characterize the natural soil conditions: 1) the corrected cone tip resistance (q_t), 2) the sleeve friction resistance (f_s), 3) the normalized soil behavior index (I_C), 4) the compression wave velocity (V_P), and 5) the shear wave velocity (V_S). These five parameters were selected for their sensitivity to changes in the density, stiffness, and state of stress of the soil (q_t and shear wave velocity) as well as for their potential influence on the effectiveness of the ground

improvement methods (soil type as identified by I_C). A site-specific median profile for each of these parameters has been calculated to be used as the baseline condition against which results from the ground improvement test panels are compared.

The q_t and I_C are calculated using the following equations from ASTM D5778-12 and Robertson 2009:

$$q_t = q_c + u_2(1 - a_n) \quad (2)$$

where q_c is the cone resistance, u_2 is the porewater pressure generated immediately behind the cone tip, and a_n is the net area ratio (ASTM D5778-12) and

$$I_C = ((3.47 - logQ_t)^2 + (logF_r + 1.22)^2)^{0.5} \quad (3)$$

where Q_t is the normalized cone penetration resistance and F_r is the normalized friction ratio (Robertson 2009). The normalized cone penetration resistance Q_t is calculated using the following equation:

$$Q_t = (q_t - \sigma_{vo})/\sigma'_{vo} \quad (4)$$

where q_t is the corrected cone tip resistance, σ_{vo} is the total vertical stress, and σ'_{vo} is the effective vertical stress (Robertson 2009). The normalized friction ratio F_r is calculated using the following equation:

$$F_r = [f_s/(q_t - \sigma_{vo})] \times 100\ \% \quad (5)$$

where f_s is the sleeve friction resistance, q_t is the corrected cone tip resistance, and σ_{vo} is the total vertical stress (Robertson 2009).

The characterization of Site 3, Site 4, and Site 6 from CPT and DPCH testing is presented in Figure 31, Figure 32, and Figure 33, respectively. The subplots of each figure show results from individual tests as well as the resulting median profile for the following parameters: (a) q_t and f_s, (b) I_C, (c) V_P, and (d) V_S.

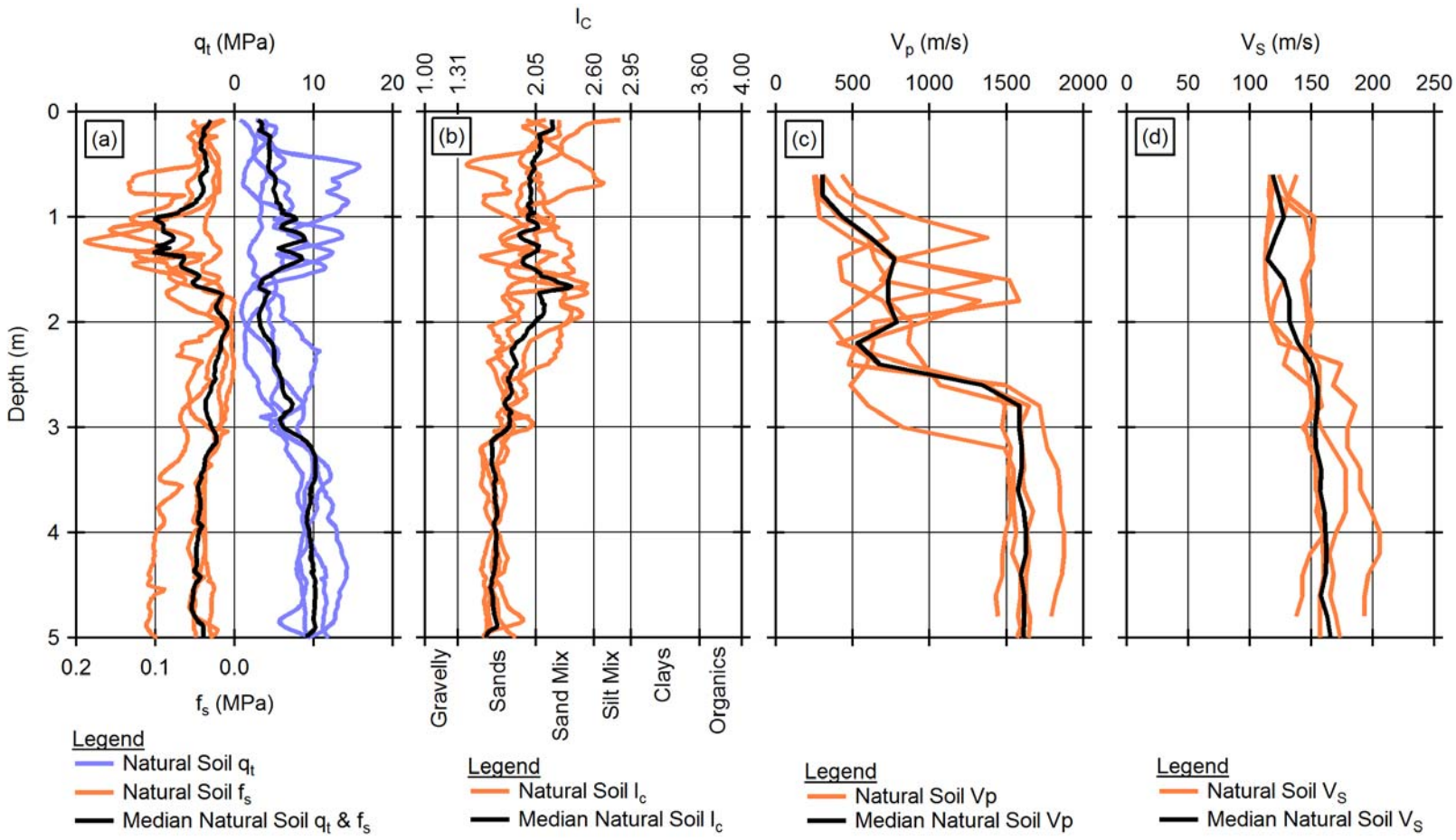

Figure 31: Characterization of the natural soil at Site 3 based on four CPTs and five DPCH profiles: (a) corrected cone tip resistance, q_t, and friction sleeve resistance, f_s, (b) normalized soil behavior index, I_c, (c) compression wave velocity, V_P, and (d) shear wave velocity, V_S.

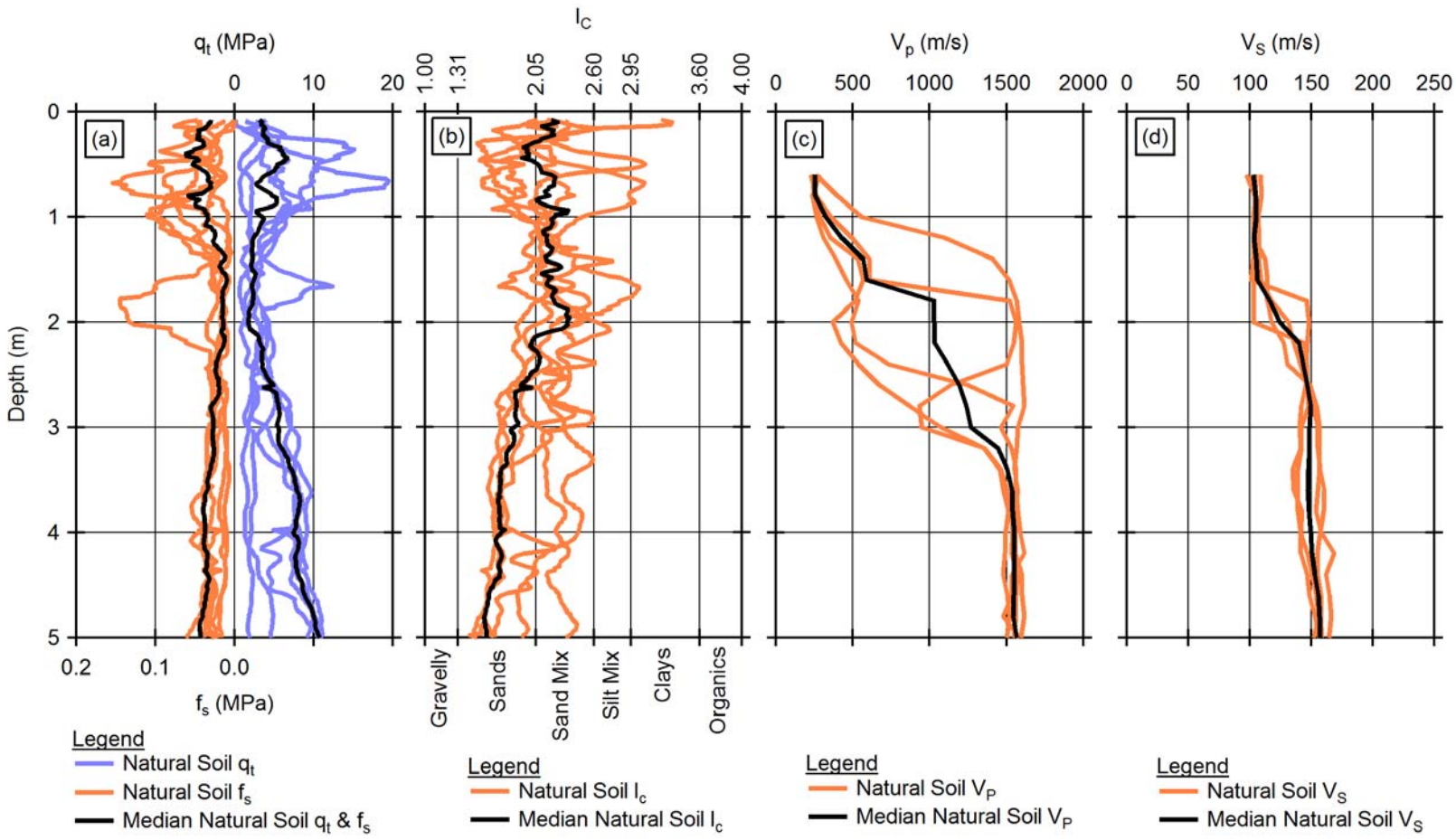

Figure 32: Characterization of the natural soil at Site 4 based on six CPTs and four DPCH profiles: (a) corrected cone tip resistance, q_t, and friction sleeve resistance, f_s, (b) normalized soil behavior index, I_c, (c) compression wave velocity, V_P, and (d) shear wave velocity, V_S.

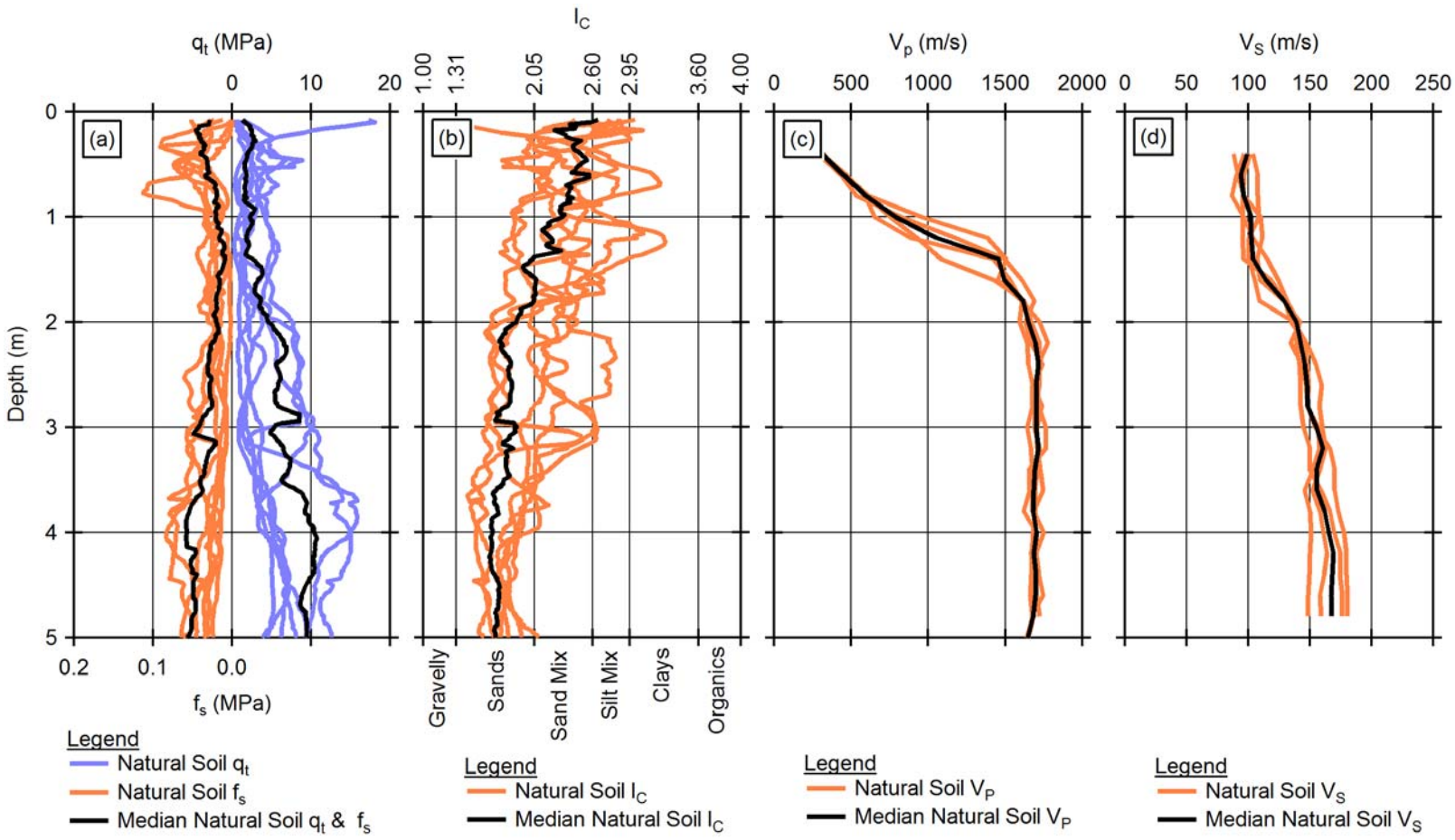

Figure 33: Characterization of the natural soil at Site 6 based on seven CPTs and four DPCH profiles: (a) corrected cone tip resistance, q_t, and friction sleeve resistance, f_s, (b) normalized soil behavior index, I_c, (c) compression wave velocity, V_P, and (d) shear wave velocity, V_S.

4.3 COMPLICATIONS IN ASSESSING THE MEDIAN SHEAR WAVE VELOCITY AT SITE 3

Developing a median shear wave velocity profile for the natural soil at Site 3 was more complicated than at Site 4 and Site 6. The two shear wave velocity profiles from DPCH testing at the 3-NS-1 test panel showed higher than expected values in the top 2.0 m below the ground surface in comparison to the profile from 3-NS-2 as well as in comparison to the natural soil profiles obtained at Sites 4 and 6. This assessment is shown in Figure 34, where the results from Site 3 are presented in subfigure (a) and the results from all three sites are presented in subfigure (b). Careful review of the time records from testing at 3-NS-1 show no indication of testing error or alternative interpretations that can explain the anomaly, so the results have been accepted as representing the soil conditions at that test panel. A possible explanation for the unexpectedly high shear wave velocity values is that this test panel was unintentionally centered under the former footprint of a single-story residence where the confining pressure would be greater than in the free field and/or construction activities associated with the residential structure densified the shallower soils. The other test panels assessed in this study were either located in the residential yard or along the edge of where residential structures once stood where the effect on increased confining pressure would be minimized.

While accepting that the shear wave velocity values at 3-NS-1 are relatively high for the natural soil in the top 2.0 m, it is not expected that the values are also high in the surrounding natural soil at Site 3 based on the comparison of results from 3-NS-1 and from Sites 4 and 6. Given the complicated situation and the fact that the 3-NS-2 DPCH test only produced one profile, the results from DPCH testing at the Single-Row-of-Beams test panel (3-SRB-1) were included to increase the number of profiles used in calculating the median natural soil profile at Site 3.

The 3-SRB-1 test panel was selected because this ground improvement method was shown to cause no measurable change to the shear wave velocity in the soil around the beams at Site 3, Site 4, and Site 6. In this case, the shear wave velocities in the depth range where one of the source-to-receiver spacings sampled through a beam was removed from the results. It is also noted in Figure 34a that the shear wave velocities at one of the 3-SRB-1 profiles is also unusually high in the bottom 2.5 to 4.8 m of the profile, but the use of a median profile reduces the effect of these outlier points as well. The resulting median shear wave velocity profile for the natural soil obtained with the inclusion of the profiles from 3-SRB-1 is considered to best represent the natural soil at Site 3.

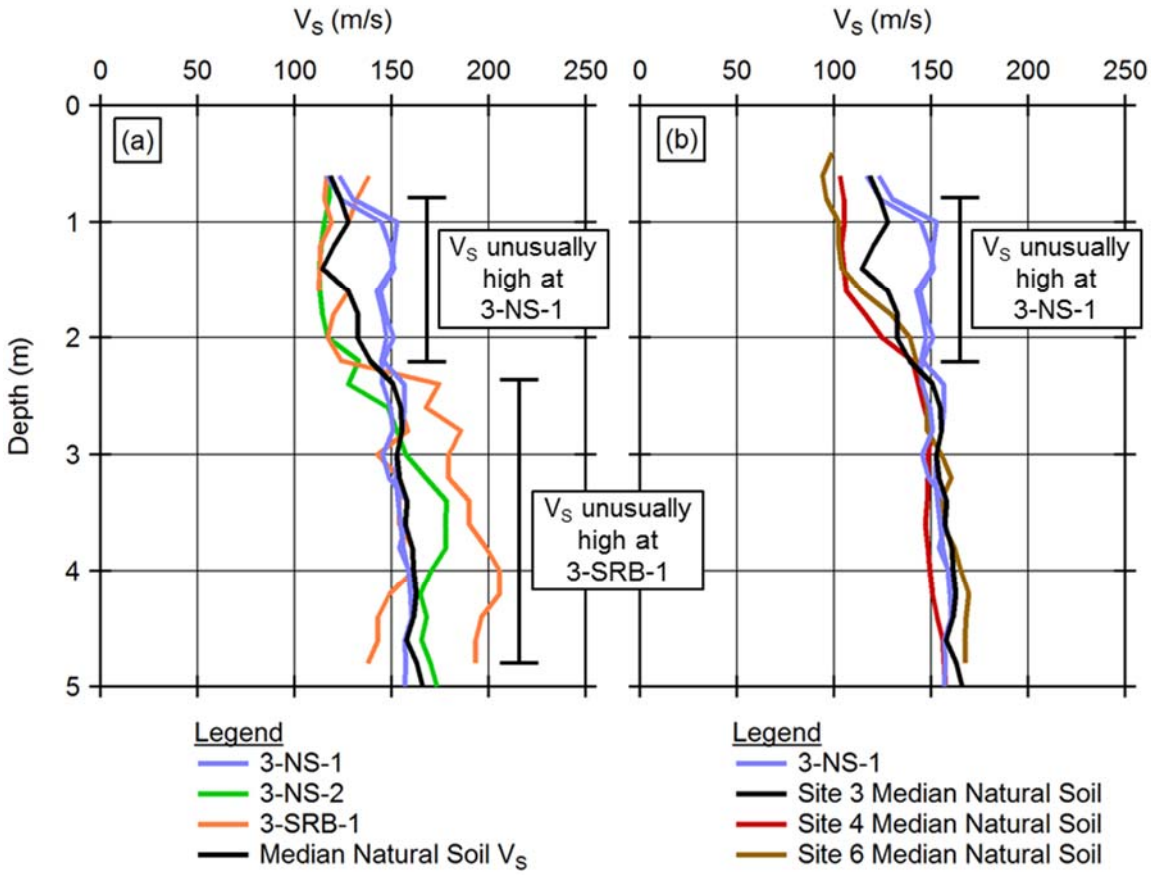

Figure 34: Assessment of the natural soil profile at Site 3 based on shear wave velocity profiles from 3-NS-1, 3-NS-2, and 3-SRB-1 (subfigure a) and in comparison to the natural soil profiles at Site 4 and Site 6 (subfigure b).

4.4 Evaluation and Comparison of Soil Layering at Site 3, Site 4, and Site 6

The trench cross-sections and summary tables for the six natural soil test panels are presented in Figure 35 and Table 3 (3-NS-1), Figure 36 and Table 4 (3-NS-2), Figure 37 and Table 5 (4-NS-1), Figure 38 and Table 6 (4-NS-2), Figure 39 and Table 7 (6-NS-1), Figure 40 and Table 8 (6-NS-2). In general, the simplified soil profile in the top 5 m of each site consists of a top layer of fill and silt layers whose total thickness ranges from 1-2 m and a second layer of sand that grades from silty sand at the top of the layer down to medium sand at the bottom. This typical profile is seen in the trench cross-sections in Figure 38 for test panel 4-NS-2 and in Figure 40 for test panel 6-NS-2. The soil profiles at the other natural soil test panels include thin layers of fine sand near the surface within the silt layers or thin layers of silt within the deeper sand layers, indicating a complex layering of materials that is typical of alluvial deposits. This interlayering of silty and sandy layers can be seen in the cross-sections in Figure 35 for test panel 3-NS-1, in Figure 36 for test panel 3-NS-2, in Figure 37 for test panel 4-NS-1, and in Figure 39 for test panel 6-NS-1.

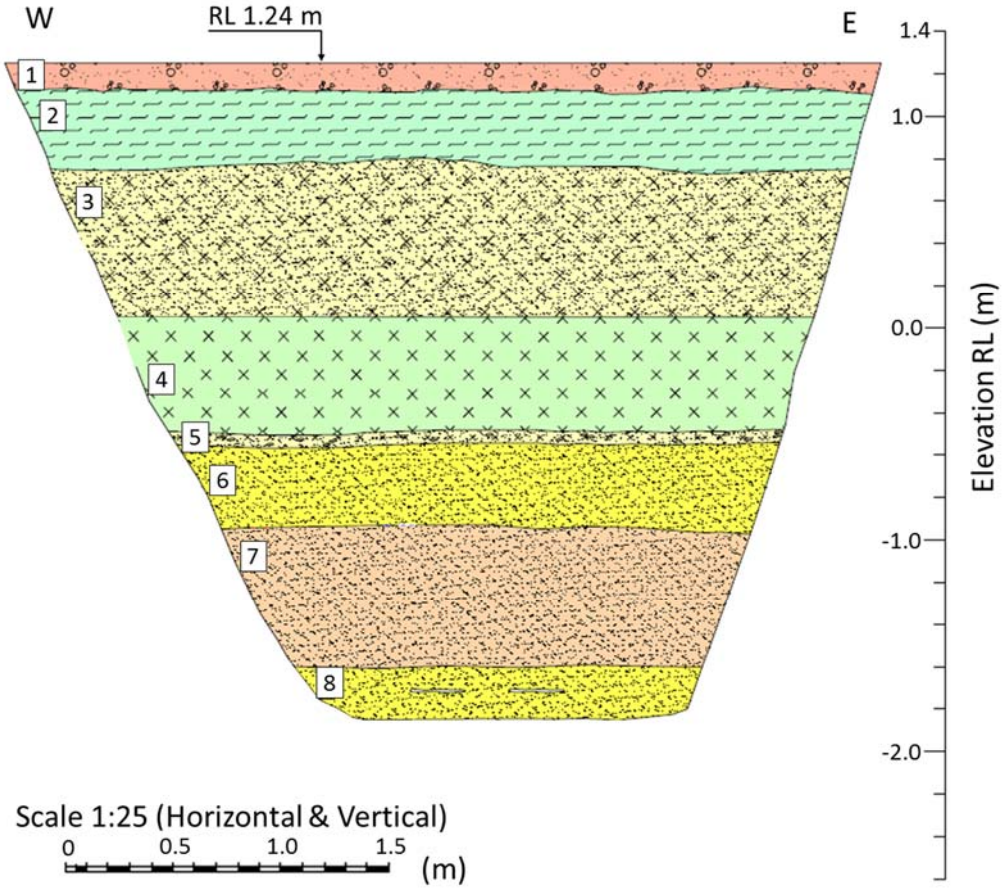

Figure 35: Cross-section of the excavation trench at the 3-NS-1 Test Panel. Modified from van Ballegooy et al. 2017.

Table 3: Soil layers, soil layer depth ranges, USCS designation, and soil description for the layers identified in the 3-NS-1 Test (van Ballegooy et al. 2017).

Layer	Depth Range	USCS	F.C.	Description
1	0 - 0.15 m			GRAVEL (FILL)
2	0.15 - 0.5 m			Topsoil (FILL)
3	0.5 - 1.3 m	SM	38 %	Silty fine SAND; yellowish brown. Loose; moist; massive; silt, non-plastic. (FILL)
4	1.3 - 1.8 m	ML	90 - 91 %	SILT with minor sand; grey mottled brown, homogeneous. Very stiff; moist; silt, non-plastic; sand, fine.
5	1.8 - 1.85 m	SM		Silty fine SAND with organic fragments.
6	1.85 - 2.3 m	SP	6 %	Fine to medium SAND with trace silt; grey, homogenous. Loose; saturated.
7	2.3 - 2.9 m	SP	1 %	Medium SAND with some organics and trace gravel; grey. Loose; saturated; gravel, fine, homogeneous; sub-rounded.
8	2.9 - 3.1 m	SP	3 %	Fine to medium SAND with trace of silt.

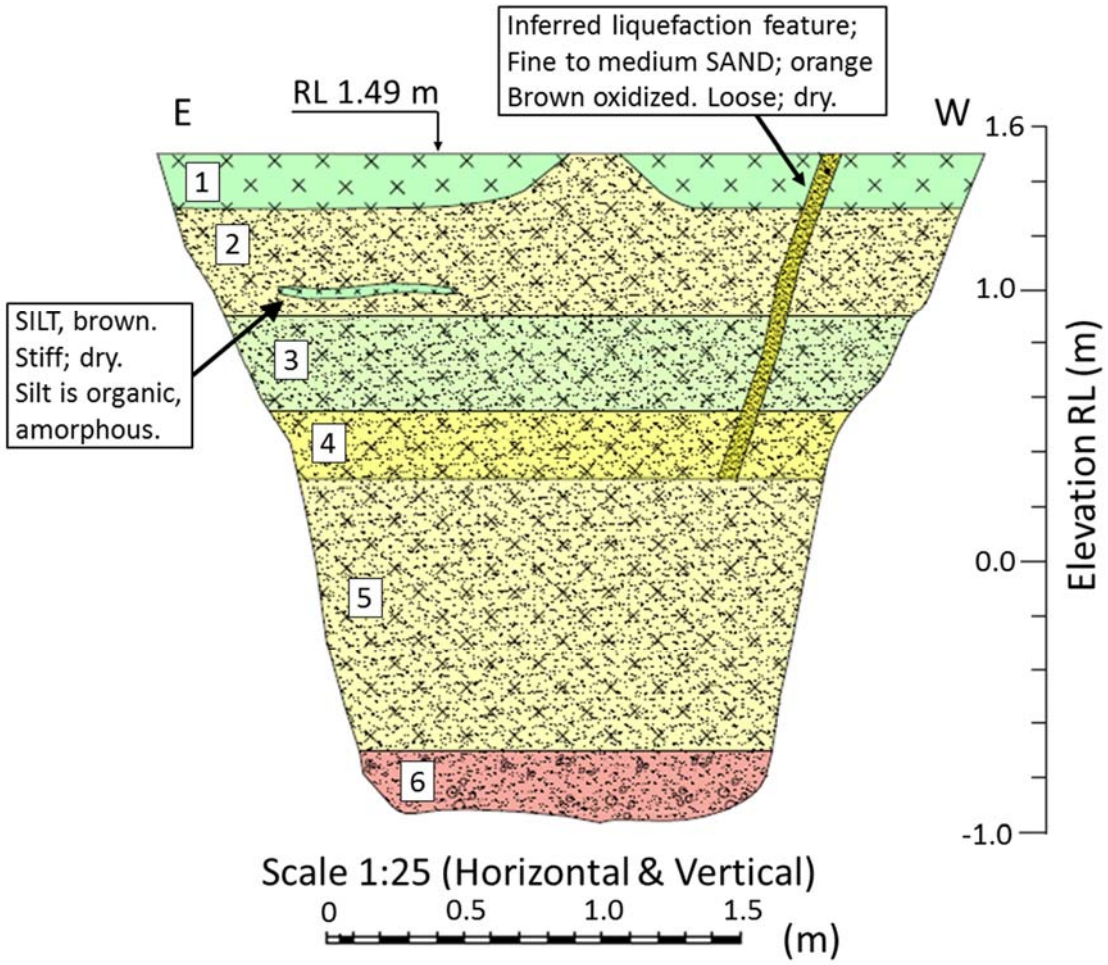

Figure 36: Cross-section of the excavation trench at the 3-NS-2 Test Panel. Modified from van Ballegooy et al. 2017.

Table 4: Soil layers, soil layer depth ranges, USCS designation, and soil description for the layers identified in the 3-NS-2 Test Panel (van Ballegooy et al. 2017).

Layer	Depth Range	USCS	F.C.	Description
1	0 - 0.2 m	SP		SILT; brown. Stiff; dry. Silt is organic, amorphous.
2	0.2 - 0.6 m	SM		Silty SAND with some silt inclusions, gravel and organics; light brown. Medium dense, dry.
3	0.6 - 0.9 m	ML	85 %	SILT with some sand with minor organics; grey mottled orange brown. Medium dense; moist; organics, rootlets.
4	0.9 - 1.2 m	SM	41 %	Silty SAND with trace organics; grey. Wet; organic, rootlets.
5	1.2 - 2.2 m	SM		Silty SAND, minor organics; grey. Wet; organics, rootlets.
6	2.2 - 2.5 m	GP-GM		Sandy GRAVEL; orange brown. Wet.

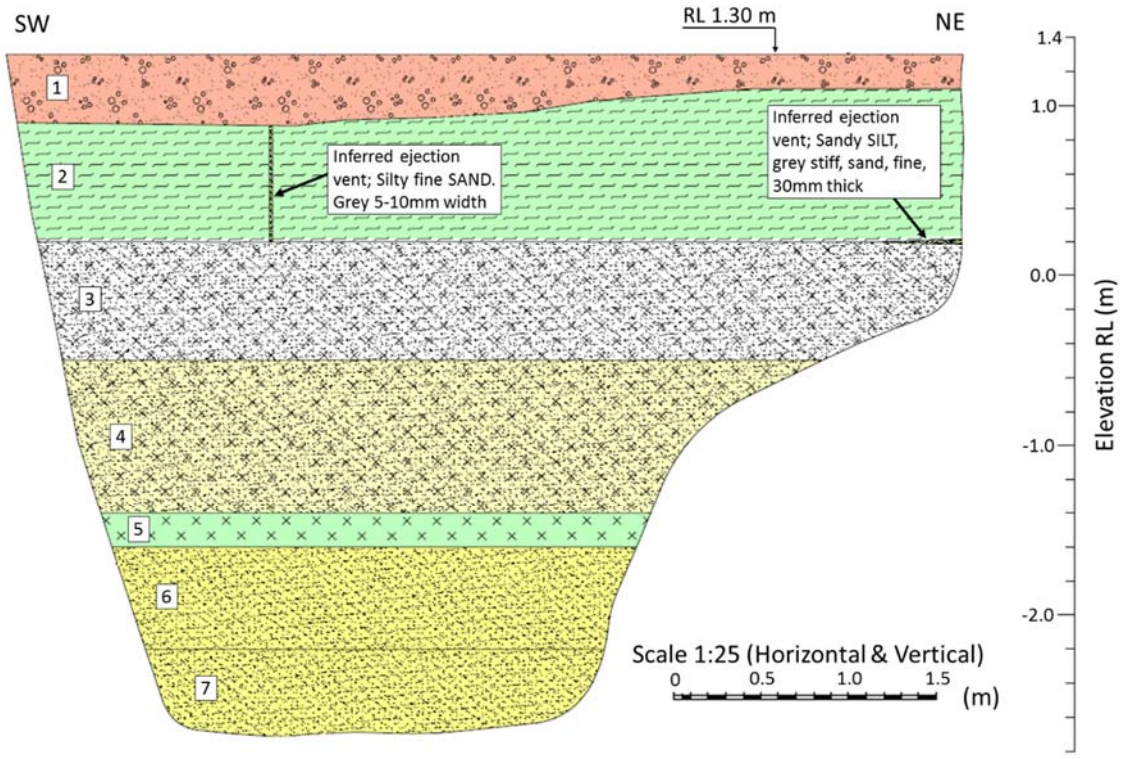

Figure 37: Cross-section of excavation trench at the 4-NS-1 Test Panel. Modified from van Ballegooy et al. 2017.

Table 5: Soil layers, soil layer depth ranges, USCS designation, and soil description for the layers identified in the 4-NS-1 Test Panel (van Ballegooy et al. 2017).

Layer	Depth Range	USCS	F.C.	Description
1	0 - 0.3 m	GP		Medium GRAVEL. Sub-angular to sub-rounded (FILL).
2	0.3 - 1.1 m	OH		SILT with some organics; dark brown. Firm to stiff, low plasticity; slightly dilatant, organic odour
3	1.1 - 1.8 m	SM		Silty fine SAND; light brown, mottled reddish brown. Loose; homogeneous.
4	1.8 - 2.7 m	SM	20 %	Fine to medium SAND with some silt and organics; dark brown. Loose; organics, fibrous.
5	2.7 - 2.9 m	OH		SILT with some organics; dark grey. Rootlets.
6	2.9 - 3.5 m	SP	1 %	Fine to medium SAND with trace silt; dark brown. Loose.
7	3.5 - 4.0 m	SP		Fine to medium SAND with trace silt; dark grey.

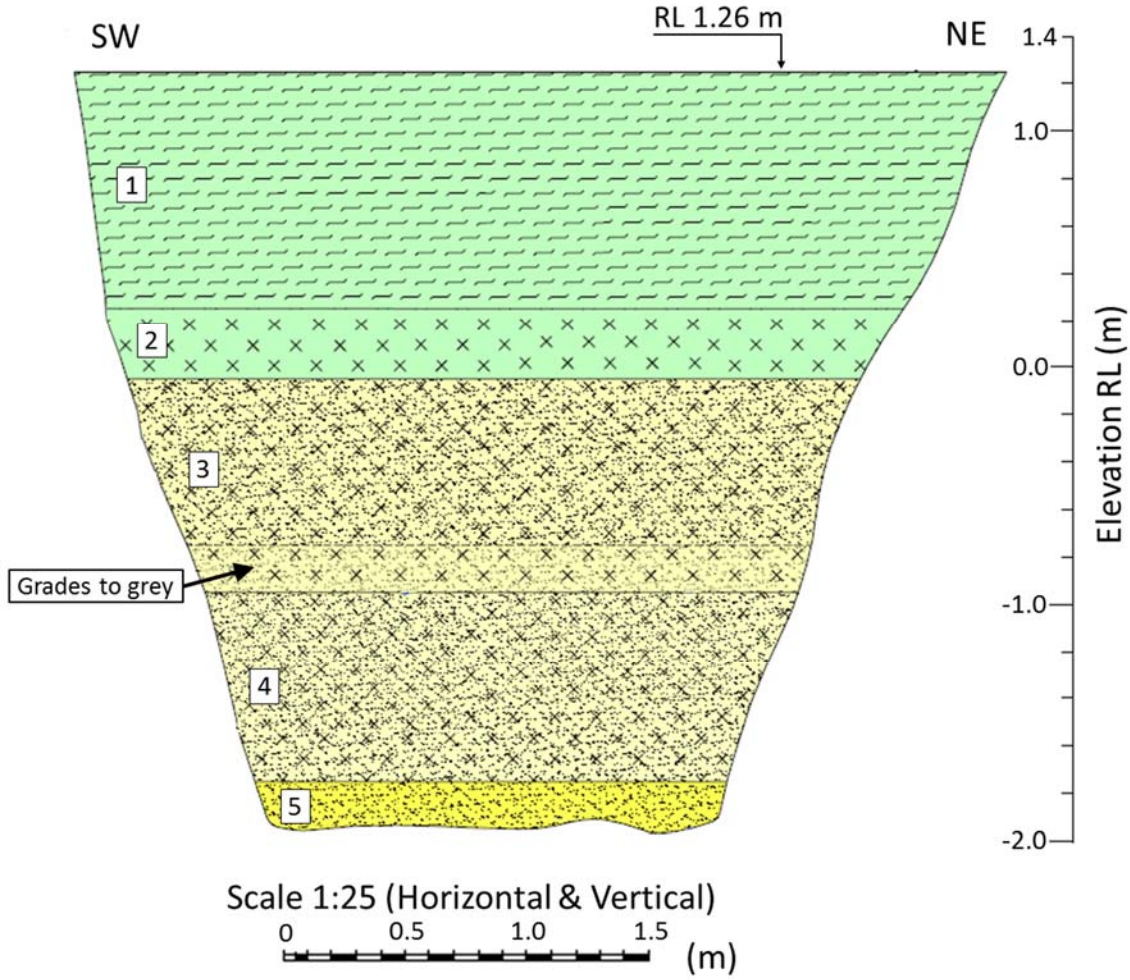

Figure 38: Cross-section of excavation trench at the 4-NS-2 Test Panel. Modified from van Ballegooy et al. 2017.

Table 6: Soil layers, soil layer depth ranges, USCS designation, and soil description for the layers identified in the 4-NS-2 Test Panel (van Ballegooy et al. 2017).

Layer	Depth Range	USCS	F.C.	Description
1	0 - 1.0 m	OH	85 % (PI=12 %)	Inter-layered Topsoil/Silt (FILL).
2	1.0 - 1.3 m	OH		SILT with some organics; black. Firm.
3	1.3 - 2.3 m	OH	30 %	Silty fine SAND with minor organic fragments; brown and grey mottled. Loose.
4	2.3 - 3.1 m	OH	20 %	Fine to medium SAND with some silt; grey. Loose.
5	3.1 - 3.3 m	SP	5 %	Fine to medium SAND with minor silt; grey. Loose.

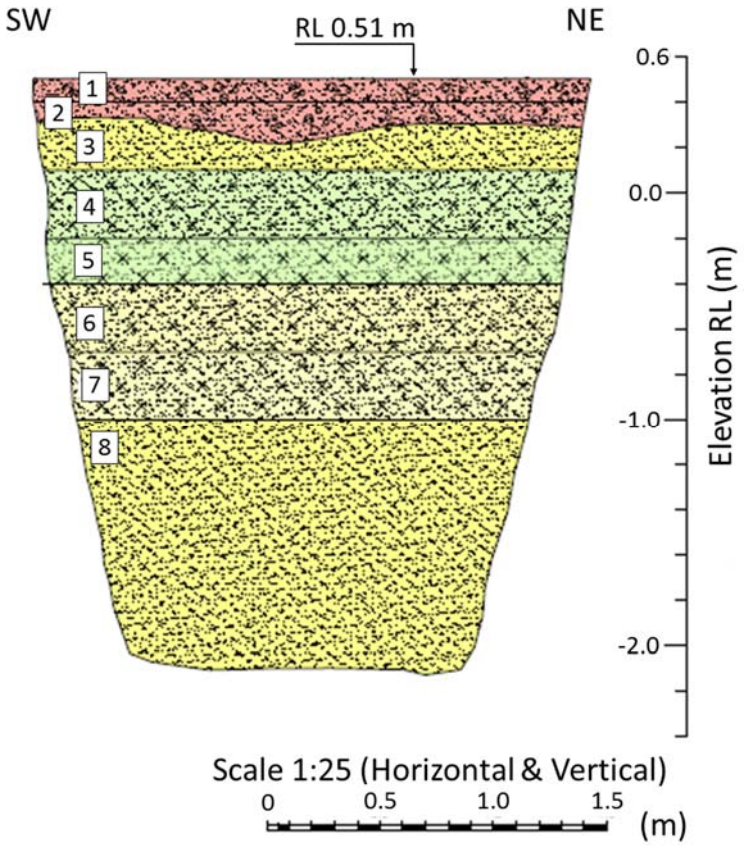

Figure 39: Cross-section of excavation trench at the 6-NS-1 Test Panel. Modified from van Ballegooy et al. 2017.

Table 7: Soil layers, soil layer depth ranges, USCS designation, and soil description for the layers identified in the 6-NS-1 Test Panel (van Ballegooy et al. 2017).

Layer	Depth Range	USCS	F.C.	Description
1	0 - 0.1 m	GP		Sandy GRAVEL; grey. Loose (FILL)
2	0.1 - 0.2 m	SP-SM		Gravelly SAND with minor silt and organics; brown. Moist. (FILL)
3	0.2 - 0.4 m	SP		Fine to medium SAND with trace silt; grey. Moist (FILL)
4	0.4 - 0.7 m	ML & SP		Interbedded sandy SILT, SILT and SAND with trace silt with trace gravel and brick fragments; brown, bedded. Moist; bedding, horizontal. (FILL)
5	0.7 - 0.9 m	ML	90 %	Sandy SILT with trace organics; grey. Firm; moist; slightly plastic; organics, rootlets.
6	0.9 - 1.2 m	SM	56 %	Grades to silty fine SAND with trace organics; grey. Moist; organics, rootlets.
7	1.2 - 1.5 m	SM	56 %	Grades to fine to medium SAND with some silt and trace organics; grey. Wet; organics, rootlets.
8	1.5 - 2.6 m	SP	11 %	Grades to fine to medium SAND with trace silt and trace organics; grey. Wet; organics, rootlets.

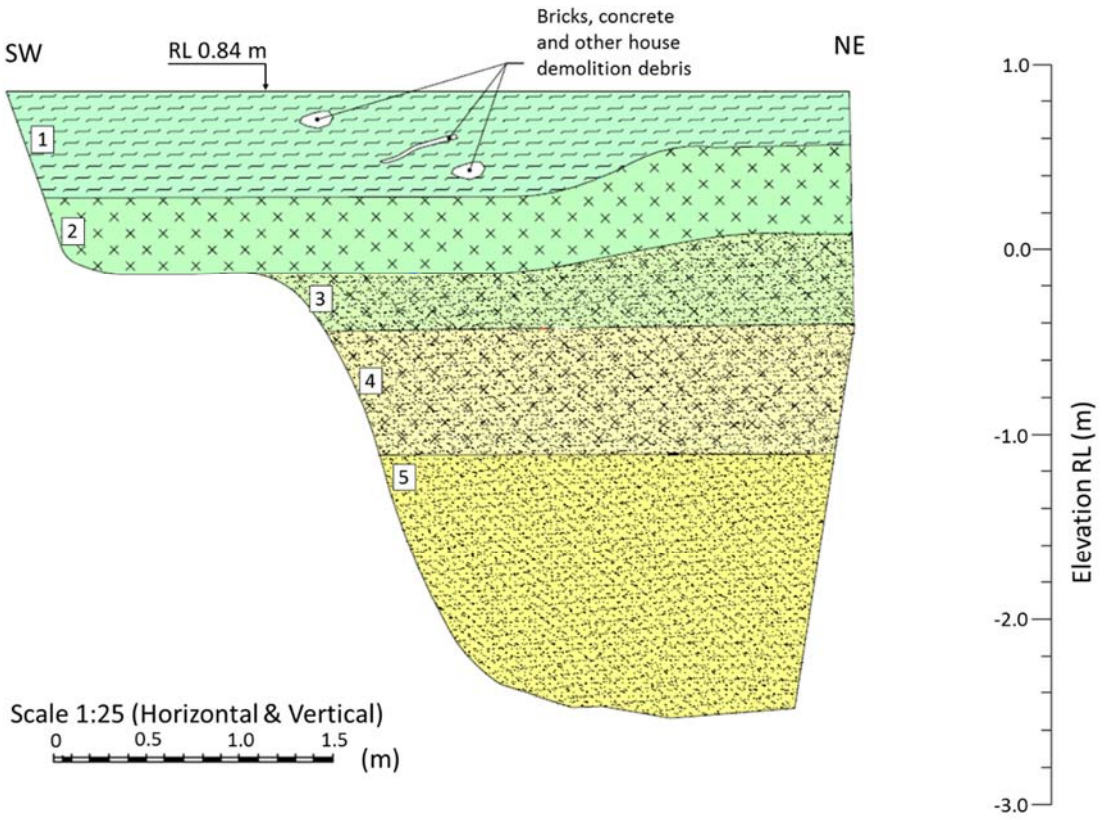

Figure 40: Cross-section of excavation trench at the 6-NS-2 Test Panel. Modified from van Ballegooy et al. 2017.

Table 8: Soil layers, soil layer depth ranges, USCS designation, and soil description for the layers identified in the 6-NS-2 Test Panel (van Ballegooy et al. 2017).

Layer	Depth Range	USCS	F.C.	Description
1	0 - 0.6 m	SP-SM		Fine to medium SAND some organics; dark brown. Loose; moist; organics, rootlets; abundant rubbish. (FILL)
2	0.6 - 1.0 m	ML	96 %	SILT with trace organics; mottled grey and brownish orange, homogenous. Stiff; non-plastic; dilatent; organics, rootlets.
3	1.0 - 1.25 m	ML	74 %	Sandy SILT; grey, homogenous. Stiff, non-plastics; dilatent.
4	1.25 - 1.9 m	SM	3 - 25 %	Silty fine SAND; grey, homogenous. Loose; wet.
5	1.9 - 3.3 m	SW	3 %	Fine to medium SAND with trace silt.

The trench cross-sections and laboratory testing on specimens taken from the trenches show that several of the silt layers contain traces of organic materials and pockets of material with plasticity indexes as high as 90 %. The majority of the silt layers, however, are firm and non-plastic with measured fines contents as high as 91 %.

Results from the CPT also provide insight into the layering and soil composition at the natural soil profiles, allowing general comparisons across sites. The summary in Table 9 shows the average distribution of the I_C value in the top 4 m of the soil profile, categorized by various normalized soil behavior types. The majority of the soils at Site 3, Site 4, and Site 6 fall into the two categories sands and sand mix based on the I_C value, confirming the results from the trench excavations that described soils primarily ranging from sands to silts. With the largest proportion of a soil profile corresponding to an I_C value less than 2.05, the sands at Site 3 appear in general to have lower fines contents than those at Site 4 or Site 6, whose proportions are similarly distributed. Overall, however, the sites have quite similar profiles consisting of thick silt layers at the surface that are underlain by several meters of sands whose fines content decreases with depth.

Table 9: Average distribution of the Soil Behavior Type Index, I_C, over the top 4 m at Site 3, Site 4, and Site 6.

I_C Value	Soil Behavior Type	Site 3 % of top 4 m	Site 4 % of top 4 m	Site 6 % of top 4 m
$1.31 < I_C < 2.05$	Sands	71	50	58
$2.05 < I_C < 2.60$	Sand Mix	28	45	31
$2.60 < I_C < 2.95$	Silt Mix	1	3	8
$2.95 < I_C < 3.60$	Clays	0	2	2

4.5 COMPRESSION WAVE VELOCITY AND DEPTH OF THE 100 % SATURATION

One of the conditions considered necessary for soil liquefaction is a degree of saturation close to 100 %. Compression wave velocity results from DPCH tests show that the actual depth to 100 % saturation is from about 1.0 to 3.0 m below the depth to the water table at the three test sites. The compression wave velocity profiles in Figure 41 show the large variation in depths to saturation below the ground water table at each of the three test sites, as signified by the depth at which compression wave velocity equals or exceeds 1,450 m/s. The depth to continuous saturation below the ground surface ranges from 2.7 to 3.2 m at Site 3 (2.0 to 2.5 m below the water table), 1.6 to 3.4 m at Site 4 (0.9 to 2.7 m below the water table), and 1.4 to 1.7 m at Site 6 (0.9 to 1.2 m below the water table. These results even show temporary, perched zones of 100 % saturation at depths 1.6 to 1.8 m below the ground surface at 3-NS-2 and 1.8 to 2.4 m at 4-NS-2, revealing a complicated transition zone starting from the unsaturated conditions above the water table down to the fully saturated soils several meters below the water table.

These test results show the natural variation in the degree of saturation below the water table, which is separate from de-saturation that may result from the construction methods of various ground improvement types. At the time of testing in 2013, the tide in the Avon River due to its proximity to the Pacific Ocean was responsible for an average fluctuation to the water table elevation of ± 20 centimeters; this fluctuation is too small to have much influence on the depth to 100 % saturation relative to the ground water table.

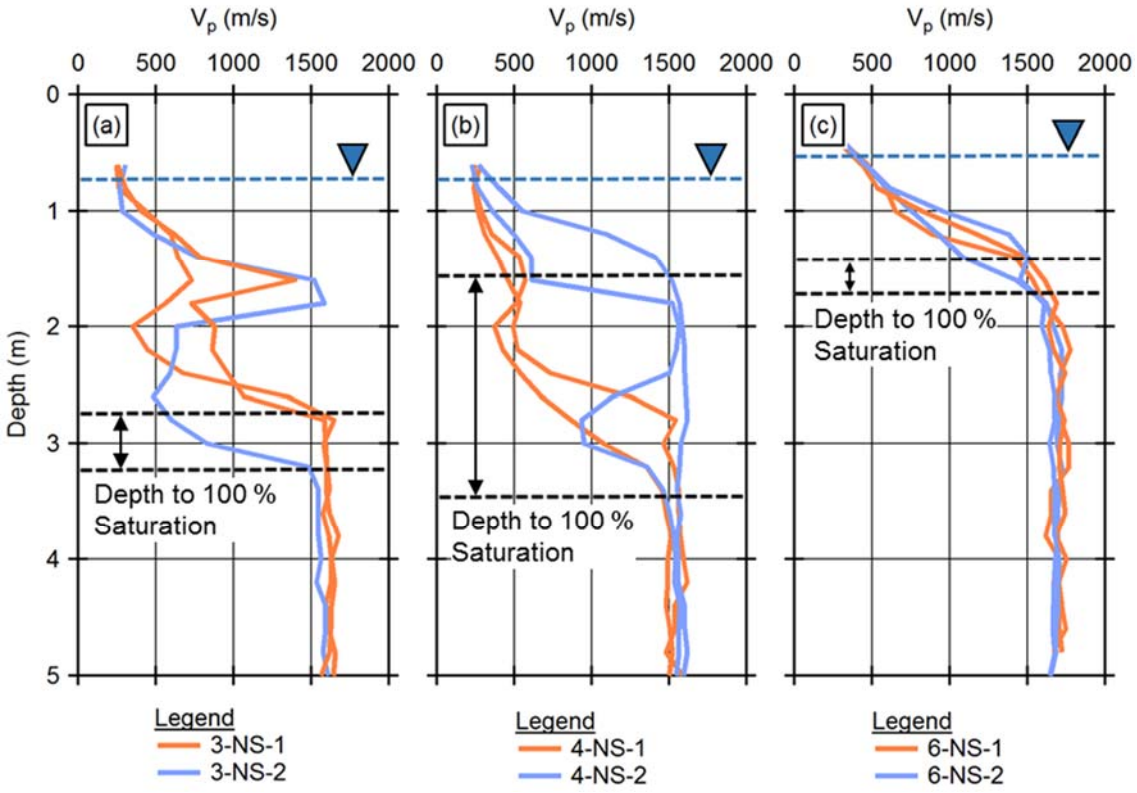

Figure 41: Compression wave velocity profiles from the natural soil test panels at: (a) Site 3, (b) Site 4, and (c) Site 6.

4.6 SUMMARY

The focus of this chapter was the characterization of the natural soils at Site 3, Site 4, and Site 6. CPT tests were used to investigate the subsurface layering and to develop median profiles of corrected cone tip resistance q_t, sleeve friction resistance f_s, and normalized soil behavior type index I_c for Site 3, Site 4, and Site 6. DPCH tests were used to develop median compression and shear wave velocity profiles for Site 3, Site 4, and Site 6. These median profiles represent the natural ground conditions at each of the test sites and serve as the baseline against which the ground improvement methods will be assessed. The excavation trenches were used to visually confirm the layering at each of the natural soil test panels and to obtain disturbed soil samples for laboratory testing.

Chapter 5: Evaluation of the RIC, RAP, and LMG Ground Improvement Methods Using CPT and DPCH

5.1 INTRODUCTION

The three ground improvement methods RIC, RAP, and LMG were evaluated using CPT and DPCH tests to determine their effectiveness at increasing the density and stiffness of the natural soil as indicated by the cone tip resistance and shear modulus, respectively. The effectiveness of each ground improvement method was evaluated by comparing the test results from CPT and DPCH tests at the ground-improved test panels against the CPT and DPCH tests of the natural soils. The analysis focuses specifically on relative changes in q_t and G_{max} rather than absolute changes and also on understanding this variation as a function of depth down to 4.0 m below the ground surface, the maximum depth to which these ground improvement methods were intended to improve the soil. To create a fair comparison of results between the CPT and DPCH tests, data from depths shallower than 0.6 m were omitted because the DPCH test started at a depth of 0.6 m at Site 3 and Site 4. This also has the benefit of further simplifying the analysis because it eliminates soils that are above the water table.

Information from the excavation trenches was used to visually assess construction quality of the ground improvement methods and identify soil layering that may contribute or inhibit the effectiveness of the ground improvement methods.

5.2 EVALUATION OF THE RIC GROUND IMPROVEMENT METHOD

The RIC ground improvement method aims to reduce the risk of soil liquefaction by densifying the natural soil in the top 4.0 m of the ground surface. The q_t parameter from CPT testing and the shear wave velocity from DPCH testing are sensitive to changes in soil density, making them both useful tools for evaluating the effectiveness of the RIC ground improvement method.

5.2.1 RIC – Variation in q_t from CPT Testing

The CPTs pushed between RIC impact points at each test panel were performed at time intervals 14, 28, and 90 days after the construction of the test panel to observe the effect on time. The results show no meaningful effect of time on the effectiveness of the ground improvement method and therefore the effect of time is not considered any further. The q_t traces presented in Figure 42a through Figure 42c show the results from CPT testing at the RIC test panels as well as the median natural soil q_t profile for Site 3, Site 4, and Site 6, respectively. The relative change in q_t due to the RIC ground improvement at all three sites is shown in Figure 42d and is calculated using the median q_t profile for the given test panel in comparison to the median natural soil q_t profile for each site using the following formula:

$$\frac{\left(q_{t,RIC} - q_{t,Natural\ Soil}\right)}{q_{t,Natural\ Soil}} \times 100\ \% \qquad (6)$$

Only results down to a depth of 4.0 m are used to assess the relative change in q_t because the ground improvement method was only intended to improve down to that depth. The results also omit data shallower than 0.6 m for fair comparison against the shear wave velocity results from DPCH testing that start at a depth of 0.6 m. For each profile of relative change in q_t at the 3-RIC-1, 4-RIC-1, and 6-RIC-1 test panels, the median, mean, minimum, and maximum values as well as the standard deviation were calculated to help understand the variation of q_t within a single test panel. These statistical parameters are summarized in Table 10.

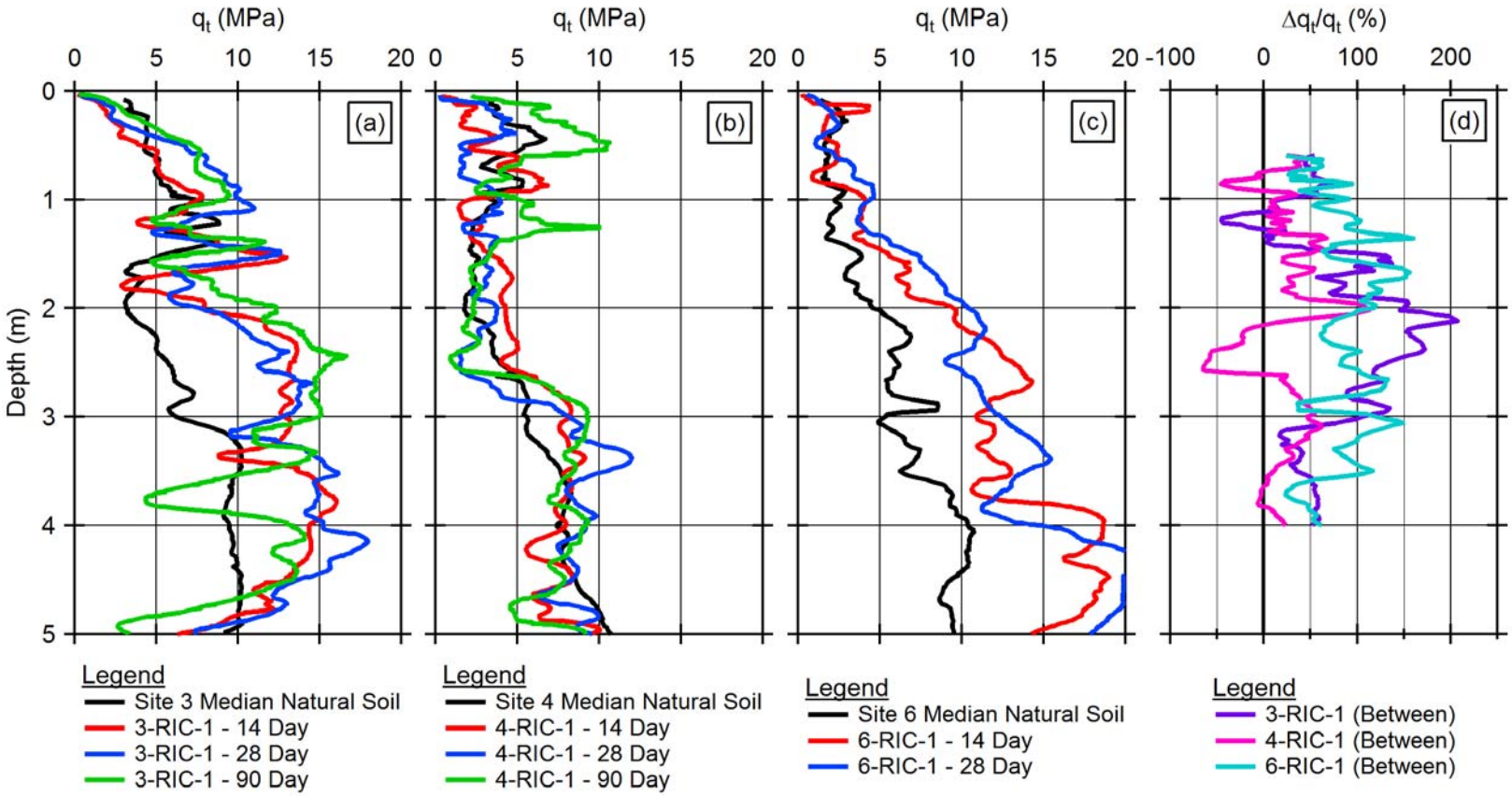

Figure 42: Profiles of q_t from CPT testing between the RIC impact points at (a) Site 3, (b) Site 4, and (c) Site 6 with the median natural soil profiles for each respective site. The relative change in q_t in subplot (d) shows the variation of q_t in relation to the median natural soil q_t profile at each site.

Table 10: Summary of statistical parameters for the relative variation in q_t resulting from the RIC ground improvement method at the 3-RIC-1, 4-RIC-1, and 6-RIC-1 test panels.

	3-RIC-1 $\Delta q_t/q_t$ (%)	4-RIC-1 $\Delta q_t/q_t$ (%)	6-RIC-1 $\Delta q_t/q_t$ (%)
Median:	60	24	86
Mean:	78	19	85
Standard Deviation:	56	35	33
Minimum:	-46	-65	23
Maximum:	207	112	160

The q_t parameter shows a large variation in the effectiveness of the RIC ground improvement method to consistently densify soil within the zone of interest 0.6 to 4.0 m as well as across test panels. The relative change in q_t ranges from -46 to 207 % at the 3-RIC-1 test panel, from -65 to 112 % at the 4-RIC-1 test panel, and from 23 to 160 % at the 6-RIC-1 test panel. Further, the results of CPT testing at the 4-RIC-1 test panel indicate little to no consistent densification in the top 4 m with a median increase in q_t of only 24 % (and a standard deviation of 35 %) while the results at Site 6 indicate greater increases in density with a median increase in q_t of 86 %. The results at Site 3 also show improvement with a median increase in q_t of 60 %, though with less consistency than at Site 6 as indicated by a larger standard deviation (56 % for 3-RIC-1 versus 33 % for 6-RIC-1). Median increases in q_t of 60 % at 3-RIC-1, 24 % at 4-RIC-1, and 86 % at 6-RIC-1 all indicate that the RIC ground improvement method is densifying the natural soil, but it is difficult to know precisely how it influences the liquefaction susceptibility of the soil any further than this simple comparative study and whether it is sufficient for achieving its goals.

5.2.2 RIC – Variation in V_S from DPCH Testing

Shear wave velocities were measured using DPCH testing both between and across the RIC impact points to assess the increase in stiffness caused by the densification of the soil. Performing DPCH testing between and across the impact points also provided an opportunity to see if there is any meaningful variation in densification of the soil directly beneath the impact point versus the soil adjacent to the impact point.

The shear wave velocity profiles presented in Figure 43a through Figure 43c show the results from DPCH testing between the impacts points at the RIC test panels as well as the median natural soil V_S profile for Site 3, Site 4, and Site 6, respectively. The V_S profiles from DPCH testing across the impact points with the median natural soil V_S profile for Site 3, Site 4, and Site 6, respectively, are shown in Figure 44a through Figure 44c.

The relative change in G_{max} between impact points due to the RIC ground improvement at all three sites is shown in Figure 43d and is calculated using the median G_{max} profile between impact points for the given test panel in comparison to the median natural soil G_{max} profile for each site using the following formula:

$$\frac{\left(G_{max,RIC\ (between)} - G_{max,Natural\ Soil}\right)}{G_{max,Natural\ Soil}} \times 100\ \% \qquad (7)$$

The relative change in G_{max} across impact points due to the RIC ground improvement at all three sites is shown in Figure 44d and is calculated using the median G_{max} profile across impact points for the given test panel in comparison to the median natural soil G_{max} profile for each site using the following formula:

$$\frac{\left(G_{max,RIC\ (across)} - G_{max,Natural\ Soil}\right)}{G_{max,Natural\ Soil}} \times 100\ \% \qquad (8)$$

Only results down to a depth of 4.0 m are used to assess the relative change in G_{max} because the ground improvement method was only intended to improve down to that depth.

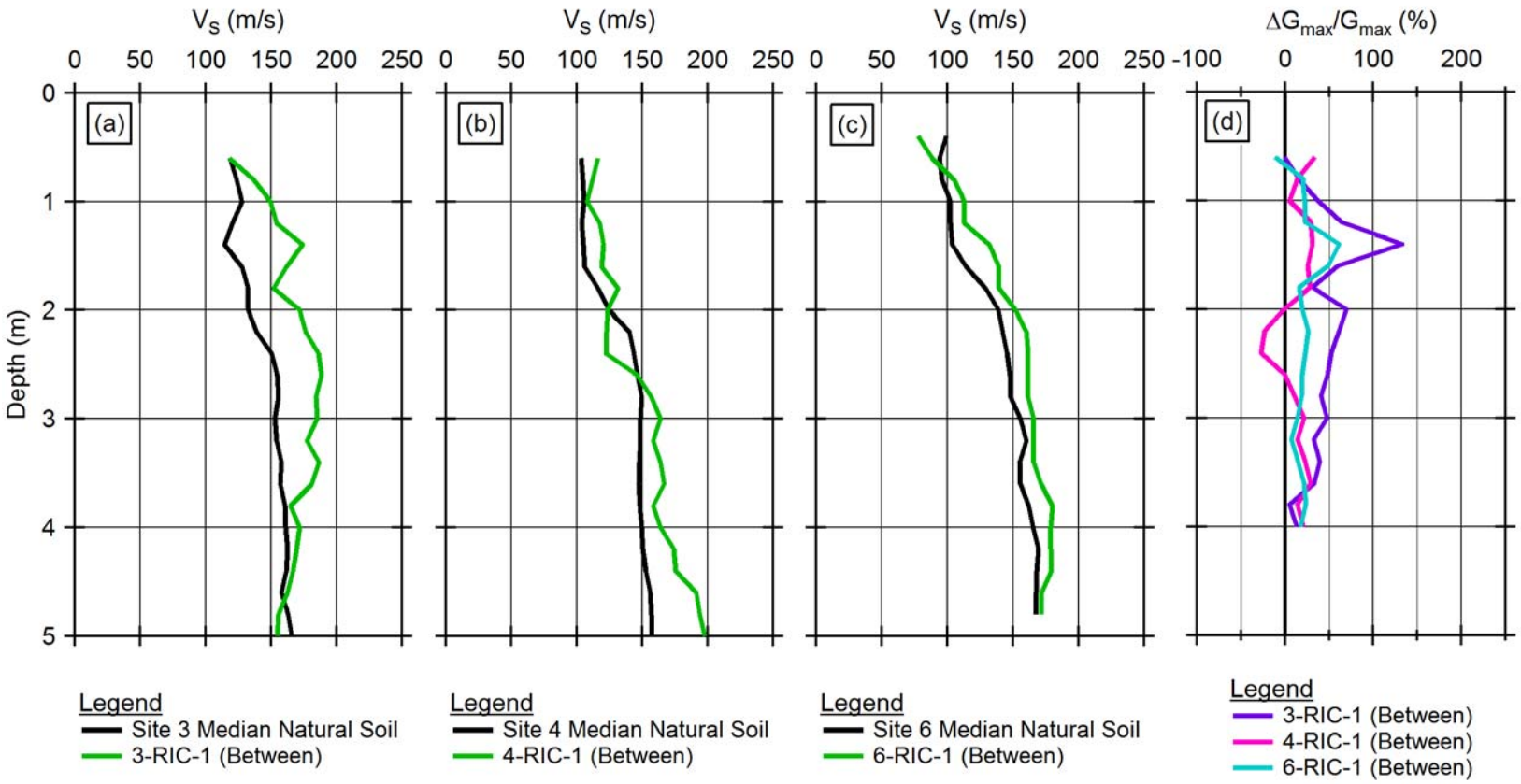

Figure 43: Shear wave velocity profiles from DPCH testing between the RIC impact points at (a) Site 3, (b) Site 4, and (c) Site 6 with the median natural soil profiles for each respective site. The relative change in G_{max} in subplot (d) shows the variation of G_{max} in relation to the median natural soil G_{max} profile at each site.

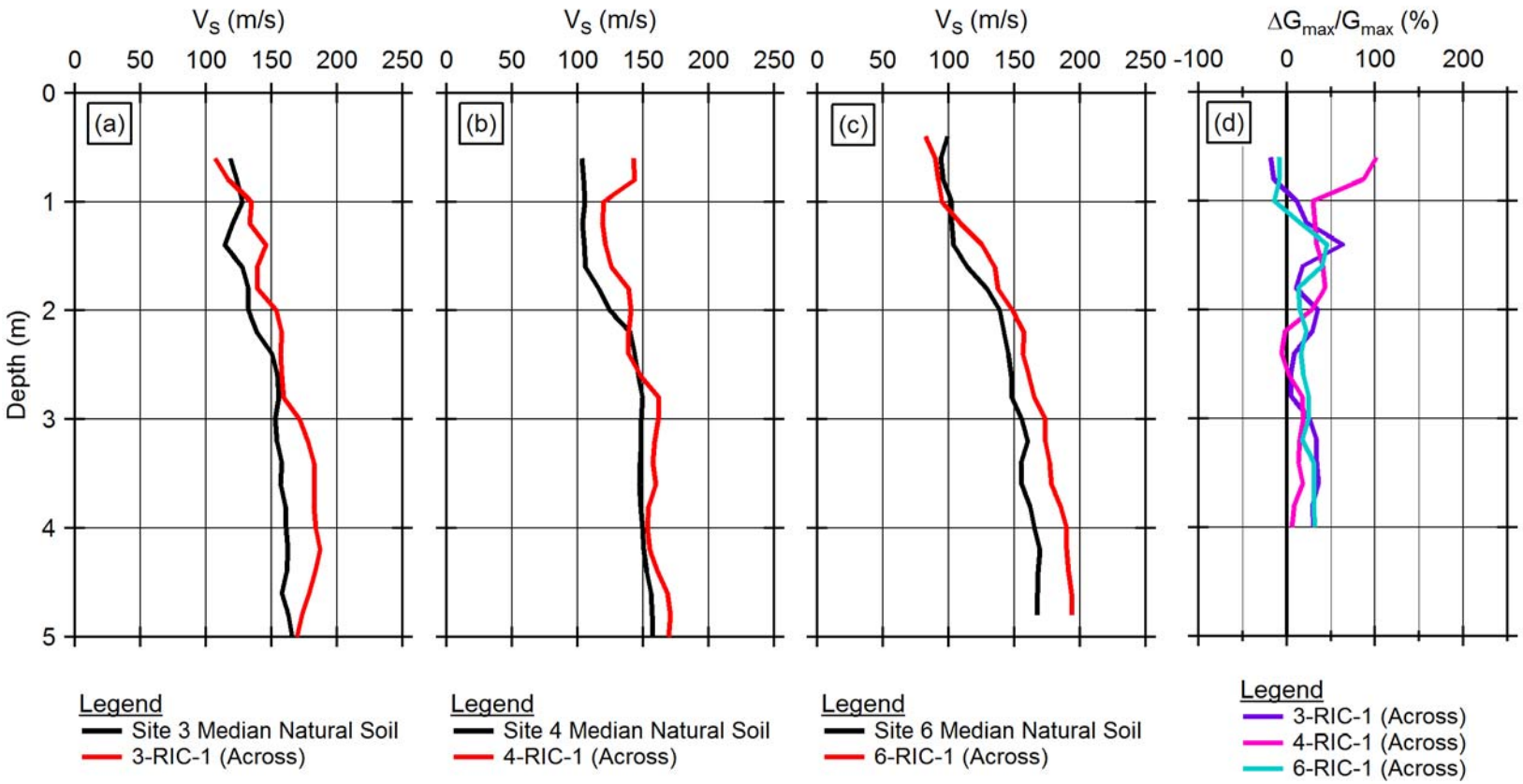

Figure 44: Shear wave velocity profiles from DPCH testing across the RIC impact points at (a) Site 3, (b) Site 4, and (c) Site 6 with the median natural soil profiles for each respective site. The relative change in G_{max} in subplot (d) shows the variation of G_{max} in relation to the median natural soil G_{max} profile at each site.

For each profile of relative change in G_{max} at the 3-RIC-1, 4-RIC-1, and 6-RIC-1 test panels, the median, mean, minimum, and maximum values as well as the standard deviation were calculated to help understand the variation of G_{max} within a single test panel. These statistical parameters for the relative variation in G_{max} between RIC impact points are summarized in Table 11 and for the relative variation in G_{max} across RIC impact points are summarized in Table 12.

Table 11: Summary of statistical parameters for the relative variation in G_{max} between impact points resulting from the RIC ground improvement method at the 3-RIC-1, 4-RIC-1, and 6-RIC-1 test panels.

	3-RIC-1 (Between) $\Delta G_{max}/G_{max}$ (%)	4-RIC-1 (Between) $\Delta G_{max}/G_{max}$ (%)	6-RIC-1 (Between) $\Delta G_{max}/G_{max}$ (%)
Median:	40	17	20
Mean:	43	14	21
Standard Deviation:	30	18	15
Minimum:	0	-27	-12
Maximum:	132	33	61

Table 12: Summary of statistical parameters for the relative variation in G_{max} across impact points resulting from the RIC ground improvement method at the 3-RIC-1, 4-RIC-1, and 6-RIC-1 test panels.

	3-RIC-1 (Across) $\Delta G_{max}/G_{max}$ (%)	4-RIC-1 (Across) $\Delta G_{max}/G_{max}$ (%)	6-RIC-1 (Across) $\Delta G_{max}/G_{max}$ (%)
Median:	24	18	20
Mean:	20	27	19
Standard Deviation:	20	28	16
Minimum:	-18	-6	-14
Maximum:	63	102	46

The median relative changes in G_{max} at test panels 4-RIC-1 and 6-RIC-1 are almost identical for values measured between and across the RIC impact points, indicating the RIC ground improvement method consistently densified the soil throughout the test panel

without large variations between impact points. The results at test panel 3-RIC-1 show large increases in G_{max} between the RIC impact points that exceed values seen at any of the other test panels, but the results from the 3-RIC-1 test panel measured across the impact points are similar in magnitude to those at test panels 4-RIC-1 and 6-RIC-1. In all cases, the minimum relative change in G_{max} is zero or negative, indicating that it is difficult to densify the soil at all depths within the top 4.0 m. In general, the negative values of change in G_{max} occur in the top 1.0 m of the profile; this loosening may result from insufficient overburden pressure in the soil to prevent heave during the impaction process.

In the case of test panel 4-RIC-1, however, there is a zone in the depth range of 2.2 to 2.6 m that is noticeably softer than the surrounding soil in both the between and across impact point G_{max} profiles. This soft zone is also observed in the CPT results for the relative change in q_t shown in Figure 42d, but the reason for this soft spot in unknown, particularly since according to the trench cross-section illustrated in Figure 47, the soft spot appears to be located in the middle of a thick, silty sand layer that gives no indication of being softer than the surrounding soil.

5.2.3 RIC – Comparison of Results Across Test Methods

In general, the results from CPT and DPCH testing show that the RIC ground improvement method can create modest increases in the overall density as well as build up horizontal stresses in the soil but also that there are isolated portions of the profile where the soil is likely to be loosened. The main difference between the CPT and DPCH testing results is that CPT method showed large variations in the median level of improvement between test panels (ranging from 24 to 86 % increase in q_t) while the DPCH testing both between and across impact points showed the median level of improvement was very consistent between test panels (17 – 24 % increase in G_{max}, not including the outlier from DPCH testing at the 3-RIC-1 test panel between impact points).

Remarkably both test methods identify depths at which the q_t or G_{max} of the RIC test panel is less than the corresponding values in the natural soil, indicating either that the RIC ground improvement method loosened the soil at depth or that there is a soft layer at the 4-RIC-1 test panel that is not present at the other test panels at Site 4. In Figure 45, the median, mean, minimum, and maximum values of relative change in q_t and G_{max} evaluated at test panels 3-RIC-1, 4-RIC-1, and 6-RIC-1 are presented for comparison. A comparison of these statistical parameters from each of the test methods reveals the following four conclusions. First, the relative change in q_t and G_{max} between impact points shows similar trends at 3-RIC-1 and 4-RIC-1, though at 6-RIC-1 the relative change in q_t indicates greater improvement in the test panel than the relative change in G_{max}. Second, the improvement in the soil between impact points at 4-RIC-1 as measured by the relative change in q_t and G_{max} is consistently lower than at the other sites. Third, the minimum value of relative change in q_t and G_{max} is zero or negative at all RIC test panels, indicating loosening of the

soil at some depths. Fourth, the median relative change in G_{max} between and across impact points is relatively constant across all three of the test panels.

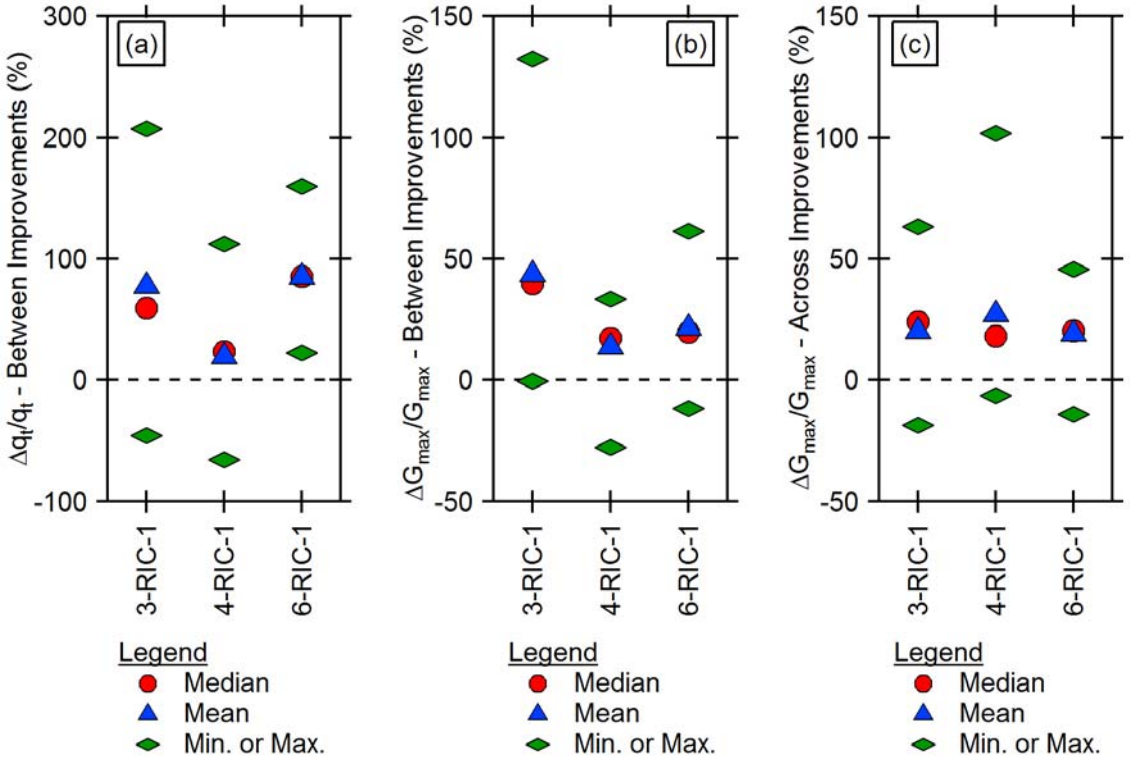

Figure 45: Summary of the median, mean, minimum, and maximum values of relative change caused by the RIC ground improvement at Site 3, Site 4, and Site 6 as evaluated by (a) the change in q_t between the impact points, (b) the change in G_{max} between impact points, and (c) the change in G_{max} across the impact points in comparison to the natural soil.

5.2.4 RIC – Trench Cross-Sections

The excavation of the RIC test panels provided an opportunity to visually identify and categorize soil layers in the subsurface and to obtain samples for laboratory testing. The trench cross-sections for 3-RIC-1, 4-RIC-1, and 6-RIC-1 are presented in Figure 46 through Figure 48, respectively. The details regarding layer thickness, USCS designation, estimated fines content, and soil description are summarized in Table 13 through Table 15 for test panels 3-RIC-1, 4-RIC-1, and 6-RIC-1, respectively.

The soil profile at 3-RIC-1 match closely with the natural soil test panels at Site 3. The soil profile at 4-RIC-1 features significantly less silt in the top 1.5 m in comparison to the natural soil test panels at Site 4 and is overall a predominantly sandy profile. The soil profile at 6-RIC-1 matches very closely to the natural soil test panel 6-NS-1 and is less silty than the natural soil test panel 6-NS-2.

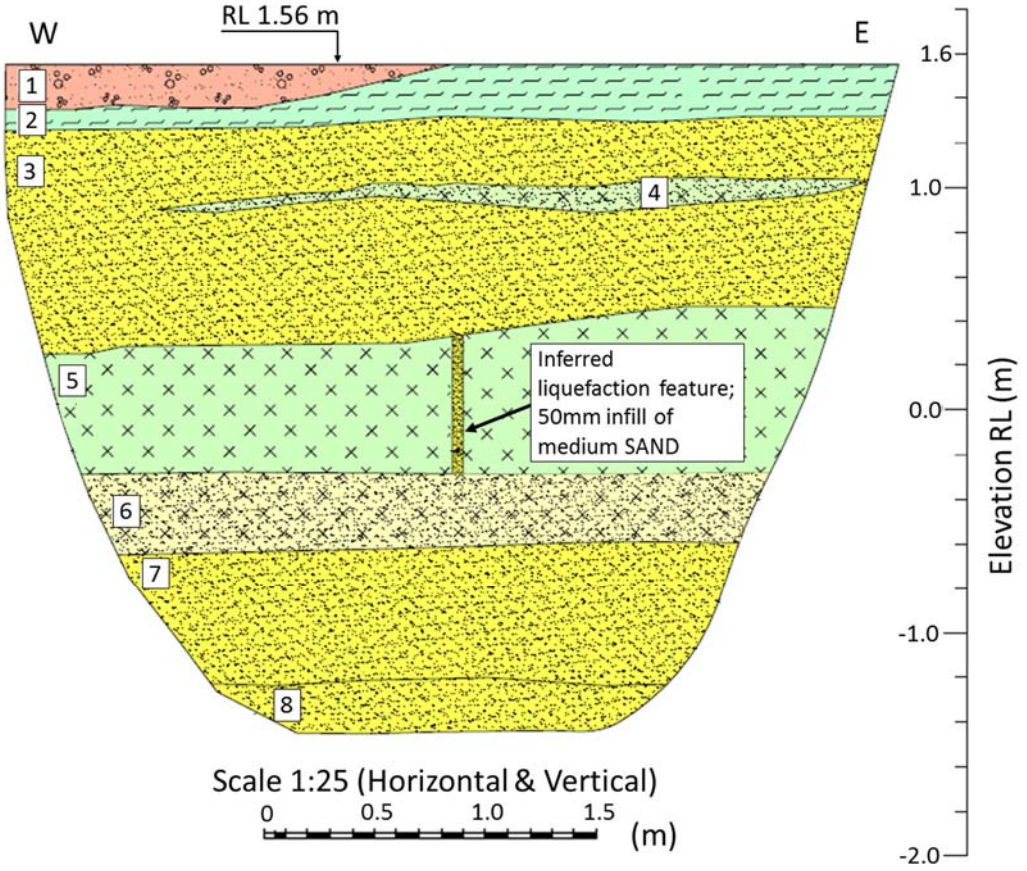

Figure 46: Cross-section of the excavation trench at the 3-RIC-1 Test Panel. Modified from van Ballegooy et al. 2017.

Table 13: Soil layers, soil layer depth ranges, USCS designation, and soil description for the layers identified in the 3-RIC-1 Test Panel (van Ballegooy et al. 2017).

Layer	Depth Range	USCS	F.C.	Description
1	0 - 0.2 m	GP		Medium GRAVEL. Loose; poorly graded. (FILL)
2	0 - 0.3 m	OL		Topsoil with rootlets. (FILL)
3	0.3 - 1.2 m	SP		Fine to medium SAND, yellowish brown. Loose to very loose; moist; massive. (FILL)
4	0.5 - 0.55 m (lens)	ML		Sandy SILT with minor organic fragments and lensoid inclusions; brownish black. Very stiff; moist; non-plastic; inclusions are silt, grey, medium dense, moist, non-plastic. (FILL)
5	1.2 - 1.9 m	CL	89 % (PI = 8 %)	SILT with minor sand; grey. Very stiff, moist, low plasticity; sand, fine to medium, occur as occasional thin laminae.
6	1.9 - 2.2 m	SM	31 %	Silty fine to medium SAND; grey. Loose, saturated.
7	2.2 - 2.8 m	SP		Fine to medium SAND; grey. Loose, saturated.
8	2.8 - 3.0 m	SP		Medium SAND; grey. Loose; saturated; poorly graded.

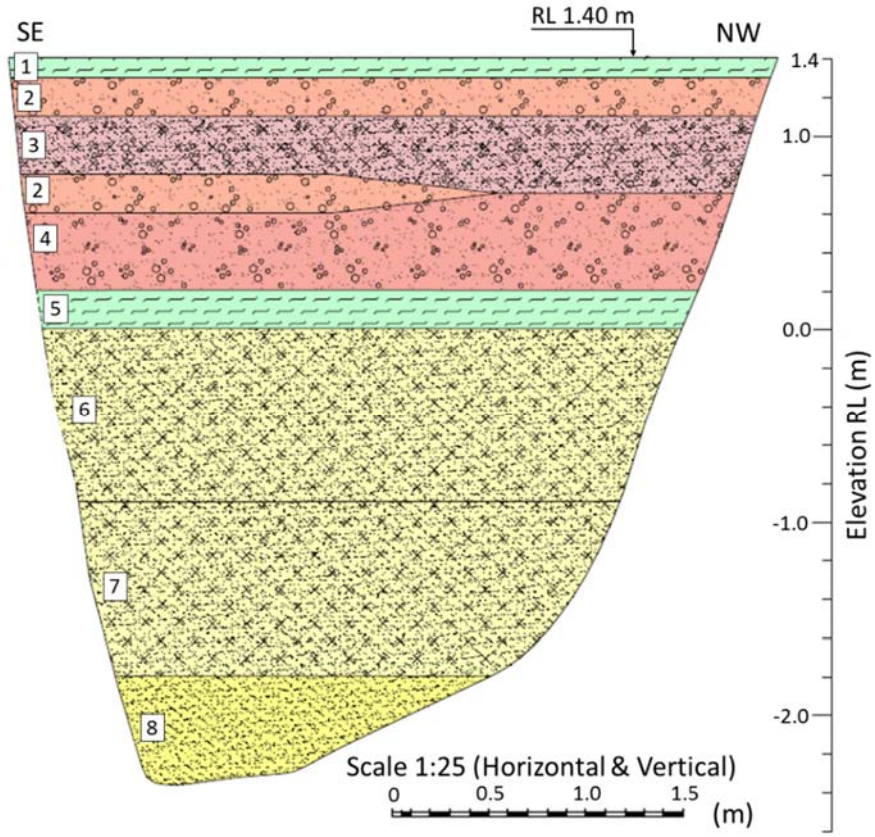

Figure 47: Cross-section of excavation trench at the 4-RIC-1 Test Panel. Modified from van Ballegooy et al. 2017.

Table 14: Soil layers, soil layer depth ranges, USCS designation, and soil description for the layers identified in the 4-RIC-1 Test Panel (van Ballegooy et al. 2017).

Layer	Depth Range	USCS	F.C.	Description
1	0 - 0.1 m	OL		Topsoil
2	0.1 - 0.3 m 0.6 - 0.8 m	GP		Medium GRAVEL (FILL).
3	0.3 - 0.6 m	SP		Silty SAND with some gravel; grey, homogeneous (FILL).
4	0.7 - 1.2 m	SP		Gravelly fine to medium SAND; brown. Loose.
5	1.2 - 1.4 m	OL	84 %	SILT with organics; black. Firm to stiff; low plasticity; slightly dilatent; organics, amorphous, odorous.
6	1.4 - 2.3 m	SM	43 - 74 %	Silty fine SAND with minor organics; grey, bedded. Loose; organics, rootlets; bedding, horizontal bedded laminae of silt with minor fine sand in places.
7	2.3 - 3.2 m	SM	43 %	Silty fine SAND with some organics; grey. Loose; organics, fibrous & wood up to 80mm diameter.
8	3.2 - 3.8 m	SP	4 %	Fine to medium SAND with trace silt; grey. Loose.

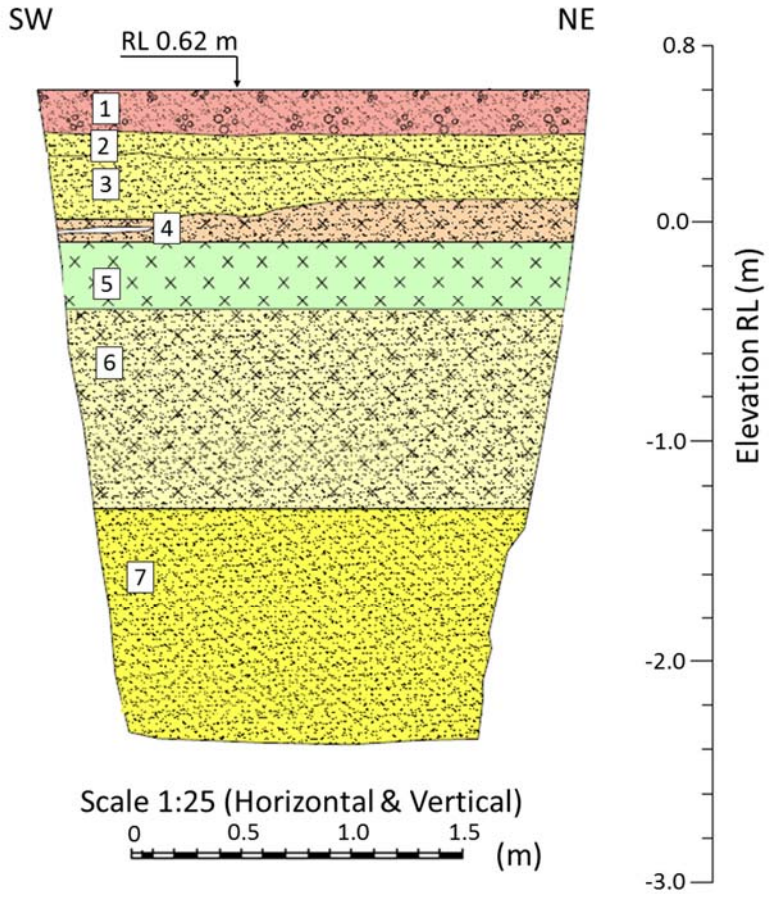

Figure 48: Cross-section of excavation trench at the 6-RIC-1 Test Panel. Modified from van Ballegooy et al. 2017.

Table 15: Soil layers, soil layer depth ranges, USCS designation, and soil description for the layers identified in the 6-RIC-1 Test Panel (van Ballegooy et al. 2017).

Layer	Depth Range	USCS	F.C.	Description
1	0 - 0.2 m	GM		Sandy GRAVEL with some organic silt; grey. Dry; organics, rootlets. (FILL)
2	0.2 - 0.3 m	SP		Fine to medium SAND with trace silt and organics; grey. Moist. (FILL).
3	0.3 - 0.5 m	SP		Fine to medium SAND with trace silt; light brown. Moist; silt is in clasts. (FILL).
4	0.5 - 0.7 m			Silty SAND interbedded with SILT with minor sand; brown. Moist. Occasional fine to coarse gravel.
5	0.7 - 1.0 m	CL-ML	90 % (PI=5 %)	SILT with minor sand and minor organics; grey. Wet; organics, rootlets.
6	1.0 - 1.9 m	SP	11 %	Grade to silty fine to medium SAND with trace organics; grey. Wet; organics, rootlets.
7	1.9 - 2.9 m	SP	2 %	Grades to SAND with trace silt; grey. Wet.

5.3 ASSESSMENT OF THE RAP GROUND IMPROVEMENT METHOD

The RAP ground improvement method aims to reduce the risk of soil liquefaction by creating stiff piers of gravel and densifying the soil surrounding the piers. The q_t parameter from CPT testing and the shear wave velocity from DPCH testing are sensitive to changes in soil density and increases in horizontal stresses, making them both useful for evaluating the effectiveness of the RAP to densify the soil surrounding the gravel piers. However, only the DPCH test is able to evaluate the increase in stiffness due to the gravel piers themselves by measuring the shear wave velocity across the piers.

5.3.1 RAP – Variation in q_t from CPT Testing

The CPTs pushed between RAP gravel piers at each test panel were performed at time intervals 14, 28, and 90 days after the construction of the test panel to observe the effect on time. The results show no meaningful effect of time on the effectiveness of the ground improvement method and therefore the effect of time is not considered any further. The q_t traces presented in Figure 49a through Figure 49c show the results from CPT testing at the RAP test panels as well as the median natural soil q_t profile for Site 3, Site 4, and Site 6, respectively. The relative change in q_t due to the RAP ground improvement at all three sites is shown in Figure 49d and is calculated using the median q_t profile for the given test panel in comparison to the median natural soil q_t profile for each site using the following formula:

$$\frac{\left(q_{t,RAP} - q_{t,Natural\ Soil}\right)}{q_{t,Natural\ Soil}} \times 100\ \% \qquad (9)$$

Only results down to a depth of 4.0 m are used to assess the relative change in q_t because the ground improvement method was only intended to improve down to that depth. The results also omit data shallower than 0.6 m for fair comparison against the shear wave velocity results from DPCH testing that start at a depth of 0.6 m.

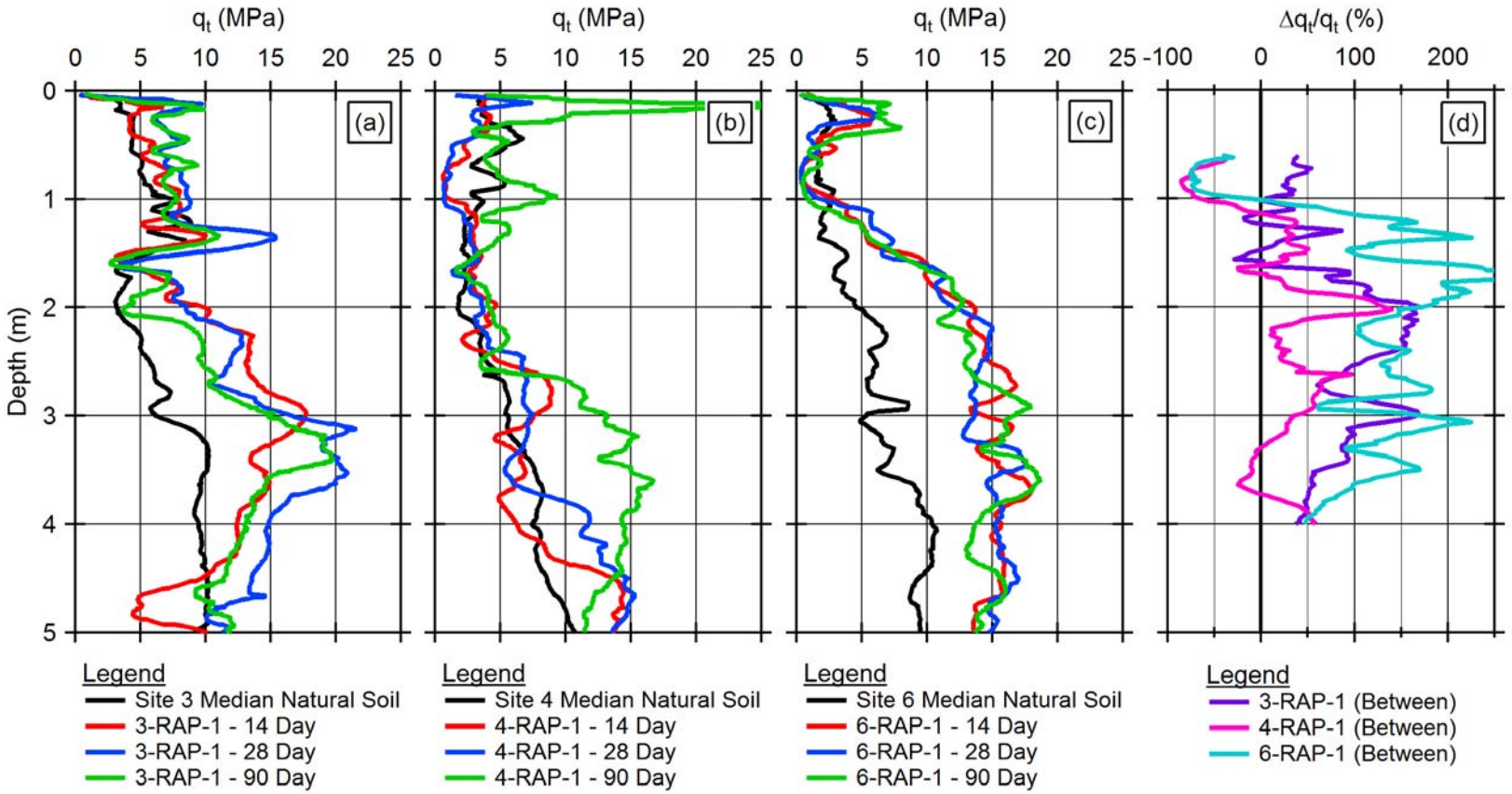

Figure 49: Profiles of q_t from CPT testing between the RAP gravel piers at: (a) Site 3, (b) Site 4, and (c) Site 6 with the median natural soil profiles for each respective site. The relative change in q_t in subplot (d) shows the variation of q_t in relation to the median natural soil q_t profile at each site.

For each profile of relative change in q_t at the 3-RAP-1, 4-RAP-1, and 6-RAP-1 test panels, the median, mean, minimum, and maximum values as well as the standard deviation were calculated to help understand the variation of q_t within a single test panel. These statistical parameters are summarized in Table 16.

Table 16: Summary of statistical parameters for the relative variation in q_t resulting from the RAP ground improvement method at the 3-RAP-1, 4-RAP-1, and 6-RAP-1 test panels.

	3-RAP-1 $\Delta q_t/q_t$ (%)	**4-RAP-1 $\Delta q_t/q_t$ (%)**	**6-RAP-1 $\Delta q_t/q_t$ (%)**
Median:	71	24	128
Mean:	77	18	113
Standard Deviation:	52	47	83
Minimum:	-29	-86	-75
Maximum:	171	140	294

Across test sites, the RAP ground improvement method provides similar increases in q_t, assumed to indicate increases in density of the soil, in the top 4.0 m in comparison to the RIC ground improvement method, but with even greater amounts of variability. Results from test panels 4-RAP-1 and 6-RAP-1 in the top 1.0 m show large changes in q_t down to -86 and -75 %, respectively, perhaps resulting from low confining pressures in the soil that are unable to resist heave in response to large lateral forces from the energetic ramming of the adjacent gravel piers. The 3-RAP-1 test panel does not exhibit consistent, large increases in q_t until depths greater than 1.5 m while the overall increase in q_t is inconsistent at all depths at the 4-RAP-1 test panel. The 6-RAP-1 test panel appears to exhibit the best performance with sustained and consistent increases in q_t at depths greater than 1.0 m. Overall improvement at each of the RAP test panels, however, is tempered by the relatively large standard deviations ranging from 47 to 83 % that reflect the inconsistent magnitude of increases over the depth range of 0.6 to 4.0 m.

The main limitation associated with the evaluation of the RAP ground improvement by pushing CPTs at locations between the gravel piers is that it cannot directly assess the main ground improvement mechanism, which is the gravel piers themselves. The relative change in q_t as measured between the gravel piers at best provides an indirect and imprecise evaluation of the RAP ground improvement's effectiveness in increasing the resistance of the soil to soil liquefaction. In this case, the q_t parameter shows that there is an overall, if highly variable, increase in the density and horizontal stresses of the soil between the gravel piers.

5.3.2 RAP – Variation in V_S from DPCH Testing

Shear wave velocities were measured using DPCH testing both between and across the RAP gravel piers to assess the increase in stiffness caused by the densification of the soil as well as by the presence of the stiff gravel piers. The shear modulus G_{max} is calculated from the shear wave velocity to quantify the increase in stiffness due to the RAP ground improvement; however, G_{max} reported for the measurements across the gravel piers is a loose approximation because the travel path for the shear wave across the gravel piers includes both soil and gravel but the G_{max} value is calculated using a mass density corresponding only to the soil. The accuracy of results from DPCH testing across the gravel pier is further challenged because the true travel path of the shear wave velocity is unknown (e.g. through the middle of the pier or refracted around the outside of the pier). Despite these concerns, the values of shear wave velocity and G_{max} corresponding to the DPCH test across the gravel piers is still useful for a comparative analysis across test sites and in comparison to results obtained between the gravel piers.

The shear wave velocity profiles presented in Figure 50a through Figure 50c show the results from DPCH testing between gravel piers at the RAP test panels as well as the median natural soil shear wave velocity profile for Site 3, Site 4, and Site 6, respectively. The shear wave velocity profiles from DPCH testing across the gravel piers with the median natural soil shear wave velocity profile for Site 3, Site 4, and Site 6, respectively, are shown in Figure 51a through Figure 51c.

The relative change in G_{max} between gravel piers due to the RAP ground improvement at all three sites is shown in Figure 50d and is calculated using the median G_{max} profile between gravel piers for the given test panel in comparison to the median natural soil G_{max} profile for each site using the following formula:

$$\frac{\left(G_{max,RAP\ (between)} - G_{max,Natural\ Soil}\right)}{G_{max,Natural\ Soil}} \times 100\ \% \qquad (10)$$

The relative change in G_{max} across gravel piers due to the RAP ground improvement at all three sites is shown in Figure 51d and is calculated using the median G_{max} profile across gravel piers for the given test panel in comparison to the median natural soil G_{max} profile for each site using the following formula:

$$\frac{\left(G_{max,RAP\ (across)} - G_{max,Natural\ Soil}\right)}{G_{max,Natural\ Soil}} \times 100\ \% \qquad (11)$$

Only results down to a depth of 4.0 m are used to assess the relative change in G_{max} because the ground improvement method was only intended to improve down to that depth.

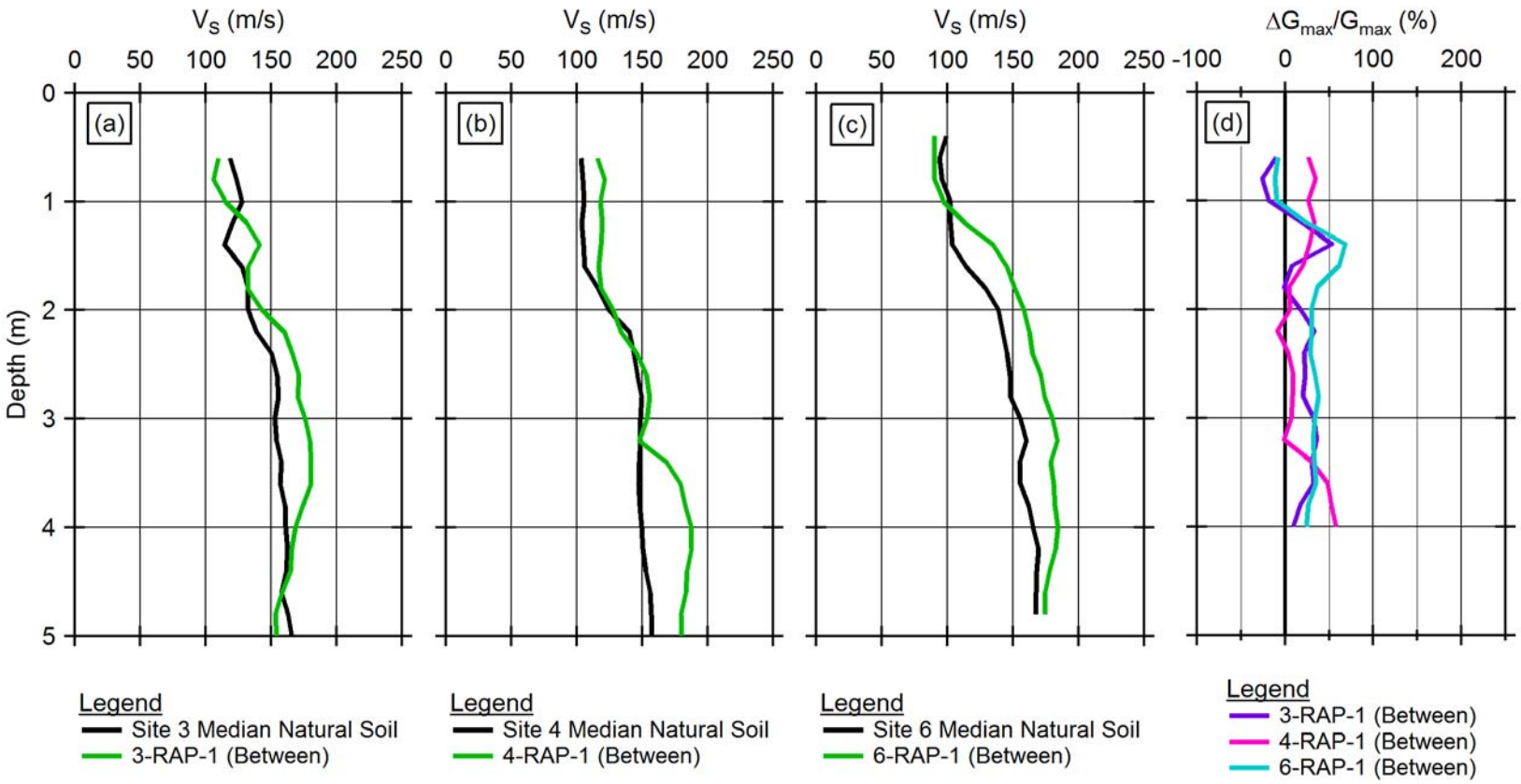

Figure 50: Shear wave velocity profiles from DPCH testing between the RAP gravel piers at (a) Site 3, (b) Site 4, and (c) Site 6 with the median natural soil profiles for each respective site. The relative change in G_{max} in subplot (d) shows the variation of G_{max} in relation to the median natural soil G_{max} profile at each site.

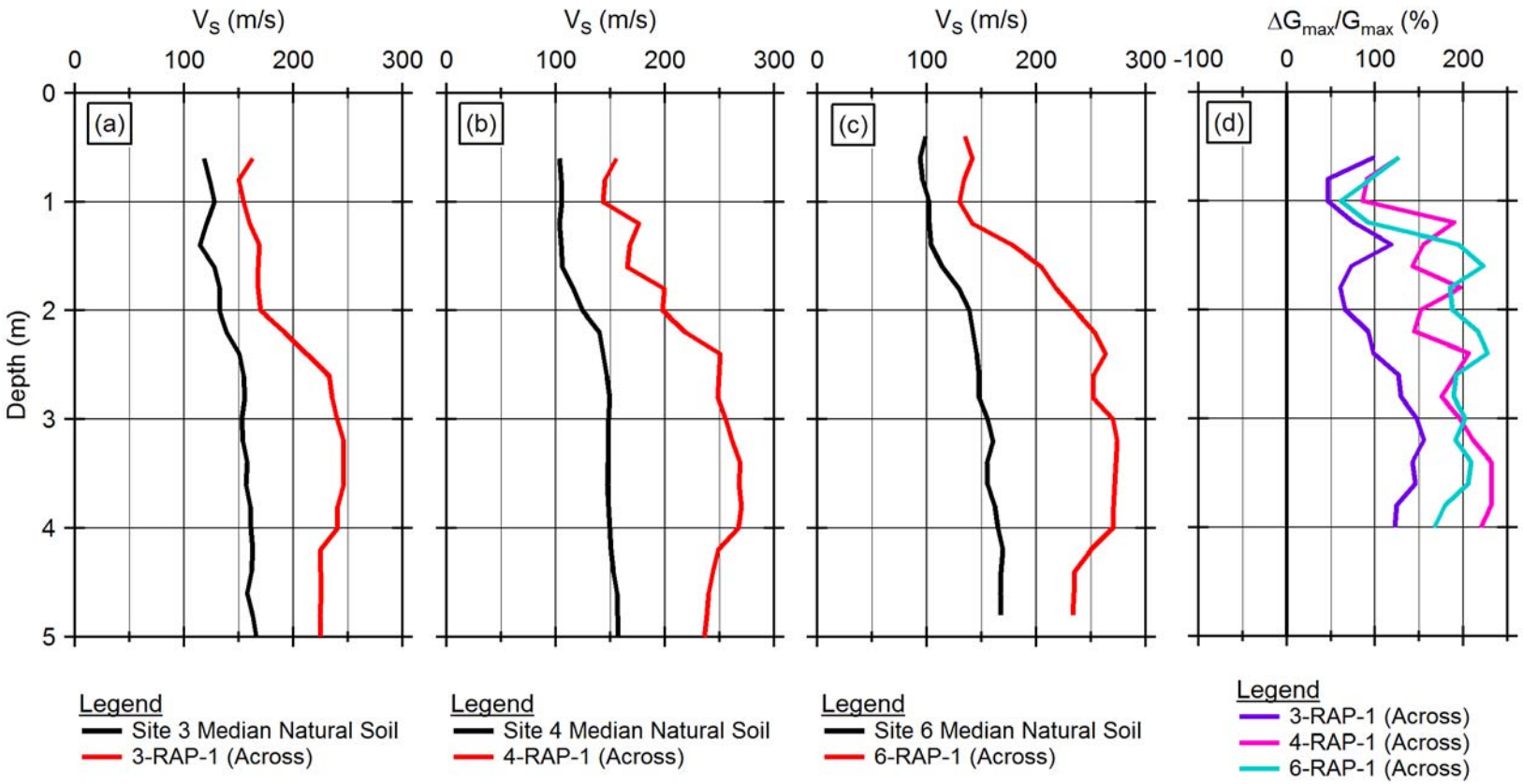

Figure 51: Shear wave velocity profiles from DPCH testing across the RAP gravel piers at (a) Site 3, (b) Site 4, and (c) Site 6 with the median natural soil profiles for each respective site. The relative change in G_{max} in subplot (d) shows the variation of G_{max} in relation to the median natural soil G_{max} profile at each site.

For each profile of relative change in G_{max} at the 3-RAP-1, 4-RAP-1, and 6-RAP-1 test panels, the median, mean, minimum, and maximum values as well as the standard deviation were calculated to help understand the variation of G_{max} within a single test panel. These statistical parameters for the relative variation in G_{max} between RAP gravel piers are summarized in Table 11 and for the relative variation in G_{max} across RAP gravel piers are summarized in Table 12.

Table 17: Summary of statistical parameters for the relative variation in G_{max} between gravel piers resulting from the RAP ground improvement method at the 3-RAP-1, 4-RAP-1, and 6-RAP-1 test panels.

	3-RAP-1 (Between) $\Delta G_{max}/G_{max}$ (%)	4-RAP-1 (Between) $\Delta G_{max}/G_{max}$ (%)	6-RAP-1 (Between) $\Delta G_{max}/G_{max}$ (%)
Median:	19	23	31
Mean:	16	21	28
Standard Deviation:	20	19	21
Minimum:	-26	-9	-12
Maximum:	53	58	68

Table 18: Summary of statistical parameters for the relative variation in G_{max} across gravel piers resulting from the RAP ground improvement method at the 3-RAP-1, 4-RAP-1, and 6-RAP-1 test panels.

	3-RAP-1 (Across) $\Delta G_{max}/G_{max}$ (%)	4-RAP-1 (Across) $\Delta G_{max}/G_{max}$ (%)	6-RAP-1 (Across) $\Delta G_{max}/G_{max}$ (%)
Median:	109	190	190
Mean:	104	176	175
Standard Deviation:	36	46	48
Minimum:	46	86	61
Maximum:	155	232	228

With the RAP ground improvement method, the changes in G_{max} relative to the natural soil that are evaluated between gravel piers come only from variations in the soil state whether it be changes in density or in horizontal stresses. The changes in G_{max} relative

to the natural soil that are evaluated across gravel piers come from the changes in the soil state as well as the presence of gravel, which is a significantly stiffer material than the natural soil.

Looking first at the relative change in G_{max} between the gravel piers, the median value of increase across all three sites ranges from 19 to 31 %, which is similar to the increases seen at the RIC test panels that ranged from 17 to 40 %. Both the RIC and RAP ground improvement methods appear to achieve similar increases in the stiffness of the natural soil. Further, the statistical parameters for measurements between the gravel piers at all three sites are remarkably similar, an indication that for the soil between the gravel piers, the RAP ground improvement method has consistent performance across sites. As with the RIC ground improvement method, however, the minimum relative change in G_{max} between gravel piers is negative at all three test panels. For test panels 3-RAP-1 and 6-RAP-1, this softening occurs in the top 1.0 m of the profile and is possibly caused by low confining pressures in the soil that are unable to prevent heave during the construction process. The relative softening at test panel 4-RAP-1 occurs at depth as it did at the 4-RIC-1 test panel, though not with the same pattern. As with the results from 4-RIC-1, it is not clear why the 4-RAP-1 test panel shows little to no improvement in the depth range of 1.8 to 3.2 m between gravel piers.

In the evaluation of DPCH testing across gravel piers, the statistical parameters for the relative change in G_{max} at test panels 4-RAP-1 and 6-RAP-1 show very similar increases in stiffness along the length of the profile and the magnitude of these increases is very large. The median relative change in G_{max} across piers at the 3-RAP-1 test panel is 109 %, which is considerably smaller than the 190 % median increase seen at the 4-RAP-1 and 6-RAP-1 test panels, however the shapes of the shear wave velocity profiles at all three of the test panels are similar. The minimum relative change in G_{max} across the gravel piers is

positive at all of the RAP test panels and ranges from 46 to 86 %. Even though these results for DPCH test across the gravel piers may not be fully representative of the gravel piers, they show that the gravel piers are significantly and consistently stiffer than the surrounding, natural soil.

5.3.3 RAP – Comparison of Results Across Test Methods

The results from CPT and DPCH testing at the RAP test panels in general show modest but inconsistent increases in density of the soil between gravel piers and large increases in the stiffness across gravel piers. The CPT and DPCH test methods performed between gravel piers identify depths at which the q_t or G_{max} of the RAP test panel is less than the corresponding values in the natural soil, indicating a loosening of the soil. In Figure 52, the median, mean, minimum, and maximum values of relative change in q_t and G_{max} evaluated at test panels 3-RAP-1, 4-RAP-1, and 6-RAP-1 are presented for comparison. A comparison of these statistical parameters from each of the test methods reveals some conclusions from the results: 1) the minimum values of relative change in q_t and G_{max} between gravel piers at all three sites are negative, indicating loosening of the soil at some depths, 2) the median relative change in G_{max} across gravel piers is consistently and significantly larger than the values between gravel piers, 3) the median relative change in G_{max} between gravel piers is relatively constant across all three test panels, indicating homogenous densification.

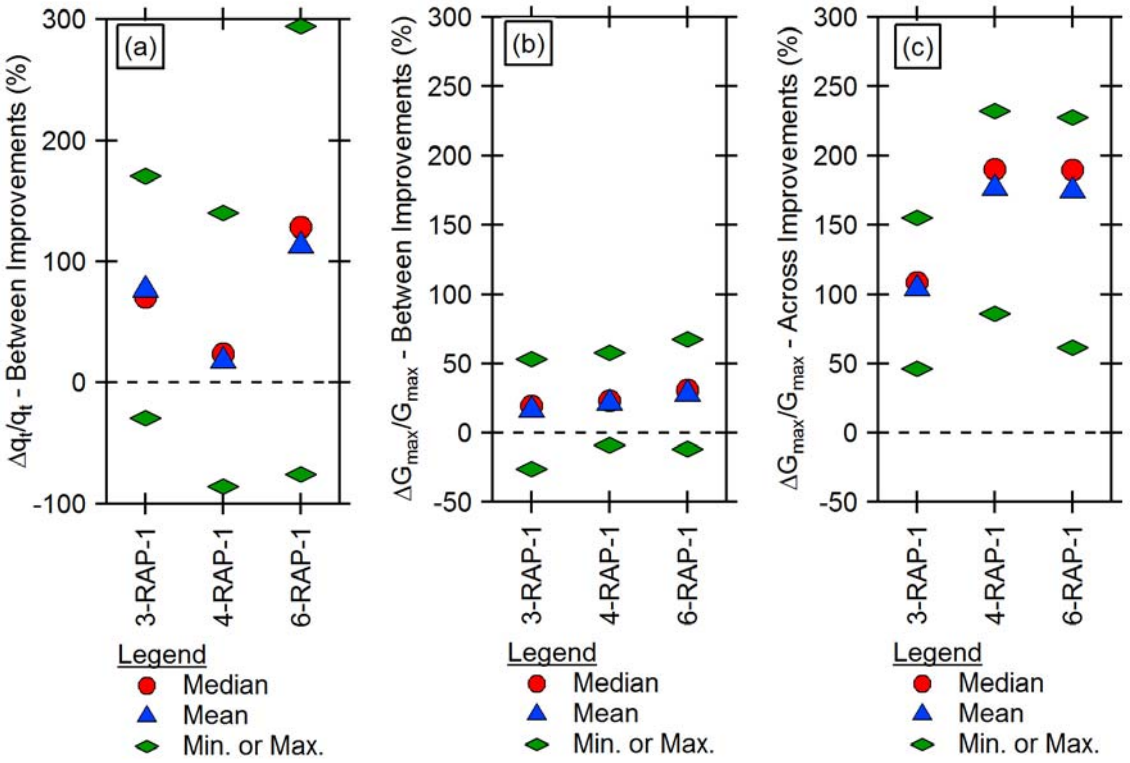

Figure 52: Summary of the median, mean, minimum, and maximum values of relative change caused by the RAP ground improvement at Site 3, Site 4, and Site 6 as evaluated by the change (a) in q_t between the gravel piers, (b) in G_{max} between gravel piers, and (c) in G_{max} across the gravel piers in comparison to the natural soil.

5.3.4 RAP – Trench Cross-Sections

The excavation of the RAP test panels provided an opportunity to visually identify and categorize soil layers in the subsurface, obtain samples for laboratory testing, and to inspect the construction quality of the gravel piers. The trench cross-sections for 3-RAP-1, 4-RAP-1, and 6-RAP-1 are presented in Figure 53 through Figure 55, respectively. The details regarding layer thickness, USCS designation, estimated fines content, and soil description are summarized in Table 19 through Table 21 for test panels 3-RAP-1, 4-RAP-1, and 6-RAP-1, respectively.

The soil profiles at the 3-RAP-1 and 4-RAP-1 test panels appear to have fewer and thinner silt layers than the natural soil test panels at Site 3 and Site 4, respectively, but in general follow a pattern of decreasing fines content and increasing coarseness of the sand particles with depth. The soil profile at 6-RAP-1 matches very closely to the natural soil test panel 6-NS-1 and is less silty than the natural soil test panel 6-NS-2.

In terms of construction quality, it appears that these the gravel piers are well-formed. The piers are vertically-plumb and at test panels 3-RAP-1 and 4-RAP-1 the piers have relatively constant 0.5-m diameters. It is unclear whether or not the piers at 6-RAP-1 were purposely bulbed and tapered near the ground surface; the diameter of these piers below the bulbs near the ground surface are also considerably smaller than the target 0.5 m. Despite the issues with the dimensions of the piers at the 6-RAP-1 test panel, the continuity and integrity of the piers at each of the sites appears to be intact and confirms good quality control by the contractor during installation.

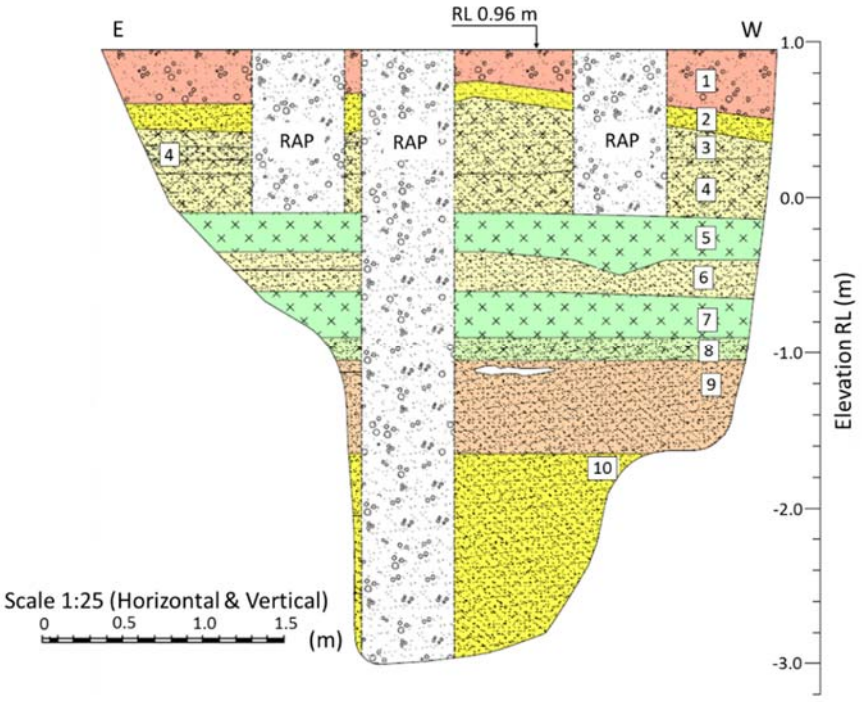

Figure 53: Cross-section of excavation trench at the 3-RAP-1 Test Panel. Modified from van Ballegooy et al. 2017.

Table 19: Soil layers, soil layer depth ranges, USCS designation, and soil description for the layers identified in the 3-RAP-1 Test Panel (van Ballegooy et al. 2017).

Layer	Depth Range	USCS	F.C.	Description
1	0 - 0.4 m	GP-GM		Medium to coarse GRAVEL; grey. Loose. (FILL).
2	0.4 - 0.6 m	SW		Fine to medium SAND; yellowish brown, homogeneous. Loose; moist; well graded. (FILL).
3	0.6 - 0.8 m	SM		Silty fine SAND; yellowish brown, homogeous. Medium dense; moist; non-plastic. (FILL).
4	0.8 - 1.1 m	SM		Silty fine SAND with minor organics, dark grey. Medium dense; moist; silt, non-plastic; organics, inclusions/fragments. (FILL).
5	1.1 - 1.4 m	ML		SILT; grey mottled brown, homogeneous. Very stiff; moist; slightly to non-plastic; low dilatency. (FILL).
6	1.4 - 1.65 m	SM	14 - 77 % (PI = 8 %)	Fine to medium SAND with some silt; greyish brown. Medium dense; moist; silt, non-plastic. (FILL).
7	1.65 - 1.9 m	ML		SILT with trace organics; grey homogeneous. Moist; stiff; slightly to non-plastic.
8	1.9 - 2.0 m	SM	40 %	Interbedded fine to medium SAND, SILT and sandy SILT with minor fine organic fragments.
9	2.0 - 2.6 m	SM	22 %	Fine to medium SAND with minor organics and trace gravel; yellowish brown, lensoidal. Loose; wet; organics, wood fragments up to 150mm diameter; gravel, fine, sub-rounded.
10	2.6 - 4.0 m	SP-SM	2 - 9 %	Fine to medium SAND; grey, homogeneous. Loose; saturated.

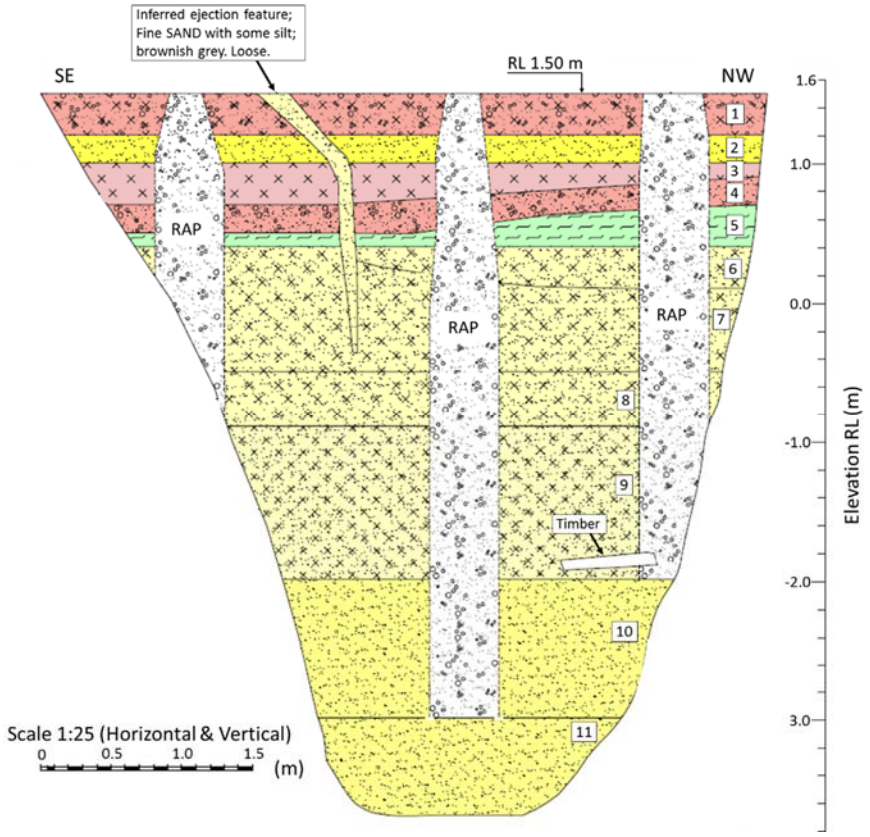

Figure 54: Cross-section of excavation trench at the 4-RAP-1 Test Panel. Modified from van Ballegooy et al. 2017.

Table 20: Soil layers, soil layer depth ranges, USCS designation, and soil description for the layers identified in the 4-RAP-1 Test Panel (van Ballegooy et al. 2017).

Layer	Depth Range	USCS	F.C.	Description
1	0 - 0.3 m	ML		Gravely SILT (FILL).
2	0.3 - 0.5 m	SM		Fine to medium SAND (FILL).
3	0.5 - 0.7 m	ML		SILT with minor gravel (FILL).
4	0.7 - 0.9 m	SP-SM		Gravely SAND (FILL).
5	0.9 - 1.1 m	OL	68 % (PI=15 %)	SILT with some organics and minor sand; mottled black and brown. Firm; slightly plastic; organics, amorphous.
6	1.1 - 1.4 m	SM	57 %	Silty fine SAND. Loose.
7	1.1 - 2.0 m	SM	15 - 57 %	Silty fine SAND; mottled brown and grey; loose.
8	2.0 - 2.4 m	SM	15 %	Silty fine SAND; grey. Loose.
9	2.4 - 3.5 m	SM	10 %	Fine to medium SAND with some silt and minor organics; grey. Loose; organics, woody and fibrous.
10	3.5 - 4.5 m	SP	3 %	Fine to medium SAND with trace silt.
11	4.5 - 5.2 m	SP	10 %	Fine to medium SAND with trace silt; grey. Loose.

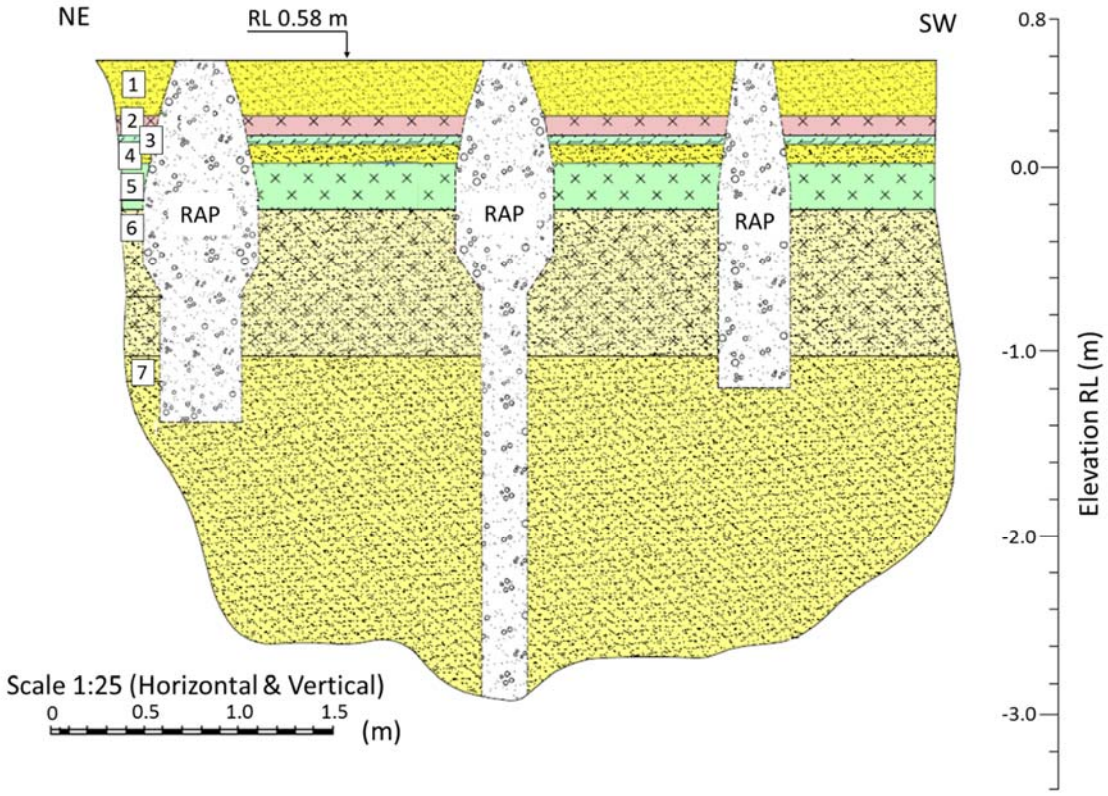

Figure 55: Cross-section of excavation trench at the 6-RAP-1 Test Panel. Modified from van Ballegooy et al. 2017.

Table 21: Soil layers, soil layer depth ranges, USCS designation, and soil description for the layers identified in the 6-RAP-1 Test Panel (van Ballegooy et al. 2017).

Layer	Depth Range	USCS	F.C.	Description
1	0 - 0.3 m	SP		Fine to medium SAND; grey. (FILL).
2	0.3 - 0.4 m	ML		SILT with minor gravel; grey mottled brown. (FILL).
3	0.4 - 0.45 m	PT		PEAT; fibrous. (FILL).
4	0.45 - 0.55 m	SP		Fine to medium SAND; greyish brown. (FILL).
5	0.55 - 0.7 m	ML	94 % (PI=18 %)	SILT with trace organics; grey, m oist. Stiff; low to moderately plastic.
6	0.7 - 1.6 m	SM	21 %	Silty fine SAND; grey. Loose.
7	1.6 - 3.2 m	SP	1 - 3 %	Fine to medium SAND with trace silt; grey . Loose.

5.4 ASSESSMENT OF THE LMG GROUND IMPROVEMENT METHOD

The LMG ground improvement method aims to reduce the risk of soil liquefaction by creating stiff columns of grout and densifying the soil surrounding the columns. The q_t parameter from CPT testing and the shear wave velocity from DPCH testing are sensitive to changes in soil density, making them both useful for evaluating the effectiveness of the LMG ground improvement to densify the soil surrounding the grout columns. However, only the DPCH test is able to evaluate the increase in stiffness due to the grout columns themselves by measuring the shear wave velocity across the columns.

5.4.1 LMG – Variation in q_t from CPT Testing

The CPTs pushed between LMG grout columns at each test panel were performed at time intervals 14, 28, and 90 days after the construction of the test panel to observe the effect on time; the results show no meaningful effect of time on the effectiveness of the ground improvement method and therefore the effect of time is not considered any further. The q_t traces presented in Figure 56a through Figure 56c show the results from CPT testing at the LMG test panels as well as the median natural soil q_t profile for Site 3, Site 4, and Site 6, respectively. The relative change in q_t due to the LMG ground improvement at all three sites is shown in Figure 56d and is calculated using the median q_t profile for the given test panel in comparison to the median natural soil q_t profile for each site using the following formula:

$$\frac{\left(q_{t,LMG} - q_{t,Natural\ Soil}\right)}{q_{t,Natural\ Soil}} \times 100\ \% \qquad (12)$$

Only results down to a depth of 4.0 m are used to assess the relative change in q_t because the ground improvement method was only intended to improve down to that depth. The results also omit data shallower than 0.6 m for fair comparison against the shear wave velocity results from DPCH testing that start at a depth of 0.6 m.

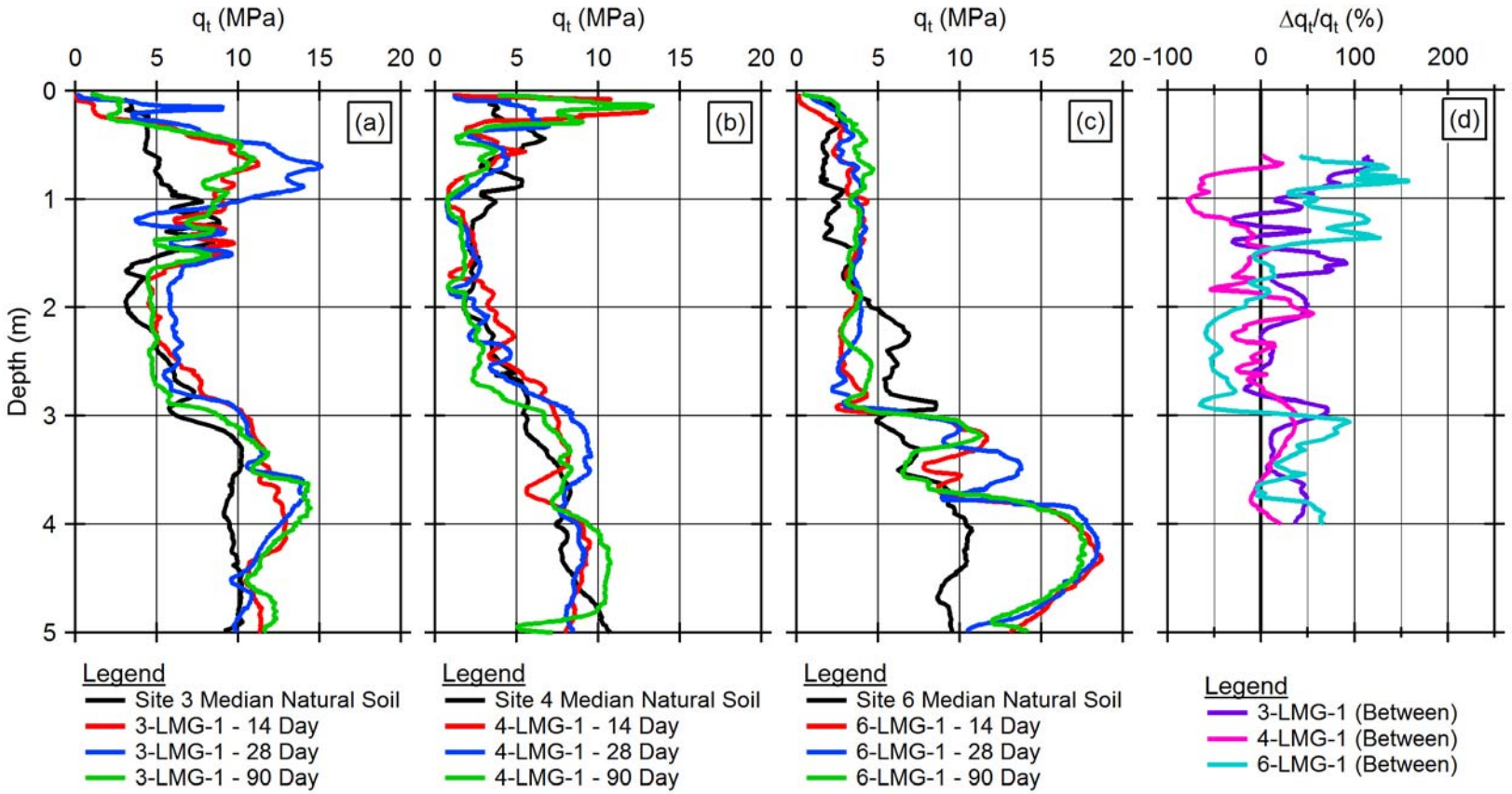

Figure 56: Profiles of q_t from CPT testing between the LMG grout columns at (a) Site 3, (b) Site 4, and (c) Site 6 with the median natural soil profiles for each respective site. The relative change in q_t in subplot (d) shows the variation of q_t in relation to the median natural soil q_t profile at each site.

For each profile of relative change in q_t at the 3-LMG-1, 4-LMG-1, and 6-LMG-1 test panels, the median, mean, minimum, and maximum values as well as the standard deviation were calculated to help understand the variation of q_t within a single test panel. These statistical parameters are summarized in Table 22.

Table 22: Summary of statistical parameters for the relative variation in q_t resulting from the LMG ground improvement method at the 3-LMG-1, 4-LMG-1, and 6-LMG-1 test panels.

	3-LMG-1 $\Delta q_t/q_t$ (%)	**4-LMG-1** $\Delta q_t/q_t$ (%)	**6-LMG-1** $\Delta q_t/q_t$ (%)
Median:	29	-4	15
Mean:	31	-6	21
Standard Deviation:	33	30	56
Minimum:	-31	-79	-66
Maximum:	119	56	157

By evaluation of the q_t from CPT testing, the LMG ground improvement method provides little to no improvement in the soil between grout columns. The median increases in q_t range from -4 % at the 4-LMG-1 test panel to 29 % at the 3-LMG-1 test panel. In the case of every test panel, the values of relative change in q_t one standard deviation below the mean value are negative, indicating that significant portions of the profile in the depth range of 0.6 to 4.0 m are being loosened by the ground improvement method rather than densified as intended. While proving that densification through this method is possible, as reflected in the large increases of q_t up to 119 % at the 3-LMG-1 test panel and 157 % at the 6-LMG-1 test panel, the lack of consistency and evidence of significant loosening suggests this ground improvement method is not appropriate as a liquefaction-mitigation technique as applied in this project.

5.4.2 LMG – Variation in V_S from DPCH Testing

Shear wave velocities were measured using DPCH testing both between and across the LMG grout columns to assess the increase in stiffness caused by the densification of the soil as well as by the presence of the stiff grout columns. The shear modulus G_{max} is calculated from the shear wave velocity to quantify the increase in stiffness due to the LMG ground improvement; however, G_{max} reported for the measurements across the grout columns is a loose approximation because the travel path for the shear wave across the grout columns includes both soil and grout but the G_{max} value is calculated using a mass density corresponding only to the soil. The accuracy of results from DPCH testing across the grout column is further challenged because the true travel path of the shear wave velocity is unknown (e.g. through the middle of the column or refracted around the outside of the column). Despite these concerns, the values of V_S and G_{max} corresponding to the DPCH test across the grout columns is still useful for a comparative analysis across test sites and in comparison to results obtained between the grout columns.

The V_S profiles presented in Figure 50a through Figure 50c show the results from DPCH testing between grout columns at the LMG test panels as well as the median natural soil V_S profile for Site 3, Site 4, and Site 6, respectively. The V_S profiles from DPCH testing across the grout columns with the median natural soil V_S profile for Site 3, Site 4, and Site 6, respectively, are shown in Figure 51a through Figure 51c.

The relative change in G_{max} between grout columns due to the LMG ground improvement at all three sites is shown in Figure 50d and is calculated using the median G_{max} profile between grout columns for the given test panel in comparison to the median natural soil G_{max} profile for each site using the following formula:

$$\frac{\left(G_{max,LMG\ (between)} - G_{max,Natural\ Soil}\right)}{G_{max,Natural\ Soil}} \times 100\ \% \qquad (13)$$

The relative change in G_{max} across grout columns due to the LMG ground improvement at all three sites is shown in Figure 51d and is calculated using the median G_{max} profile across grout columns for the given test panel in comparison to the median natural soil G_{max} profile for each site using the following formula:

$$\frac{\left(G_{max,LMG\ (across)} - G_{max,Natural\ Soil}\right)}{G_{max,Natural\ Soil}} \times 100\ \% \qquad (14)$$

Only results down to a depth of 4.0 m are used to assess the relative change in G_{max} because the ground improvement method was only intended to improve down to that depth.

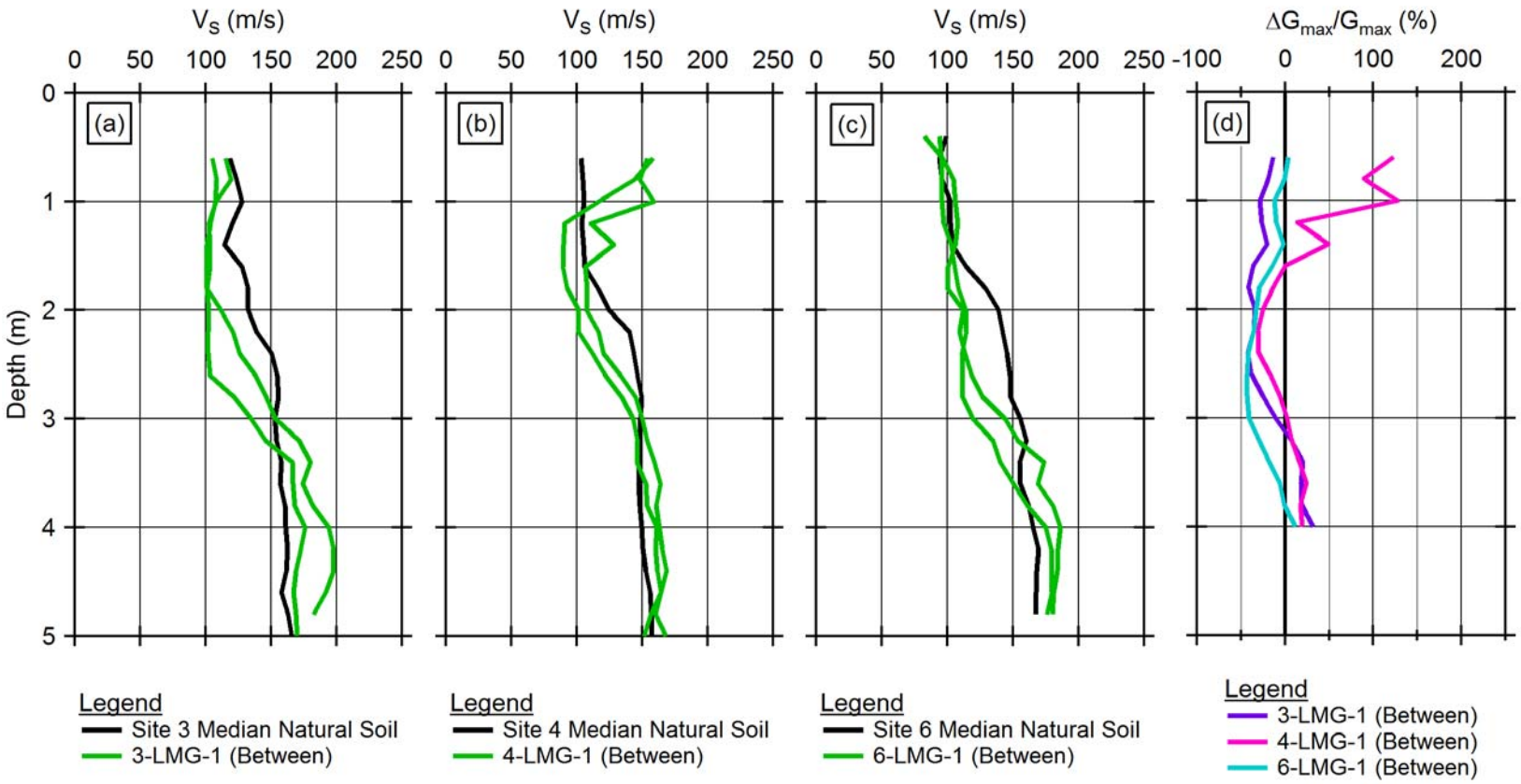

Figure 57: Shear wave velocity profiles from DPCH testing between the LMG grout columns at Site 3, Site 4, and Site 6 in comparison to the median natural soil profiles for each respective site.

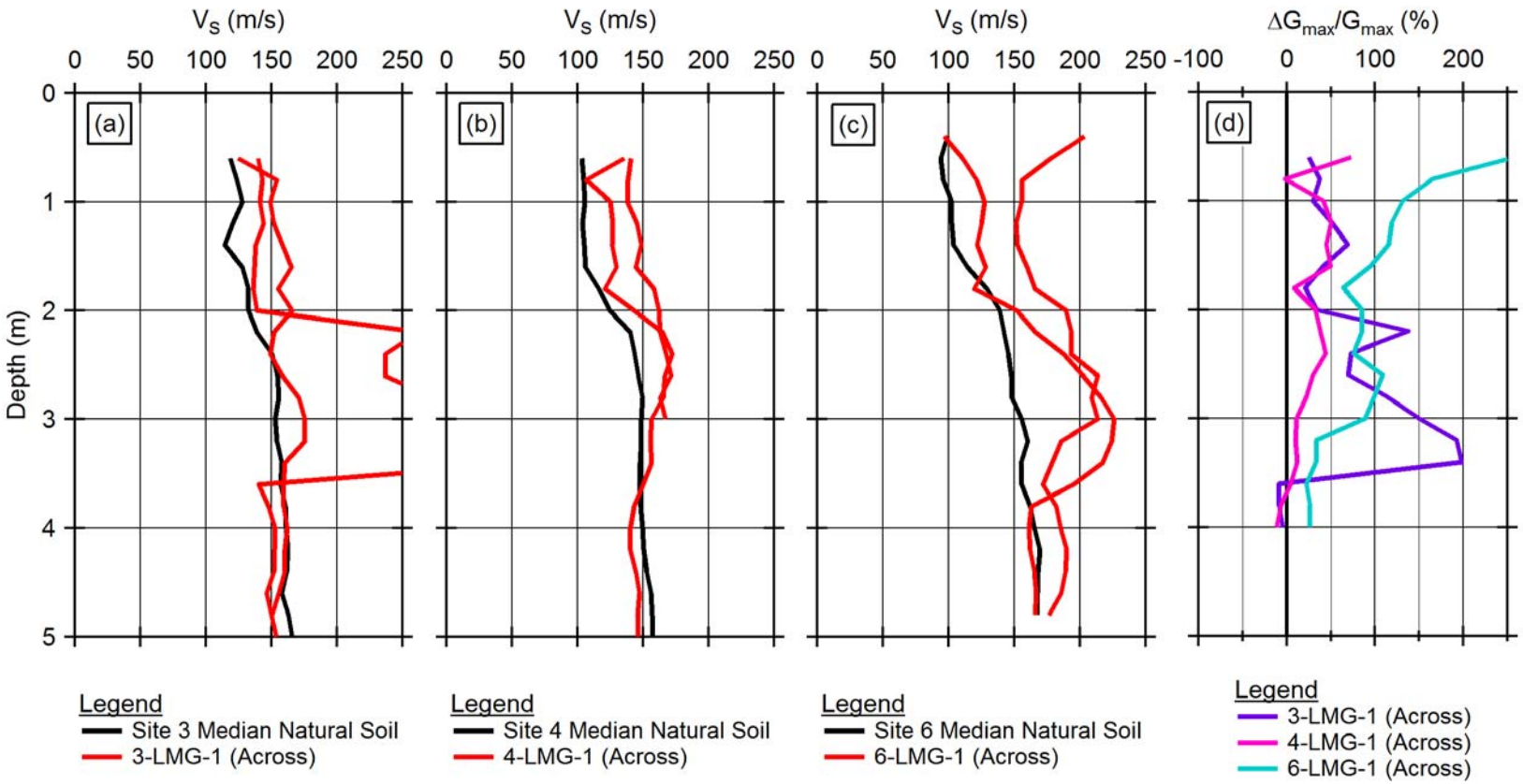

Figure 58: Shear wave velocity profiles from DPCH testing across the LMG grout columns at Site 3, Site 4, and Site 6 in comparison to the median natural soil profiles for each respective site.

For each profile of relative change in G_{max} at the 3-LMG-1, 4-LMG-1, and 6-LMG-1 test panels, the median, mean, minimum, and maximum values as well as the standard deviation were calculated to help understand the variation of G_{max} within a single test panel. These statistical parameters for the relative variation in G_{max} between LMG grout columns are summarized in Table 11 and for the relative variation in G_{max} across LMG grout columns are summarized in Table 12.

Table 23: Summary of statistical parameters for the relative variation in G_{max} between grout columns resulting from the LMG ground improvement method at the 3-LMG-1, 4-LMG-1, and 6-LMG-1 test panels.

	3-LMG-1 (Between) $\Delta G_{max}/G_{max}$ (%)	4-LMG-1 (Between) $\Delta G_{max}/G_{max}$ (%)	6-LMG-1 (Between) $\Delta G_{max}/G_{max}$ (%)
Median:	-23	11	-16
Mean:	-15	20	-19
Standard Deviation:	24	48	18
Minimum:	-42	-31	-43
Maximum:	32	127	12

Table 24: Summary of statistical parameters for the relative variation in G_{max} across grout columns resulting from the LMG ground improvement method at the 3-LMG-1, 4-LMG-1, and 6-LMG-1 test panels.

	3-LMG-1 (Across) $\Delta G_{max}/G_{max}$ (%)	4-LMG-1 (Across) $\Delta G_{max}/G_{max}$ (%)	6-LMG-1 (Across) $\Delta G_{max}/G_{max}$ (%)
Median:	46	26	87
Mean:	68	25	91
Standard Deviation:	65	23	58
Minimum:	-9	-12	22
Maximum:	198	73	257

With the LMG ground improvement method, the changes in G_{max} relative to the natural soil that are evaluated between grout columns are intended to come only from variations in the soil state whether it be changes in density or in horizontal stress. There

are cases, however, in which it appears that grout from adjacent injection points spread laterally into the travel path of the DPCH testing between grout columns, resulting in higher than expected values of shear wave velocity. The changes in G_{max} relative to the natural soil that are evaluated between grout columns come from the changes in the soil state as well as the presence of grout, which is a significantly stiffer material than the natural soil.

Looking first at the relative change in G_{max} between grout columns, the median relative change in G_{max} at the 3-LMG-1 and 6-LMG-1 test panels are negative, indicating significant loosening of the soil over the length of the profile. The median relative change in G_{max} at the 4-LMG-1 test panel is 11 %, which is lower than any of the median values reported at the RIC test panels or RAP test panels. The maximum values of relative change in G_{max} between the grout columns are very low at 32 % for the 3-LMG-1 test panel and 12 % for the 6-LMG-1 test panel. It is believed that the values of shear wave velocity in the top 1.0 m at the 4-LMG-1 test panel are too high to represent densified natural soil and instead probably reflect the presence of grout along the travel path. As a result, the maximum relative change in G_{max} between grout columns at 4-LMG-1 is more likely to be 50 % rather than the report 127 %. The results from DPCH testing between the grout columns show extensive softening of the soil, which may leave the soil more vulnerable to soil liquefaction than before the ground improvement method was implemented.

In the evaluation of DPCH testing across grout columns, there is a wide range of median values for the relative change in G_{max} across the three sites. The median value of relative change in G_{max} is the lowest with 26 % at the 4-LMG-1 test panel, in the middle with 46 % at the 3-LMG-1 test panel, and the greatest with 87 % at the 6-LMG-1 test panel. Two of the test panels, 3-LMG-1 and 4-LMG-1, have minimum values of relative change in G_{max} that are negative, reflecting a softening of the soil that is unexpectedly occurring toward the bottom of the profile in the range of 3.6 to 4.0 m. The large standard deviations

at test panel 3-LMG-1 (65 %) and test panel 6-LMG-1 (58 %) show how highly variable the improvement is along the length of the profile with the LMG ground improvement method. While the grout itself is measurably stiffer than the natural soil in some locations, the overall increase in stiffness lacks continuity and consistency over the depth range of interest for the goal of liquefaction remediation.

5.4.3 LMG – Comparison of Results Across Test Methods

The results from CPT and DPCH testing at the LMG test panels in general show little to no increases, and in some cases decreases, in the density of the soil between grout columns as well as moderate increases in the stiffness across grout columns. The CPT and DPCH tests performed between grout columns identify significant portions of the profile at which the q_t or G_{max} of the LMG test panel is less than the corresponding values in the natural soil, indicating a loosening of the soil. In Figure 59, the median, mean, minimum, and maximum values of relative change in q_t and G_{max} evaluated at test panels 3-LMG-1, 4-LMG-1, and 6-LMG-1 are presented for comparison. A comparison of these statistical parameters from each of the test methods reveals some conclusions from the results: 1) the minimum values of relative change in q_t and G_{max} between grout columns at all three site are negative, indicating a loosening of the soil at some depths, 2) the median relative change in q_t is positive at test panels 3-LMG-1 and 6-LMG-1 and negative at test panel 4-LMG-1 while the median relative change in G_{max} is negative at test panels 3-LMG-1 and 6-LMG-1 and positive at test panel 4-LMG-1, indicating that densification within each test panel is highly variable because the CPT and DPCH tests are at different locations within a given test panel, 3) the median relative change in G_{max} between grout columns at test panels 3-LMG-1 and 6-LMG-1 and the median relative change in q_t at test panel 4-LMG-1 are negative, indicating significant portions of the soil between the grout columns was loosened by the LMG ground improvement method.

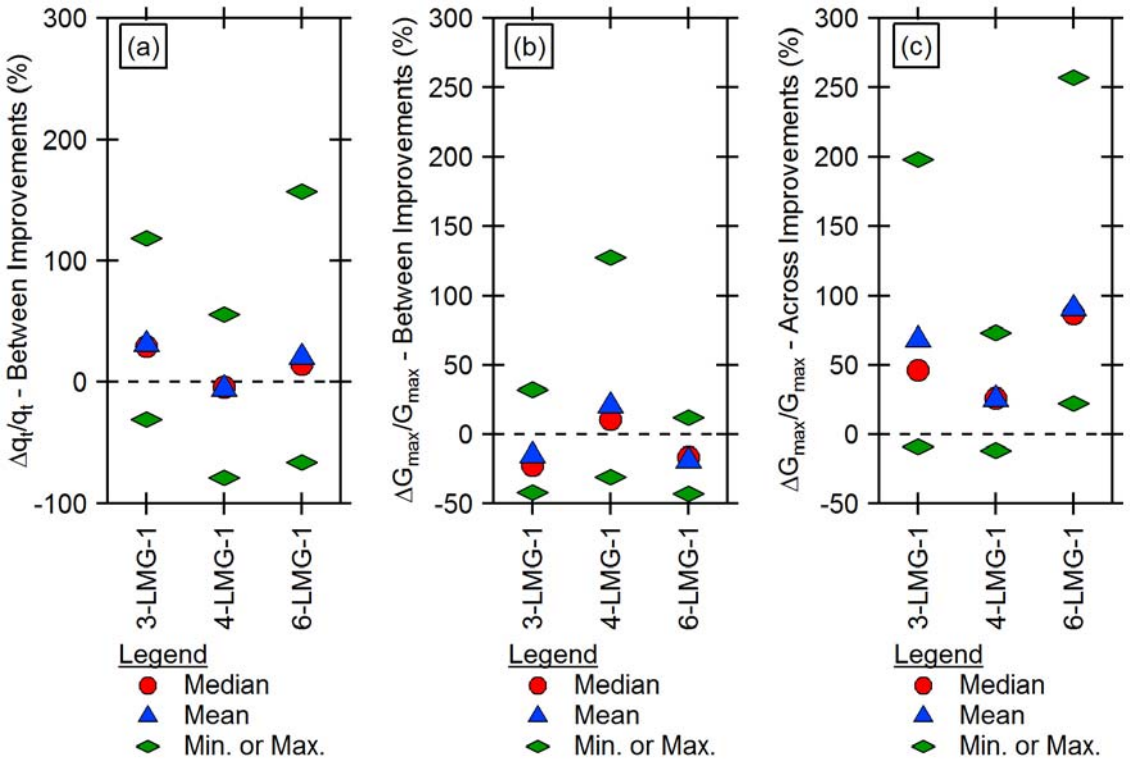

Figure 59: Summary of the median, mean, minimum, and maximum values of relative change caused by the LMG ground improvement at Site 3, Site 4, and Site 6 as evaluated by the change (a) in q_t between the grout columns, (b) in G_{max} between grout columns, and (c) in G_{max} across the grout columns in comparison to the natural soil.

5.4.4 LMG – Trench Cross-Sections

The excavation of the LMG test panels provided an opportunity to visually identify and categorize soil layers in the subsurface, obtain samples for laboratory testing, and to inspect the construction quality of the grout columns. The trench cross-sections for 3-LMG-1, 4-LMG-1, and 6-LMG-1 are presented in Figure 60 through Figure 62, respectively. The details regarding layer thickness, USCS designation, estimated fines content, and soil description are summarized in Table 25 through Table 27 for test panels 3-LMG-1, 4-LMG-1, and 6-LMG-1, respectively.

The soil profiles at the 3-LMG-1 and 6-LMG-1 agree well with the natural soil test panels at Site 3 and Site 6, respectively, while the soil profile at 4-LMG-1 appears to have slightly less of a silt content than the natural soil test panels at Site 4 but is overall similar. These trench cross-sections all show the general trend of silty layers near the ground surface underlain by sand layers.

In terms of construction quality, the grout columns are poorly formed with lack of integrity along the length of the column. Instead of creating a column of grout bulbs, the pressure-injected grout in some cases flowed laterally as seen in Figure 60 for the trench cross-section of test panel 3-LMG-1. The trench cross-section of test panel 6-LMG-1 in Figure 62 shows fractures in the soil along the edge of the grout column near the ground surface that most likely resulted from the grouting process. Overall it appears that there is little control over the placement of the grout, an inability to create columns with continuous integrity, and evidence that the process loosens the surrounding soil rather than systematically densifying it.

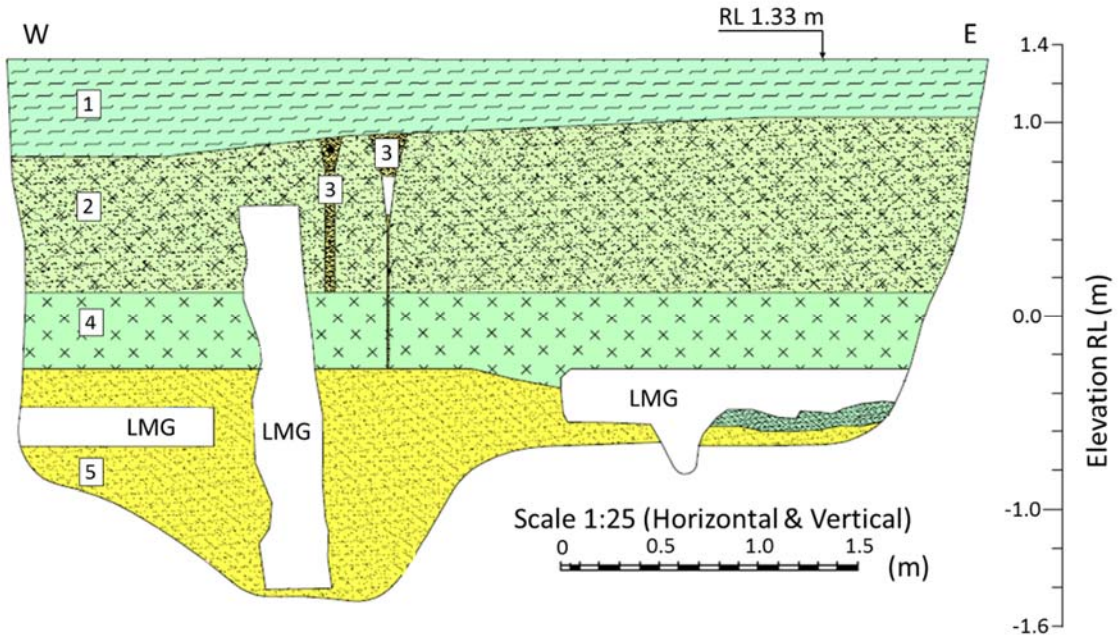

Figure 60: Cross-section of excavation trench at the 3-LMG-1 Test Panel. Modified from van Ballegooy et al. 2017.

Table 25: Soil layers, soil layer depth ranges, USCS designation, and soil description for the layers identified in the 3-LMG-1 Test Panel (van Ballegooy et al. 2017).

Layer	Depth Range	USCS	F.C.	Description
1	0 - 0.4 m			Topsoil. (FILL).
2	0.4 - 1.2 m	ML	53 - 56 %	Sandy SILT; brown, homogeneous. Loose to medium dense; moist; non-plastic; sand, fine. (FILL).
3	0.4 - 1.2 m Vertical fissures	SW		Fine to medium SAND with trace silt; light brown, homogeneous. Loose.
4	1.2 - 1.6 m	ML	60 %	SILT with minor organics; grey with brown mottling. Very stiff; moist.
5	1.6 - 2.8 m	SW	3 - 6 %	Fine to medium SAND; grey, homogeneous. Loose; moist.

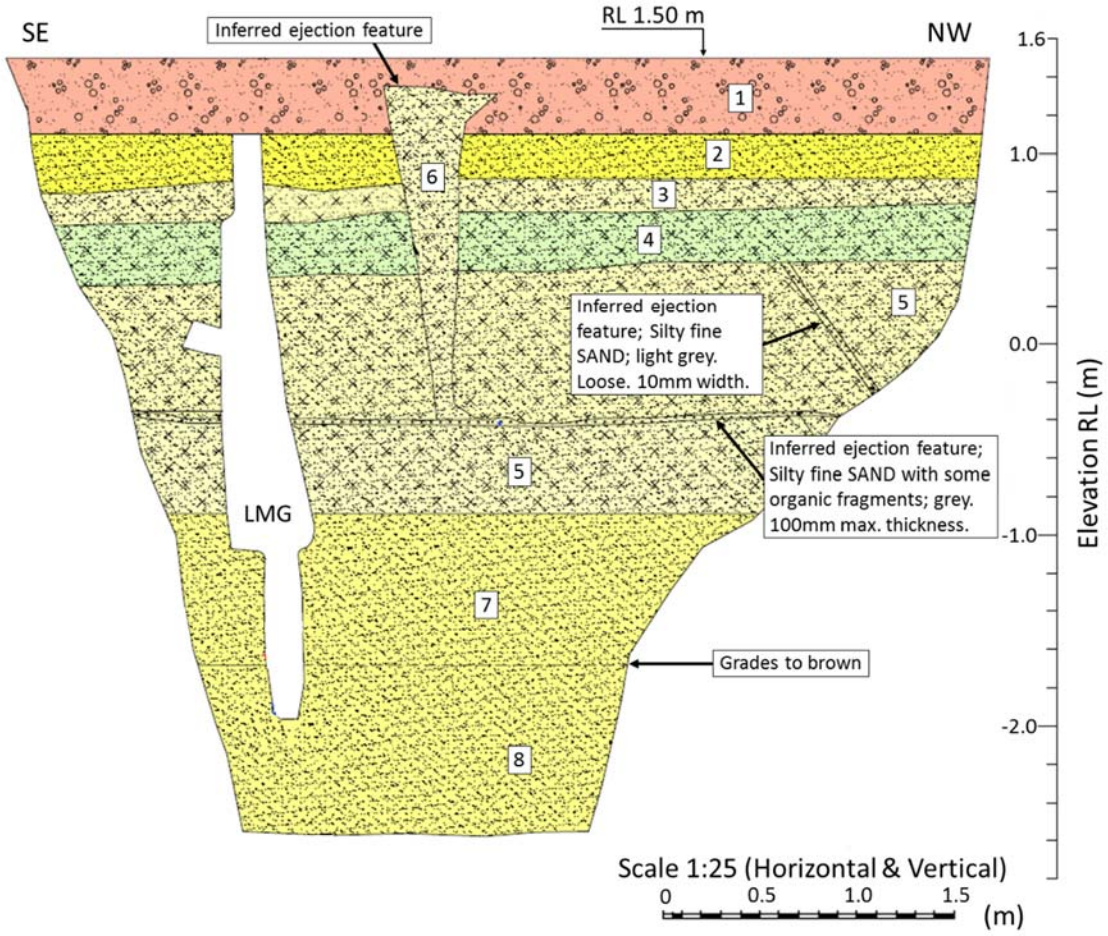

Figure 61: Cross-section of excavation trench at the 4-LMG-1 Test Panel. Modified from van Ballegooy et al. 2017.

Table 26: Soil layers, soil layer depth ranges, USCS designation, and soil description for the layers identified in the 4-LMG-1 Test Panel (van Ballegooy et al. 2017).

Layer	Depth Range	USCS	F.C.	Description
1	0 - 0.4 m	GP		Fine to medium GRAVEL (FILL).
2	0.4 - 0.7 m	SP		Fine to medium SAND (FILL).
3	0.7 - 0.9 m	SM		Silty SAND; brown grey (FILL).
4	0.9 - 1.2 m	OL	65 % (PI=12 %)	Sandy SILT with minor organics; brown. Firm; organic ordour; sand, fine
5	1.2 - 2.4 m	SM	22 - 81 %	Silty fine SAND, dark grey. Loose.
6	0.2 - 1.9 m Vertical fissure	SM		Fine to medium SAND with some silt; light grey.
7	2.4 - 4.1 m	SW	10 - 11 %	Fine SAND with minor silt; grayish brown. Loose

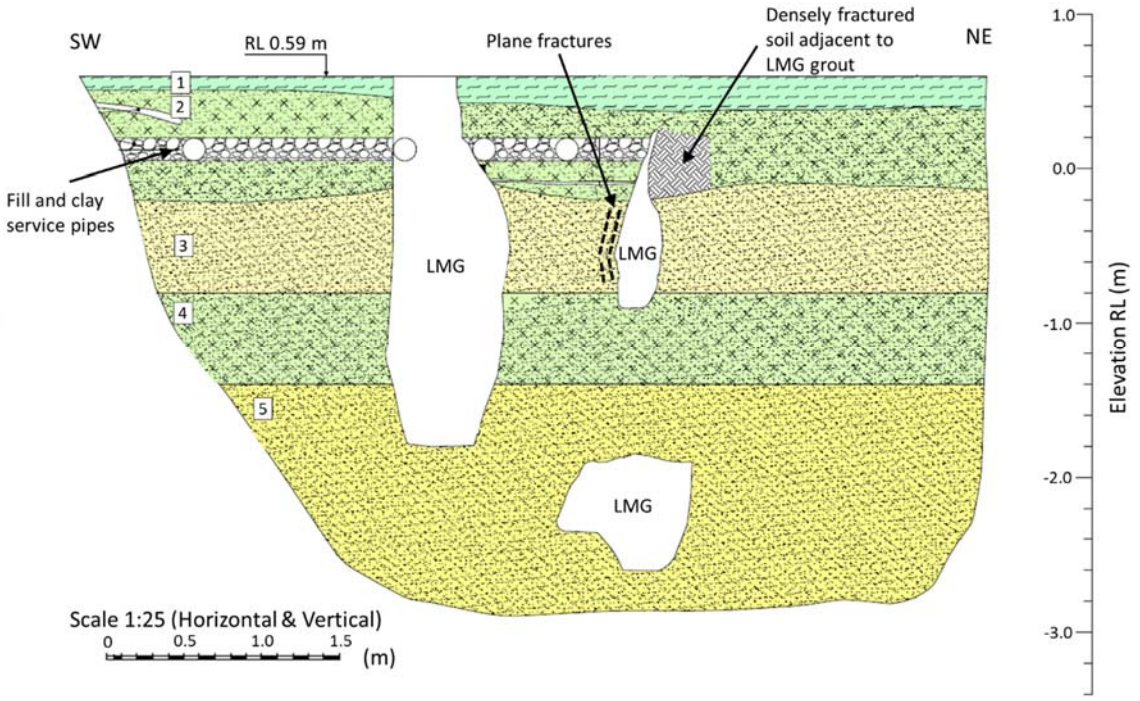

Figure 62: Cross-section of excavation trench at the 6-LMG-1 Test Panel. Modified from van Ballegooy et al. 2017.

Table 27: Soil layers, soil layer depth ranges, USCS designation, and soil description for the layers identified in the 6-LMG-1 Test Panel (van Ballegooy et al. 2017).

Layer	Depth Range	USCS	F.C.	Description
1	0 - 0.2 m	OL		Topsoil.
2	0.2 - 0.8 m	ML	71 %	Sandy SILT; brown with grey mottling. Stiff; moist; non-plastic; slightly dilatant; sand, fine.
3	0.8 - 1.4 m	SM	7 - 14 %	Fine SAND with some to minor silt and trace organics; grey; homogeneous. Loose; moist.
4	1.4 - 2.0 m	SP	18 %	Fine to medium SAND interbedded with sandy SILT; dark grey. Sand, loose, moist; silt, moist, non-plastic.
5	2.0 - 3.4 m	SP-ML	2 %	Fine to medium SAND with trace silt; saturated; organic odour.

5.5 SUMMARY

This chapter covered the use of CPT and DPCH testing and excavation trenches at Site 3, Site 4, and Site 6 to evaluate the effectiveness of the RIC, RAP, and LMG test panels.

The q_t from CPT testing and shear modulus from DPCH testing were used to measure changes in the density and stiffness, respectively, due to the ground improvement methods in comparison to the natural soil. The median increase in corrected cone tip resistance between improvements ranged from 24 to 86 % for the RIC ground improvement method, from 24 to 128 % for the RAP ground improvement method, and -4 to 29 % for the LMG ground improvement method at the three test sites. The median increase in shear modulus between improvements ranged from 17 to 40 % for the RIC ground improvement method, 19 to 31 % for the RAP ground improvement method, and -23 to 11 % for the LMG ground improvement method at the three test sites. The median increase in shear modulus across improvements ranged from 18 to 24 % for the RIC ground improvement method, from 109 to 190 % for the RAP ground improvement method, and from 26 to 87 % for the LMG ground improvement method.

These comparisons showed that across test sites and within test panels, the RIC and RAP ground improvement methods were able to consistently and effectively densify the natural soil, with the caveat that within the profile this densification can be highly variable with instances of soil being loosened or softened at some depths. Many times the areas of softening occurred near the ground surface but there are also instances where it occurred several meters below the ground surface as in the 4-RIC-1 test panel. The LMG ground improvement method had the least amount of improvement are measured by the CPT and DPCH tests between grout columns in comparison to the RAP and RIC ground improvement methods, and in some cases even in comparison to the natural soil. At Site 4,

the median q_t value of the LMG test panel was less than the median q_t value from the natural soil test panels. At Site 3 and Site 6, the median shear modulus value of the LMG test panel was less than the median shear modulus value from the natural soil test panels. Because of the presence of the stiff grout, the median shear modulus across grout columns was uniformly larger than the median shear modulus of the natural soil, but the only situation in which the LMG had better performance than the natural soil at all three test sites.

The trench cross-sections provided invaluable information regarding the construction quality of the RAP and LMG ground improvement methods. The gravel piers of the RAP test panels are well-formed and mostly match the design expectations. The quality of construction revealed in the trench cross-section also bolster the positive results from CPT and DPCH testing. The grout columns of the LMG test panels, however, consist of disjointed, irregularly formed bulbs and instances where the grout spread laterally through the soil instead of forming bulbs. Evidence of soil fracturing is also noted in one of the LMG trench cross-sections. The LMG trench cross-sections revealed that the injection of low-mobility grout under these conditions was difficult to control and resulted in poor construction. These findings of poor construction agree with the results from CPT and DPCH testing that indicated highly variable changes in soil density and many instances in which the ground improvement method have probably increased the susceptibility to soil liquefaction.

Chapter 6: Overview of the Staged Shake Testing with T-Rex

Staged shake testing with T-Rex is a large-scale, in-situ method for inducing small to moderate levels of shear strains ($0.0001 < \gamma < 1.0$ %) in the soil for use in studying the nonlinear behavior of soil under dynamic loading conditions. In this study, the application includes the generation of pore pressures in leading to the triggering of soil liquefaction. The current version of this field shaking test has evolved from and has improved upon previous work of Chang (2002), Cox (2006), and Roberts (2014).

6.1 INSTRUMENTATION

By the end of the project in Christchurch, 76, two-dimensional velocity transducers (geophone sensors) and 72 pore pressure transducers (PPTs) had been custom-built and installed at the test panels across all three sites. In some cases, the sensors were recovered when the test panels were trenched and many were successfully re-used after field verification testing. The designs of these sensors are very similar to the those used for liquefaction shake tests in 2012 at the Wildlife Liquefaction Array (WLA) in Imperial Valley, California (Roberts J. N., 2014), with some modifications.

6.1.1 Two-Dimensional Velocity Transducers

Two-dimensional velocity transducers were used to measure the particle velocity of the soil in the vertical and inline horizontal directions during shake testing with T-Rex. Each sensor contains two, 28-Hz-resonance frequency geophones from Geospace (model GS-14-L3) that are orthogonally oriented with one geophone in the vertical direction and the other geophone in the inline horizontal direction. The relatively stiff spring in the 28-Hz geophones allows the geophones to be oriented vertically or horizontally and still operate well. The geophones are encased in a custom-designed hard polycarbonate cone-

tipped cylinder. The cone tip, which facilitates pushing the two-dimensional velocity transducers into the soil, has an angle of 60° just like a typical CPT cone. The diameter of the polycarbonate cylinder is 3.8 cm and the height, including the cone tip, is approximately 10.8 cm. The approximate unit weight of the sensor, 16.5 kN/m^3 (105 pcf), is designed to be very close to the assumed unit weight of the soil (17 kN/m^3 above the water table and 19.5 kN/m^3 below the water table). This design of the sensor to have a unit weight similar to the soil helps minimize impedance contrast between the sensor and soil as well as ensuring the sensor will not float or sink during shake testing as the excess pore pressure increases.

The top of the sensor is capped with an aluminum top cap that includes an orientation pin near the edge. When prepared for installation, the orientation rod prevents rotation between the steel connector rod and the sensor by slipping into the machined key in the face of the steel connector rod. The other end of the steel connector rod threads into standard, steel CPT rods. A two-dimensional velocity transducer is shown in Figure 63 with its main components identified and a steel connector rod is shown in Figure 64.

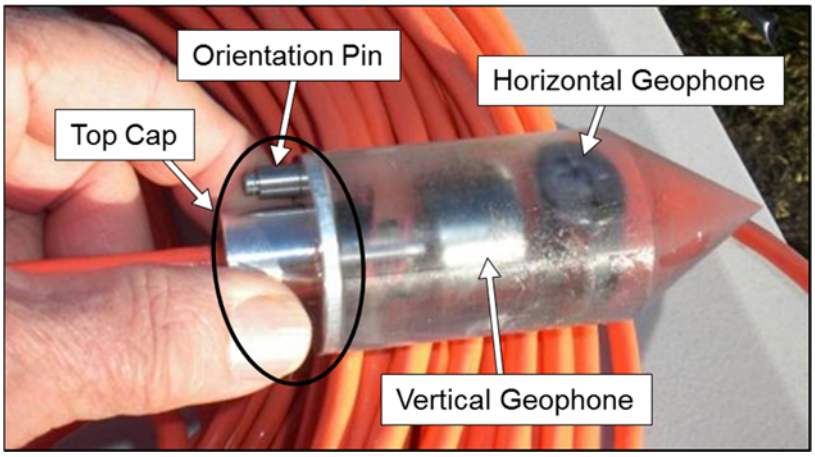

Figure 63: Components of an assembled two-dimensional velocity transducer including the top cap, orientation pin, and two geophones.

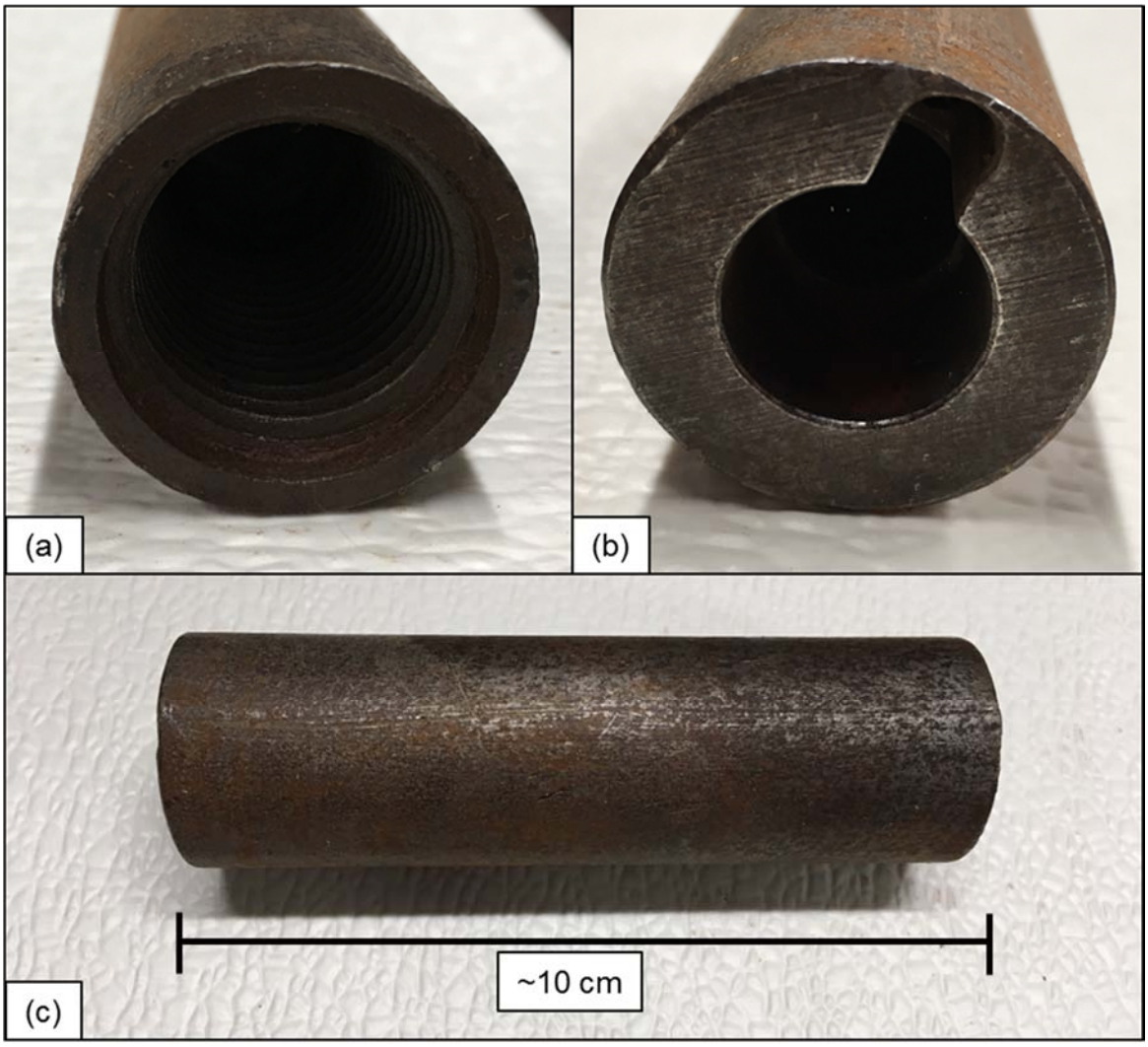

Figure 64: Steel connector rod used to connect the sensors to the steel CPT rods during installation: (a) view of the connector rod end with threads, (b) view of the connector rod end with machined key, and (c) side-view of the connector rod.

Prior to building the sensors, each geophone was calibrated on a shake table using a downward, stepped-sine sweep from 202 Hz to 2 Hz in 1 Hz increments. The resulting calibration curve is used to convert the voltage output from the geophone into units of in./sec during the subsequent analysis processing. The graph in Figure 65 shows the typical calibration curve for one of the 28-Hz geophones.

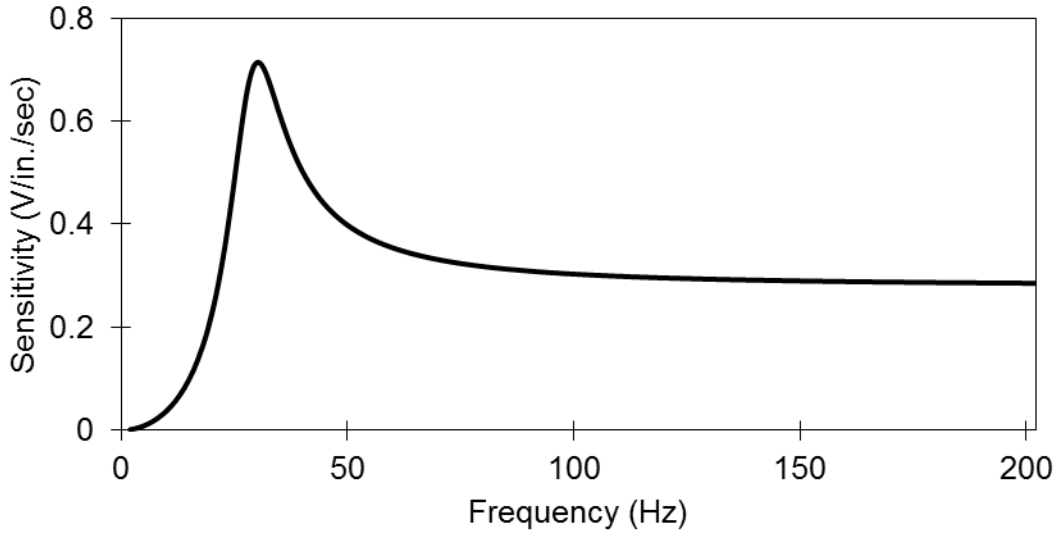

Figure 65: Example calibration curve for a 28-Hz geophone.

The verification process for determining if a recovered sensor can be re-used in another test panel involves analyzing the free-vibration decay response of each geophone from a forced-displacement starting position. This method was used because it is difficult to accurately re-calibrate the geophones on the shake table once they are encased in the sensor and also because this method can be performed in the field with minimal equipment. In this setup, a constant ~1-volt DC voltage is applied across the positive and negative terminals of a geophone and then instantaneously released while the response of the geophone was recorded. An example free-vibration decay record for a 28-Hz-resonance frequency geophone is shown in Figure 66.

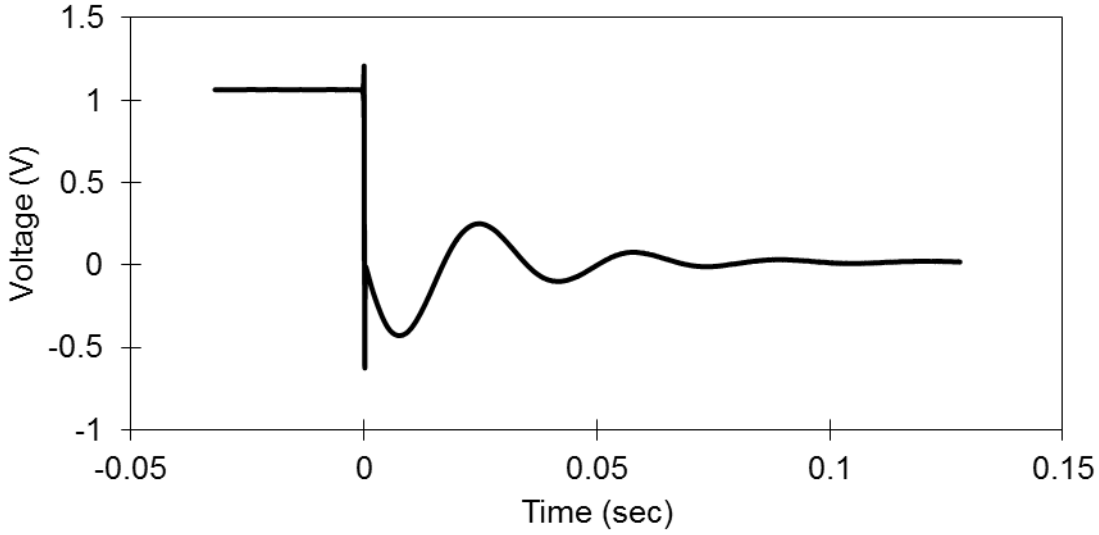

Figure 66: Example free-vibration decay curve of a 28-Hz-resonance frequency geophone used to re-verify the two-dimensional velocity transducers.

6.1.2 Pore Pressure Transducers (PPTs)

Pore pressure transducers (PPTs) are used to measure the static and dynamic water pressure in the ground before, during, and after shake testing with T-Rex. The PPTs were built using two kinds of Druck PDCR 1830 Submersible Pressure Transducers; one set of these sensors are rated to operate in conditions up to 10 psi and have a sensitivity of 0.98 mV/V/psi and the other set are rated to operate in conditions up to 15 psi and have a sensitivity of 0.69 mV/V/psi. Two types of sensors were used because the supplier was not able to supply a sufficient quantity of either sensor type alone; the use of different sensor types has no effect on the quality of pore pressure measurements in the experiments.

Each pressure transducer was encased in a hard, polycarbonate cone-tipped cylinder with dimensions 3.8 cm in diameter and 15.2 cm in length. In contrast to the two-dimensional velocity transducers, the cone tip on these sensors are removable and therefore replaceable. The cone tips also include replaceable porous stones on opposite faces of the side, allowing water to freely pass through the casing to the membrane of the pressure

transducer while keeping soil on the outside. The filters used on this project are sintered bronze with a 20 micron filtration grade from Capstan California. The tops of the PPTs are capped with the same aluminum top caps, just as done for the two-dimensional velocity transducers to control the orientation of the PPT during installation. An assembled PPT ready for installation is shown in Figure 67.

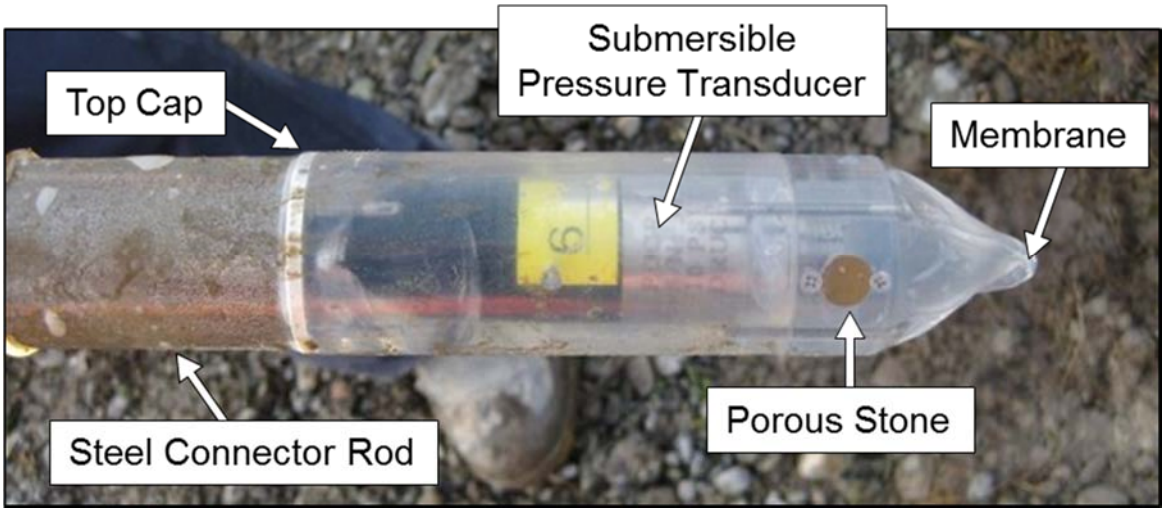

Figure 67: Components of an assembled pore pressure transducer (PPT) including the steel connector rod, top cap, submersible pressure transducer, and porous stone. The flexible membrane is added just before insertion into the ground.

6.1.3 Sensor Installation

Both the two-dimensional velocity transducers and the PPTs were installed using steel CPT rods and the pushing mechanism on the back of T-Rex. A ~10-cm long steel connector rod was used as an adapter to connect the sensor to the steel CPT rods: one end forms a compression fit with the aluminum top cap on the top of the sensor and the other end of the connector rod screws into a steel CPT rod. During installation, the horizontal geophones on the two-dimensional velocity transducers and the filters on the PPTs were oriented in line with the eventual direction of shaking for the shake tests with T-Rex. Once the sensors were pushed to the target depth using the steel CPT rods, the sensors were

decoupled from the steel connector rod by pouring water down the center of the hollow steel CPT rods to increase the pressure on the top of the sensor and gently retracting the rods. The holes were backfilled with bentonite pellets after retraction of the pushing rods.

The PPTs required additional preparation prior to installation to fully saturate the components of the sensor. The filters were boiled in distilled water for a minimum of 30 minutes and the sensors were assembled in a bucket of distilled water. The PPTs were also covered with a thin, rubber membrane so that they would remain saturated in the transition from the water bucket to their final position in the ground below the water table. During the installation process, over-sized pilot holes allowed the PPTs to be lowered by hand to a depth below the water table before using the pushing mechanism on the back of T-Rex. This step in the installation process prevented the membrane from ripping off until after the sensor was below the water table.

6.2 OVERVIEW OF SHAKE TESTING SETUP

In this project, the sensor array for shake testing with T-Rex was composed of four or five two-dimensional velocity transducers and five or six pore pressure transducers (PPTs) that were installed below the ground surface and within the plan dimensions of the baseplate of T-Rex (2.3 by 2.3 m^2). These sensors captured the response of the soil during each stage of shaking by recording the soil particle velocity and the water pressure.

The exact configuration of the two-dimensional velocity transducers and PPTs varied by test site (Site 3, Site 4, or Site 6). In the case of Site 4, the sensor configuration also varied with the ground improvement method. The sensor array used at Site 3 consisted of four, two-dimensional velocity transducers and five PPTs configured as shown in Figure 68. The sensor array used at the 4-NS-1 and 4-RAP-1 test panels of Site 4 consisted of five, two-dimensional velocity transducers and six PPTs configured as shown in Figure 69. The sensor array used at the 4-RIC-1 and 4-LMG-1 test panels of Site 4 consisted of five, two-dimensional velocity transducers and six PPTs configured as shown in Figure 70. The sensor array used at the Site 6 consisted of four, two-dimensional velocity transducers and five PPTs configured as shown in Figure 71.

While similar in configuration, each modification to the sensor array was made for an explicit purpose. The sensors at Site 3 and Site 4 were placed deeper than those at Site 6 because the depth to the liquefiable layer is greater at those sites and the sensor array was positioned primarily to capture the behavior of the liquefiable material. Additional sensors were added to the arrays at Site 4 because testing at Site 4 took place approximately 2 months after testing at Site 3 and Site 6. This change was made because the test results from Sites 3 and 6 showed the potential value of adding additional sensors to the instrumentation arrays. The variation in array configuration between the array used at 4-

NS-1 and 4-RAP-1 and the array used at 4-RIC-1 and 4-LMG-1 was due to challenges encountered during installation.

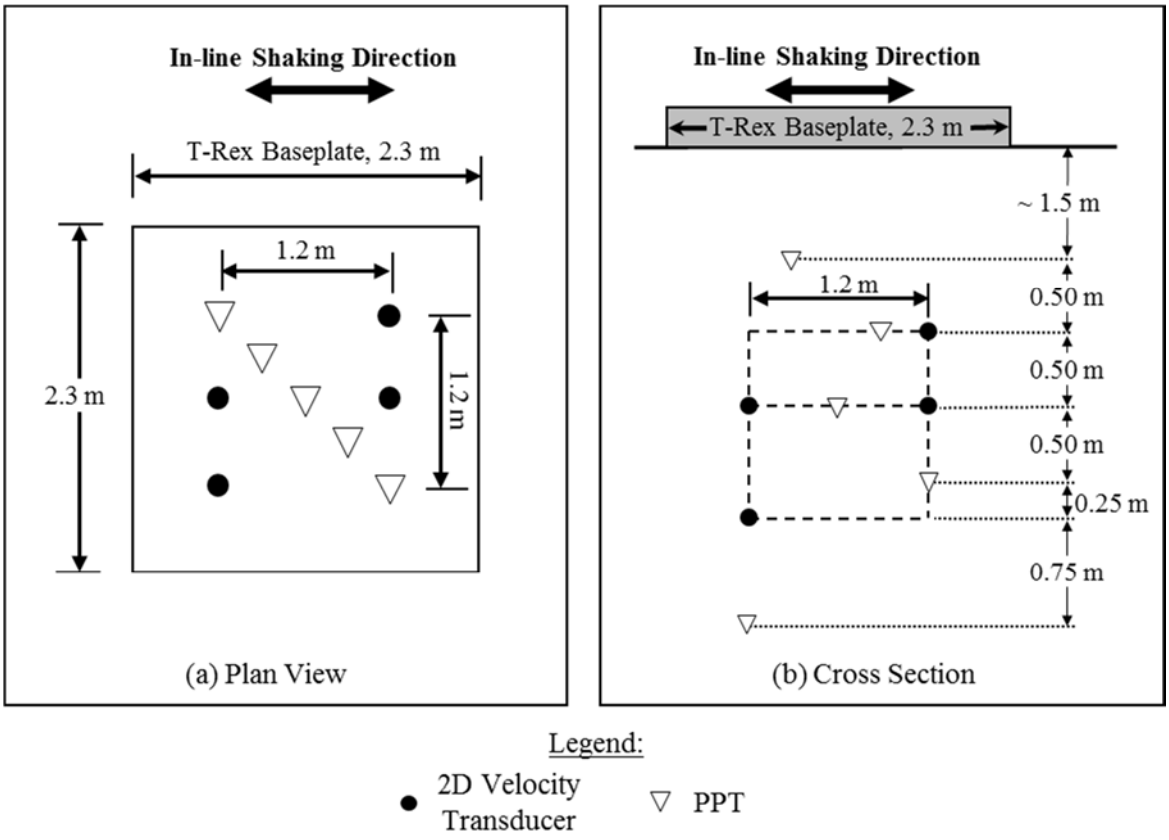

Figure 68: Plan and cross-sectional views ((a) and (b), respectively) of the instrumentation array used at Site 3 for shake testing with T-Rex.

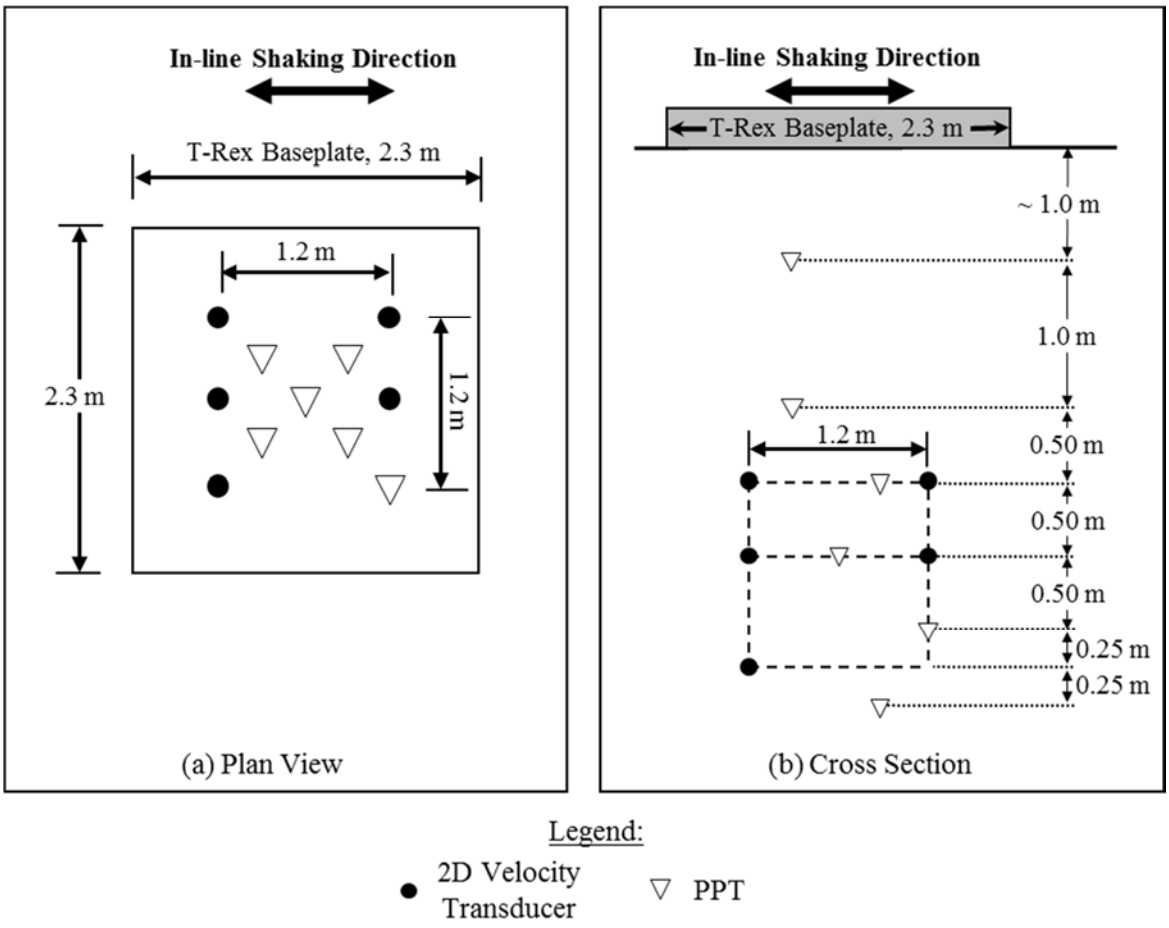

Figure 69: Plan and cross-sectional views ((a) and (b), respectively) of the instrumentation array used at Site 4 for shake testing with T-Rex at test panels 4-NS-1 and 4-RAP-1.

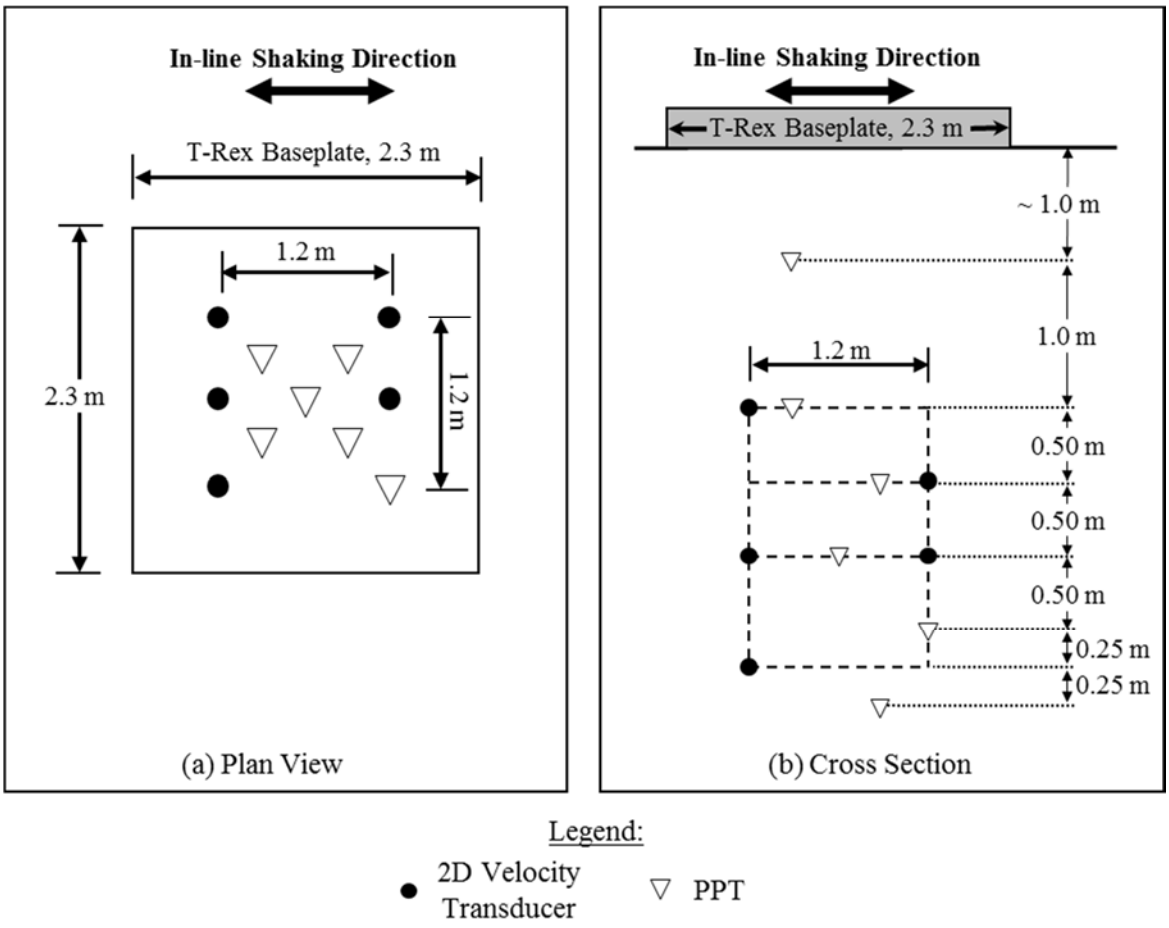

Figure 70: Plan and cross-sectional views ((a) and (b), respectively) of the instrumentation array used at Site 4 for shake testing with T-Rex at test panels 4-RIC-1 and 4-LMG-1.

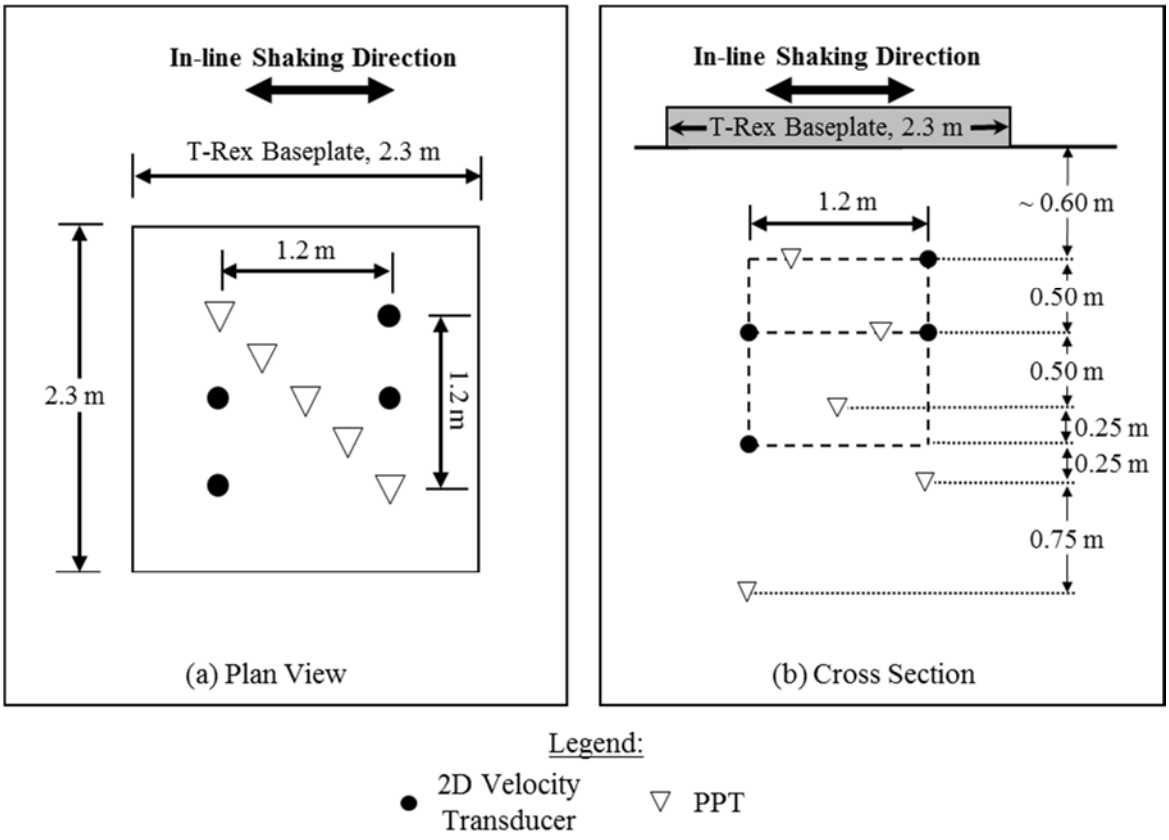

Figure 71: Plan and cross-sectional views ((a) and (b), respectively) of the instrumentation array used at Site 6 for shake testing with T-Rex.

In these tests, T-Rex is used as a controlled source of downward-propagating, horizontally oriented, sinusoidal shear waves. As shown in the theoretical force output plot in Figure 72, T-Rex is capable of shaking horizontally at force levels up to 133 kN in the frequency range of 5 to 180 Hz. A typical shake testing experiment is broken into five or six separate stages, with each stage consisting of 100 cycles at 10 Hz and a different constant input force amplitude. Starting at the lowest level of shaking for the first stage (13.3 kN), each subsequent stage of shaking is performed with a larger input force amplitude, with a maximum force level ranging between 106.4 to 133 kN depending on how the test was progressing. While the exact force amplitude at a given stage number

varies between experiments, the typical experimental load levels used for five stages of shaking on this project is shown in Table 28.

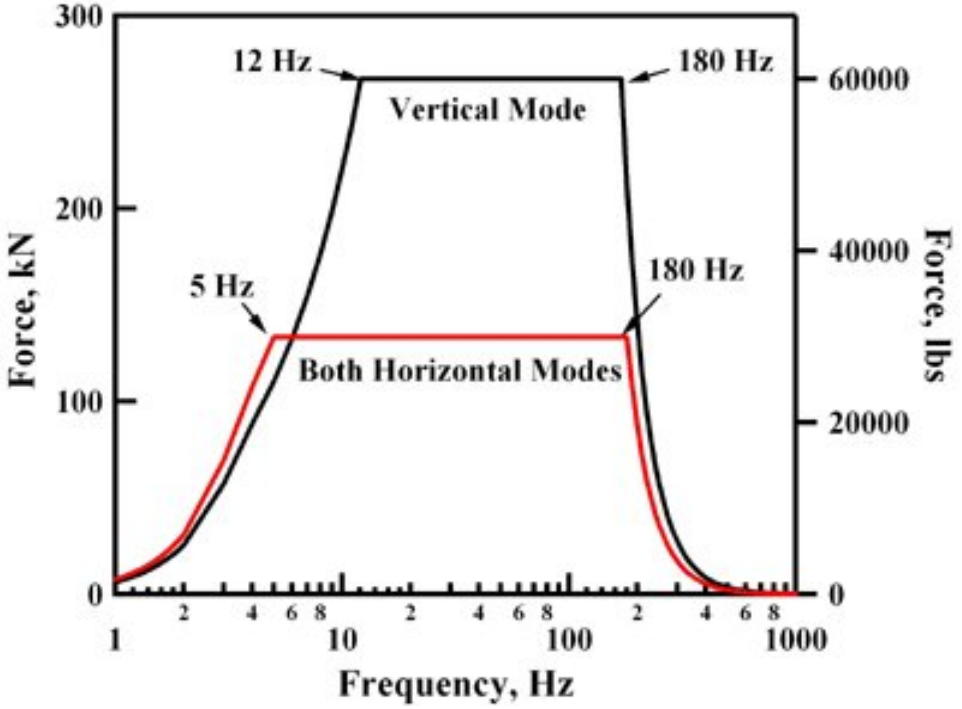

Figure 72: Theoretical force output of T-Rex shaking a rigid half space in both the vertical and horizontal modes (from Menq et al. 2008).

Table 28: Typical load levels used in the five stages of shake testing with T-Rex in Christchurch.

Stage #	Number of Cycles, N	Frequency (Hz)	Force (kN)	Force (lbs)
1	100	10	13.3	3,000
2	100	10	26.6	6,000
3	100	10	39.9	9,000
4	100	10	66.5	15,000
5	100	10	106.4	24,000

6.3 EVALUATION OF EXCESS PORE PRESSURE RATIO

Excess pore pressure generated from cyclic shear strains are composed of two distinct components. The dynamic excess pore pressure is the component that responds immediately to the applied shear stress but is transient in nature and less detrimental to the stability of soil deposits than the residual excess pore pressure. The residual excess pore pressure is the component of pore pressure that is generated in response to cyclic loading at shear strains that are large enough to induce permanent volume change in the soil. In shake testing with T-Rex, the residual excess pore pressure is evaluated by passing the pore pressure time record through a low-pass filter to eliminate frequencies greater than 3 Hz, which has the effect of removing the dynamic excess pore pressure component from the time record.

The excess pore pressure ratio (r_u) is defined as the ratio between the change in pore pressure from the hydrostatic condition (Δu) and the initial vertical effective stress in the soil (σ_v'):

$$r_u = \frac{\Delta u}{\sigma_v'} \times 100\ \% \qquad (15)$$

Liquefaction is triggered when r_u is equal to 100 %, corresponding to a total loss of confining pressure in the soil. The initial vertical effective stress in the soil was evaluated using a total unit weight of 17 kN/m^3 for soils above the water table and 19.5 kN/m^3 for soils below the water table. The initial, hydrostatic water pressure was determined from measurements taken by the PPTs immediately before each stage of shake testing.

In this study, the residual excess pore pressure ratio after 30 cycles of loading was used analysis. 30 cycles was selected as the optimal number of cycles for two reasons: (1) the first ~10 cycles of shaking sometimes exhibited erratic pore pressure generation before settling into more consistent patterns and (2) the residual excess pore pressure sometimes

experienced a plateau after ~50 cycles. The plateau in residual excess pore pressure may be caused by the simultaneous dissipation of excess pore pressure laterally and downward into soils outside the main loading zone below the baseplate of T-Rex.

6.4 EVALUATION OF SHEAR STRAIN

Shear strain induced in the soil during shake testing with T-Rex was evaluated using a modification of the displacement-based method that utilizes a single, 4-node element as described by Chang (2002), Rathje et al. (2004), and Cox (2006). While previous research involved a single, 4-node element, these ground improvement trials expanded the instrumentation array by vertically stacking two to three 4-node elements and eliminating sensors from some of the nodal points in the 4-node element due to time and cost considerations. The impact of calculating shear strains with fewer than four sensors in a single 4-node element is discussed in Section 6.4.1 and the impact of stacking 4-node elements is discussed in Section 6.4.2.

6.4.1 Calculation of Shear Strains with a Reduced Number of Sensors

The objective of eliminating sensors from select nodes in the 4-node element was to minimize installation disturbance to the soil and limit the number of sensors installed at each test site for time and cost considerations. By taking advantage of the symmetric nature of the 4-node elements and the assumption of plane-wave propagation during the shake tests, two-dimensional velocity transducers were eliminated from one or two corners of a 4-node element with minimal impact integrity of the results as discussed below. The velocity time records at the node without a sensor were simulated by using the time records from the two-dimensional velocity transducer located at the horizontally-adjacent node at the same elevation. In this modification, the horizontal component of the velocity time record remained unaltered while the vertical component of the velocity record is polarized to capture the mild rocking nature of the horizontal shaking from T-Rex.

The validity of this modification was assessed by evaluating shear strain at three locations along the centerline of an element with sensors at two nodes, three nodes, and four nodes. These three, 4-node element variations are illustrated in Figure 73. The data

used in this assessment come from shake testing at test panels 4-NS-1 and 4-RAP-1, both of which includes six stages of shaking. These are the only test panels whose instrumentation array included a 4-node element with two-dimensional velocity transducers at all four nodes.

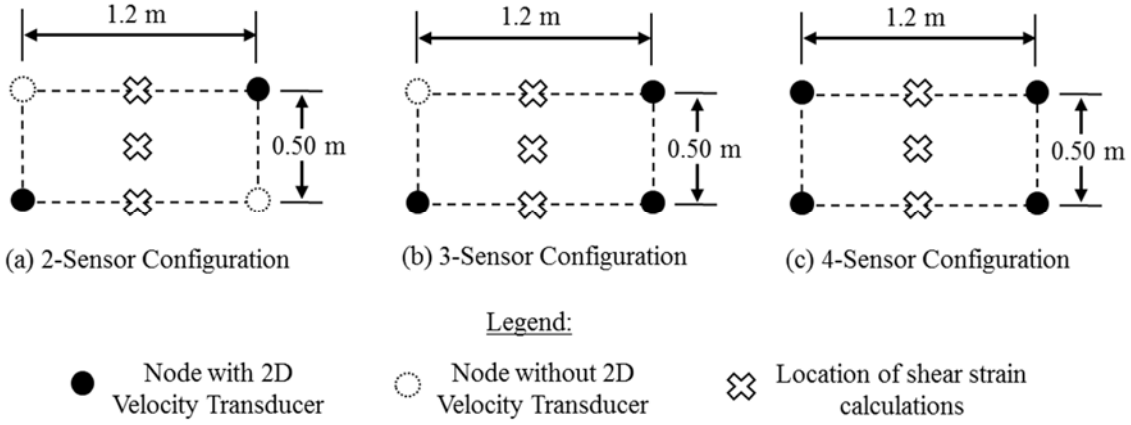

Figure 73: Schematic diagram showing the various configurations of the 4-node element: (a) sensors at two of the four corners, (b) sensors at three of the four corners, and (c) sensors at all four corners.

The results of the shear strain calculations at each of the three locations along the centerline of the 4-node array at three different elevations are shown in the following figures for the two test panels. For results from test panel 4-NS-1, variations in shear strains along the centerline of the 4-node element are presented for the top of the array in Figure 74, the center of the array are presented in Figure 75, and the bottom of the array are presented in Figure 76. For results from test panel 4-RAP-1, variations in shear strains along the centerline of the 4-node element are presented for the top of the array in Figure 77, the center of the array are presented in Figure 78, and the bottom of the array are presented in Figure 79.

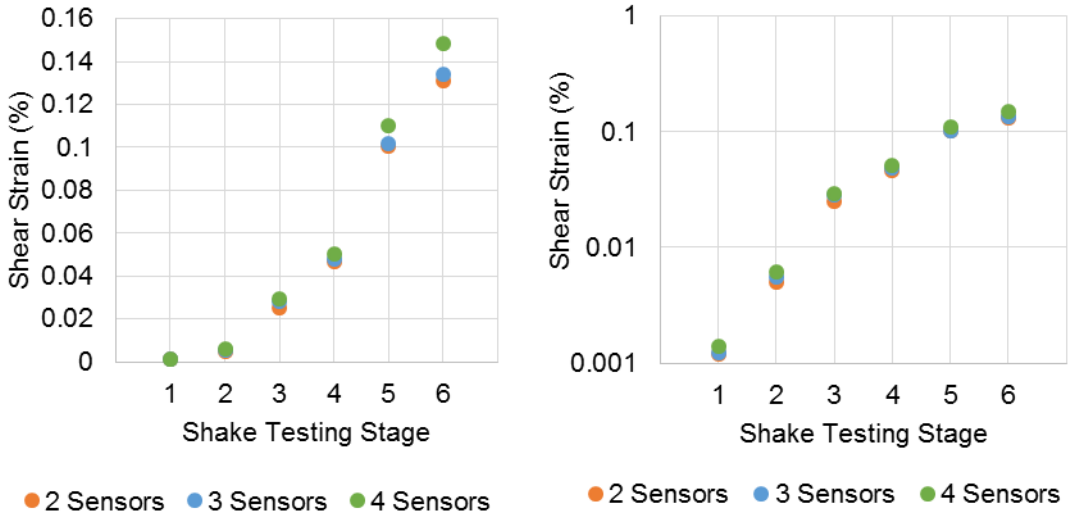

(a) Shear strain on an arithmetic scale (b) Shear strain on a logarithmic scale

Figure 74: Evaluation of shear strains at the horizontal midpoint and top of the 4-node element using two, three, and four sensors for each of the six stages of shaking at the 4-NS-1 test panel.

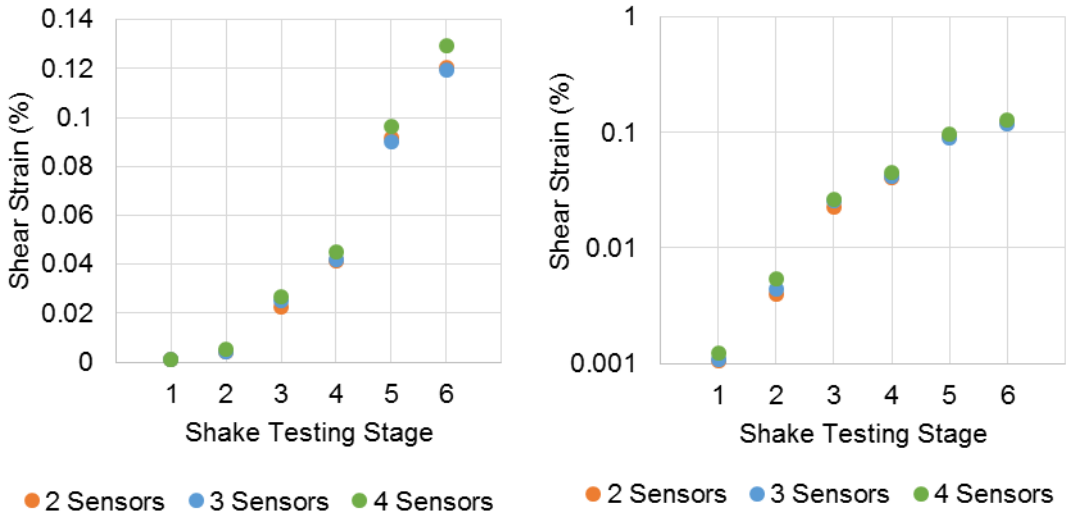

(a) Shear strain on an arithmetic scale (b) Shear strain on a logarithmic scale

Figure 75: Evaluation of shear strains at the horizontal midpoint and vertical midpoint of the 4-node element using two, three, and four sensors for each of the six stages of shaking at the 4-NS-1 test panel.

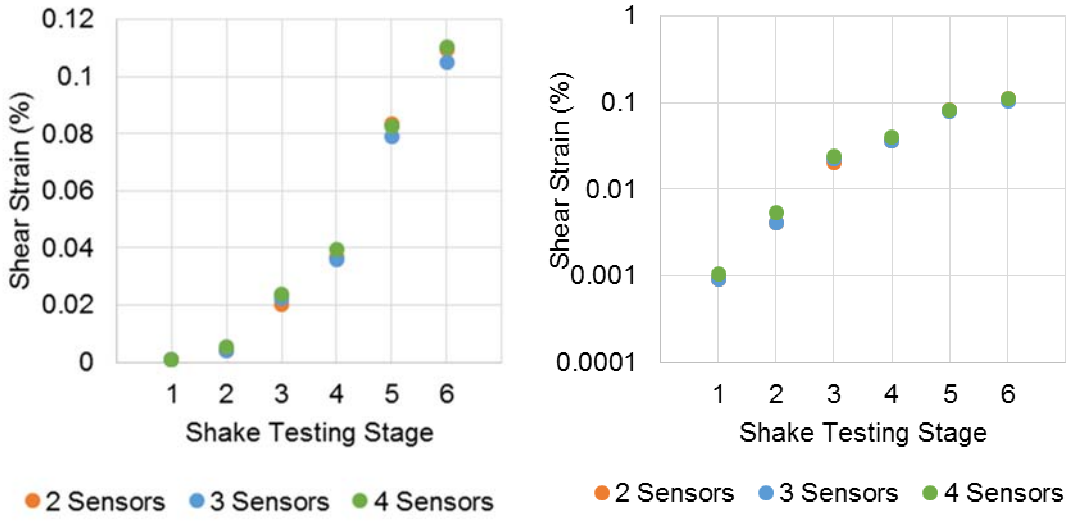

(a) Shear strain on an arithmetic scale (b) Shear strain on a logarithmic scale

Figure 76: Evaluation of shear strains at the horizontal midpoint and bottom of the 4-node element using two, three, and four sensors for each of the six stages of shaking at the 4-NS-1 test panel.

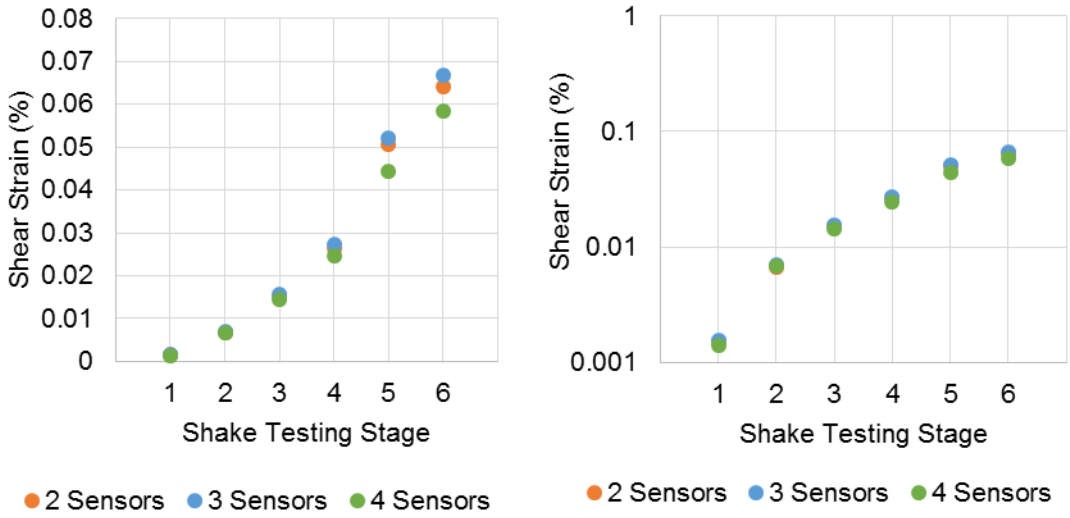

(a) Shear strain on an arithmetic scale (b) Shear strain on a logarithmic scale

Figure 77: Evaluation of shear strains at the horizontal midpoint and top of the 4-node element using two, three, and four sensors for each of the six stages of shaking at the 4-RAP-1 test panel.

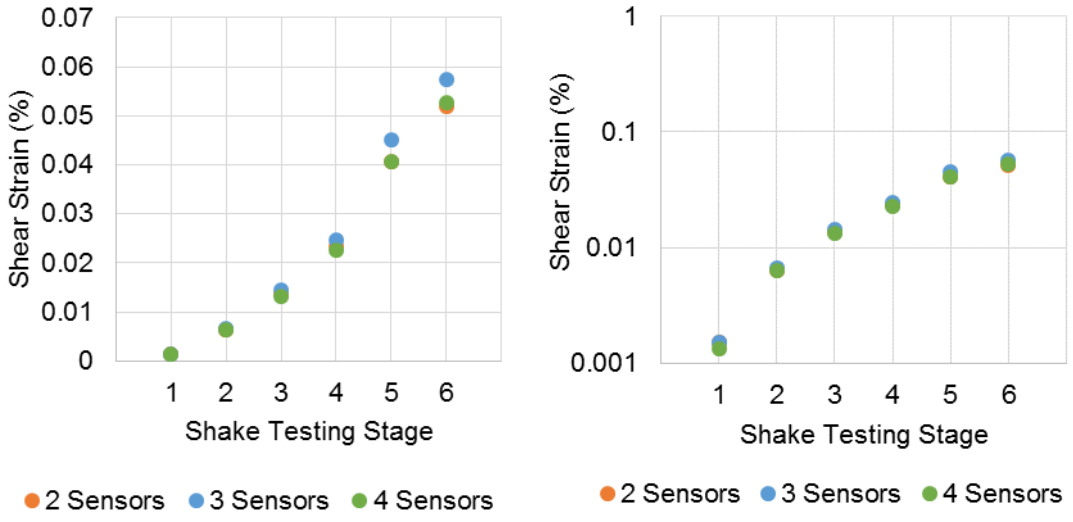

(a) Shear strain on an arithmetic scale (b) Shear strain on a logarithmic scale

Figure 78: Evaluation of shear strains at the horizontal midpoint and vertical midpoint of the 4-node element using two, three, and four sensors for each of the six stages of shaking at the 4-RAP-1 test panel.

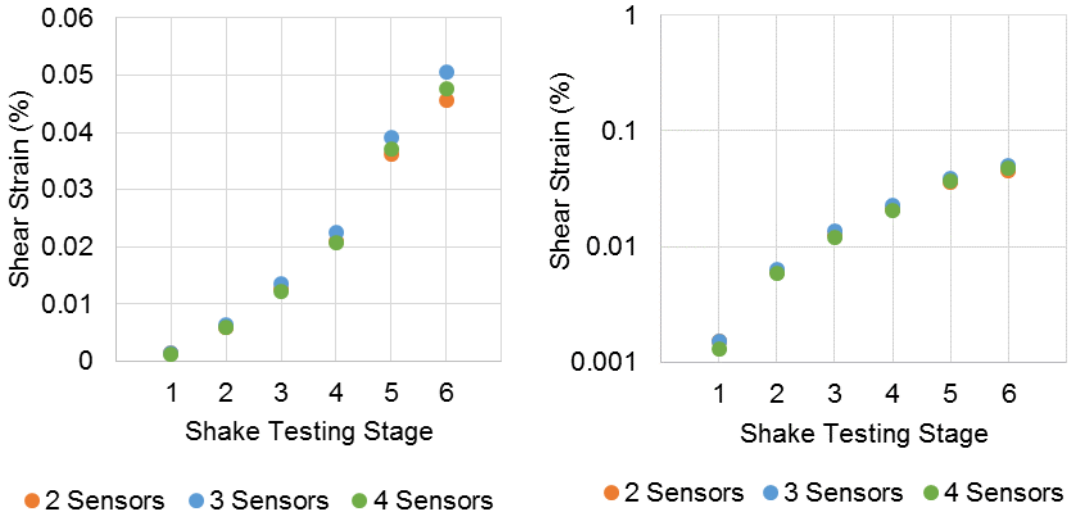

(a) Shear strain on an arithmetic scale (b) Shear strain on a logarithmic scale

Figure 79: Evaluation of shear strains at the horizontal midpoint and bottom of the 4-node element using two, three, and four sensors for each of the six stages of shaking at the 4-RAP-1 test panel.

In comparison to the shear strains calculated using four sensors, the shear strains calculated using three sensors vary by -4 % to -34 % (median value -19 %) and the shear strains calculated using two sensors vary by -8 to -35 % (median value -22 %) at test panel 4-NS-1. At test panel 4-RIC-1, the shear strains calculated using three sensors vary by -13 % to 17 % (median value 1 %) and the shear strains calculated using two sensors vary by -22 % and 14 % (median value -5 %) in comparison to the shear strains calculated using four sensors. In two-thirds of calculations at both the 4-NS-1 and 4-RIC-1, the shear strain calculation using two sensors under- or overestimates the value of shear strain calculated using four sensors to a greater degree than the calculation using three sensors. In other words, the calculation of shear strain using two sensors is less accurate than using three sensors, though there are many exceptions in which the reverse is true and many times the values are closer to each other than they are to the shear strains calculated using four sensors. Further, it is important to note that using two or three sensors to calculate shear strains typically results in an underestimate of the shear strains in comparison to those calculated using four sensors.

On a logarithmic scale, a variation in shear strain of up to 35 % will not have a large impact on the overall analysis, but it still large enough to be of concern. It is also worrisome that the shear strains calculated using fewer than four sensors consistently underestimates the values of shear strains calculated using four sensors. While it was not optimal to use fewer than four sensors in each 4-node element because of this loss in accuracy in calculating shear strains, this modification allowed significantly more data to be collected from shake testing with T-Rex. Given the limitations of time and cost in this study, the author believes that the benefits of reducing the number of sensors greatly outweigh the risks, but the risks should not be forgotten.

The design of an instrumentation array with fewer than four sensors for a 4-node element should be used with an additional note of caution. This modification can only be used with a reasonably symmetric plane wave propagating vertically that is also centered along the centerline of the array. Further, an installed sensor can only simulate the particle motion at a node that is at the same depth and same lateral distance from the centerline as its position, requiring a minimum of two sensors located at different depths in the 4-node element. The greatest foreseen risk in using fewer than four sensors is the failure of a non-redundant sensor during shaking, which would eliminate the opportunity to evaluate shear strains using the 4-node element configuration.

6.4.2 Horizontal Variation in the Evaluation of Shear Strain

The expanded instrumentation array provided significantly greater insight into the behavior of the soil during shake testing but a known shortcoming of the stacked array configuration is the development of a discontinuity in evaluated shear strain at the interface between the stacked, 4-node elements. To eliminate the discontinuity in shear strain at the boundary, shear strain was evaluated along the centerline at three depths within each 4-node element (top, center or location of a PPT, and bottom of the element) and a French curve was used to interpolate values of shear strain within the elements as well as extrapolate values of shear strain above and below the elements at depths that correspond with the location of PPTs. An example of this analysis is shown in Figure 80.

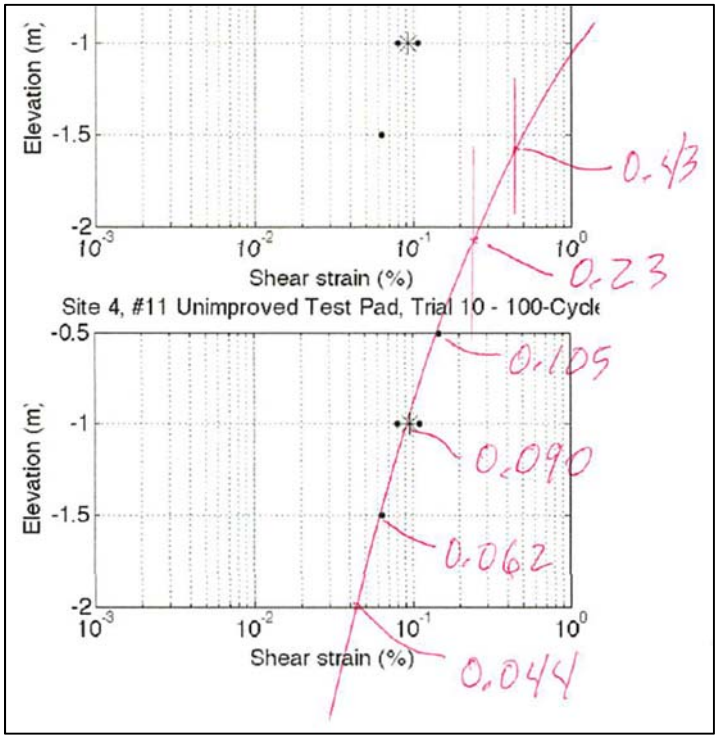

Figure 80: Example extrapolation of shear strain values using a French curve at one stage of shake testing at the 4-NS-1 test panel.

Because these values of shear strain are ultimately paired with water pressure measurements from PPTs that are predominantly not located along the centerline of the instrument array, this centerline-interpolation approach requires the shear strain to be relatively constant at a given elevation across the 4-node element. The results of shake testing at the 6-NS-1 test panel were used to assess the validity of this assumption by evaluating shear strains at 25 locations within an array with two, stacked, 4-node elements. The cross-section of the instrumentation array with two-dimensional velocity transducers and PPTs is presented in Figure 81a and the location of the 25 shear strain evaluations are shown in Figure 81b. The horizontal position of these locations are -0.6 m, -0.3 m, 0 m, 0.3 m, and 0.6 m relative to the center line. Shear strain was evaluated twice at locations 11 through 15, once using the top, 4-node element and once using the bottom, 4-node element to investigate the discontinuity in shear strain that develops at the interface between two elements.

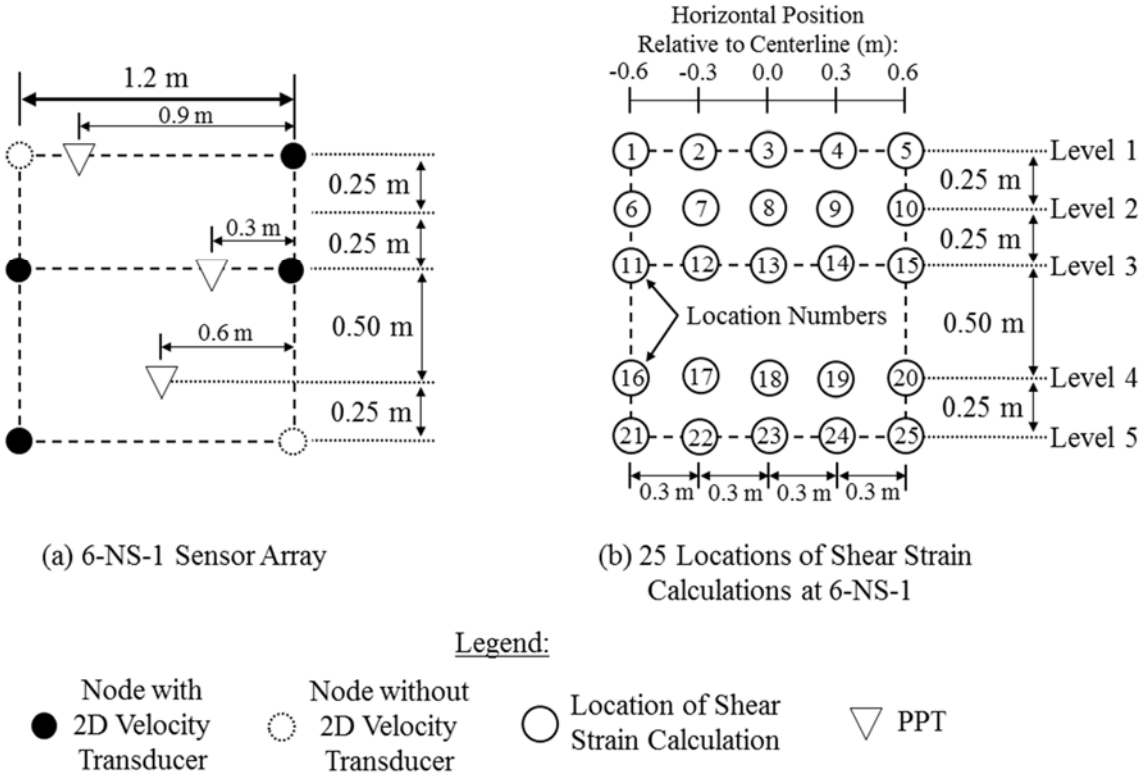

Figure 81: Schematic used for evaluating the horizontal distribution of shear strain across the 4-node element: (a) partial instrumentation array at 6-NS-1 test panel showing the sensors used in the analysis and (b) location of shear strain calculations at 25 points overlaid on the 6-NS-1 sensor array.

Figure 82 through Figure 87. The maximum variation in shear strain at the outermost edge of the 4-node element compared to shear strain at the centerline increases with increasing levels of shaking as the shake test stages progress. The maximum magnitude of variation is 2.9 % at the lowest level of shaking in Stage 1 while the maximum magnitude of variation is 7.2 % at the largest level of shaking in Stage 5. This variation in shear strain is considered negligible particularly since the shear strains are typically presented on a logarithmic scale and the comparisons focus on the variation in shear strains over two to three orders of magnitude.

This horizontal variation in shear strains also needs to be considered with regard to the shear strain discontinuity that exists for values evaluated at the boundary between the two, 4-node elements. The data in Figure 88 show the variation in shear strain values evaluated at the same location using two different 4-node elements, the upper element and the lower element. The variations presented in Figure 88 range from 30.1 % to 75.3 % and are much larger than those associated with horizontal variation across the 4-node element. Rectifying this discontinuity is the main reason for using a center-line interpolation and on the basis of this analysis, it is concluded that the assumption of constant shear strain values at a given elevation within the 4-node element is sufficiently valid for this test setup.

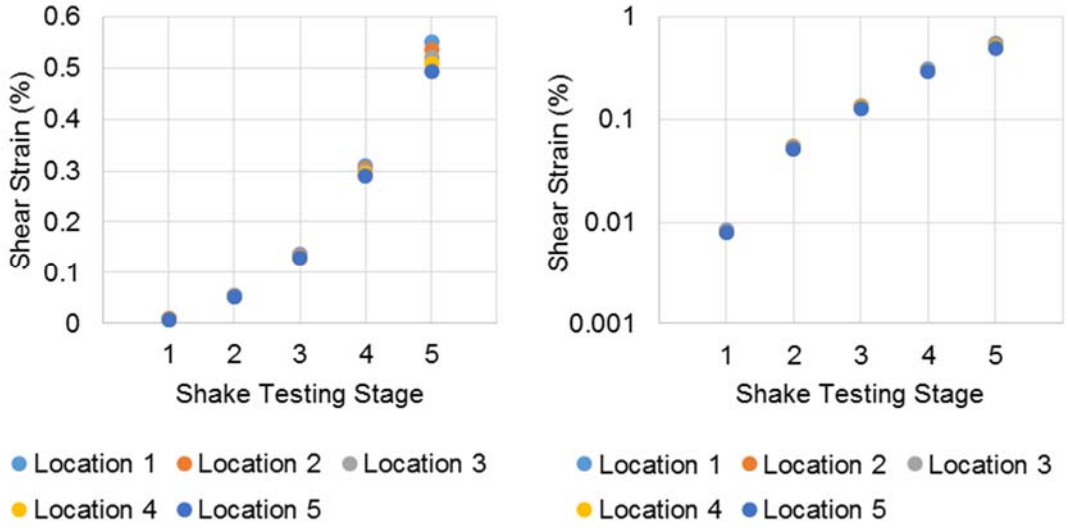

(a) Shear strain on an arithmetic scale (b) Shear strain on a logarithmic scale

Figure 82: Evaluation of shear strains at Locations 1 through 5 along Level 1 using the top array in each of the five stages of shake testing at the 6-NS-1 test panel.

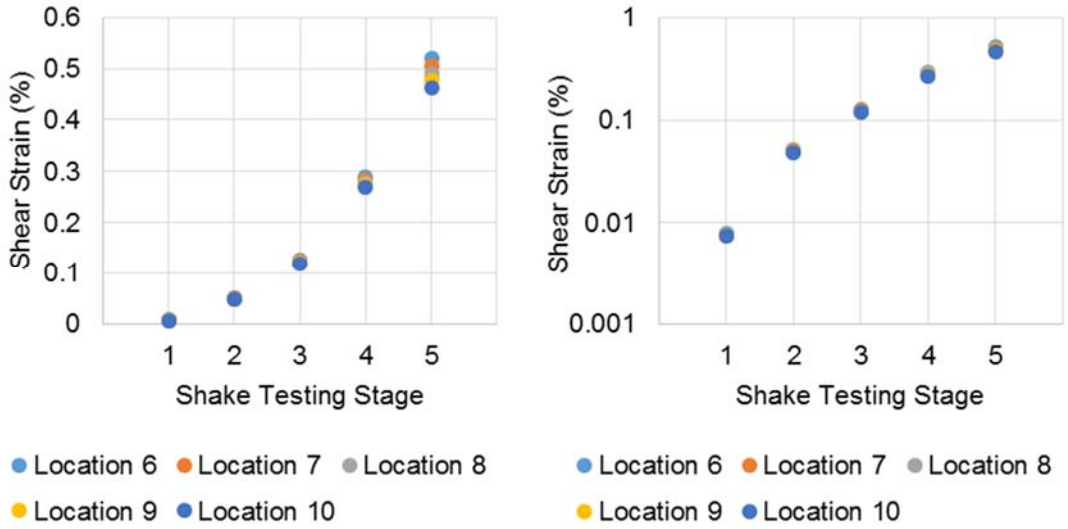

(a) Shear strain on an arithmetic scale (b) Shear strain on a logarithmic scale

Figure 83: Evaluation of shear strains at Locations 6 through 10 along Level 2 using the top array in each of the five stages of shake testing at the 6-NS-1 test panel.

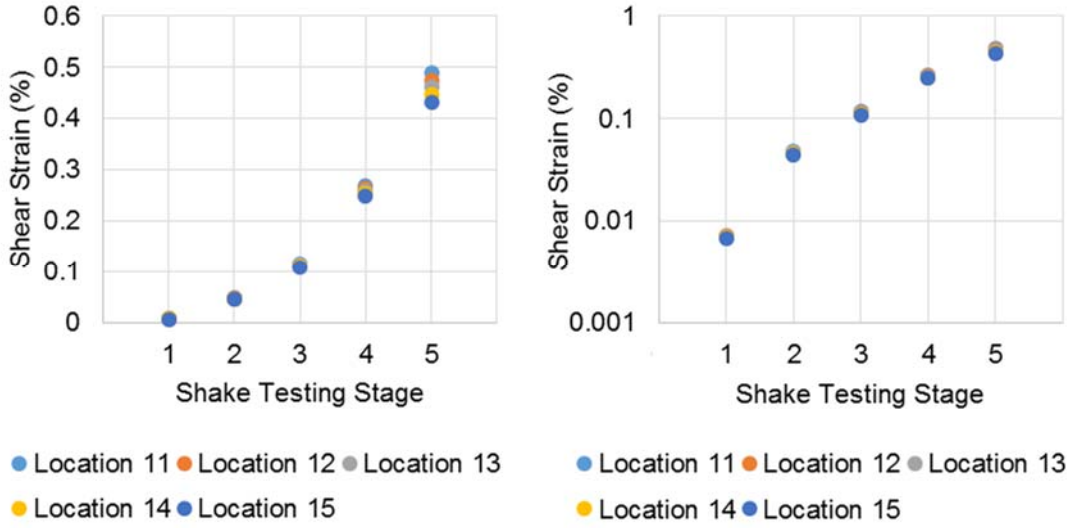

(a) Shear strain on an arithmetic scale (b) Shear strain on a logarithmic scale

Figure 84: Evaluation of shear strains at Locations 11 through 15 along Level 3 using the top array in each of the five stages of shake testing at the 6-NS-1 test panel.

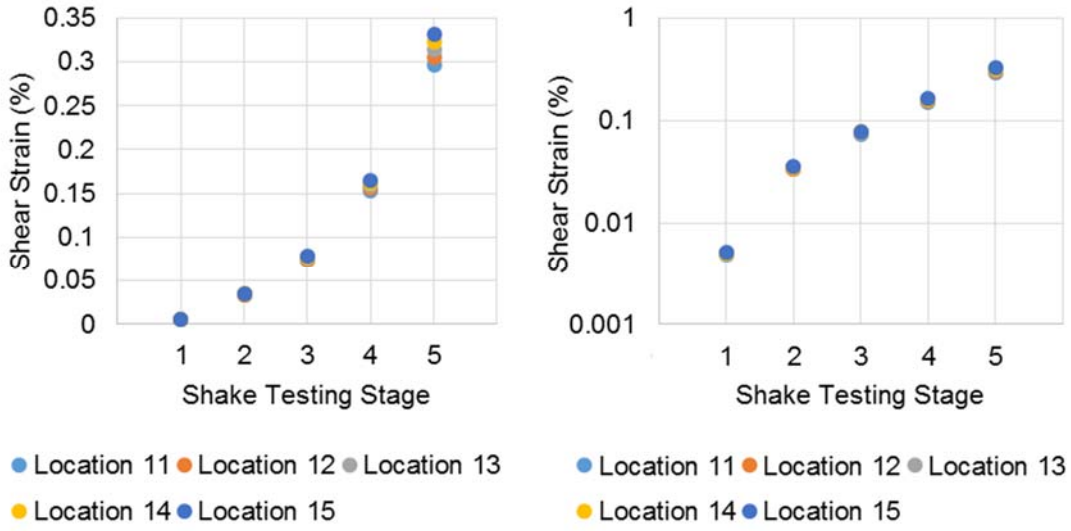

(a) Shear strain on an arithmetic scale (b) Shear strain on a logarithmic scale

Figure 85: Evaluation of shear strains at Locations 11 through 15 along Level 3 using the bottom array in each of the five stages of shake testing at the 6-NS-1 test panel.

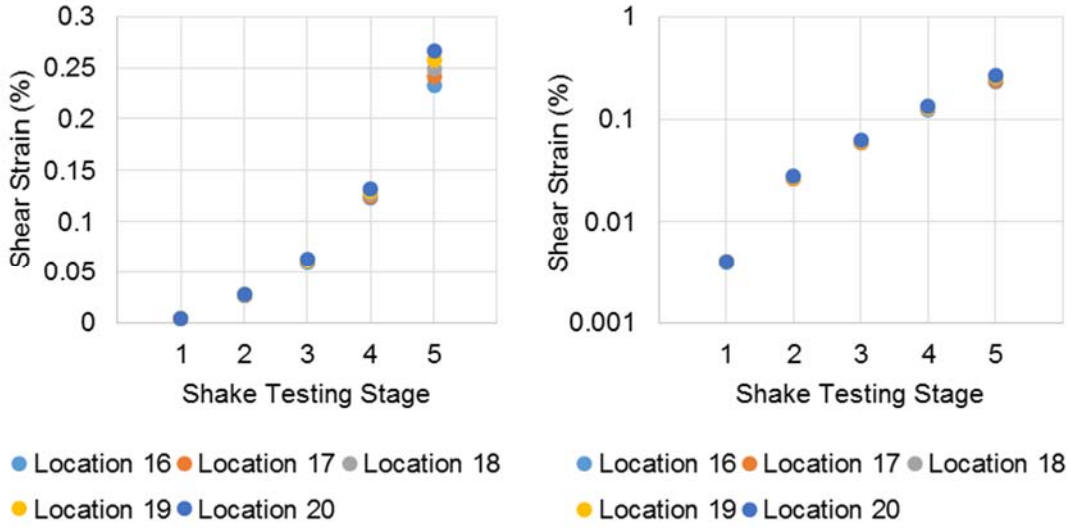

(a) Shear strain on an arithmetic scale (b) Shear strain on a logarithmic scale

Figure 86: Evaluation of shear strains at Locations 16 through 20 along Level 4 using the bottom array in each of the five stages of shake testing at the 6-NS-1 test panel.

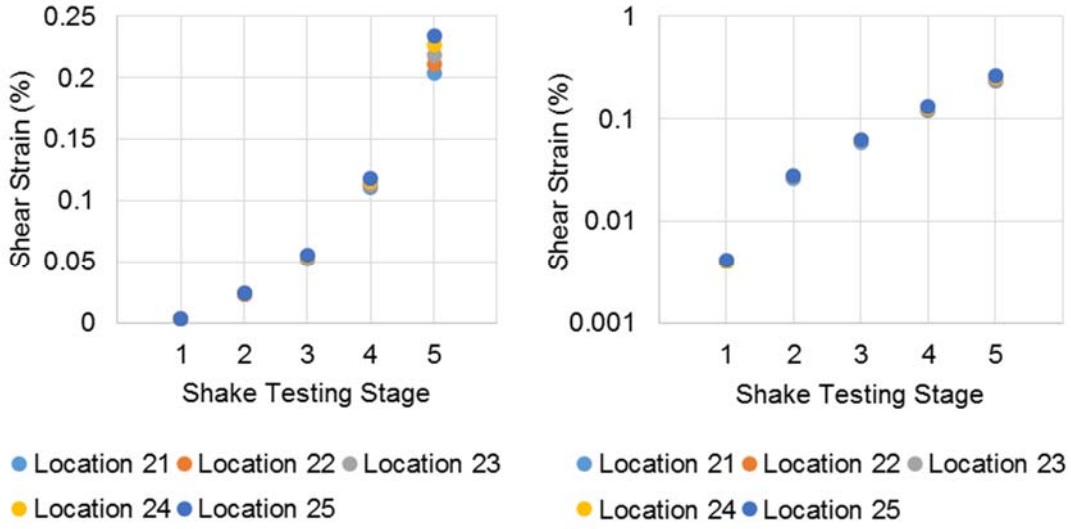

(a) Shear strain on an arithmetic scale (b) Shear strain on a logarithmic scale

Figure 87: Evaluation of shear strains at Locations 21 through 25 along Level 5 using the bottom array in each of the five stages of shake testing at the 6-NS-1 test panel.

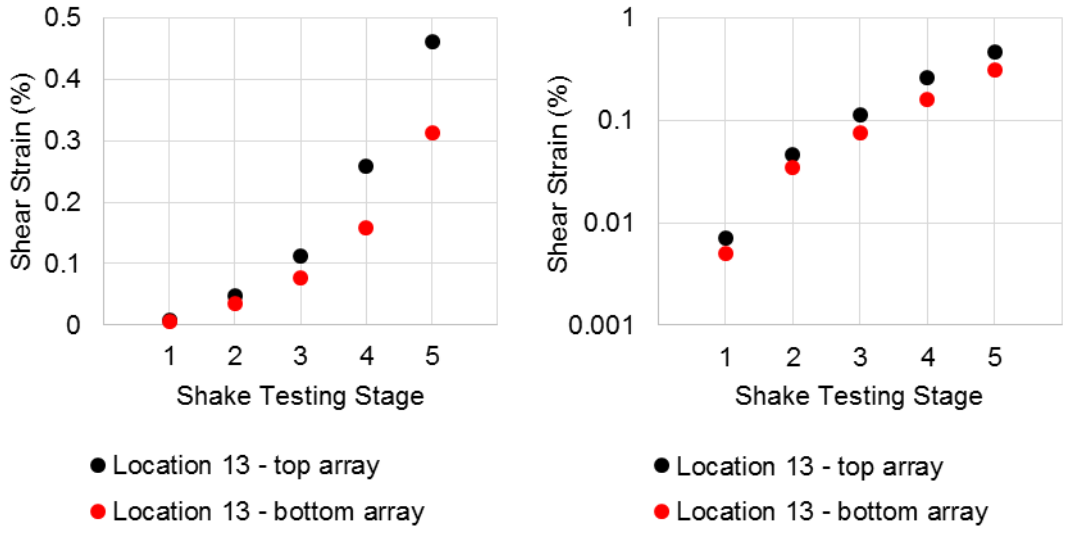

(a) Shear strain on an arithmetic scale (b) Shear strain on a logarithmic scale

Figure 88: Evaluation of shear strains at Location 13 using the top and bottom arrays in each of the five stages of shake testing at the 6-NS-1 test panel.

6.5 EVALUATION OF CYCLIC RESISTANCE RATIO

The cyclic resistance ratio (CRR) of a soil describes its susceptibility to liquefaction in binary terms, categorizing soils as either liquefiable or non-liquefiable. The most common way to evaluate the CRR of soils in situ is to use empirically-derived equations that correlate stress-normalized values of blow counts from SPT testing, cone tip resistance from CPT testing, or shear wave velocity from crosshole testing to values of CRR. In their most basic form, the equations apply to fully-saturated, clean sands on level ground that are subjected to the loading of a 7.5-magnitude earthquake. These CRR calculation methods also include correction factors that account for situations such as varying levels of fines content, thin layers, earthquake magnitudes other than 7.5, and non-level ground surface conditions (Youd et al 2001).

Of the three test methods that can be used to estimate the CRR of the soil, only the shear wave velocity-based method as described by Andrus and Stokoe (2000) was found suitable for estimating the CRR of the soils in the top 4.0 m of the natural soil and ground-improved test panels. The SPT-based method was not considered because SPT tests were not performed at any of the test sites. The CPT-based method was considered but rejected because the evaluations of CRR were inconsistent with the behavior of the soil seen during shake testing with T-Rex. It is believed that the stress-normalization correction factor used in the CPT-based method is inappropriate for evaluation of CRR in this case because almost all of the sensors installed at the test panels have vertical effective stresses less than 35 kPa. The authors of the CPT-based method state that the “expressions were not derived or validated for very low effective stresses”, which in this case refers to effective vertical stresses less than 0.35 atm (~35 kPa) (Boulanger & Idriss 2014).

Using the shear wave velocity-based method by Andrus and Stokoe (2000), the CRR is calculated using the following equation:

$$CRR = \left\{ a\left(\frac{V_{S1}}{100}\right)^2 + b\left(\frac{1}{V_{S1}^* - V_{S1}} - \frac{1}{V_{S1}^*}\right)\right\} \quad (16)$$

where V_{S1} is the overburden stress-corrected shear wave velocity, V_{S1}^* is the limiting upper value of V_{S1} for cyclic liquefaction occurrence and "a" and "b" are curve fitting parameters equal to 0.022 and 2.8, respectively The overburden stress-corrected shear wave velocity (V_{S1}) is calculated using the following equation:

$$V_{S1} = V_S\left(\frac{P_a}{\sigma_v'}\right)^{0.25} \quad (17)$$

where V_S is the shear wave velocity, Pa is atmospheric pressure, and σ_v' is vertical effective stress. The limiting upper value of V_{S1} for cyclic liquefaction occurrence (V_{S1}^*) is calculated using the following equations:

$$V_{S1}^* = 215\ m/s, \text{ for sands with FC} \leq 5\ \% \quad (18)$$

$$V_{S1}^* = 215 - 0.5(FC - 5)\ m/s, \text{ for sands with } 5\ \% < \text{FC} < 35\ \% \quad (19)$$

$$V_{S1}^* = 200\ m/s, \text{ for sands with FC} \geq 35\ \% \quad (20)$$

where FC is the fines content of the soil.

6.6 SUMMARY

This chapter provides an overview of shake testing with T-Rex. The sensors used in this test method include two-dimensional velocity transducers and PPTs to measure the particle velocity and pore water pressure of the soil. A hydraulic ram on the back of T-Rex was used to installed the sensors by pushing them into the ground with steel CPT rods. At each test panel, the sensors were installed in one of four instrumentation array patterns; the instrumentation array varied between Site 3, Site 4, and Site 6, and in the case of the test panels at Site 4 it varied between ground improvement methods. Each shake test with T-Rex at a given test panel consisted of five or six stages of loading at increasingly larger force levels. Each stage of shaking consisted of 100 cycles at a frequency of 10 Hz.

The time records from the two-dimensional velocity transducers and the PPTs were used to evaluate the shear strain and residual excess pore pressure after 30 cycles of shaking. The effect of eliminating two-dimensional velocity transducers from one or two nodes of the 4-node element that is used to calculate shear strain is investigated using the results of shake testing at test panels 4-NS-1 and 4-RIC-1. The impact of neglecting the horizontal variation in shear strain across the 4-node element to allow the interpolation and extrapolation of shear strains using stacks of 4-node elements is investigated using the results of shake testing at test panel 6-NS-1.

Chapter 7: Use of Stiffness Profiles to Understand Shear Strains Induced During Shake Tests with T-Rex

7.1 Introduction to Stiffness Profiles

An advantage of performing large-scale shake testing in situ with T-Rex is the ability to assess the moderate- to large-strain behavior of the ground improvement methods under cyclic loading. One metric of evaluation used in this study is informally called the stiffness profile, which is an observation of the variation in shear strain as a function of depth for a given level of shear stress applied at the ground surface by T-Rex. The shear stress at the ground surface is used rather than the shear stress at depth because the shear stress at depth is not directly measureable and is difficult to accurately estimate. Therefore, the stiffness profiles provide a comparative rather than absolute assessment of the shear strains that were developed during cyclic loading at the natural soil and ground-improved test panels.

7.2 EVALUATION OF T-REX-INDUCED SHEAR STRESS AT THE GROUND SURFACE

T-Rex is capable of outputting very large cyclic loads but it is also a very complex, electro-mechanical nonlinear machine. Precisely calculating the cyclic shear stress induced by T-Rex at the ground surface is non-trivial, but can be done using the recorded force output and accelerations recorded from sensors on the baseplate and reaction mass. The following equation can be used to calculate the force output from T-Rex applied to the baseplate:

$$F_{output} = m_{RM} \times a_{RM} + m_{BP} \times a_{BP} \quad (21)$$

where m_{RM} is the mass of the reaction mass, a_{RM} is the recorded acceleration of the reaction mass during shaking, m_{BP} is the mass of the baseplate, and a_{BP} is the recorded acceleration of the baseplate during shaking (Menq et al. 2008).

The shear stress imposed by the baseplate of T-Rex at the ground surface is obtained by dividing the force output by the surface area of the baseplate that is in contact with the soil:

$$\tau_{T-Rex} = F_{output}/A_{BP} \quad (22)$$

where $\tau_{T\text{-}Rex}$ is the shear stress at the ground surface induced by T-Rex and A_{BP} is the surface area of the baseplate in contact with the ground surface. The dimensions of the square baseplate are 2.3 by 2.3 m^2 (7.5 by 7.5 ft^2), which corresponds to a baseplate area of 5.29 m^2 (56.25 ft^2).

7.3 NORMALIZATION OF SHEAR STRESS AT THE GROUND SURFACE

Given the nonlinear nature of T-Rex as a dynamic source, it is not possible to ensure the same force level of shaking for a given stage of shaking between test panels. The variation in output force level for a given input signal is a function of the soil stiffness, the limited maximum displacement of the baseplate during shaking, and the nonlinear electro-mechanical nature of T-Rex itself. Therefore, the shear strains induced in the soil at each stage of shaking across all test panels were caused by different levels of shear stress, complicating an analysis of the variation in shear strains due to ground improvements.

To overcome this complication, the shear stresses and shear strains were linearly interpolated to match the closest of one of the following nominal shear stress levels: 0.75 kPa, 1.5 kPa, 5 kPa, 10 kPa, 15 kPa, 20 kPa, and 25 kPa. The relationship between shear stress induced by T-Rex at the ground surface and shear strain developed at depth is highly non-linear, an example of which is shown in Figure 89. The data in Figure 89 from the five test panels at Site 6 (6-NS-1, 6-NS-2, 6-RIC-1, 6-RAP-1, and 6-LMG-1) show the non-unique relationships between shear stress induced by T-Rex at the ground surface versus shear strain evaluated at depths ranging from 0.60 to 0.66 m, which corresponds to the depth of shallowest PPTs at these test panels. Figure 90 shows how linear interpolation between adjacent data points was used to estimate the shear strains at various levels of shear stress.

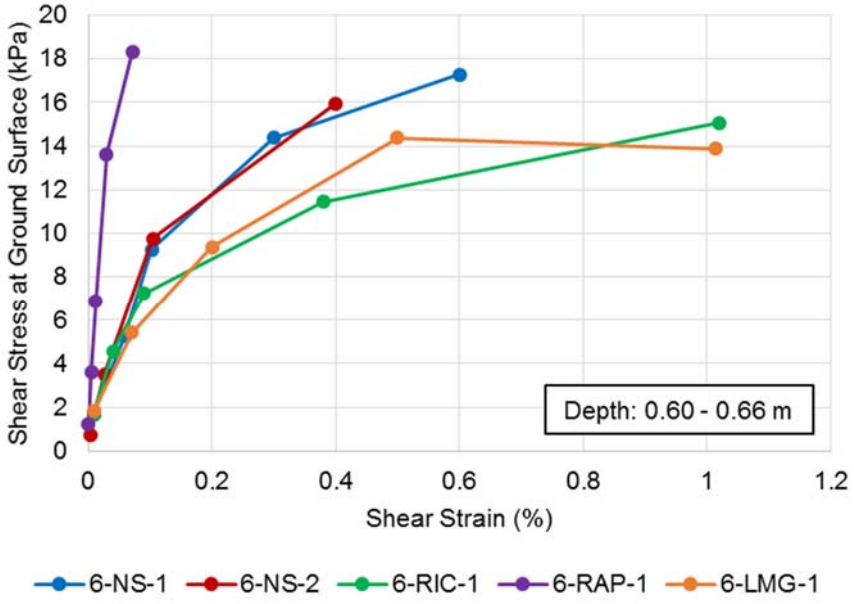

Figure 89: Variation in shear stress induced by T-Rex at the ground surface versus shear strain evaluated at depths ranging from 0.60 to 0.66 m at the five test panels at Site 6.

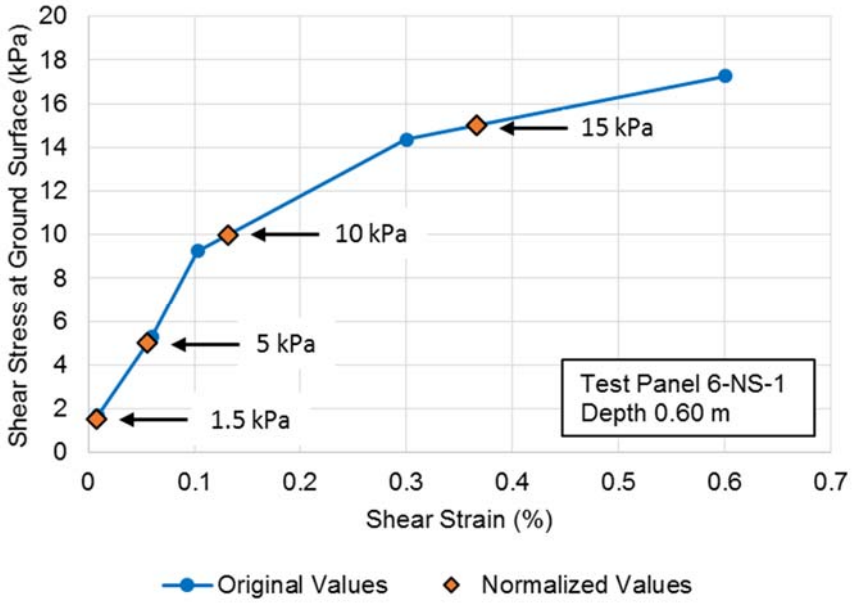

Figure 90: Estimate of shear strain values for shear stresses of 1.5, 5, 10, and 15 kPa using linear interpolation between adjacent data points for the 6-NS-1 test panel at a depth of 0.60 m.

The original values of shear stress and shear strain from the 6-NS-1 test panel are presented in Table 29 for all five stages of shaking and five depths while the nominal values of shear stress and the linearly-adjusted values of shear strain are presented in Table 30. It was common across all test panels for the shear stresses and shear strains of last two stages of shaking to be adjusted to the same nominal shear stress as shown in Table 30 because T-Rex was unable to effectively transfer increasingly large shear stresses into the soil at the largest levels of shaking.

In a situation seen only in testing at Site 3, the increases in shear stresses between shaking stages were sufficiently large enough to skip over 10 kPa as a nominal stress level, eliminating 10 kPa as nominal shear stress level to be used in comparisons. Further, the maximum adjusted shear stress levels at Site 6 never exceeded 15 kPa even though it consistently reached 20 kPa or 25 kPa at Site 3 and Site 4. The minimum nominal shear stress value of 0.75 kPa was only used for one test panel, 6-NS-2, where the lower force outputs were used during testing because of complications with the system electronics of T-Rex. Of the seven nominal shear stress levels used (0.75 kPa, 1.5 kPa, 5 kPa, 10 kPa, 15 kPa, 20 kPa, and 25 kPa), only three nominal stress levels were consistently achieved at almost all 18 of the test panels: 1.5 kPa, 5 kPa, and 15 kPa. These three nominal stress levels were used to compare the linearly-adjusted shear strains as a function of depth across all of the test panels to observe differences in response at the ground-improved test panels in comparison to the natural soil test panels.

Table 29: Original values of shear strain evaluated at the 6-NS-1 test panel over five stages of shaking and at five depths.

Test Panel 6-NS-1

Shaking Stage:	Stage 1	Stage 2	Stage 3	Stage 4	Stage 5
Original Stress (kPa):	1.69	5.28	9.25	14.36	17.26

Depth	$\gamma_{original}$	$\gamma_{original}$	$\gamma_{original}$	$\gamma_{original}$	$\gamma_{original}$
(m)	(%)	(%)	(%)	(%)	(%)
0.6	0.0090	0.0600	0.1030	0.3000	0.6000
1.1	0.0060	0.0400	0.0900	0.2000	0.4000
1.6	0.0040	0.0270	0.0580	0.1200	0.2400
2.1	0.0029	0.0170	0.0320	0.0700	0.1400
2.85	0.0012	0.0073	0.0130	0.0300	0.0630

Table 30: Linearly-adjusted values of shear strain evaluated at the 6-NS-1 test panel over five stages of shaking and at five depths.

Test Panel 6-NS-1

Shaking Stage:	Stage 1	Stage 2	Stage 3	Stage 4	Stage 5
Nominal Stress (kPa):	1.50	5.00	10.00	15.00	15.00

Depth	$\gamma_{adjusted}$	$\gamma_{adjusted}$	$\gamma_{adjusted}$	$\gamma_{adjusted}$	$\gamma_{adjusted}$
(m)	(%)	(%)	(%)	(%)	(%)
0.6	0.0080	0.0560	0.1318	0.3659	0.3659
1.1	0.0053	0.0374	0.1061	0.2439	0.2439
1.6	0.0035	0.0252	0.0671	0.1464	0.1464
2.1	0.0026	0.0159	0.0375	0.0854	0.0854
2.85	0.0011	0.0068	0.0155	0.0372	0.0372

7.4 PRESENTATION AND DISCUSSION OF STIFFNESS PROFILES

Stiffness profiles at three nominal levels of shear stress were evaluated for all test panels subjected to shake testing except 3-NS-2. Testing at test panel 3-NS-2 resulted in only one shaking stage that closely matched one of the three nominal shear stress levels, making it impossible to compare shear strains across a range of shear stresses. For this reason, the results from shake testing at test panel 3-NS-2 are omitted from this stiffness analysis.

In the initial set of figures, the stiffness profiles are organized by test site. The results in Figure 91 show the stiffness profiles from Site 3 for test panels 3-NS-1, 3-RIC-1, 3-RAP-1, and 3-LMG-1. The results in Figure 92 show the stiffness profiles from Site 4 for test panels 4-NS-1, 4-NS-2, 4-RIC-1, 4-RAP-1, and 4-LMG-1. The results in Figure 93 show the stiffness profiles from Site 6 for test panels 6-NS-1, 6-NS-2, 6-RIC-1, 6-RAP-1, and 6-LMG-1. Each test panel stiffness profile contains five to six data markers, the depths of which corresponds to the depths of the PPTs within that test panel where the shear strains were evaluated. The stiffness profiles range in depths from 0.74 to 4.01 m at Site 3, 0.57 to 3.68 m at Site 4, and 0.6 to 2.9 m at Site 6.

For the most part, the variation in shear strain with respect to depth is fairly linear in a semi-logarithmic space with shear strain decreasing logarithmically as depth increases arithmetically, due primarily to the increasing distance from the baseplate of T-Rex, which is the source of the cyclic loading. Two notable exceptions to this trend are the stiffness profiles at 4-RIC-1 and 6-RAP-1. The stiffness profile at the 4-RIC-1 test panel shows higher strains than expected in the 2.0 to 3.0 m depth range for the 5 kPa and 15 kPa shear stress levels, possibly indicating the presence of a soft zone in the subsurface profile. As further evidence toward this theory, both the CPT and DPCH test results also showed the presence of a zone that was less dense and softer than the natural soil in a similar depth

range of 2.0 to 2.6 m at the 4-RIC-1 test panel. As such, this soft zone certainly may be large and soft enough to be responsible for the increase in shear strain seen at the 4-RIC-1 test panel during shake testing at the 5 kPa and 15 kPa shear stress levels in the 2.0 to 3.0 m depth range.

On the other hand, the curvature of the 6-RAP-1 stiffness profile is not easily explained by variations in density or stiffness within the soil profile; in fact, this stiffness profile behaves in a manner opposite to what it expected. The results of the CPT and DPCH testing showed that the soil in the top 1.0 m below the ground surface at the 6-RAP-1 test panel was looser and softer than the median profiles for the natural soil at Site 6. The results from shake testing, however, indicate that the top 1.0 m is much stiffer than expected with shear strains that are almost an order of magnitude smaller than those at a similar depth in the 6-NS-1 and 6-NS-2 test panels and they are even smaller than shear strains within the same profile in the 1.0 to 2.0 m depth range.

In general, it appears that the stiffness profiles at the ground-improved test panels show smaller shear strains for a given level of loading, indicating the ground improvement methods were able to impart greater stiffness to the soil in comparison to the natural soil. At Site 3 and Site 6, the stiffness profiles maintain similar shapes and relative positions in comparison to the other stiffness profiles at the same site across all three nominal levels of shear stress, indicating fairly uniform, relative performance of the soil at small strains (~0.001 %) up to moderate strains (~0.5 %).

In contrast, there is greater variability in the shapes and relative positions of the stiffness profiles at Site 4 across all three nominal levels of shear stress. In particular, the shapes of the 4-NS-1 and 4-RIC-1 are quite different at the 1.5 kPa shear stress level than at the 5 and 15 kPa shear stress levels. Further, the relative position of the 4-LMG-1 stiffness profile at the 5 kPa shear stress level in comparison to the other test panel stiffness

profiles is significantly different than at the 1.5 and 15 kPa stress levels, which perhaps can be attributed as an anomaly in the data. In general there is more variation in the relative positions of each test panel's stiffness profile at Site 4 between levels of shear stress than at Site 3 or Site 6, indicating less uniformity in performance at varying levels of shear stress at the Site 4 test panels. The reason for this variation at Site 4 is not understood.

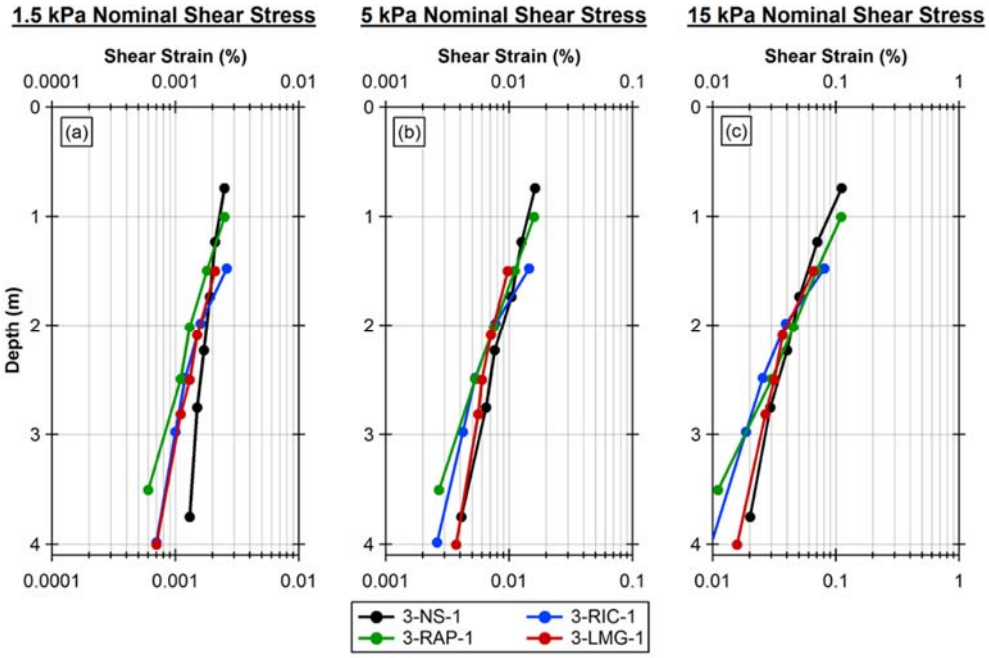

Figure 91: Profiles showing the stiffness profiles from the 3-NS-1, 3-RIC-1, 3-RAP-1, and 3-LMG-1 test panels at Site 3 for three levels of shear stress applied by T-Rex at the ground surface: (a) 1.5 kPa, (b) 5 kPa, and (c) 15 kPa.

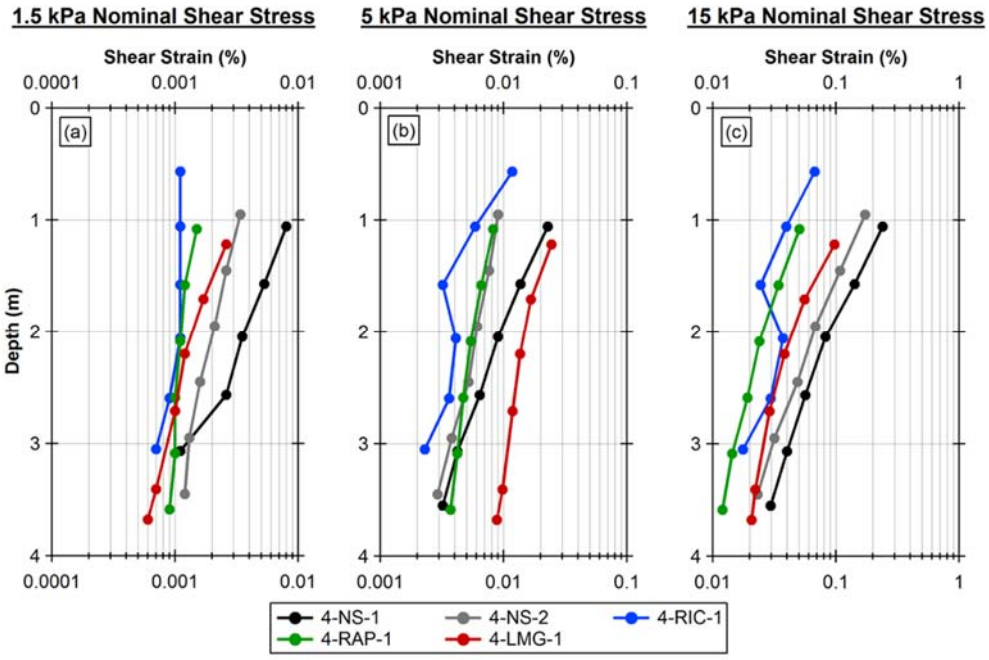

Figure 92: Profiles showing the stiffness profiles from the 4-NS-1, 4-NS-2, 4-RIC-1, 4-RAP-1, 4-LMG-1 test panels at Site 4 for three levels of shear stress applied by T-Rex at the ground surface: (a) 1.5 kPa, (b) 5 kPa, and (c) 15 kPa.

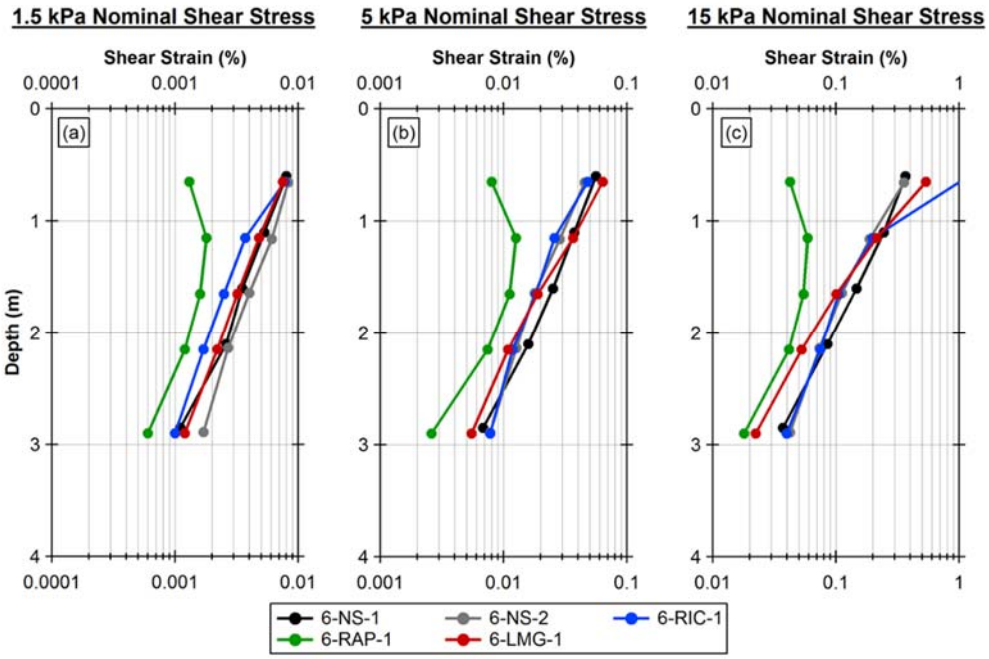

Figure 93: Profiles showing the stiffness profiles from the 6-NS-1, 6-NS-2, 6-RIC-1, 6-RAP-1, 6-LMG-1 test panels at Site 6 for three levels of shear stress applied by T-Rex at the ground surface: (a) 1.5 kPa, (b) 5 kPa, and (c) 15 kPa.

7.5 Relative Change in Stiffness Profiles Due to Ground Improvements

The relative position of the stiffness profiles from the ground-improved test panels in comparison to the natural soil test panels from the same test site provide quantitative insight into the effect the ground improvement methods have on the non-linear cyclic behavior of the soil over a large range of shear strain values (~0.0006 to 1.0 %). The relative change in shear strain between ground-improved test panels and the natural soil test panels can be calculated at any given depth using the following equations for the RIC, RAP, and LMG test panels:

$$\frac{(\gamma_{RIC} - \gamma_{NS})}{\gamma_{RIC}} \times 100\ \% \quad (23)$$

$$\frac{(\gamma_{RAP} - \gamma_{NS})}{\gamma_{RAP}} \times 100\ \% \quad (24)$$

$$\frac{(\gamma_{LMG} - \gamma_{NS})}{\gamma_{LMG}} \times 100\ \% \quad (25)$$

Because the shear strain was evaluated at five or six depths with values that vary between test panels, the shear strain values used in this comparison were linearly interpolated between the data points to provide continuous profiles of shear strain over the depths ranging from the shallowest to the deepest evaluated shear strain data points.

To control for variations between test sites, each site has its own representative natural soil stiffness profile for comparison against the ground-improved stiffness profiles from the same site. At Site 3, the results from shake testing at the second natural soil test panel 3-NS-2 were not included in the stiffness profile analysis so the representative natural soil profile is the same as the 3-NS-1 stiffness profile. At Site 4, the representative natural soil stiffness profile is an average of the 4-NS-1 and 4-NS-2 stiffness profiles. At Site 6, the representative soil stiffness profile is an average of the 6-NS-1 and 6-NS-2 stiffness profiles.

7.5.1 Assessment of the RIC Ground Improvement Method

The relative changes in stiffness profiles due to the RIC ground improvement method is presented in Figure 94 for the three levels of nominal shear stress 1.5 kPa, 5 kPa, and 15 kPa. The median changes in shear strain over the length of each profile due to the RIC ground improvement method is summarized in Table 31, also for the three levels of nominal shear stress 1.5 kPa, 5 kPa, and 15 kPa.

The average median change in shear strain due to the RIC ground improvement is -30 %, indicating that on average, the shear strains at 3-RIC-1, 4-RIC-1, and 6-RIC-1 were reduced by 30 % in comparison to the representative natural soil stiffness profiles for Site 3, Site 4, and Site 6 at all depths. The median change in shear strain for the RIC ground improvement ranged from -3 % at 6-RIC-1 for the 15 kPa shear stress level up to -54 % at the 4-RIC-1 test panel also for the 15 kPa shear stress level. For a given test panel, the median change in shear strain at the 3-RIC-1 and 4-RIC-1 test panels is relatively constant between nominal levels of shear stress, indicating that the RIC and natural soil test panels at those sites have similar trends in non-linear behavior over a large range of shear strains. The 6-RIC-1 test panel, however, shows a consistent decrease in the magnitude of median change in shear strain as the shear stress increases, indicating that it is stiffer than the natural soil at lower levels of shear stress but starts to behave more like the natural soil at larger levels of shear stress.

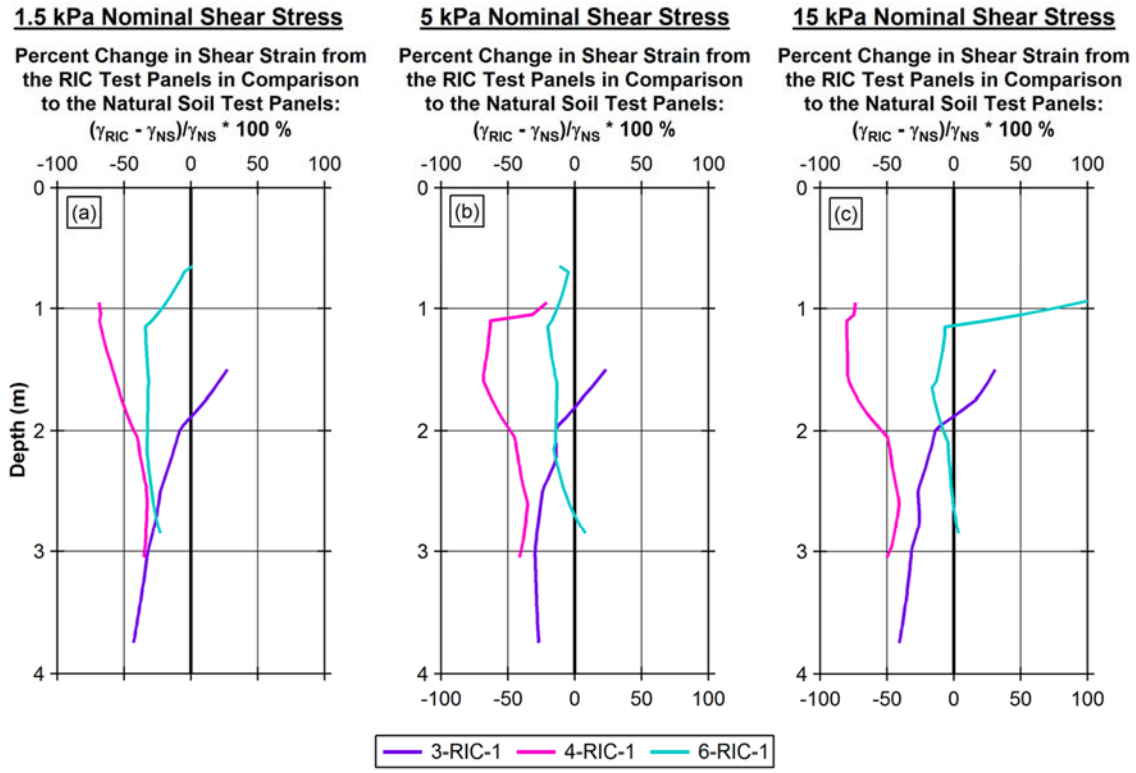

Figure 94: Variation in shear strain at the RIC test panels in comparison to the Natural Soil test panels from Site 3, Site 4, and Site 6 at three nominal levels of shear stress induced by T-Rex at the ground surface: (a) 1.5 kPa, (b) 5 kPa, and (c) 15 kPa.

Table 31: Median values of the relative change in shear strain, γ, at the 3-RIC-1, 4-RIC-1, and 6-RIC-1 test panels in comparison to the 3-NS-1, 4-NS-1 and 4-NS-2, and 6-NS-1 and 6-NS-2 test panels, respectively.

	1.5 kPa Shear Stress* Median Percent Change in Shear Strain, γ: ($(\gamma_{RIC}-\gamma_{NS})/\gamma_{NS}$ * 100 %)	**5 kPa Shear Stress*** Median Percent Change in Shear Strain, γ: ($(\gamma_{RIC}-\gamma_{NS})/\gamma_{NS}$ * 100 %)	**15 kPa Shear Stress*** Median Percent Change in Shear Strain, γ: ($(\gamma_{RIC}-\gamma_{NS})/\gamma_{NS}$ * 100 %)
3-RIC-1:	-25	-26	-26
4-RIC-1:	-43	-44	-54
6-RIC-1:	-32	-14	-3

*Nominal shear stress applied by the baseplate of T-Rex at the ground surface

In general, the RIC ground improvement method appears to successfully reduced the cyclic shear strains for a given level of shear stress at the ground surface in comparison to the natural soil. This performance was predicted by the CPT and DPCH tests that showed median increases in the corrected cone tip resistance q_t between impact points, the small-strain modulus G_{max} between impact points, and the small-strain modulus G_{max} across impact points, indicating greater density and stiffness in the soil as a result of the ground improvement. The data in Table 32 summarize the median increases for these three parameters in addition to the median relative change in shear strain average across the three nominal levels of shear stress.

In comparing results between test panels, neither the CPT nor the DPCH test results are able to indicate which test panel will have the smallest or largest reduction in shear strains during shake testing with T-Rex. For example, CPT testing indicates the test panel 6-RIC-1 had the greatest amount of improvement, DPCH testing indicates that the test panel 3-RIC-1, and shake testing with T-Rex indicates the test panel 4-RIC-1 had the greatest amount of improvement.

Table 32: Median values of relative change due to the RIC ground improvement in corrected cone tip resistance q_t from CPT testing, small-strain modulus G_{max} between impact points from DPCH testing, small-strain modulus G_{max} across impact points from DPCH testing, and shear strain γ from shake testing with T-Rex.

	CPT $\frac{(q_{t,RIC} - q_{t,NS})}{q_{t,NS}} \times 100\ \%$ **Between Improvements**	**DPCH** $\frac{(G_{max,RIC} - G_{max,NS})}{G_{max,NS}} \times 100\ \%$ **Between Improvements**	**DPCH** $\frac{(G_{max,RIC} - G_{max,NS})}{G_{max,NS}} \times 100\ \%$ **Across Improvements**	**Shake Testing** $\frac{(\gamma_{RIC} - \gamma_{NS})}{\gamma_{NS}} \times 100\ \%$ **Between Improvements**
3-RIC-1:	60	40	24	-26
4-RIC-1:	24	17	18	-47
6-RIC-1:	86	20	20	-16

7.5.2 Assessment of the RAP Ground Improvement Method

The relative changes in stiffness profiles due to the RAP ground improvement method is presented in Figure 95 for the three levels of nominal shear stress 1.5 kPa, 5 kPa, and 15 kPa. The median changes in shear strain over the length of each profile due to the RAP ground improvement method is summarized in Table 33, also for the three levels of nominal shear stress 1.5 kPa, 5 kPa, and 15 kPa.

The average median change in shear strain due to the RAP ground improvement is -37 %, indicating that on average, the shear strains at 3-RAP-1, 4-RAP-1, and 6-RAP-1 were reduced by 37 % in comparison to the representative natural soil stiffness profiles for Site 3, Site 4, and Site 6 at all depths. The median change in shear strain for the RAP ground improvement ranged from -6 % at 3-RAP-1 for the 15 kPa shear stress level up to -65 % at the 4-RAP-1 test panel also for the 15 kPa shear stress level. For a given test panel, the median change in shear strain at the 6-RAP-1 test panel is relatively constant between nominal levels of shear stress, indicating that the RAP and natural soil test panels at Site 6 have similar trends in non-linear behavior over a large range of shear strains. The 3-RAP-1 test panel, however, shows a consistent decrease in the magnitude of median change in shear strain as the shear stress increases, indicating that it is stiffer than the natural soil at lower levels of shear stress but starts to behave more like the natural soil at larger levels of shear stress. The test results at the 4-RAP-1 test panel fit neither of the patterns seen at the other sites with a -32 % reduction in shear strain at the 1.5 kPa shear stress level, -23 % reduction in shear strain at the 5 kPa shear stress level, and a -65 % reduction in shear strain at the 15 kPa shear stress level.

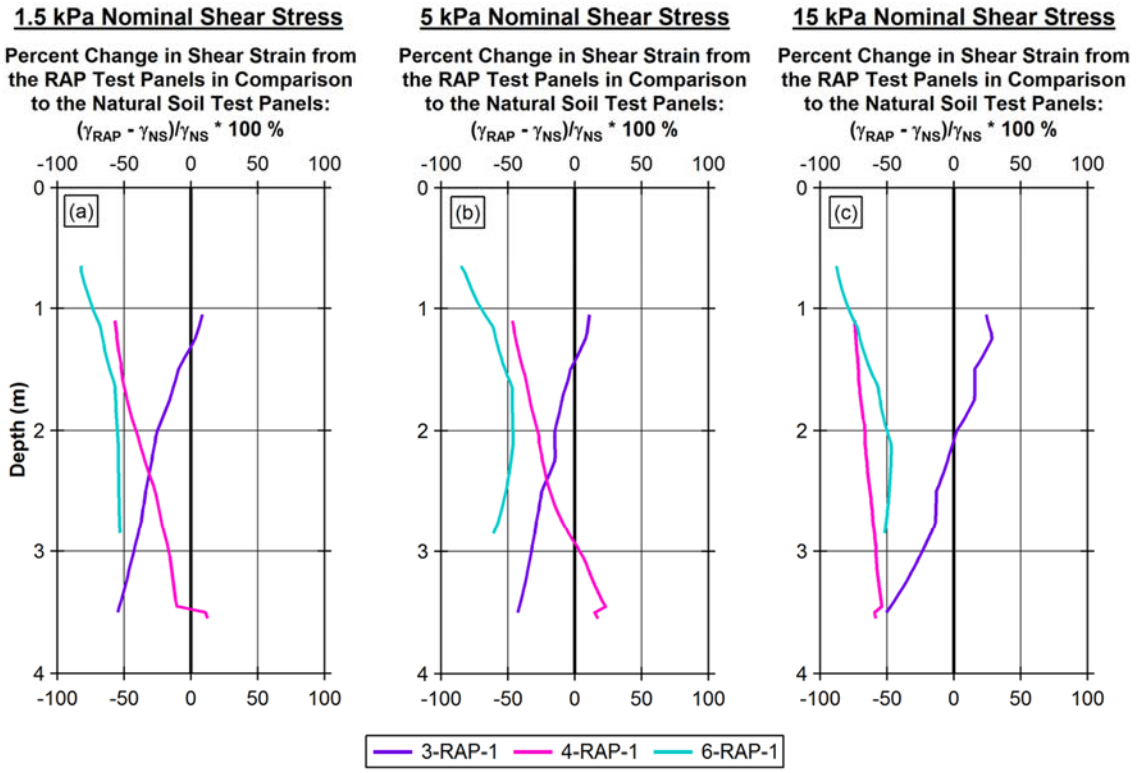

Figure 95: Variation in shear strain at the RAP test panels in comparison to the Natural Soil test panels from Site 3, Site 4, and Site 6 at three nominal levels of shear stress induced by T-Rex at the ground surface: (a) 1.5 kPa, (b) 5 kPa, and (c) 15 kPa.

Table 33: Median values of the relative change in shear strain, γ, at the 3-RAP-1, 4-RAP-1, and 6-RAP-1 test panels in comparison to the 3-NS-1, 4-NS-1 and 4-NS-2, and 6-NS-1 and 6-NS-2 test panels, respectively.

	1.5 kPa Shear Stress* Median Percent Change in Shear Strain, γ: $((\gamma_{RAP}-\gamma_{NS})/\gamma_{NS} * 100\ \%)$	**5 kPa Shear Stress*** Median Percent Change in Shear Strain, γ: $((\gamma_{RAP}-\gamma_{NS})/\gamma_{NS} * 100\ \%)$	**15 kPa Shear Stress*** Median Percent Change in Shear Strain, γ: $((\gamma_{RAP}-\gamma_{NS})/\gamma_{NS} * 100\ \%)$
3-RAP-1:	-30	-16	-6
4-RAP-1:	-32	-23	-65
6-RAP-1:	-56	-54	-55

*Nominal shear stress applied by the baseplate of T-Rex at the ground surface

In general, the RAP ground improvement method appears to successfully reduced the cyclic shear strains for a given level of shear stress at the ground surface in comparison to the natural soil. This performance was predicted by the CPT and DPCH tests that showed median increases in the corrected cone tip resistance q_t between impact points, the small-strain modulus G_{max} between impact points, and the small-strain modulus G_{max} across impact points, indicating greater density and stiffness in the soil as a result of the ground improvement. The data in Table 34 summarize the median increases for these three parameters in addition to the median relative change in shear strain average across the three nominal levels of shear stress.

In this case, the CPT, DPCH, and shake testing with T-Rex all show that the 6-RAP-1 test panel has achieved greater levels of improvement in comparison to the 3-RAP-1 and 4-RAP-1 test panels. There is less consensus between the test methods at the 3-RAP-1 and 4-RAP-1 test panels where the CPT shows the least amount of improvement at the 4-RAP-1 test panel while DPCH and shake testing with T-Rex show the 3-RAP-1 test panel to be the worst performing.

Table 34: Median values of relative change due to the RAP ground improvement in corrected cone tip resistance q_t from CPT testing, small-strain modulus G_{max} between impact points from DPCH testing, small-strain modulus G_{max} across impact points from DPCH testing, and shear strain γ from shake testing with T-Rex.

	CPT $\frac{(q_{t,RAP} - q_{t,NS})}{q_{t,NS}} \times 100\ \%$ Between Improvements	DPCH $\frac{(G_{max,RAP} - G_{max,NS})}{G_{max,NS}} \times 100\ \%$ Between Improvements	DPCH $\frac{(G_{max,RAP} - G_{max,NS})}{G_{max,NS}} \times 100\ \%$ Across Improvements	Shake Testing $\frac{(\gamma_{RAP} - \gamma_{NS})}{\gamma_{NS}} \times 100\ \%$ Between Improvements
3-RAP-1:	71	19	109	-17
4-RAP-1:	24	23	190	-40
6-RAP-1:	128	31	190	-55

7.5.3 Assessment of the LMG Ground Improvement Method

The relative changes in stiffness profiles due to the LMG ground improvement method is presented in Figure 96 for the three levels of nominal shear stress 1.5 kPa, 5 kPa, and 15 kPa. The median changes in shear strain over the length of each profile due to the LMG ground improvement method is summarized in Table 35, also for the three levels of nominal shear stress 1.5 kPa, 5 kPa, and 15 kPa.

The average median change in shear strain due to the LMG ground improvement is -21 %, indicating that on average, the shear strains at 3-LMG-1, 4-LMG-1, and 6-LMG-1 were reduced by 21 % in comparison to the representative natural soil stiffness profiles for Site 3, Site 4, and Site 6 at all depths. This average does not include the anomalously high value of +106 % from the 4-LMG-1 test panel at a nominal shear stress level of 5 kPa, which the author does not believe reflects the true behavior of the LMG test panel in comparison to the natural soil and is likely an artifact of normalization process used to adjust shear strains to matching nominal levels of shear stress.

Excluding the anomalous data point, the median change in shear strain for the LMG ground improvement ranged from -8 % at 3-LMG-1 for the 15 kPa shear stress level up to -40 % at the 4-LMG-1 test panel also for the 15 kPa shear stress level. For a given test panel, the median change in shear strain at the 6-LMG-1 test panel is relatively constant between nominal levels of shear stress, indicating that the LMG and natural soil test panels at Site 6 have similar trends in non-linear behavior over a large range of shear strains. The 3-LMG-1 test panel, however, shows a consistent decrease in the magnitude of median change in shear strain as the shear stress increases, indicating that it is stiffer than the natural soil at lower levels of shear stress but starts to behave more like the natural soil at larger levels of shear stress. The 4-LMG-1 test panel shows an increase in the magnitude of median change in shear strain from the 1.5 kPa to 15 kPa shear stress levels, but without

a valid value at the 5 kPa shear stress level, it is impossible to know if this indicates a trend or random variation.

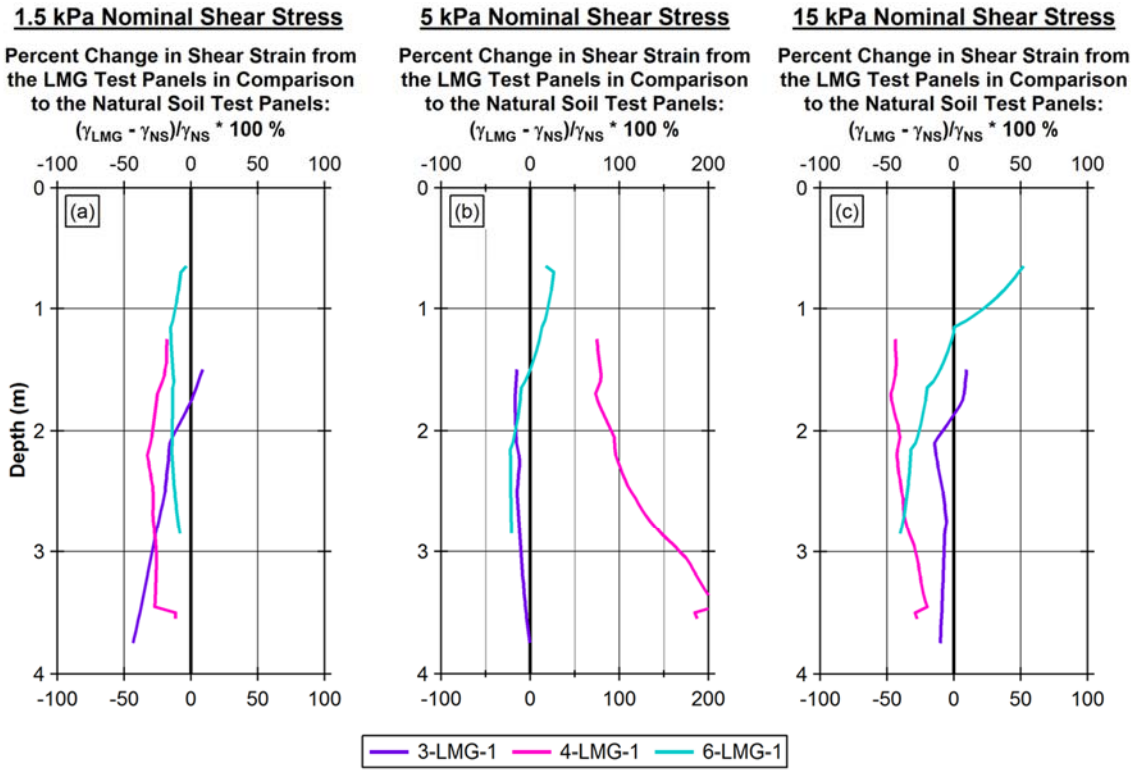

Figure 96: Variation in shear strain at the LMG test panels in comparison to the Natural Soil test panels from Site 3, Site 4, and Site 6 at three nominal levels of shear stress induced by T-Rex at the ground surface: (a) 1.5 kPa, (b) 5 kPa, and (c) 15 kPa.

Table 35: Median values of the relative change in shear strain, γ, at the 3-LMG-1, 4-LMG-1, and 6-LMG-1 test panels in comparison to the 3-NS-1, 4-NS-1 and 4-NS-2, and 6-NS-1 and 6-NS-2 test panels, respectively.

	1.5 kPa Shear Stress* Median Percent Change in Shear Strain, γ: $((\gamma_{LMG}-\gamma_{NS})/\gamma_{NS} * 100\ \%)$	**5 kPa Shear Stress*** Median Percent Change in Shear Strain, γ: $((\gamma_{LMG}-\gamma_{NS})/\gamma_{NS} * 100\ \%)$	**15 kPa Shear Stress*** Median Percent Change in Shear Strain, γ: $((\gamma_{LMG}-\gamma_{NS})/\gamma_{NS} * 100\ \%)$
3-LMG-1:	-22	-13	-8
4-LMG-1:	-27	106	-40
6-LMG-1:	-14	-11	-21

*Nominal shear stress applied by the baseplate of T-Rex at the ground surface

In general, the LMG ground improvement method appears to successfully reduced the cyclic shear strains for a given level of shear stress at the ground surface in comparison to the natural soil. This performance was not well predicted by the CPT and DPCH tests that showed both median increases and decreases in the corrected cone tip resistance q_t between impact points, the small-strain modulus G_{max} between impact points, and the small-strain modulus G_{max} across impact points, indicating greater density and stiffness in the soil as a result of the ground improvement. The data in Table 36 summarize the median increases for these three parameters in addition to the median relative change in shear strain average across the three nominal levels of shear stress.

In comparing results between test types, it is interesting to see that while the CPT and DPCH tests show cases in which the LMG ground improvement on the whole loosened and softened the soil conditions, albeit for different test panels, the stiffness profiles from shake testing with T-Rex all show reductions in shear strain in comparison to the natural soil test panels indicating an overall increase in stiffness. On their own, the results from CPT or DPCH testing fail to consistently identify which of the three LMG test panels had the largest increase in density or stiffness. Neither the CPT nor DPCH test results satisfactorily predict the relative performance of the three LMG test panels during shake testing with T-Rex. Overall, the CPT, DPCH, and shake testing with T-Rex have share little consensus assessing performance at the LMG test panels, indicating that changes in the soil due to the LMG ground improvement method are very complicated and/or highly variable.

Table 36: Median values of relative change due to the LMG ground improvement in corrected cone tip resistance q_t from CPT testing, small-strain modulus G_{max} between impact points from DPCH testing, small-strain modulus G_{max} across impact points from DPCH testing, and shear strain γ from shake testing with T-Rex.

	CPT $\frac{(q_{t,LMG} - q_{t,NS})}{q_{t,NS}} \times 100\ \%$ **Between Improvements**	**DPCH** $\frac{(G_{max,LMG} - G_{max,NS})}{G_{max,NS}} \times 100\ \%$ **Between Improvements**	**DPCH** $\frac{(G_{max,LMG} - G_{max,NS})}{G_{max,NS}} \times 100\ \%$ **Across Improvements**	**Shake Testing** $\frac{(\gamma_{LMG} - \gamma_{NS})}{\gamma_{NS}} \times 100\ \%$ **Between Improvements**
3-LMG-1:	29	-23	46	-14
4-LMG-1:	-4	11	26	-34
6-LMG-1:	15	-16	87	-15

7.6 SUMMARY

For the most part, this comparative analysis of the stiffness profiles shows that the shear strains from the ground-improved test panels are smaller than those at the natural soil test panels, indicating the ground improvement methods were successful at stiffening the soil in the top ~4.0 m. The average decrease in shear strain was 21 % at the LMG test panels, 30 % at the RIC test panels, and 37 % at the RAP test panels, all of which represent changes less than an order of magnitude (a decrease in one order of magnitude is equal to a 90 % reduction in shear strain, a decrease in two orders of magnitude is equal to a 99.0 % reduction in shear strain). It is difficult to know if these levels of shear strain reduction are sufficient enough to have a meaningful impact on decreasing the liquefaction susceptibility of these natural soil deposits given that soil liquefaction is a phenomenon in which shear strains can vary several orders of magnitude between the initial generation of excess pore pressure and the eventual triggering of soil liquefaction.

Based on the assessment of stiffness profiles developed from shake testing with T-Rex, it appears that the RAP ground improvement method is most effective at reducing the shear strain induced in the soil over a large range of shear strains with an average reduction of 37 %. The RIC ground improvement method performed the second best of the group with an average reduction in shear strain of 30 %, followed by the LMG ground improvement with an average reduction in shear strain of 21 %. Both the RAP and RIC ground improvements were shown with the CPT and DPCH tests to increase the density of the natural soil with relatively similar success, so the main difference expected between the performance of the two ground improvements is the inclusion of very stiff gravel piers in the RAP test panels that presumably are responsible for the additional 7 % reduction in shear strain in comparison to the RIC ground improvement method.

The performance of the LMG test panels during shake testing, however, is surprising given that both the CPT and DPCH tests showed minimal to no improvement (and instances in which the ground conditions were worsened). These test panels were expected to perform as poorly or worse than the natural soil test panels under cyclic loading conditions, but the results show an average reduction of shear strain equal to 21 %. Again, though, it is difficult to quantify what effect this might have on liquefaction susceptibility of these test panels.

The CPT and DPCH tests at the natural soil and ground improved test panels were intended to help explain the performance of the test panels during shake testing with T-Rex. It was hoped that the CPT and/or DPCH tests would adequately predict the performance of the ground-improved test panels compared to the natural soil test panels under earthquake-like loading conditions to validate their use as tools for verifying the effectiveness of ground improvements. In general, the CPT and DPCH tests both indicated that there were increases in density and stiffness at the ground-improved sites in comparison to the natural soil sites, and this matched well with the results from shake testing with T-Rex. However, these tests struggle to adequately rank the performance of test panels for a given ground improvement method between test sites. In other words, there was little consistent consensus between the CPT, DPCH, and shake testing with T-Rex regarding the variation in performance between test sites for a given ground improvement method.

Several contributing factors may help explain why the CPT, DPCH, and shake testing with T-Rex all indicate different levels of performance between the same ground improvement method at different test panels. First is that CPT, DPCH, and shake testing with T-Rex at ground-improved test panels are all performed at different locations within the same test panel. Second, the representative natural soil profile from CPT testing comes

from CPTs that were pushed in the natural soil at various locations around the test sites in between test panels while the representative natural soil profiles from DPCH and shake testing with T-Rex come from testing performed at the designated natural soil test panels. Third, the CPT, DPCH, and shake testing with T-Rex each impose different stress conditions on the soil during testing and measure different soil properties and parameters.

Chapter 8: Coupled Behavior of Shear Strain & Excess Pore Pressure Ratio

8.1 INTRODUCTION

The relationship between cyclic shear strain and the generation of excess pore pressure is critical to understanding liquefaction triggering. The work of Dobry et al. 1982 and Vucetic & Dobry 1986 has shown that the cyclic behavior of soil leading to the triggering of soil liquefaction can be well understood using a strain-based approach. Under the strain-based approach, the cyclic threshold strain is identified as the strain above which residual excess pore pressure begins to generate; in clean, fully-saturated, loose sands, this cyclic threshold strain is typically found to be in the range of 0.01 to 0.03 %. Dobry further shows that liquefaction in clean, fully-saturated, loose sands is predicted to be triggered at a strain level of ~ 0.5 % after 30 cycles of loading.

These results that were first shown using strain-controlled cyclic triaxial tests and strain-controlled direct-simple shear tests in the laboratory by Dobry et al. 1982 and Vucetic & Dobry 1986 have been supported by similar results from shake testing with T-Rex in the field (Cox 2006 and Roberts 2014). One of the advantages of shake testing with T-Rex over laboratory tests is the ability to test in situ a wide range of undisturbed samples that have varying soil types, densities, and degrees of saturation. Shake testing with T-Rex was performed at the 18 test panels previously discussed and included a total of 81 installed PPT sensors at depths that ranged from 0.56 to 4.01 m, in soil types that ranged from silts to clean sands, and in soil conditions that ranged from completely unsaturated to fully saturated. The test results from each PPT are considered separately and the soil surrounding the PPT is considered an individual test specimen for the purposes of this analysis. The values of excess pore pressure ratio are taken at 30 cycles of loading during shake testing with T-Rex. The results of shake testing with T-Rex at the test panel 3-NS-2 are omitted

from the analysis because the data showed unusual results and the soil was later shown to have unexplained artesian pressure conditions. As a result, this analysis includes the results of 75 specimens from a total of 17 test panels.

Shake testing with T-Rex revealed four potential behavioral categories that describe the relationship between cyclic shear strain and the residual excess pore pressure ratio: Category 1) a relationship similar to Dobry's pore water prediction model for liquefiable sands, Category 2) generation of positive excess pore pressure but not rapidly enough to be considered highly susceptible to liquefaction triggering, Category 3) generation of little to no generation of excess pore pressure regardless of shear strain level, and Category 4) generation of negative excess pore pressure. Examples of the typical relationships between excess pore pressure ratio and shear strain for each of the four categories are shown in Figure 97.

Also in Figure 97 is the Dobry prediction model for excess pore pressure as a function of shear strain to show the typical behavior of liquefiable sands for different numbers of cycles (10 and 50) and different cyclic threshold strains (0.01 % and 0.02 %). Soils that are highly susceptible to liquefaction in the field have been shown to exhibit behavior similar to the Dobry prediction model (Cox 2006 and Roberts 2014). The Dobry prediction model (Dobry et al. 1982) as calibrated for sands from the Wildlife Site in Imperial Valley, California, (Vucetic & Dobry 1986) is defined as follows:

$$r_u = \frac{1.04 \times N \times 2.6(\gamma - \gamma_t^c)^{1.7}}{1 + N \times 2.6(\gamma - \gamma_t^c)^{1.7}} \qquad (26)$$

where N is the number of cycles, γ is the cyclic shear strain, and γ_t^c is the cyclic threshold strain for the material.

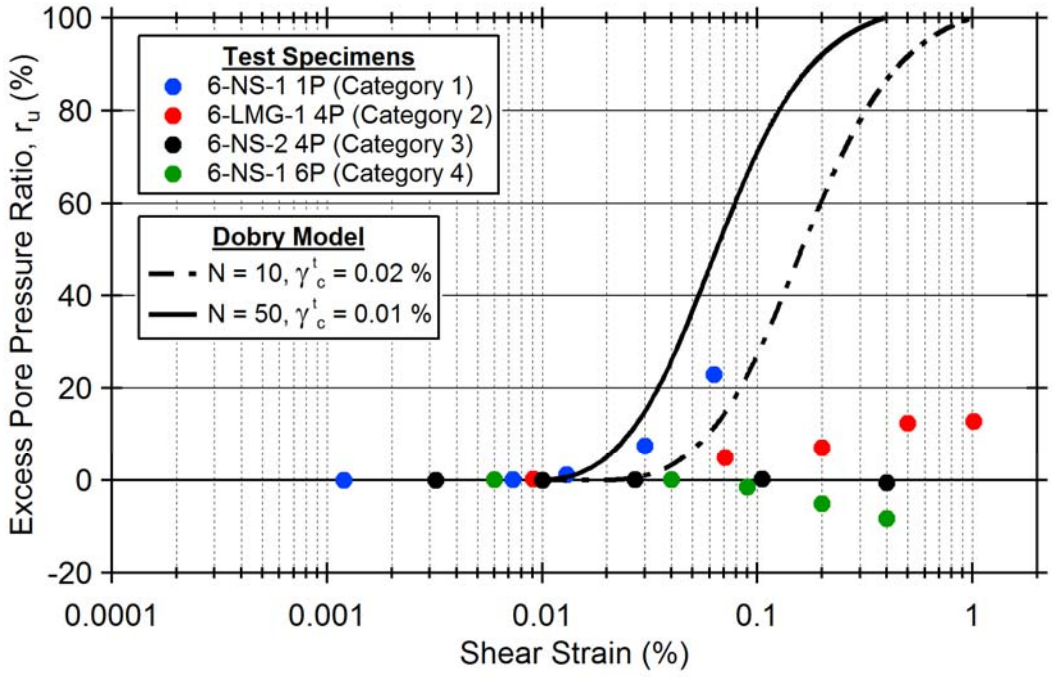

Figure 97: Example of typical relationships between excess pore pressure ratio and shear strain for the four identified categories of soil behavior.

The three main soil characteristics that appear to have the greatest influence on the relationship between the generation of excess pore pressure and shear strain are 1) soil type, 2) relative density, and 3) degree of saturation. The soil type for each of the 75 specimens was inferred via visual inspection of the soil during trenching as well as laboratory classification tests on samples that were taken from the trenches, as reported in previous chapters. The relative density of the in situ soil is incredibly difficult to ascertain even from indirect methods because empirical correlations using the CPT are inappropriate for these soils with wide-ranging fines contents and laboratory estimates of minimum and maximum void ratios are not particularly accurate for fine materials. Instead of assessing the relative density, the shear wave velocity-based CRR is used as a rough proxy for the relative density of the soil: a low value of CRR indicates relatively loose soils with high

probability of liquefaction triggering while a high value or undefined value indicates relatively dense soils with low to no probability of liquefaction triggering (Andrus & Stokoe 2000). The shear wave velocity is a good parameter to use in this case because it is sensitive to changes in relative density. Similarly, the compression wave velocity is used as a proxy for the degree of saturation in the soil. As stated in Section 4.1.2, soils with compression wave velocities greater than 750 m/s are believed to have fully-saturated behavior under dynamic loading while soils with compression velocities less than 750 m/s are believed to have partially-saturated behavior.

8.2 CATEGORY 1 – HIGHLY SUSCEPTIBLE TO LIQUEFACTION TRIGGERING

The soils in Category 1 have the highest risk of triggering soil liquefaction under dynamic loading and follow a relationship between the generation of excess pore pressure ratio and shear strain that is similar to the Dobry prediction model. Of the 75 specimens, seven were identified as exhibiting Category 1 behavior. The results of shake testing with T-Rex for these seven specimens are shown in Figure 98 and a summary of their parameters and properties are presented in Table 37. All seven of these specimens have compression wave velocities greater than 750 m/s and include soil types that range from SP to SM. The median CRR value is 0.235, which is a fairly low value and indicates soils with relatively low resistance to liquefaction triggering. There are two outlier CRR values, with specimen 6-RAP-1 5P having an undefined CRR value and 6-NS-2 1P having a CRR value of 0.464, which is relatively high. In general, these seven specimen have similar characteristics in terms of soil type (SP to SM), relative density (loose), and degree of saturation (S_r > 99.6 %).

The cyclic threshold strain of these soils is in the range of 0.007 to 0.02 %, which matches reasonably well with the threshold strain reported in other liquefiable, clean sands (Vucetic & Dobry 1986, Cox 2006, Roberts 2014). Unfortunately, the largest excess pore pressure ratio recorded for this ground of specimen is only 24.7 % at a shear strain of 0.08 %, so the full behavior of these soils up to the triggering of soil liquefaction at an excess pore pressure ratio of 100 % is not captured. Because these specimens are typically located on the bottom half of the instrumentation array where the sands have lower fines content and the degree of saturation is higher than 99.6 %, the shear strains induced by T-Rex are proportionally smaller with distance from the ground surface, thus making it difficult to capture the behavior at larger shear strains. It must be noted that some of these specimens

may ultimately exhibit Category 2 behavior at larger shear strains, but it is impossible to know without additional data.

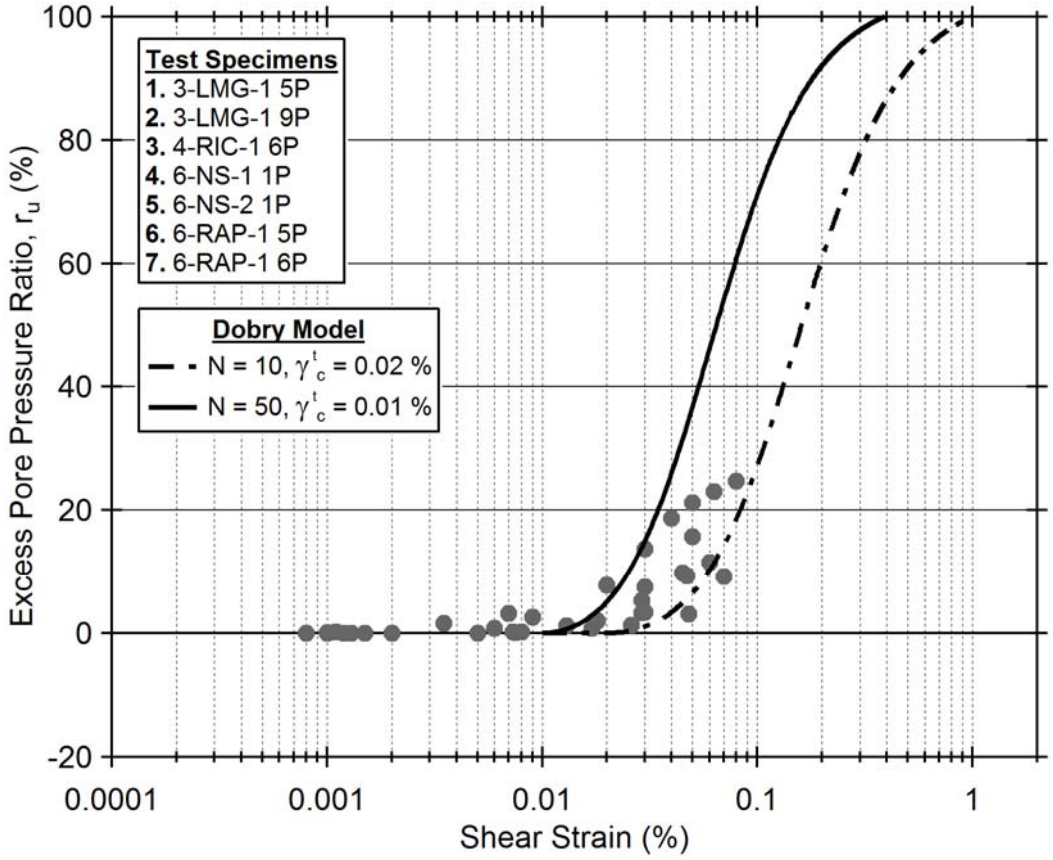

Figure 98: Results from shake testing with T-Rex that show a relationship between excess pore pressure ratio and shear strain that exhibit Category 1 behavior.

Table 37: Summary of parameters and properties of the specimens that exhibit Category 1 behavior.

Specimen	Depth (m)	FC min. (%)	FC max. (%)	V_P (m/s)	V_S (m/s)	$V_{S,1}$ (m/s)	CRR*	USCS
3-LMG-1 5P	2.5	3	6	771	117	160	0.139	SP
3-LMG-1 9P	2.815	3	6	1299	135	179	0.167	SP
4-RIC-1 6P	1.57	33	75	1340	122	183	0.235	SM
6-NS-1 1P	2.85	1	5	1728	146	196	0.238	SP
6-NS-2 1P	2.89	1	5	1676	155	208	0.464	SP
6-RAP-1 6P	1.15	20	28	894	110	177	0.178	SM
6-RAP-1 5P	1.65	3	21	1565	147	221	Undefined	SP-SM

*CRR calculated using the Andrus & Stokoe (2000) shear wave velocity-based method.

8.3 CATEGORY 2 – POSITIVE EXCESS PORE PRESSURE BUT NOT LIKELY TO TRIGGER SOIL LIQUEFACTION

The specimens in Category 2 appear to have a lower risk of triggering soil liquefaction under dynamic loading, and perhaps could be considered moderate-to-low risk. Of the 75 specimens, 16 were identified as exhibiting Category 2 behavior. The results of shake testing with T-Rex for these 16 specimens are shown in Figure 99 and a summary of their parameters and properties are presented in Table 38. These specimens generate positive excess pore pressure, but less than is expected for highly liquefiable soils that follow the Dobry prediction model.

The properties and parameters of 16 specimens vary significantly between one another, representing the full range of soils tested using shake testing with T-Rex. The soil types range from SP to ML. The proportion of specimens by soil type in Category 2 are 33 % of SP soils, 20 % of SP-SM soils, 13 % of SM soils, and 25 % of ML soils. In terms of degree of saturation, there is an even 50/50 split between specimens with compression wave velocities above and below 750 m/s. The median CRR value for these specimens is a very low 0.152 (even lower than for Category 1), but without accounting for soil type this appears to mischaracterize the soils of this category. Among the 16 specimens, the median CRR value for SP soils is 0.266 (with one SP specimen having an undefined CRR), for SP-SM soils is 0.145, for SM soils is 0.148, and for ML soils is 0.166. Based on the observed behavior of these specimens, it appears that the fines content correction for the $V_{S,1}$ used in calculating the CRR results in overestimating the liquefaction susceptibility of these soils that have a fines content greater than 5 %, which include soils classified as SP-SM, SM, and ML. The shear wave based CRR method also lacks further corrections for fines content larger than 35 %, despite the large differences in behavior for a soil with 35 % and one with 100 % (Polito & Martin 2001, Liu & Mitchell 2006).

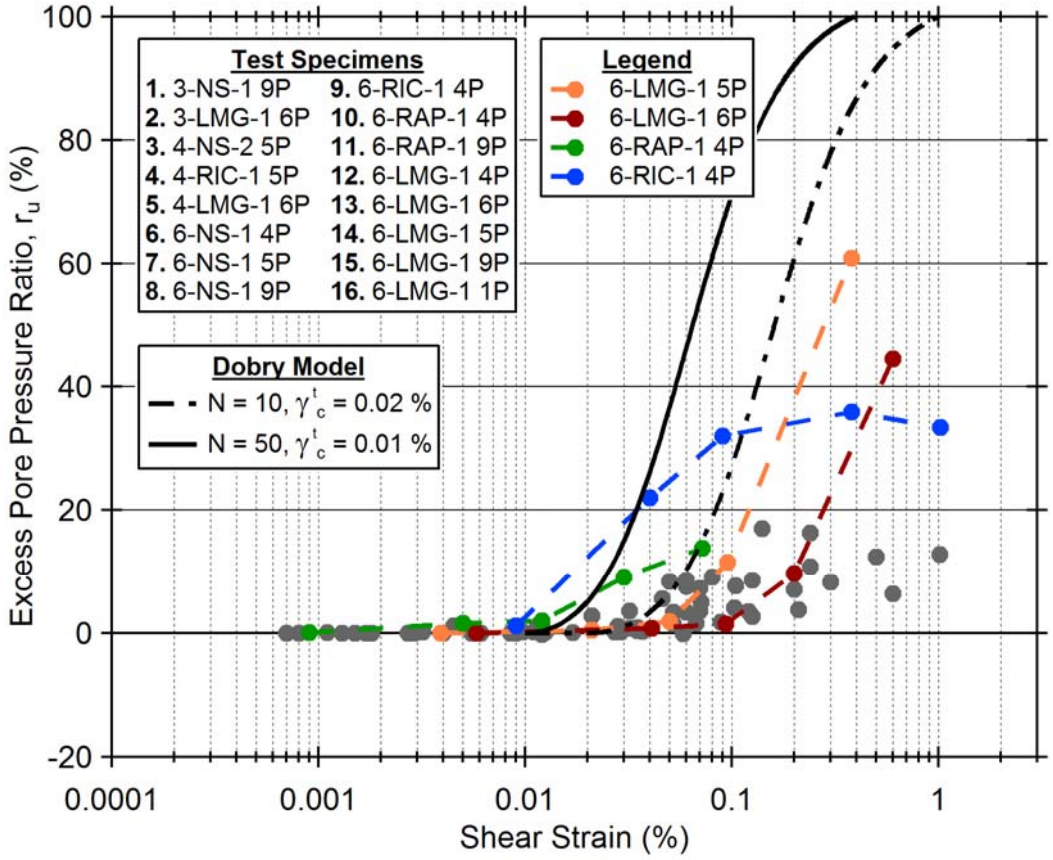

Figure 99: Results from shake testing with T-Rex that show a relationship between excess pore pressure ratio and shear strain that exhibit Category 2 behavior. The relationships of four specimen (6-LMG-1 5P, 6-LMG-1 6P, 6-RIC-1 4P, and 6-RAP-1 4P) are highlighted for clarity.

Table 38: Summary of parameters and properties of the specimens that exhibit Category 2 behavior.

Specimen	Depth (m)	FC min. (%)	FC max. (%)	V_P (m/s)	V_S (m/s)	$V_{S,1}$ (m/s)	CRR*	USCS
3-NS-1 9P	2.755	1	5	1522	153	204	0.353	SP
3-LMG-1 6P	2.09	3	6	655	109	154	0.134	SP
4-NS-2 5P	2.453	20	30	1398	146	200	0.615	SM
4-RIC-1 5P	2.059	33	48	1546	132	187	0.291	SM
4-LMG-1 6P	2.20	15	30	1451	109	153	0.132	SM
6-NS-1 4P	0.6	80	96	453	91	165	0.154	ML
6-NS-1 5P	1.6	3	15	1570	117	177	0.165	SP-SM
6-NS-1 9P	2.1	1	5	1699	139	199	0.266	SP
6-RIC-1 4P	0.65	20	50	505	92	163	0.151	SM
6-RAP-1 4P	0.65	94	95	443	90	161	0.146	ML
6-RAP-1 9P	2.15	2	5	1618	161	230	Undefined	SP
6-LMG-1 4P	0.65	70	74	475	97	173	0.179	ML
6-LMG-1 6P	1.15	7	14	436	102	165	0.145	SP-SM
6-LMG-1 5P	1.65	10	20	449	103	156	0.137	SP-SM
6-LMG-1 9P	2.15	2	2	387	112	160	0.139	SP
6-LMG-1 1P	2.90	1	3	1659	126	168	0.148	SP

*CRR calculated using the Andrus & Stokoe (2000) shear wave velocity-based method.

A further look at the effect of soil type on the behavior of the soil show distinct differences between in the generation of pore pressure for soil types ranging from SP to ML. The four graphs in Figure 100 highlight the data from each of the four soil types: (a) soil type SP, (b) soil type SP-SM, (c) soil type SM, and (d) soil type ML. These graphs show that as the fines content increases (soil type transitioning from SP to ML), the rate of pore pressure generation as a function of shear strain decreases, resulting in a "flattening" of the excess pore pressure ratio versus shear strain curve to the point of being more linear for strains above the cyclic threshold strain for SM and ML soil types. The relationship between the excess pore pressure ratio and shear strain for SP and SP-SM soils has a similar curvature to the Dobry prediction model, though with a slightly decreased slope. The SP and SP-SM soils in Category 2 are borderline Category 1 soils, and may still have considerable susceptibility to liquefaction triggering. On the other hand, the SM and ML soils in Category 2 appear to lack the potential to generate the very large excess pore pressures required for triggering liquefaction.

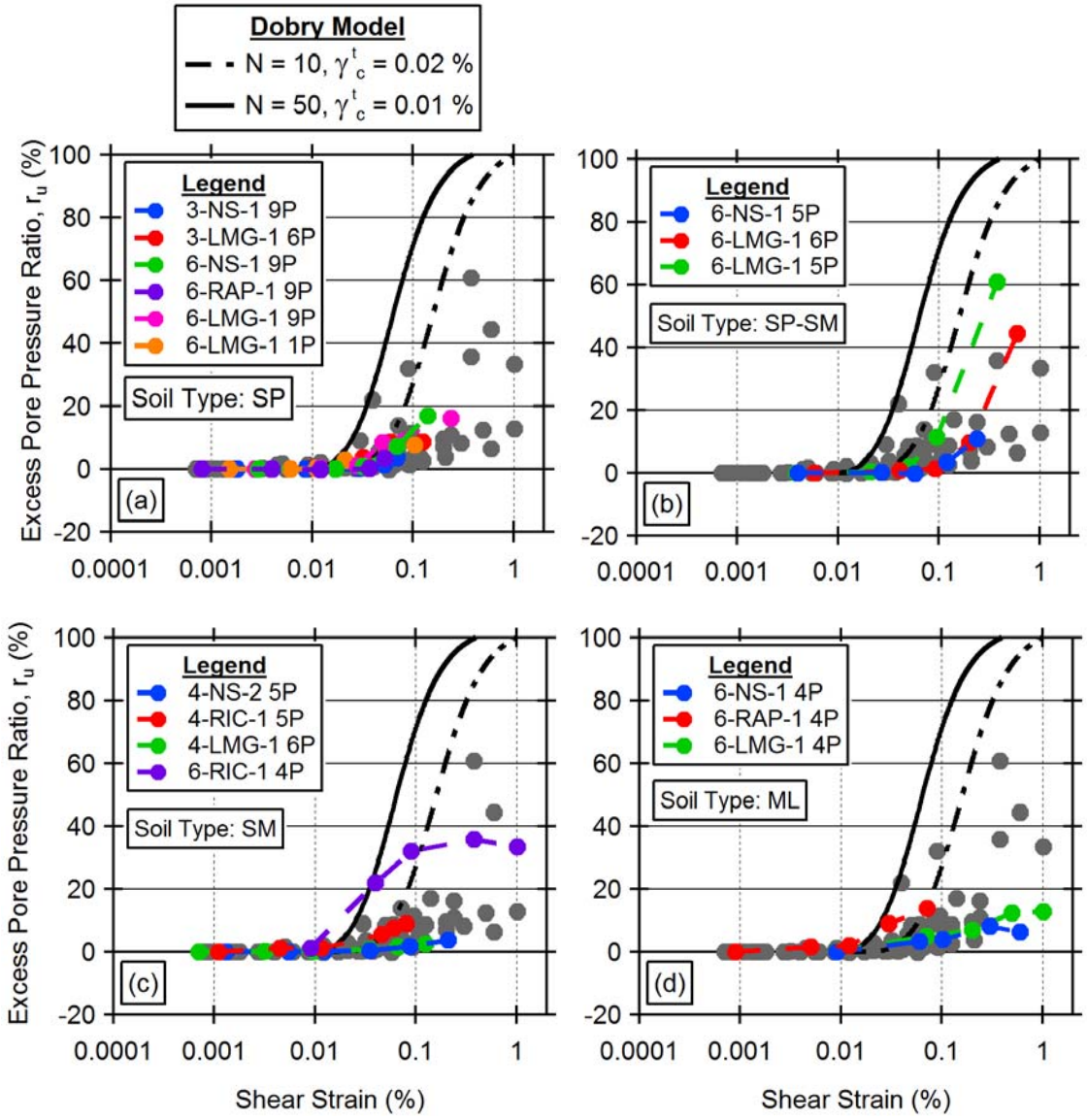

Figure 100: Data from shake testing with T-Rex that fit into Category 2 behavior. The figures are separated by soil type: (a) SP soils, (b) SP-SM soils, (c) SM soils, and (d) ML soils.

The range of values for the cyclic threshold strain of these Category 2 soils is larger than those in Category 1, which almost certainly is a factor in increasing the resistance to liquefaction triggering. For SP and SP-SM soils, the cyclic threshold strain ranges from

approximately 0.05 to 0.1 %. For SM and ML soils, the cyclic threshold strain ranges from approximately 0.01 to 0.1 %. The effect of a larger cyclic threshold strain value on the SP and SP-SM soils is that while these soils can still generate significant excess pore pressure, it takes larger levels of shear strain that Category 1 soils before this generation can occur, resulting is less susceptibility to liquefaction triggering. The SM and ML soils show that even with low cyclic threshold strains that are similar to the Category 1 soils (cyclic threshold strains ranged from 0.007 to 0.02 % for Category 1 soils), they lack the ability to quickly generate large excess pore pressure as the shear strains continue to increase.

It is difficult to identify the affect of degree of saturation on these soils in Category 2. Fully half of the specimens have a compression wave velocity less than 750 m/s and some of these specimens produce the largest values of excess pore pressure ratios. For example, the 6-LMG-1 5P and 6-LMG-1 6P specimens in Figure 100b for SP-SM soils can be considered boderline Category 1/Category 2 behavior. Both of these specimens have low CRR values (0.145 and 0.137) yet also have very low compression wave velocities (436 m/s and 449 m/s, respectively). It is possible that in this case, the low degree of saturation is the factor that pushes these specimens into Category 2 behavior rather than Category 1 behavior. On the other hand, specimen 6-NS-1 5P is also in the SP-SM category in Figure 100b; this specimen has a CRR value of 0.165 and a compression wave velocity of 1,570 m/s yet it generates much less pore pressure for a given level of shear strain than the other two specimens 6-LMG-1 5P and 6-LMG-1 6P. It is also true that all of the ML soils have a compression wave velocity less than 750 m/s and these soils were shown to have a much reduced generation of excess pore pressure at large shear strains in Figure 100d. Unfortunately, the geology of these test sites is such that the fines content decreases with depth and the degree of saturation increases with depth. Therefore it is difficult to separate out the effects of soil type degree of saturation because the shallower finer-grained

soils tend to have lower degrees of saturation at these test sites. The effect is that the two characteristics that are known to inhibit the triggering of liquefaction (less than fully saturated conditions and high fines contents) are strongly correlated in these soils and the two characteristics known to increase the triggering of liquefaction susceptibility (fully saturated conditions and low fines contents) are also strongly correlated in these soils.

8.4 CATEGORY 3 – LITTLE TO NO GENERATION OF EXCESS PORE PRESSURE

The soils in Category 3 are not at risk of triggering soil liquefaction under dynamic loading. Of the 75 specimens, 42 were identified as exhibiting Category 3 behavior, which is limited to specimens whose excess pore pressure ratios range only from -2.5 % to +2.5 %. The results of shake testing with T-Rex for these 42 specimens are shown in Figure 101 and a summary of their parameters and properties are presented in Table 39.

As with the specimens that exhibited Category 2 behavior, the specimens in Category 3 have soil types that range from SP to ML and saturation conditions ranging from unsaturated to fully-saturated. The proportion of specimens by soil type in Category 3 are 39 % of SP soils, 40 % of SP-SM soils, 73 % of SM soils, and 58 % of ML soils. Within each of the four soil type groups, specimens are most likely to exhibit Category 3 behavior. In terms of saturation conditions, 18 of the 42 specimens have compression wave velocities less than 750 m/s.

The median CRR value for Category 3 is 0.269, with 10 of the 42 specimens having undefined values of CRR. In general, the CRR values are larger than those for specimens that exhibited Category 1 and Category 2 behavior. This indicates that these soils probably have a higher relative density than those in Category 1 or Category 2. As organized by soil type, the median CRR is undefined for SP soils, 0.277 for SP-SM soils, 0.301 for SM soils, and 0.162 for ML soils. The median CRR values for the ML soils stand out as being too low for a soil that generates little to no excess pore pressure over a large range of shear strains, again indicating that the shear wave-based CRR appears to overestimate the risk of liquefaction triggering for soils with high fines contents.

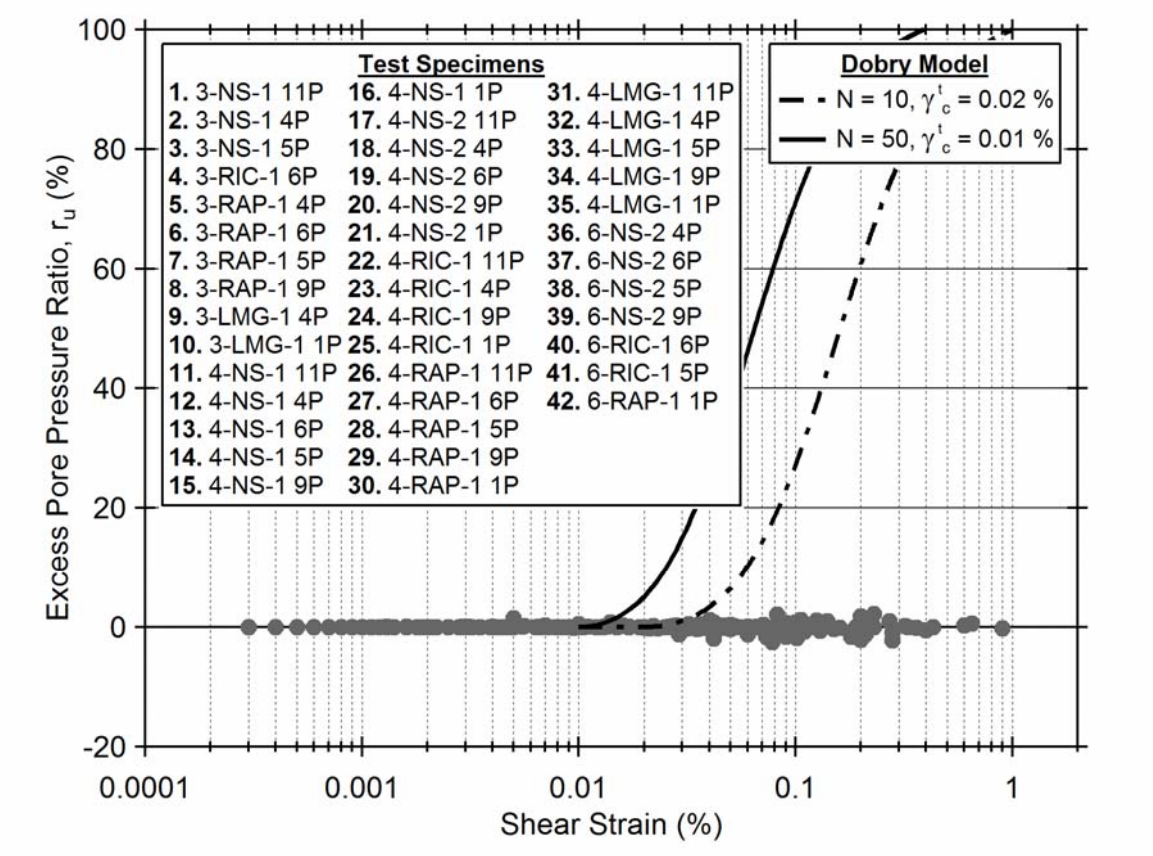

Figure 101: Results from shake testing with T-Rex that show a relationship between excess pore pressure ratio and shear strain that exhibit Category 3 behavior.

Table 39: Summary of parameters and properties of the specimens that exhibit Category 3 behavior.

Specimen	Depth (m)	FC min. (%)	FC max. (%)	V_P (m/s)	V_S (m/s)	$V_{S,1}$ (m/s)	CRR*	USCS
3-NS-1 11P	0.74	34	43	274	125	211	Undefined	SM
3-NS-1 4P	1.235	34	43	627	150	234	Undefined	SM
3-NS-1 5P	2.23	6	6	679	146	204	0.340	SP-SM
3-RIC-1 6P	1.98	29	33	685	161	230	Undefined	SM
3-RAP-1 4P	1.005	20	35	397	116	187	0.244	SM
3-RAP-1 6P	1.495	11	18	526	137	207	0.878	SM
3-RAP-1 5P	2.015	22	22	681	144	206	Undefined	SM
3-RAP-1 9P	2.495	22	22	1508	169	230	Undefined	SM
3-LMG-1 4P	1.5	53	77	607	102	154	0.135	ML
3-LMG-1 1P	4.005	3	6	1606	185	228	Undefined	SP
4-NS-1 11P	1.06	60	85	291	105	168	0.162	ML
4-NS-1 4P	1.57	20	34	506	111	166	0.152	SM
4-NS-1 6P	2.05	15	25	441	126	179	0.180	SM
4-NS-1 5P	2.57	17	21	911	146	198	0.348	SM
4-NS-1 9P	3.07	1	1	1328	156	203	Undefined	SP
4-NS-1 1P	3.55	1	2	1518	158	199	0.268	SP
4-NS-2 11P	0.95	75	88	557	105	171	0.172	ML
4-NS-2 4P	1.45	30	30	1057	103	156	0.137	SM
4-NS-2 6P	1.95	26	32	1573	125	180	0.196	SM
4-NS-2 9P	2.95	19	22	1330	142	187	0.218	SM
4-NS-2 1P	3.45	4	7	1532	137	174	0.157	SP
4-RIC-1 11P	0.56	1	20	384	129	233	Undefined	SM
4-RIC-1 4P	1.05	1	20	468	115	184	0.255	SM
4-RIC-1 9P	2.59	10	33	1540	147	198	0.414	SM
4-RIC-1 1P	3.05	43	43	1603	162	211	2.681	SM
4-RAP-1 11P	1.08	68	73	483	119	190	0.346	ML
4-RAP-1 6P	2.09	13	17	1256	130	184	0.193	SM
4-RAP-1 5P	2.59	10	18	1555	153	207	0.788	SM
4-RAP-1 9P	3.09	10	11	1611	151	197	0.270	SP-SM
4-RAP-1 1P	3.59	3	3	1661	178	225	Undefined	SP
4-LMG-1 11P	1.219	62	69	430	102	159	0.142	ML
4-LMG-1 4P	1.709	22	50	1247	99	146	0.126	SM
4-LMG-1 5P	2.714	7	13	1479	134	180	0.173	SP-SM
4-LMG-1 9P	3.409	10	12	1553	153	195	0.250	SP-SM
4-LMG-1 1P	3.679	10	12	1560	158	198	0.285	SP-SM
6-NS-2 4P	0.66	96	96	493	102	182	0.201	ML
6-NS-2 6P	1.16	74	74	1094	99	159	0.143	ML
6-NS-2 5P	1.64	3	25	1473	113	171	0.160	SM
6-NS-2 9P	2.14	1	5	1665	143	204	0.348	SP
6-RIC-1 6P	1.15	20	45	538	109	177	0.191	SM
6-RIC-1 5P	1.65	9	13	1531	138	207	0.679	SP-SM
6-RAP-1 1P	2.90	1	3	1687	177	237	Undefined	SP

*CRR calculated using the Andrus & Stokoe (2000) shear wave velocity-based method.

The behavior of the soils in Category 3, which is marked by the generation of little to no excess pore pressure, is caused by one of two possibilities: 1) the cyclic threshold strain was not exceeded during testing or 2) the soils do not generate excess pore pressure under cyclic loading. For the SP and SP-SM soils, the increased cyclic threshold strain appears to be due to a higher relative density (median 0.340 CRR value for SP and SP-SM specimens combined) rather than being influenced by fines content (fines content < 12 %) or degree of saturation (85 % of the 13 SP and SP-SM specimens have a compression wave velocity greater than 1,450 m/s).

The SM soils on the whole also appear to have a higher relative density, as indicated by the relatively large CRR values for this soil type group (6 of the 22 specimens have an undefined CRR value). While 11 of the 22 SM specimens have compression wave velocities less than 750 m/s, the degree of saturation does not seem to have as much of an influence as CRR on the lack of pore pressure generation. The higher fines content of SM soils in comparison to SP and SP-SM soils likely has a contributing effect as well to the lack of pore pressure generation.

The ML soils in Category 3 are mostly unsaturated with compression wave velocities less than 750 m/s for 6 of the 7 specimens. The median CRR value 0.162 is very low considering the lack of excess pore pressure, but this is probably due to the inability of the shear wave velocity based CRR method to account for soils with very high fines contents.

8.5 CATEGORY 4 – GENERATION OF NEGATIVE EXCESS PORE PRESSURE

The soils in Category 4 have the lowest risk of triggering soil liquefaction under dynamic loading of all of the categories because they generate negative excess pore pressure. Of the 75 specimens, ten were identified as exhibiting Category 4 behavior. The results of shake testing with T-Rex for these ten specimens are shown in Figure 102 and a summary of their parameters and properties are presented in Table 40. All ten of these specimens have compression wave velocities greater than 750 m/s and include soil types that range from SP to ML. Eight of the ten specimens (80 %) have an undefined CRR value, classifying these soils as non-liquefiable and indicating that they are relatively dense. The generation of negative excess pore pressure substantiates the idea that these soils are a non-risk for liquefaction triggering. Interestingly, the two outlier specimens with defined CRR values, 4-RAP-1 4P and 6-NS-1 6P, have very low CRR values (0.182 and 0.161, respectively) as well as compression wave velocities greater than 750 m/s and soil type SM, characteristics that would seem to indicate a soil that is highly susceptible to soil liquefaction triggering and more suitable to Category 1 behavior.

The cyclic threshold strain of the soils in Category 4 ranges from approximately 0.02 % to 0.08 %, but varies by soil type. The SP and SP-SM soils have a cyclic threshold of approximately 0.02 % to 0.03 %, while the SM and ML soils have a cyclic threshold of approximately 0.08 %. In this case, it appears that an increase in fines content has the general effect of increasing the cyclic threshold strain.

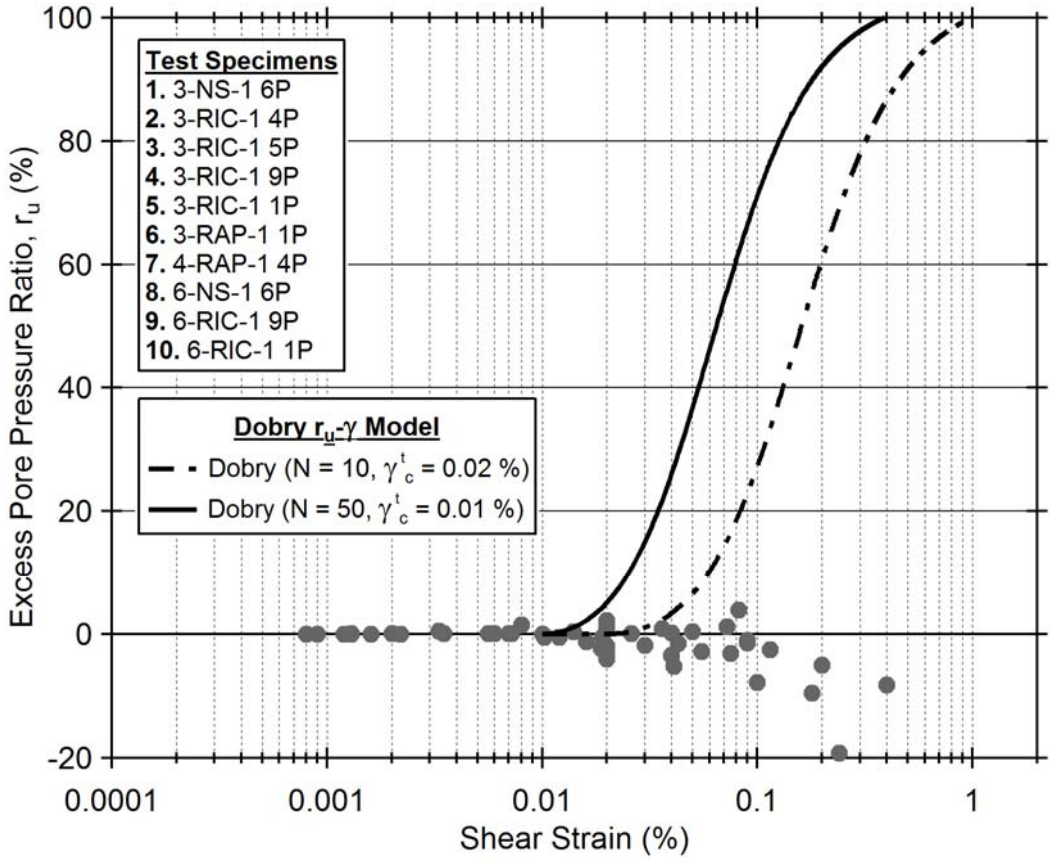

Figure 102: Results from shake testing with T-Rex that show a relationship between excess pore pressure ratio and shear strain that exhibit Category 4 behavior.

Table 40: Summary of parameters and properties of the specimens that exhibit Category 4 behavior.

Specimen	Depth (m)	FC min. (%)	FC max. (%)	V_P (m/s)	V_S (m/s)	$V_{S,1}$ (m/s)	CRR*	USCS
3-NS-1 6P	1.735	90	91	780	145	213	Undefined	ML
3-RIC-1 4P	1.475	85	93	1013	156	236	Undefined	ML
3-RIC-1 5P	2.485	5	5	1559	172	235	Undefined	SP
3-RIC-1 9P	2.98	5	5	1626	178	233	Undefined	SP
3-RIC-1 1P	3.985	5	5	1647	177	219	Undefined	SP
3-RAP-1 1P	3.505	2	9	1707	181	229	Undefined	SP-SM
4-RAP-1 4P	1.58	15	57	761	117	174	0.182	SM
6-NS-1 6P	1.1	50	50	883	105	172	0.161	SM
6-RIC-1 9P	2.15	2	5	836	157	223	Undefined	SP
6-RIC-1 1P	2.9	1	3	1607	167	223	Undefined	SP

*CRR calculated using the Andrus & Stokoe (2000) shear wave velocity-based method.

8.6 Effect of Ground Improvement Method on the Relationship Between the Generation of Excess Pore Pressure and Shear Strain

The specimens from the ground-improved test panels exhibit a different distribution of behavior than specimens from the natural soil test panels, indicating that the ground improvement methods are able to affect change on the moderate-to-large strain behavior of the soil. The data in Table 41 show the distribution of specimens by behavioral category (Category 1, Category 2, Category 3, or Category 4) for a given test panel type (natural soil, RIC, RAP, or LMG). The median CRR values of the specimens by test panel type and soil type are similarly summarized in Table 42. If a ground improvement method had no effect on the soil, the distribution of specimens should be the same as the distribution for the natural soil. Similarly, larger median CRR values indicate a ground improvement method densified the soil in comparison to the natural soil while lower median CRR values indicate a ground improvement method loosened the soil in comparison to the natural soil.

Table 41: Distribution of specimens subjected to shake testing with T-Rex by behavioral category as a percentage of total specimens for a given test panel type (Natural Soil, RIC, RAP, or LMG).

	Category 1	Category 2	Category 3	Category 4
Natural Soil:	7 %	19 %	67 %	7 %
RIC:	6 %	13 %	44 %	38 %
RAP:	13 %	13 %	63 %	13 %
LMG:	13 %	44 %	44 %	0 %

Table 42: Median CRR values of specimens subjected to shake testing with T-Rex by test panel type (Natural Soil, RIC, RAP, or LMG) and soil type (SP, SP-SM, SM, and ML).

	SP Soils	SP-SM Soils	SM Soils	ML Soils	All Soil Types
Natural Soil:	0.308	0.253	0.196	0.167	0.218
RIC:	Undefined	0.679	0.291	Undefined	Undefined
RAP:	Undefined	Undefined	0.516	0.246	0.833
LMG:	0.144	0.173	0.129	0.142	0.144

Specimens from the RIC test panels on the whole have lower susceptibility to liquefaction triggering than specimens from the natural soil test panels based on the relationship between the generation of excess pore pressure and shear strain. There is roughly the same percentage of specimens from the RIC test panels than from the natural soil test panels in Category 1 (6 % of RIC versus 7 % of natural soil specimens), a lower percentage in Category 2 (13 % of RIC versus 19 % of natural soil specimens) and Category 3 (44 % of RIC versus 67 % of natural soil specimens), and a higher percentage in Category 4 than the natural soil specimens (38 % of RIC versus 7 % of natural soil specimens). The RIC ground improvement appears to have densified the soils sufficiently enough to have shifted the change the generation of excess pore pressure and reduce the risk of liquefaction triggering. Further, fully 50 % of the RIC specimens have an undefined CRR value, which in comparison to 15 % of specimens from the natural soil test panels with an undefined CRR, indicates an effective densification of the soils at depth by the RIC ground improvement method. The median CRR value of the all specimens subjected to the RIC ground improvement method is 2.681 versus a median CRR value of 0.218 for all specimens from the natural soil test panels.

Based on the relationship between the generation of excess pore pressure and shear strain, specimens from the RAP test panels have a similar distribution of categorical behavior to the specimens from the natural soil test panel with small differences. The RAP ground improvement has a higher percentage of specimens than the natural soil in Category 1 (13 % of RAP versus 7 % of natural soil specimens) but a lower percentage of specimens in Category 2 (13 % of RAP versus 19 % of natural soil specimens). It also has a lower percentage of specimens in Category 3 (63 % of RAP versus 67 % of natural soil specimens) but a higher percentage in Category 4 (13 % of RAP versus 7 % of natural soil specimens). This pattern indicates the RAP ground improvement method perhaps had a

small effect of loosening some soils, pushing them toward Category 1 from Category 2 behavior while also densifying other soils, pushing them toward Category 4 from Category 3 behavior. The distribution of behavior between specimens from the natural soil and RAP test panels, however, is overall very similar, suggesting that the RAP test panel had little effect on changing the behavior of excess pore pressure generation under cyclic loading. Interestingly, though, 44 % of the RAP specimens have an undefined CRR value in comparison to 15 % of specimens from the natural soil test panels with an undefined CRR, and the median CRR value of the specimens subjected to the RAP ground improvement method is 0.833 versus a median CRR value of 0.218 for specimens from the natural soil test panels. The higher CRR values of the specimens from the RAP test panels compared to the specimens from the natural soil test panels indicate that the ground improvement method is densifying the soil even if that change is not captured in the relationship between pore pressure generation and shear strain.

Specimens from the LMG test panels have a higher susceptibility to liquefaction triggering than specimens from the natural soil test panels based on the relationship between the generation of excess pore pressure and shear strain. The LMG ground improvement has a higher percentage of specimens than the natural soil in Category 1 (13 % of LMG versus 7 % of natural soil specimens) and Category 2 (44 % of LMG versus 19 % of natural soil specimens). It also has a lower percentage of specimens in Category 3 (44 % of LMG versus 4 % of natural soil specimens) and Category 4 (0 % of LMG versus 7 % of natural soil specimens). The median CRR value of the specimens from the LMG test panels is 0.144, which is lower than the median CRR value of 0.218 for the specimens from the natural soil test panels. Only one specimen from the LMG test panels registered an undefined CRR value, which corresponds to 6 % of total LMG specimens and is lower than the 15 % of natural soil specimens with an undefined CRR value.

8.7 SUMMARY

The relationship between the generation of excess pore pressure and shear strain is fundamental to understanding the susceptibility of triggering soil liquefaction. Results from shake testing at 17 test panels include a total of 75 specimens whose soil type ranges from SP to ML and degrees of saturation ranging from partially saturated to fully saturated.

Four distinct categories of behavior related to the generation of excess pore pressure and shear strain were identified, each with different levels of risk for triggering soil liquefaction under cyclic loading. Category 1 includes soils that are highly liquefiable and closely follow the Dobry prediction model for pore pressure generation, which features large excess pore pressure ratios at moderate levels of shear strains. Category 2 soils also generate positive excess pore pressure but are slightly less susceptible than Category 1 soils to triggering soil liquefaction under cyclic loading because they require higher shear strains to match the same level of excess pore pressure ratios as in Category 1. The soils in Category 3 generated little to no excess pore pressure at the shear strains induced during shake testing with T-Rex, and were limited to specimens that generated excess pore pressure ratios less than 2.5 % and larger than -2.5 %. The soils in Category 4 generated negative excess pore pressures and are considered to have the lowest risk of triggering soil liquefaction under cyclic loading.

The results from shake testing with T-Rex also show the effect of soil type, degree of saturation, and relative density on this relationship between the generation of excess pore pressure and shear strain as well as the impact of the various ground improvement methods. The soil type was shown to have a large effect of the distribution of specimens among the four identified behavioral categories. In general, the SP and SP-SM soils were shown to have the greatest potential for both positive and negative generation of excess pore pressure, behavior which is distinguished as Category 1 and Category 4. As the fines

content of the soil increases toward SM and ML classifications, the increase in pore pressure as a function of shear strain was more linear and significantly reduced in comparison to the sandier materials. The behavior of SM and ML soils were largely absent from being classified as Category 1 and Category 4. Category 2 and Category 3 soils had the full range of soils types from SP to ML, though for different reasons. SP and SP-SM materials in Category 2 and Category 3 are probably either too dense or too unsaturated to have Category 1 behavior while SM and ML soils appear to lack the soil structure needed to generate large excess pore pressures under the cyclic loading levels seen with shake testing with T-Rex.

The degree of saturation as assessed by the compression wave velocity was found not to have as large of an effect on the relationship between excess pore pressure generation and shear strain as soil type and relative density. Because of the geology of the site, the ML soils near the ground surface were also the most likely to be unsaturated due to their shallow depths. This relationship makes it difficult to separate out the effect of degree of saturation from the effect of soil type, but it appears that most of the influence comes from soil type rather than degree of saturation.

The shear wave based CRR was successfully used as a proxy for the relative density of the soil. The analysis of results from shake testing with T-Rex showed that especially in SP and SP-SM soils, the CRR increased as the risk of soil liquefaction triggering decreased. The specimens in Category 1 and Category 2 had the lowest median CRR values and Category 4 had such high CRR values that 80 % of them were undefined for the specimens in that category. The CRR seems to be a better indicator of relative density for soils with lower fines content (SP and SP-SM soil types) and in particular appears to significantly underestimate the cyclic resistance of soils with high fines content such as the ML soils.

The three ground improvement methods (RIC, RAP, and LMG) had varying levels of influence on the relationship between the generation of excess pore pressure and shear strain in comparison to those of the natural soil. The specimens from the RIC test panels showed the greatest reduction in susceptibility to soil liquefaction with a larger percentage of specimens in Category 4 than any of test panel type and the largest median CRR value. The specimens from the RAP test panels performed similarly to the specimens from the natural soil test panels, though the median CRR value was larger for the RAP specimens than the natural soil specimens. Finally, the specimens from the LMG test panels had a higher susceptibility to liquefaction triggering than those from the natural soil test panels as well as the lowest median CRR value of all the test panel types. The change in liquefaction susceptibility due to the ground improvements in comparison to the natural soil was well-captured by the calculated CRR values for the specimens. In absence of a more direct way of estimating the relative density of the soil in situ, the shear-wave based CRR is a suitable proxy.

A note of caution in interpreting these results: the risk of triggering liquefaction due to cyclic loading is different than the risk of triggering liquefaction as a chain reaction from adjacent soil deposits that liquefy. For example, an isolated dense sand may generate no or even negative excess pore pressure when subjected to cyclic loading on its own, but the high permeability of the soil means that if a dense sand layer is adjacent to a highly liquefiable loose sand layer, the high pore pressures from the loose layer may trigger liquefaction in the dense layer as the pore pressures redistributes through the deposit (Cubrinovski et al. 2017). Soils with high fines content may not have this secondary risk because of their relatively lower permeabilities.

Chapter 9: Summary, Conclusions, & Recommendations

9.1 SUMMARY OF WORK

The Ground Improvement Trials funded by the New Zealand Earthquake Commission (EQC) provided a unique opportunity to evaluate a variety of ground improvement methods at full-scale. For this dissertation, the RIC, RAP, and LMG ground improvement methods were selected among the nine ground improvement methods included in the trials for an extensive evaluation using several different approaches. The main objectives of the evaluation was determine how the ground improvement methods improved the soil and what effect it had on the liquefaction susceptibility of the soil. The various assessments of the ground improvement methods were primarily comparative in nature and used results from testing the natural, unimproved soil as a baseline against which to compare the results from testing the ground-improved soil at three test sites.

The majority of the data used in this dissertation came from excavation trenches, CPT testing, DPCH testing, and shake testing with T-Rex. In total, data were collected from 15 excavation trenches, 43 CPT tests, 19 DPCH tests, and 15 shake tests with T-Rex, resulting in a highly-detailed characterization of the natural and ground-improved soils. These collective data provide information regarding soil type, density, stiffness, degree of saturation, subsurface layering, nonlinear behavior, and coupled behavior of pore pressure generation and shear strain that are all key to understanding the soil's susceptibility to liquefaction triggering under cyclic loading. This study has shown the significant complexity in understanding the soil behavior leading to the triggering of liquefaction as well as the difficulty in assessing the impact and effectiveness of various ground improvement methods. The conclusions reached in this dissertation are an attempt to untangle this complexity and explain the observed behavior as well as possible.

9.2 CONCLUSIONS

Results from CPT, DPCH, and shake testing with T-Rex were used to evaluate the effectiveness of the RIC, RAP, and LMG ground improvements in comparison to the natural soil.

9.2.1 Results from CPT and DPCH testing

The corrected cone tip resistance q_t from CPT testing and the shear modulus from DPCH testing were used to evaluate changes in the density and stiffness, respectively, of the soil due to the ground improvement methods in comparison to the natural soil. The analysis was performed over depths ranging from 0.6 to 4.0 m below the ground surface. Depths shallower than 0.6 m were omitted from the analysis because DPCH testing at Site 3 and Site 4 started at a depth of 0.6 m below the ground surface (DPCH testing at Site 6 started at 0.4 m below the ground surface). Depths greater than 4.0 m were omitted from the analysis because the ground improvement methods were only intended to improve the ground down to 4.0 m.

The results of CPT and DPCH testing between the improvements both show similar conclusions regarding the relative effectiveness of the ground improvements methods. The ranking of ground improvement methods in order from most effective to least effective is RAP, RIC, and LMG. As determined by increases in the corrected cone tip resistance and the shear modulus for the soil between improvements, the increase in density and stiffness in the soil by the RIC and RAP methods are similar. The LMG, on the other hand, exhibited at most half the improvement of the other two ground improvement methods as well as situations in which it loosened the soil in comparison to the natural soil. The median increase in corrected cone tip resistance between improvements ranged from 24 to 86 % for the RIC ground improvement method, from 24 to 128 % for the RAP ground improvement method, and -4 to 29 % for the LMG ground improvement method at the

three test sites. The median increase in shear modulus between improvements ranged from 17 to 40 % for the RIC ground improvement method, 19 to 31 % for the RAP ground improvement method, and -23 to 11 % for the LMG ground improvement method at the three test sites.

The results of DPCH testing across improvements showed that the RAP ground improvement method resulted in the greatest increases in stiffness, followed by the LMG ground improvement method and then by the RIC ground improvement method. In contrast to the CPT and DPCH testing between improvements which measured changes in density and stiffness to the soil, the DPCH across improvements measures also measured the additional stiffness imparted by the gravel in the RAP piers and the grout in the LMG columns. The median increase in shear modulus across improvements ranged from 18 to 24 % for the RIC ground improvement method, from 109 to 190 % for the RAP ground improvement method, and from 26 to 87 % for the LMG ground improvement method.

9.2.2 Results from Shake Testing with T-Rex – Stiffness Profiles

The stiffness profiles from shake testing with T-Rex show an approximation of stiffness of the natural and ground-improved soils over a large range of shear strains. The shear strains from three selected stages of shaking were normalized to three nominal levels of shear stress applied at the ground surface by the baseplate of T-Rex to allow a common comparison of test results across test panels. The three shear stress levels used were (1) 1.5 kPa, (2) 5 kPa, and (3) 15 kPa.

In comparison to the natural soil, the RAP ground improvement method resulted in the largest reduction of shear strains for a given shear stress at the ground surface. The RIC ground improvement method had the second largest reduction in shear strains, followed by the LMG ground improvement method with the smallest reduction in shear strains in

comparison to the performance of the natural soil. The median decrease in shear strain in comparison to the natural soil ranged from 16 to 47 % for the RIC ground improvement method, from 17 to 55 % for the RAP ground improvement method, and 14 to 34 % for the LMG ground improvement method.

9.2.3 Results from Shake Testing with T-Rex – Coupled Behavior of Shear Strain and Excess Pore Pressure Ratio

The relationships between shear strain and the generation of residual excess pore pressure (in terms of the excess pore pressure ratio) developed from shake testing with T-Rex provided some insight into the influence of the ground improvement methods on the liquefaction susceptibility of the soil. Four categories of soil behavior were identified based on the coupled behavior between shear strain and the generation of excess pore pressure. Soils that fall into Category 1 behavior have the potential to generate large positive excess pore pressure ratios at moderate levels of shear strain and exhibit similar behavior to Dobry's pore water prediction model for liquefiable soils (Dobry et al. 1982). Soils that fall into Category 2 behavior fall to the right of Dobry's pore water prediction model and generate relatively small levels of positive excess pore pressures at moderate levels of shear strain. Soils that fall into Category 3 behavior generate little to no excess pore pressure at any level of shear strain. And finally, soils that fall into Category 4 behavior generate negative excess pore pressure. The liquefaction susceptibility of these soils under dynamic loading ranges from highly susceptible in Category 1 to not susceptible in Category 4.

An evaluation of the ground improvement methods was done by comparing the distribution of test specimens from the natural soil test panels between each of the four behavioral categories against the distribution of test specimens from the ground improved test panels. This analysis showed the RIC ground improvement method had the greatest impact on reducing the liquefaction susceptibility of the soil in comparison to the natural

soil, followed by the RAP ground improvement method. The LMG ground improvement method, on the other hand, had the effect of increasing the liquefaction susceptibility of the ground-improved soil in comparison to the natural soil.

The shear-wave velocity based CRR calculated for each of the specimens also showed the RIC ground improvement method had the greatest increase in resistance to soil liquefaction triggering. From the RIC test panels, 8 out of 16 specimens had undefined CRR values in comparison to a median CRR value of 0.218 for the natural soil specimens. The CRR also indicated the RAP ground improvement had greater increase in resistance to soil liquefaction triggering than the natural soil with a median CRR value of 0.833 for the RAP specimens in comparison to 0.218 for the natural soil specimens. For the LMG ground improvement method, the CRR indicated a decrease in resistance to soil liquefaction triggering with a median CRR value of 0.144 in comparison to 0.218 for the natural soil.

9.2.4 Summary of Conclusions

By using the corrected cone tip resistance from CPT testing, the shear modulus from DPCH testing, and stiffness profiles from shake testing with T-Rex as metrics for performance, the RAP ground improvement method consistently performed the best in comparison to the natural soil and the other ground improvement methods. The RIC ground improvement method outperformed the natural soil and the LMG ground improvement method by each of those metrics except for the shear modulus measured across improvements. The LMG ground improvement method had variable levels of success, with the some increases in performance but also instances of worse performance in comparison to the natural soil.

However, by directly evaluating the liquefaction susceptibility of the soil with the relationship between shear strain and the generation of excess pore pressure and with the shear-wave based CRR, the RIC significantly outperformed the natural soil and the RAP and LMG ground improvement methods. It is possible that the CPT and DPCH tests as well as the stiffness profiles from shake testing with T-Rex are failing to properly capture the changes in relative density that are more critical to the liquefaction susceptibility than overall density and stiffness. It is believed that increases in stiffness that result in smaller shear strains should only be considered a secondary benefit of these ground improvement methods because they are not large enough to have a dramatic impact on the soil's resistance to liquefaction triggering. The main impact of these ground improvement methods needs to be the change in behavior under cyclic loading and the relationship between shear strain and the generation of excess pore pressure from highly susceptible to liquefaction behavior (Category 1) to non-liquefiable behavior (Category 3 and 4) under dynamic loading.

9.3 RECOMMENDATIONS & FUTURE WORK

Testing during the Ground Improvement Trials went well without any major challenges. As a result, recommendations for improving the testing procedures are relatively minor and easy to implement. Indeed, much of the future work described in this section is currently underway and implements the recommendations.

9.3.1 Disadvantages of Using a Reduced Number of Sensors

The main suggestion for future projects is to avoid eliminating ground particle motion sensors from nodes of the 4-node element that is used to calculate shear strains. As discussed in Section 6.4.1, the shear strains calculated using 4-node element with fewer than four sensors resulted in variations of up to 30 % in comparison to shear strains calculated using a 4-node element with four sensors. Further, using additional sensors makes it easier to calculate the nonlinear shear wave velocity of the soil during shake testing with T-Rex if the sensors are stacked in a reasonably vertical array. While this dissertation did not discuss the nonlinear shear wave velocities, it is an important part of understanding soil behavior during shake testing with T-Rex and is a topic currently being pursued by other graduate students.

9.3.2 Initial Site Characterization with CPT and DPCH

It is highly advantageous to perform preliminary site characterization at new test sites with the CPT and DPCH test. The CPT test can provide insight into the subsurface layering of the site and the DPCH test can identify the depth to 100 % saturation using the compression wave velocity. Knowing the subsurface layering and the depth to 100 % saturation is key to properly locating the instrumentation array below the ground surface in the intended ground conditions.

It is also important to perform the CPT and DPCH tests sufficiently close to one another as well as in close proximity to any additional tests such as shake testing with T-Rex to eliminate the effects of spatial variability as much as possible. The tests should not, however, be located too close to one another to prevent testing in the zones of disturbed soil. The appropriate minimum distance between tests is site-specific and requires engineering judgment.

9.3.3 Using Multiple Shake Trucks to Obtain Larger Shear Strains

One of the future goals of shake testing with T-Rex is to increase the magnitude of cyclic shear strains. The test procedure is currently being modified to synchronize two large shaker trucks in an effort to induce larger shear strains in the soil, and preliminary results show that it can be done. One complication with adding a second shaker truck is that it necessitates the use of a three-dimensional instrumentation array to capture motion in three dimensions. Previously iterations of the test with one shaker truck only required instrumentation and an analysis that dealt with two dimensions. Preliminary results also show that the implementation of a three-dimensional instrumentation array can be achieved without much difficulty.

9.3.4 Model the Response of the Soil from Shake Testing with T-Rex

To date, shake testing with T-Rex has been performed in the field in locations such as Imperial Valley (California, USA), Charleston (South Carolina, USA), Christchurch (New Zealand), and Longview (Washington, USA) to study the triggering of soil liquefaction. The data collected from these projects have provided great insight into the nonlinear behavior of the soil as well as the coupled response between the generation of excess pore pressure and shear strain. A natural area of future research to be done in conjunction with shake testing with T-Rex would be to model its behavior using a

numerical modeling software such as FLAC. Fortunately many of the sites where shake testing with T-Rex has been performed are very well documented with supplementary information from a number of other in situ tests and laboratory tests on specimens obtained from the sites. Success in modeling the behavior observed during shake testing with T-Rex will provide critical insight into the complex behavior.

9.3.5 Study the Nonlinear and Pore Pressure Degradation of the Shear Modulus

Resonant column testing on reconstituted specimens obtained from various test panels is underway in the Soil and Rock Dynamic Laboratory at The University of Texas at Austin by fellow graduate students Yaning Wang and Zhongze "Steve" Xu. So far these tests have provided shear modulus reduction curves that are considered fairly representative of the in-situ conditions during shake testing with T-Rex. The shear modulus reduction curves are used in conjunction with the shear strains calculated from shake testing with T-Rex to estimate the reduction in shear modulus as a result of nonlinearity as well as the cyclic shear stresses. The reduction in shear modulus predicted by the resonant column data can hopefully be corroborated by the calculation of the nonlinear shear wave velocity of the soil during shake testing with T-Rex. The nonlinear shear wave velocity, and therefore nonlinear shear modulus, should decrease as the shear strain increases in a way that is predicted by the model from resonant column testing. Calculation of the nonlinear shear wave velocity is currently being performed by fellow graduate student Benchen Zhang.

The resonant column device is currently being modified with pore pressure transducers in order to capture the coupled behavior of shear strains and the generation of excess pore pressures. If successful, this new test setup will be able to identify the contribution to shear modulus degradation due to nonlinearity and due to changes in

confining pressure from the generation of excess pore pressure, which can then be compared to results in the field. This work is currently underway.

Appendix A: Variation in shear stress induced by T-Rex at the ground surface versus shear strain evaluated at depth

The figures presented in Appendix A are supplementary from Section 7.3, on the normalization of shear stress at the ground surface.

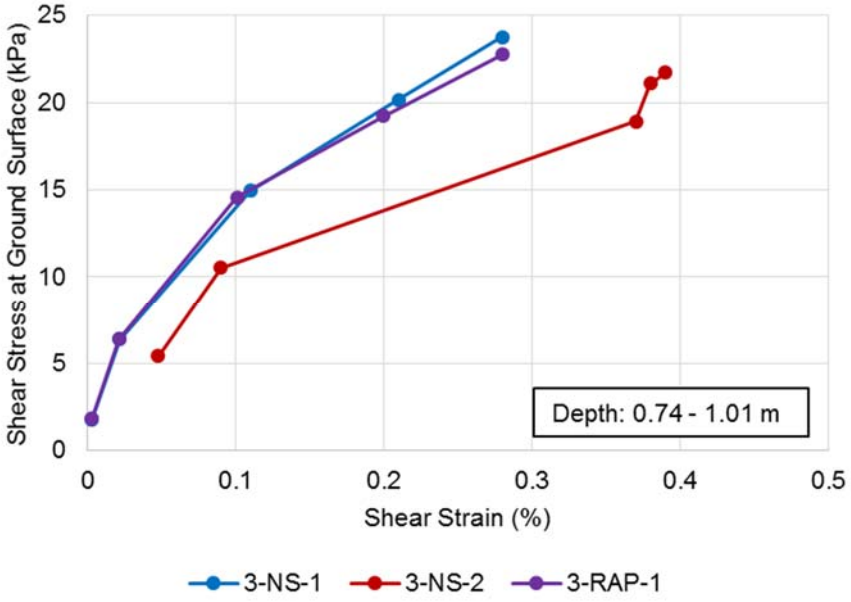

Figure 103: Variation in shear stress induced by T-Rex at the ground surface versus shear strain evaluated at depths ranging from 0.74 to 1.01 m at the 3-NS-1, 3-NS-2, and 3-RAP-1 test panels.

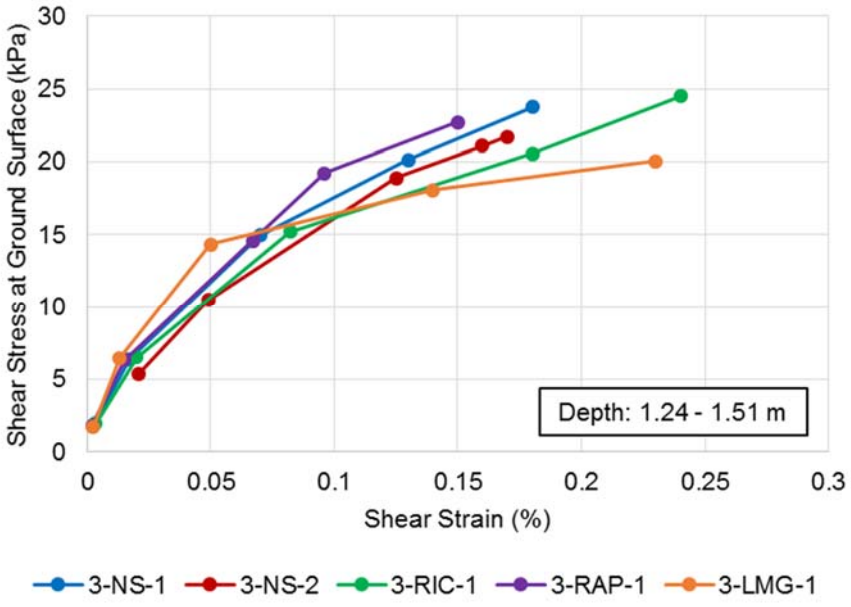

Figure 104: Variation in shear stress induced by T-Rex at the ground surface versus shear strain evaluated at depths ranging from 1.24 to 1.51 m at the 3-NS-1, 3-NS-2, 3-RIC-1, 3-RAP-1, and 3-LMG-1 test panels.

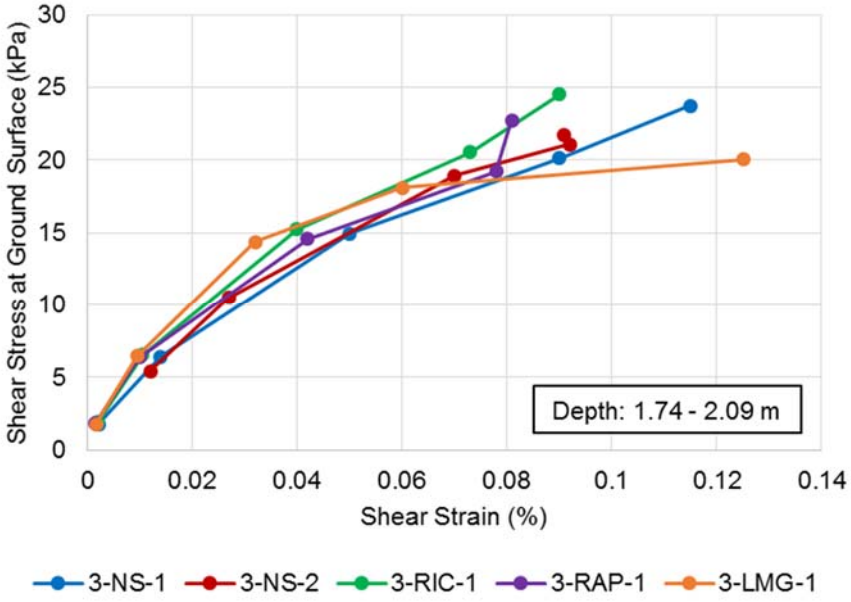

Figure 105: Variation in shear stress induced by T-Rex at the ground surface versus shear strain evaluated at depths ranging from 1.74 to 2.09 m at the 3-NS-1, 3-NS-2, 3-RIC-1, 3-RAP-1, and 3-LMG-1 test panels.

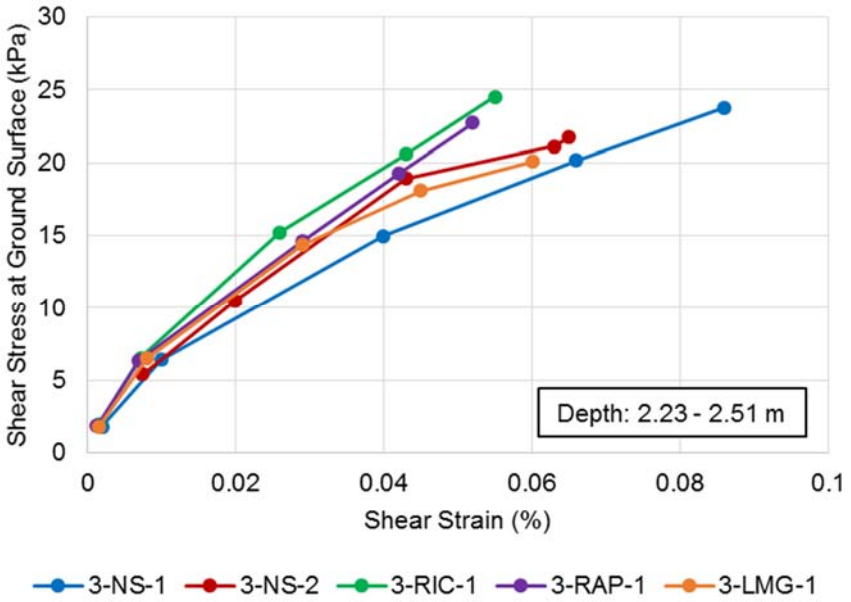

Figure 106: Variation in shear stress induced by T-Rex at the ground surface versus shear strain evaluated at depths ranging from 2.23 to 2.51 m at the 3-NS-1, 3-NS-2, 3-RIC-1, 3-RAP-1, and 3-LMG-1 test panels.

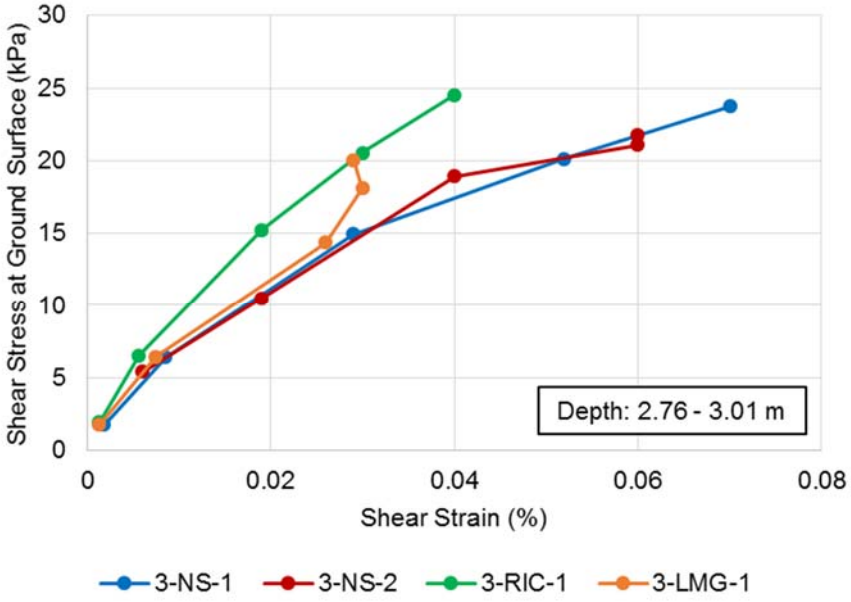

Figure 107: Variation in shear stress induced by T-Rex at the ground surface versus shear strain evaluated at depths ranging from 2.76 to 3.01 m at the 3-NS-1, 3-NS-2, 3-RIC-1, and 3-LMG-1 test panels.

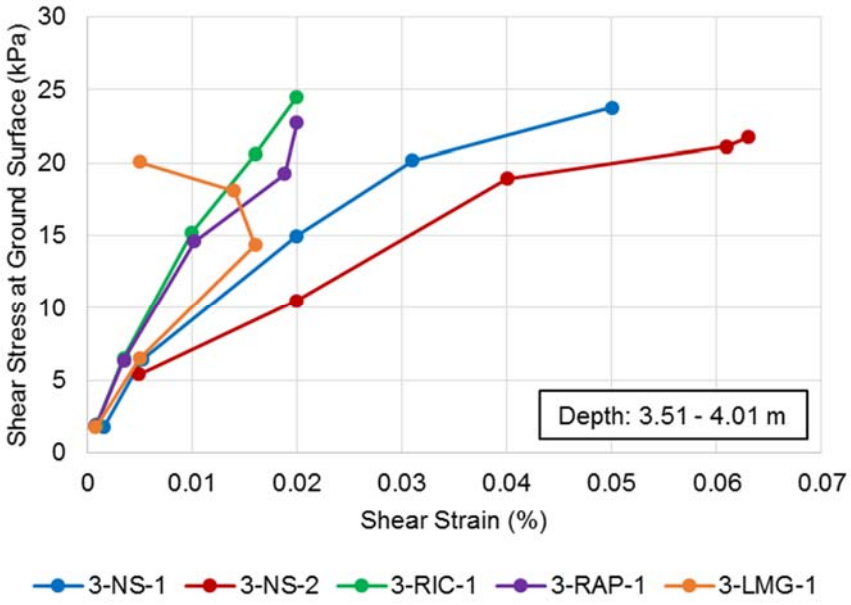

Figure 108: Variation in shear stress induced by T-Rex at the ground surface versus shear strain evaluated at depths ranging from 3.51 to 4.01 m at the 3-NS-1, 3-NS-2, 3-RIC-1, 3-RAP-1, and 3-LMG-1 test panels.

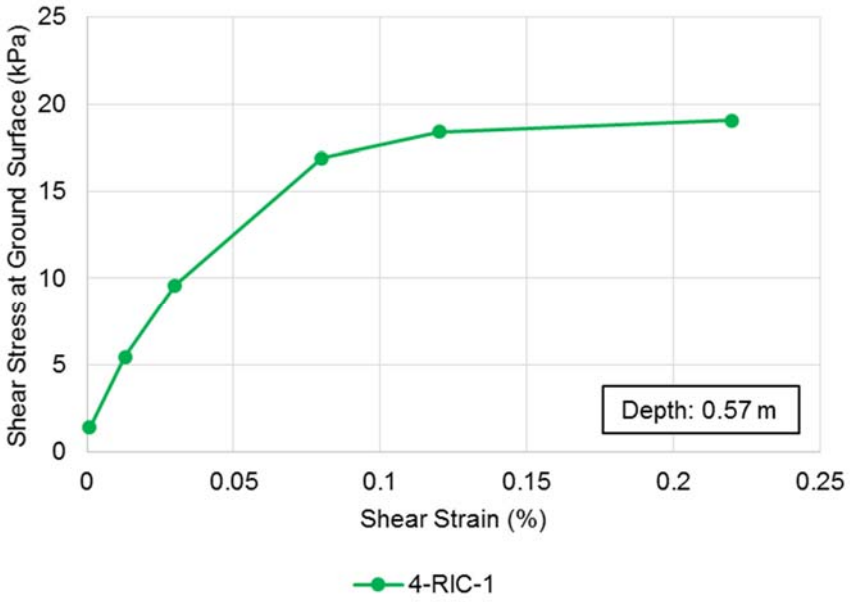

Figure 109: Variation in shear stress induced by T-Rex at the ground surface versus shear strain evaluated at a depth of 0.57 m at the 4-RIC-1 test panel.

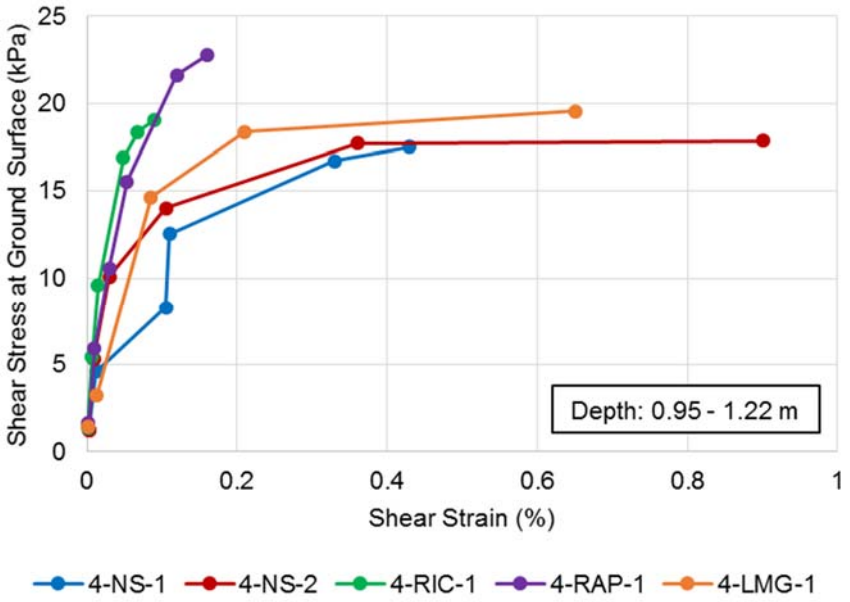

Figure 110: Variation in shear stress induced by T-Rex at the ground surface versus shear strain evaluated at depths ranging from 0.95 to 1.22 m at the 4-NS-1, 4-NS-2, 4-RIC-1, 4-RAP-1, and 4-LMG-1 test panels.

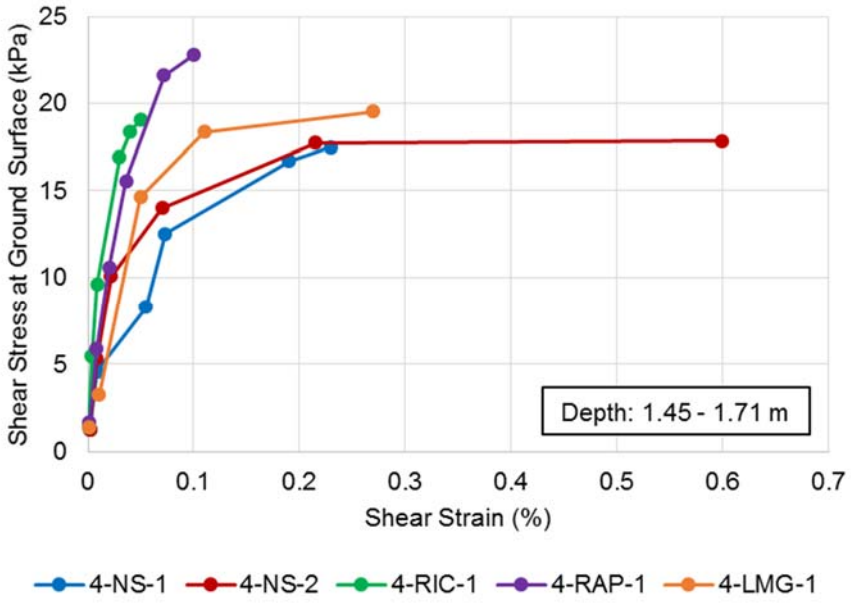

Figure 111: Variation in shear stress induced by T-Rex at the ground surface versus shear strain evaluated at depths ranging from 1.45 to 1.71 m at the 4-NS-1, 4-NS-2, 4-RIC-1, 4-RAP-1, and 4-LMG-1 test panels.

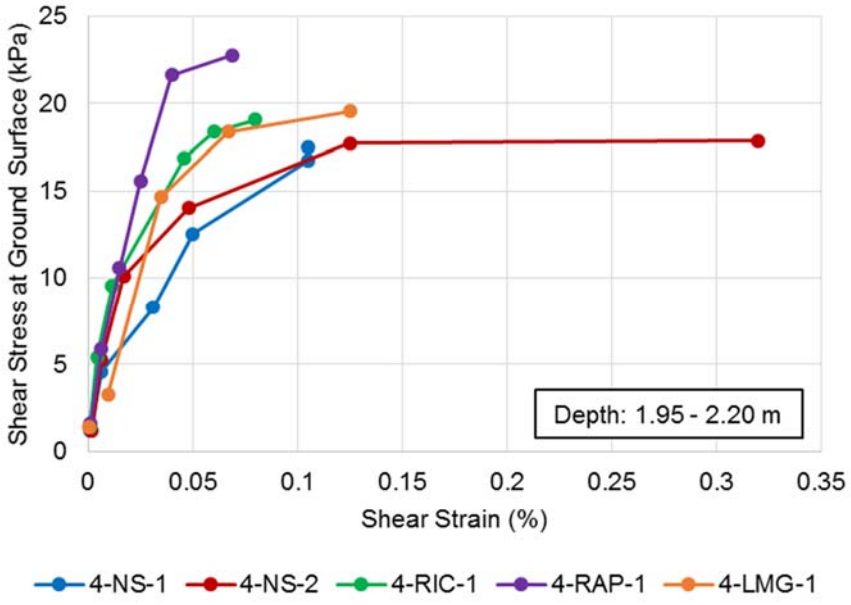

Figure 112: Variation in shear stress induced by T-Rex at the ground surface versus shear strain evaluated at depths ranging from 1.95 to 2.20 m at the 4-NS-1, 4-NS-2, 4-RIC-1, 4-RAP-1, and 4-LMG-1 test panels.

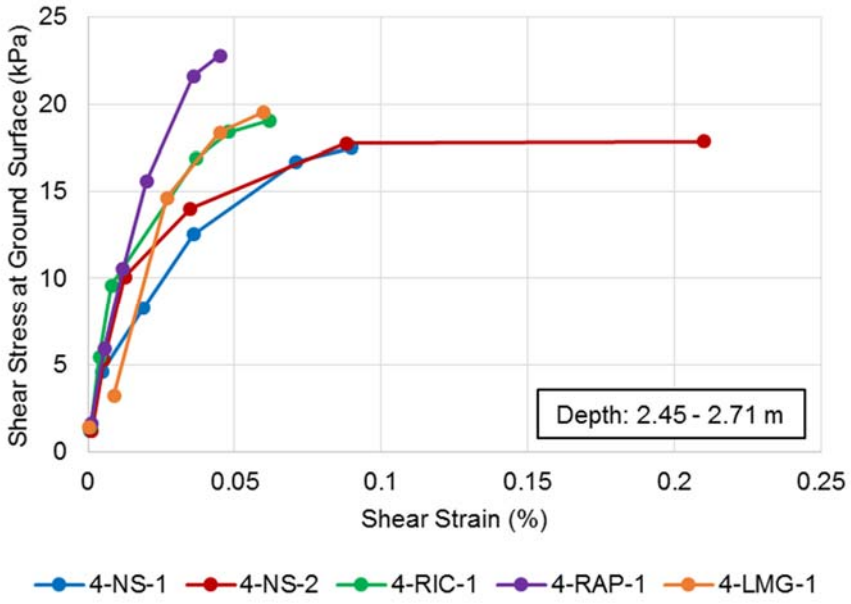

Figure 113: Variation in shear stress induced by T-Rex at the ground surface versus shear strain evaluated at depths ranging from 2.45 to 2.71 m at the 4-NS-1, 4-NS-2, 4-RIC-1, 4-RAP-1, and 4-LMG-1 test panels.

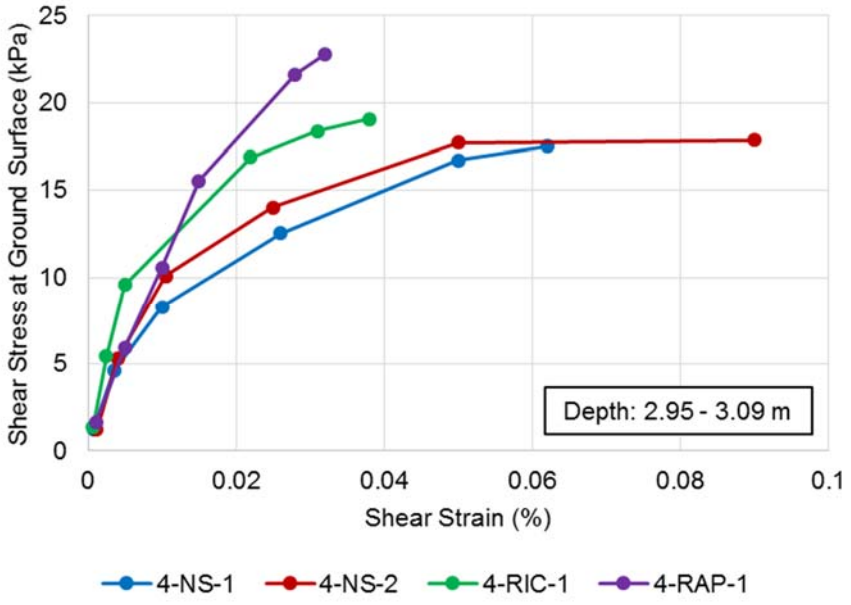

Figure 114: Variation in shear stress induced by T-Rex at the ground surface versus shear strain evaluated at depths ranging from 2.95 to 3.09 m at the 4-NS-1, 4-NS-2, 4-RIC-1, 4-RAP-1, and 4-LMG-1 test panels.

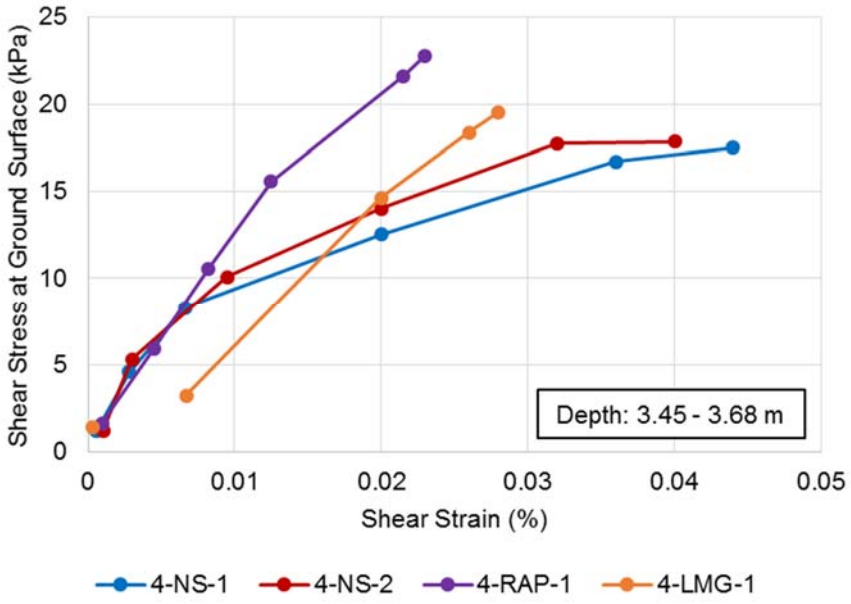

Figure 115: Variation in shear stress induced by T-Rex at the ground surface versus shear strain evaluated at depths ranging from 3.45 to 3.68 m at the 4-NS-1, 4-NS-2, 4-RAP-1, and 4-LMG-1 test panels.

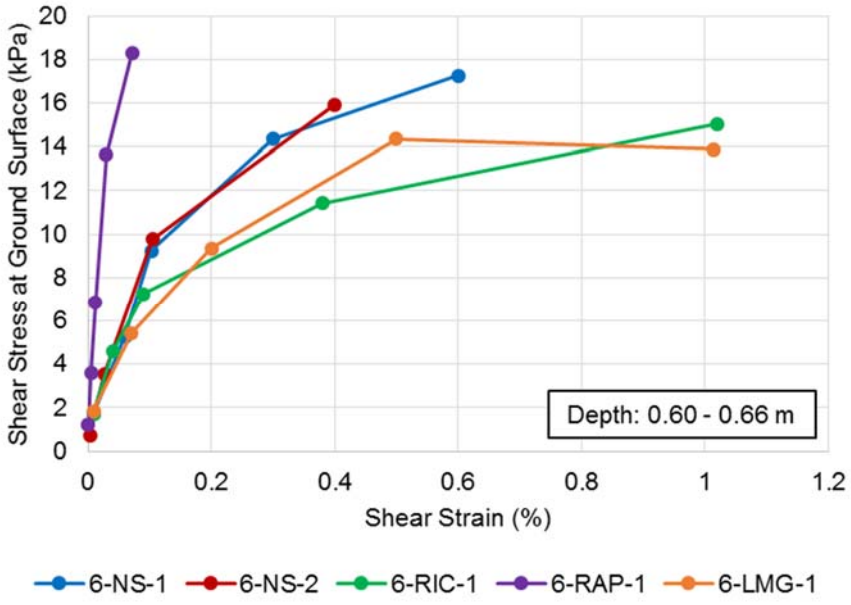

Figure 116: Variation in shear stress induced by T-Rex at the ground surface versus shear strain evaluated at depths ranging from 0.60 to 0.66 m at the 6-NS-1, 6-NS-2, 6-RIC-1, 6-RAP-1, and 6-LMG-1 test panels.

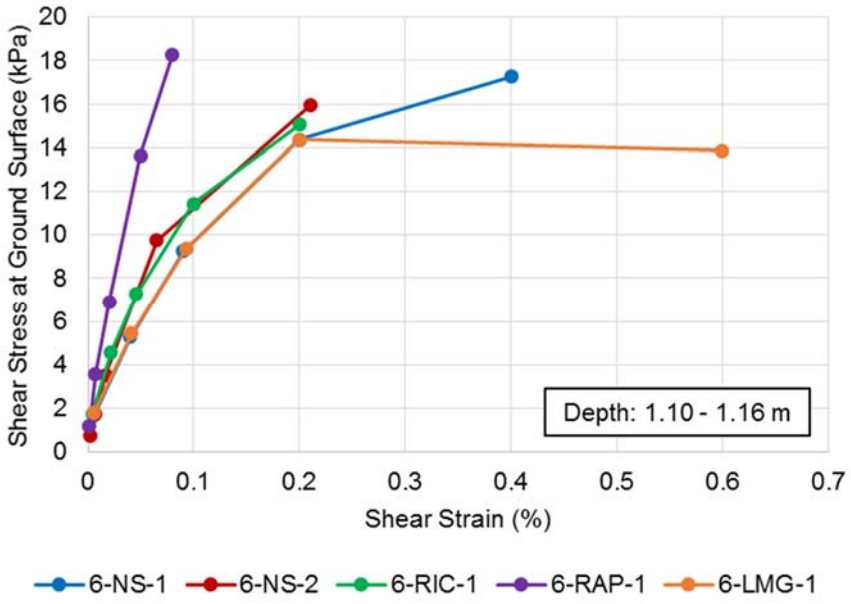

Figure 117: Variation in shear stress induced by T-Rex at the ground surface versus shear strain evaluated at depths ranging from 1.10 to 1.16 m at the 6-NS-1, 6-NS-2, 6-RIC-1, 6-RAP-1, and 6-LMG-1 test panels.

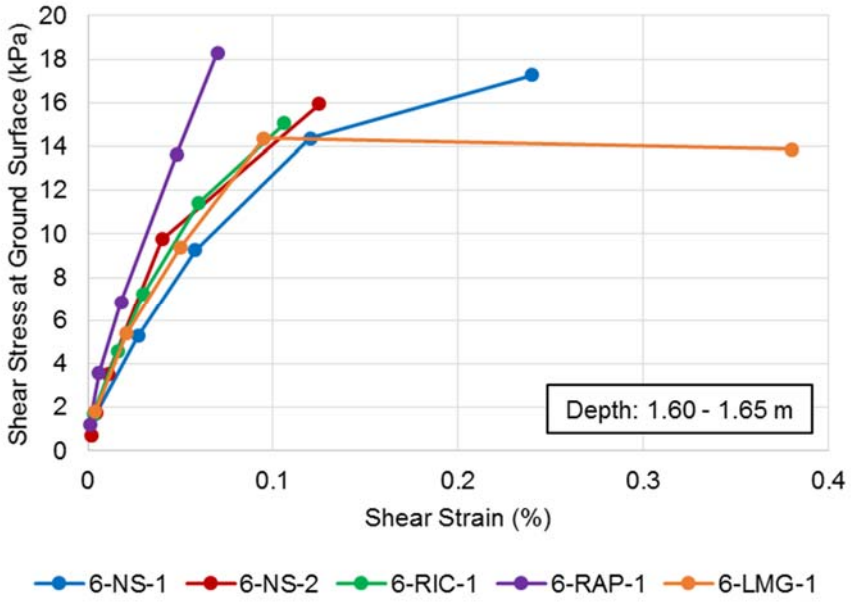

Figure 118: Variation in shear stress induced by T-Rex at the ground surface versus shear strain evaluated at depths ranging from 1.60 to 1.65 m at the 6-NS-1, 6-NS-2, 6-RIC-1, 6-RAP-1, and 6-LMG-1 test panels.

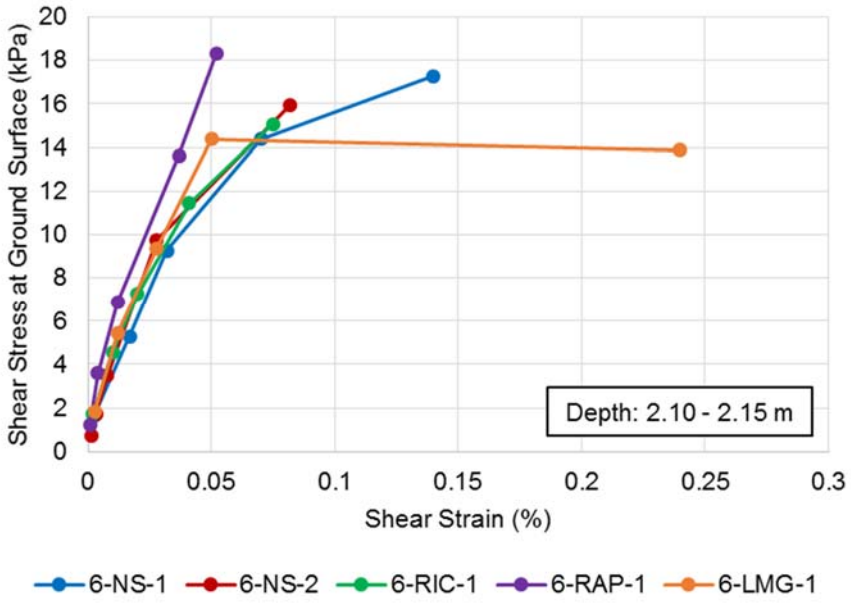

Figure 119: Variation in shear stress induced by T-Rex at the ground surface versus shear strain evaluated at depths ranging from 2.10 to 2.15 m at the 6-NS-1, 6-NS-2, 6-RIC-1, 6-RAP-1, and 6-LMG-1 test panels.

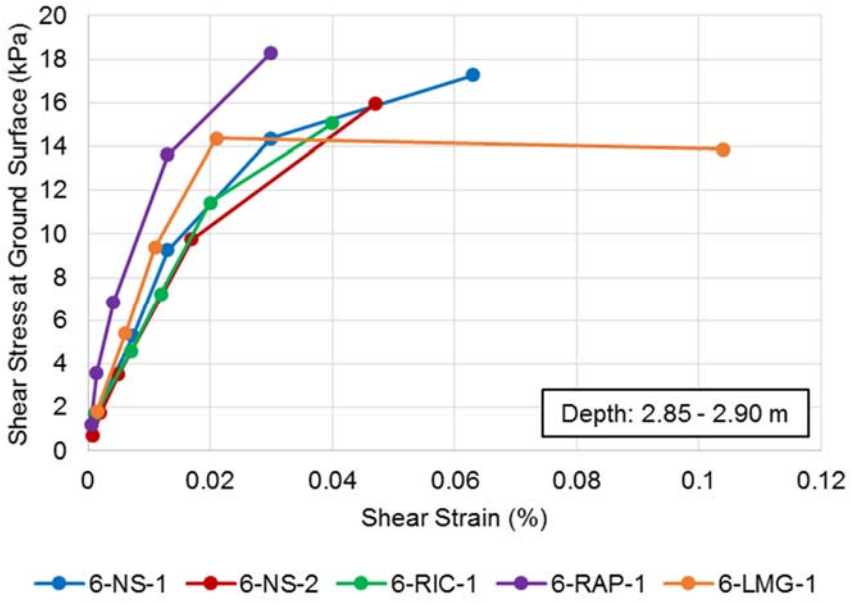

Figure 120: Variation in shear stress induced by T-Rex at the ground surface versus shear strain evaluated at depths ranging from 2.85 to 2.90 m at the 6-NS-1, 6-NS-2, 6-RIC-1, 6-RAP-1, and 6-LMG-1 test panels.

References

Amini, F., & Qi, G. Z. (2000). Liquefaction Testing of Stratified Silty Sands. *Journal of Geotechnical and Geoenvironmental Engineering, 123*(3), 208-217.

Andrus, R. D., & Stokoe II, K. H. (2000). Liquefaction Resistance of Soils from Shear-Wave Velocity. *Journal of Geotechnical and Geoenvironmental Engineering, 126*(11), 1015-1025.

Askari, F., Dabiri, R., Shafiee, A., & Jafari, M. (2010). Effects of Non-Plastic Fines Content on Cyclic Resistance and Post Liquefaction of Sand-Silt Mixtures Based on Shear Wave Velocity. *Journal of Seismology and Earthquake Engineering, 12*.

ASTM Standard D5778-12. (2012). *Standard Test Method for Electronic Friction Cone and Piezocone Penetration Testing of Soils.* West Conshohocken.

Bennet, M.J., Ponti, D.J., Tinsley III, J.C., Holzer, T.L., & Conaway, C.H. (1998). Subsurface geotechnical investigations near sites of ground deformation caused by the January 17, 1994, Northridge, California, earthquake. *U.S.G.S. Open-file Report*, 98-373.

Boulanger, R. W., & Idriss, I. (2006). Liquefaction Susceptibility Criteria for Silts and Clays. *Journal of Geotechnical and Geoenvironmental Engineering, 132*(11), 1413-1426.

Boulanger, R. W., Mejia, L. H., & Idriss, I. M. (1997). Liquefaction at Moss Landing during Loma Prieta Earthquake. *Journal of Geotechnical and Geoenvironmental Engineering, 123*(5), 453-467.

Boulanger, R. W., Meyers, M. W., Mejia, L. H., & Idriss, I. M. (1998). Behavior of a Fine-Grained Soil during the Loma Prieta Earthquake. *Canadian Geotechnical Journal, 35*, 146-158.

Boulanger, R., & Idriss, I. (2014). *CPT and SPT Based Liquefaction Triggering Procedures.* University of California, Center for Geotecnical Modeling, Department of Civil and Environmental Engineering.

Bray, J. D., Sancio, R. B., Durgunoglu, T., Onalp, A., Youd, T. L., Stewart, J. P., Seed, R.B., Cetin, O.K., Bol, E., Baturay, M.B., Christensen, C., Karadayilar, T. (2004). Subsurface Characterization at Ground Failure Sites in Adapazari, Turkey. *Journal of Geotechnical and Geoenvironmental Engineering, 130*(7), 673-685.

Bray, J. D., & Sancio, R. B. (2006). Assessment of the Liquefaction Susceptibility of Fine-Grained Soils. *Journal of Geotechnical and Geoenvironmental Engineering, 132*(9), 1165-1177.

Chang, W.-J. (2002). *Development of an In Situ Dynamic Liquefaction Test.* Dissertation, The University of Texas at Austin.

Chu, D. B., Stewart, J. P., Lee, S., Tsai, J., Lin, P.S., Chu, B.L., Seed, R.B., Hsu, S.C., Yu, M.S., Wang, M.C.H. (2004). Documentation of Soil Conditions at Liquefaction and Non-Liquefaction Sites from 1999 Chi-Chi (Taiwan) Earthquake. *Soil Dynamics and Earthquake Engineering, 24*, 647-657.

Cox, B. R. (2006). *Development of a Direct Test Method for Dynamically Assessing the Liquefaction Resistance of Soils In Situ.* Dissertation, The University of Texas at Austin.

Cubrinovksi, M., Rhodes, A., Ntritsos, N., & van Ballegooy, S. (2017). System Response of Liquefiable Deposits.

Cubrinovski, M., Rhodes, A., Ntritsos, N., & van Ballegooy, S. (2017). System Response of Liquefiable Deposits. *3rd International Conference on Performance-Based Design in Earthquake Geotechnical Engineering (PBD-III Vancouver 2017).* Vancouver.

Dobry, R., Ladd, R., Yokel, F., Chung, R., & Powell, D. (1982). *Predictions of Pore Water Pressure Buildup and Liquefaction of Sands During Earthquakes by the Cyclic Strain Method.* National Bureau of Standards, Building Science Series, U.S. Department of Commerce.

Fourie, A. B., Hofmann, B. A., Mikula, R. J., Lord, E. R., & Robertson, P. K. (2001). Partially Saturated Tailings Sand Below the Phreatic Surface. *Geotechnique, 51*(7), 577-585.

Hossain, A.M., Andrus, R.D., & Camp III, W.M. (2013). Correcting Liquefaction Resistance of Unsaturated Soil Using Wave Velocity. *Journal of Geotechnical and Geoenvironmental Engineering, 139*(2), 277-287.

Huang, Y.-T., Huang, A.-B., Kuo, Y.-C., & Tsai, M.-D. (2004). A Laboratory Study on the Undrained Strength of a Silty Sand from Central Western Tawain. *Soil Dynamics and Earthquake Engineering, 24*, 733-743.

Hwang, S., Roberts, J., Stokoe, K., Cox, B., van Ballegooy, S., & Soutar, C. (2017). Utilizing Direct-Push Crosshole Seismic Testing to Verify the Effectiveness of Shallow Ground Improvements; A Casae Study Involving Low-Mobility Grout Columns in Christchurch, New Zealand. *Grouting 2017.* Honolulu.

Ishihara, K. (1985). Stability of natural deposits during earthquakes. *Proceedings of the 11th International Conference on Soil Mechanics and Foundation Engineering*, 321-376.

Ishihara, K., Tsuchiya, H., Huang, Y., & Kamada, K. (2001). Keynote Lecture: Recent Studies on Liquefaction Resistance of Sand-Effect of Saturation. *Fourth International Conference on Recent Advances in Geotechnical Engineering and Soil Dynamics.* 30.

Ishihara, K., & Tsukamoto, Y. (2004). Cyclic strength of imperfectly saturation sands and analysis of liquefaction. *Proceedings of the Japanese Academy, 80*(B), 372-391.

Kokusho, T. (2000). Correlation of Pore-Pressure B-Value with P-Wave Velocity and Poisson's Ratio for Imperfectly Saturated Sand or Gravel. *Soils and Foundations, 40*(4), 95-102.

Lade, P. V., & Yamamuro, J. A. (1997). Effects of Nonplastic Fines on Static Liquefaction of Sands. *Canadian Geotechnical Journal, 34*, 918-928.

Liu, N., & Mitchell, J. K. (2006). Influence on Nonplastic Fines on Shear Wave Velocity-Based Assessment of Liquefaction. *Journal of Geotechnical and Geoenvironmental Engineering, 132*(8), 1091-1097.

Martin, G. R., Seed, H. B., & Finn, W. D. (1978). Effects of System Compliance on Liquefaction Tests. *Journal of Geotechnical Engineering Division, 104*(4), 463-479.

Menq, F.-Y., Stokoe II, K., Park, K., Rosenblad, B., & Cox, B. (2008). Performance of Mobile Hydraulic Shakers at nees@UTexas for Earthquake Studies. *14th World Conference of Earthquake Engineering.* Beijing.

Pitman, T., Robertson, P., & Sego, D. (1994). Influence of Fines on the Collapse of Loose Sands. *Canadian Geotechnical Journal, 31*, 728-739.

Polito, C. P., & Martin II, J. R. (2001). Effects of Nonplastic Fines on the Liquefaction Resistance of Sands. *Journal of Geotechnical and Geoenvironmental Engineering, 127*(5), 408-415.

Rathje, E., Chang, W.-J., & Stokoe, I. K. (2004). Evaluation of Ground Strain From In Situ Dynamic Response. *13th World Conference on Earthquake Engineering.* Vancouver, B.C.

Roberts, J. N. (2014). *Direct In-Situ Evaluation of Liquefaction Susceptibility.* Thesis, The University of Texas at Austin, Austin.

Roberts, J., Stokoe II, K., Hwang, S., Cox, B., Wang, Y., & Menq, F. (2016). Field Measurements of the Variability in Shear Strain and Pore Pressure Generation in Christchurch Soils. *5th International Conference on Geotechnical and Geophysical Site Characterisation.* Gold Coast.

Robertson, P. K., & Campanella, R. G. (1985). Liquefaction Potential of Sands Using the CPT. *Journal of Geotechnical Engineering, 111*(3), 384-403.

Robertson, P.K., & Wride, C.E. (1998). Evaluation cyclic liquefaction potential using the cone penetration test. *Canadian Geotechnical Journal, 35*, 442-459.

Robertson, P. K. (2009). Interpretation of cone penetration tests - a unified approach. *Canadian Geotechnical Journal, 46*, 1337-1355.

Sancio, R., Bray, J., Youd, T., Durgunoglu, H., Onalp, A., Seed, R.B., Christensen, C., Baturay, M.B., Karadayilar, T. (2002). Correlation between Ground Failure and Soil Conditions in Adapazari, Turkey. *Soil Dynamics and Earthquake Engineering, 22*, 1093-1102.

Seed, H.B., & Idriss, I.M. (1971). Simplified Procedure for Evaluation Soil Liquefaction Potential. *Journal of Geotechnical Engineering Division*, *97*(9), 1249-1273.

Seed, H.B., Idriss, I.M., & Arango, I. (1983). Evaluation of Liquefaction Potential Using Field Performance Data. *Journal of Geotechnical Engineering, 109*(3), 458-482.

Seed, H.B., Tokimatsu, K., Harder, L.F., & Chung, R.M. (1985). The Influence of SPT Procedures in Soil Liquefaction Resistance Evaluations. *Journal of Geotechnical Engineering*, ASCE, *111*(12), 1425-1445.

Sherif, M. A., Ishibashi, I., & Tsuchiya, C. (1977). Saturation Effect on Initial Soil Liquefaction. *Journal of Geotechnical Engineering Division, 103*(8), 914-917.

Singh, S. (1996). Liquefaction Characteristics of Silts. *Geotechnical and Geological Engineering, 14*, 1-19.

Sladen, J., D'Hollander, R., & Krahn, J. (1985). Back Analysis of the Nerlerk Berm Liquefaction Slides. *Canadian Geotechnical Journal, 22*, 579-588.

Stokoe II, K. H., Roberts, J., Hwang, S., Cox, B., Menq, F., & van Ballegooy, S. (2014). Effectiveness of Inhibiting Liquefaction Triggering by Shallow Ground Improvement Methods: Initial Field Shaking Trials with T-Rex at One Site in Christchurch, New Zealand. *Soil Liquefaction During Recent Large-Scale Earthquakes*, 193-202.

Stokoe II, K.H., Roberts, J.N., Hwang, S., Cox, B.R., Menq, F.Y., & van Ballegooy, S. (2014). Effectiveness of Inhibiting Liquefaction Triggering by Shallow Ground Improvement Methods: Initial Field Shaking Trials with T-Rex at One Site in Christchurch, New Zealand. *New Zealand-Japan Workshop on Soil liquefaction During Recent Large-Scale Earthquakes.* Auckland.

Stokoe II, K.H., Roberts, J.N., Hwang, S., Cox, B.R., Menq, F.Y., & van Ballegooy, S. (2016). Effectiveness of Inhibiting Liquefaction Triggering by Shallow Ground Improvement Methods: Field Shaking Trials with T-Rex at One Area in Christchurch, New Zealand. *24th Geotechnical Conference of Torino.* Torino.

Thevanayagam, S., Shenthan, T., Mohan, S., & Liang, J. (2002). Undrained Fragility of Clean Sands, Silty Sands, and Sandy Silts. *Journal of Geotechnical and Geoenvironmental Engineering, 128*(10), 849-859.

Tokimatsu, K., & Yoshimi, Y. (1983). Empirical Correlation of Soil Liquefaction Based on SPT N-Value and Fines Content. *Soils and Foundations, 23*(4).

Tsukamoto, Y., Ishihara, K., Nakazawa, H., Nakazawa, H., Kamada, K., & Huang, Y. (2002). Resistance of Partly Saturated Sand to Liquefaction with Reference to Longitudinal and Shear Wave Velocities. *Soils and Foundations, 42*(6), 93-104.

Unno, T., Kazama, M., Uzuoka, R., & Sento, N. (2008). Liquefaction of Unsaturated Sand Considering the Pore Air Pressure and Volume Compressibility of the Soil Particle Skeleton. *Soils and Foundations, 48*(1), 87-99.

Valle-Molina, C. (2006). *Measurements of Vp and Vs in Dry, Unsaturated and Saturated Sand Specimens with Piezoelectric Transducers.* PhD Thesis, The University of Texas at Austin.

Valle-Molina, C., & Stokoe, K. H. (2012). Seismic measurements in sand specimens with varying degrees of saturation using piezoelectric transducers. *Canadian Geotechnical Journal*, 671-685.

van Ballegooy, S., Roberts, J., Stokoe II, K., Cox, B., Wentz, F., & Hwang, S. (2015). Large-Scale Testing of Shallow Ground Improvements Using Controlled Stage-Loading with T-Rex. *Proceedings of the 6th International Conference on Earthquake Geotechnical Engineering.* Christchurch.

van Ballegooy, S., Wentz, F., Stokoe, K., Cox, B., Rollins, K., Ashford, S., & Olsen, M. (2017). *Christchurch Ground Improvement Trial Report.* Auckland: Tonkin & Taylor.

Vucetic, M., & Dobry, R. (1986). *Pore Pressure Build Up and Liquefaction at Level Sandy Sites During Earthquakes.* Research Report, Rensselaer Polytechnic Institute, Department of Civil Engineering, Troy.

Wang, W. (1979). *Some Findings in Soil Liquefaction.* Beijing, China: Water Conservancy and Hydroelectric Power Scientific Research Institute.

Wang, Y., Keene, A., & Stokoe, K. (2017). Evaluating the Dynamic Properties of the Material Skeleton of Liquefiable Sands at Low Confining Pressures. *16th World Conference on Earthquake Engineering.* Santiago.

Xenaki, V., & Athanasopoulos, G. (2003). Liquefaction Resistance of Sand-Silt Mixtures: An Experimental Investigation of the Effect of Fines. *Soil Dynamics and Earthquake Engineering, 23*, 183-194.

Yamamuro, J. A., & Lade, P. V. (1997). Static Liquefaction of Very Loose Sands. *Canadian Geotechnical Journal, 34*, 905-917.

Yoshimi, Y., Tanaka, K., & Tokimatsu, K. (1989). Liquefaction Resistance of a Partially Saturated Sand. *Soils and Foundations, 29*(3), 157-162.

Youd, T.L., & Noble, S.K. (1997). Magnitude Scaling Factors. *Proceedings of NCEER Workshop of Evaluation of Liquefaction Resistance of Soils,* National Center for Earthquake Engineering Research, State University of New York at Buffalo, 149-165.

Youd, T., Idriss, I., Andrus, R. D., Arango, I., Castro, G., Christian, J. T., Dobry, R., Finn, W.D.L., Harder, L.F., Hynes, M.E., Ishihara, K., Koester, J.P., Liao, S.S.C., Marcuson III, W.F., Martin, G.R., Mitchell, J.K., Moriwaki, Y., Power, M.S., Robertson, P.K., Seed, R.B., Stokoe II, K.H. (2001). Liquefaction Resistance of Soils: Summary Report from the 1996 NCEER and 1998 NCEER/NSF Workshops on Evaluation of Liquefaction Resistance of Soils. *Journal of Geotechnical and Geoenvironmental Engineering, 127*(10), 817-833.

Zlatovic, S., & Ishihara, K. (1997). Normalized Behavior of Very Loose Non-Plastic Soils: Effects of Fabric. *Soils and Foundations, 37*(4), 47-56.